A Contribution to Modeling and Control of Dephosphorization in the Oxygen Steelmaking Process

Von der Fakultät für Ingenieurwissenschaften,

Abteilung Maschinenbau und Verfahrenstechnik

der

Universität Duisburg-Essen

zur Erlangung des akademischen Grades

einer

Doktorin der Ingenieurwissenschaften

Dr.-Ing.

genehmigte Dissertation

von

Sabrine Khadhraoui
aus
Kairouan, Tunesien

Gutachter: Univ.-Prof. Dr.-Ing. Rüdiger Deike
Univ.-Prof. Dr.-Ing. Karl-Heinz Spitzer

Tag der mündlichen Prüfung: 16.02.2021

Abstract

Phosphorus has a detrimental effect on the quality of steel as it reduces its ductility and toughness. In order to ensure a good quality of the final product, the requirements for steel regarding the phosphorus content are very strict. Recently, it has been reported that the levels of phosphorus in iron ores are increasing due to a gradual shortage of low phosphorus iron ores. Thus, the phosphorus content of the hot metal charged into the BOF (Basic Oxygen Furnace) process will be increasing, which will sharpen the challenges associated with meeting the end phosphorus requirements. Steelmakers are therefore exploring the possibilities for refining high phosphorus iron ore and aim at developing solutions that ensure controlling the final phosphorus contents within the target range under those new circumstances.

A detailed study of the thermodynamics of dephosphorization reaction at conditions relevant for the BOF process is necessary in order to point out the potential as well as the limitations of phosphorus removal for different starting conditions and blowing strategies. This is important for deriving the appropriate process solution, for example, in deciding whether a single or a double slag treatment is required, or for the development of innovative process technologies and new control methods.

Even though the quaternary system $CaO\text{-}FeO_x\text{-}SiO_2\text{-}P_2O_5$ is the fundamental oxide system for low and high phosphorus refining processes, its thermochemical behavior remains unclear. Instead, it is common practice to reduce this system to its ternary sub-systems $CaO\text{-}FeO_x\text{-}SiO_2$ and $CaO\text{-}FeO_x\text{-}P_2O_5$ when studying the thermochemical behavior of low and high phosphorus systems. However, the phase diagrams available in the literature do not always cover the total temperature range of the industrial process. In addition, the effect of the oxidation state of FeO_x and that of minor oxides such as MgO or MnO on the phase boundaries of those ternary systems remains unclear.

By means of carrying out extensive evaluations of the oxide systems relevant for both low and high phosphorus refining processes, this thesis aims at providing a deep understanding of the state of industrial slags in the composition, temperature, and $p(O_2)$ ranges relevant for the entire process. In addition, an assessment of the dephosphorization potential of industrial slags under those conditions is provided. The extent of phosphorus removal from the metal phase is controlled by the dephosphorization potential of the slag phase, which is generally believed to be a strong function of the composition and temperature of the relevant oxide system.

A computational thermodynamics approach is used for the thermodynamic evaluations carried out in the present work, which involves coupling the newly developed thermodynamic database BOFdePhos to the software package FactSage ™. The non-ideal associate solution model is used for the description of the Gibbs energy of the liquid phase and the Compound Energy Formalism (CEF) for the description of the Gibbs energy of the solid solution phases while the solid stoichiometric compounds are treated with simple temperature-dependent Gibbs energy functions. This approach has been selected due to the fact that modeling approaches developed according to the CALPHAD (CALculation of PHAse Diagrams) method have a good capability for extrapolating from assessed binary and ternary sub-systems to higher-order systems. Thus, it is possible to generate new phase diagrams using experimental data from lower-order systems.

The thermodynamic evaluation of the oxide system $CaO\text{-}FeO_x\text{-}SiO_2\text{-}P_2O_5$ and its ternary subsystems were carried out for the total composition, temperature, and $p(O_2)$ ranges relevant for the process. The results were used for the assessment of the state of industrial slags by means of the analysis of plant trial measurements. The assessments indicate that industrial slags are heterogeneous throughout the major part of the process and, in most cases, saturated with the solid C2S_C3P ($2CaO.SiO_2\_3CaO.P_2O_5$) phase. However, most phosphorus distribution approaches (Lp-approaches) reported in the literature were developed for purely liquid slags. Thus, a new Lp-approach has been developed in the present work, which considers the effect of the amount, type, and composition of the different slag phases. The type and amount of phases formed during the process are found to be highly sensitive to the composition, temperature, and oxidation state of FeO_x. The risk involved with simplifying the oxide system to its main components, as well as with the non-consideration of the effect of $p(O_2)$ is underlined in this work.

This work demonstrates how new methods and strategies for enhancing dephosphorization control can be developed based on a combination of thermodynamic, experimental, and industrial evaluations. Those methods include an implementation concept for the thermodynamic database into dynamic models, the specification of a new target slag region for achieving optimal dephosphorization results, as well as the development of a new BOF method for ensuring a flexible, yet accurate, control of the slag composition towards the target region.

Kurzfassung

Phosphor wirkt sich nachteilig auf die Qualität des Stahls aus, da es seine Duktilität und Zähigkeit verringert. Um eine gute Qualität des Endprodukts zu gewährleisten, sind die Anforderungen an Stahl hinsichtlich des Phosphorgehalts sehr streng. In letzter Zeit wurde berichtet, dass die Phosphorgehalte in Eisenerzen aufgrund eines langsam wachsenden Mangels an Eisenerzen mit niedrigem Phosphorgehalt zunehmen. Der P-Gehalt des in den BOF (Basic Oxygen Furnace) -Prozess eingefüllten Roheisens wird daher zunehmen, was die Herausforderung, die Anforderung an den Endphosphorgehalt zu erfüllen, verschärfen wird. Die Stahlhersteller untersuchen daher die Möglichkeiten zur Raffination von Eisenerz mit hohem P-Gehalt und sind bestrebt, Lösungen zu entwickeln, die unter diesen neuen Umständen einen Endphosphorgehalt innerhalb des Zielbereichs gewährleisten.

Eine detaillierte Untersuchung der Thermodynamik der Entphosphorungsreaktion unter für den BOF-Prozess relevanten Bedingungen ist erforderlich, um das Potenzial und die Grenzen der Phosphorentfernung für verschiedene Startbedingungen und Blasstrategien aufzuzeigen. Dies ist wichtig, um die geeignete Prozesslösung abzuleiten, z.B. um zu entscheiden, ob eine Einzel- oder eine Doppelschlackenbehandlung erforderlich ist, oder um innovative Prozesstechnologien und neue Steuerungsmethoden zu entwickeln.

Obwohl das quaternäre Oxidsystem $CaO\text{-}FeO_x\text{-}SiO_2\text{-}P_2O_5$ das grundlegende Oxidsystem für den BOF-Prozess ist, bleibt sein thermochemisches Verhalten unklar. Daher ist es üblich, dieses System auf seine ternären Komponenten zu reduzieren. Diese Phasendiagramme decken jedoch nicht immer den gesamten Temperaturschwankungsbereich für den industriellen Prozess ab. Darüber hinaus bleibt die Auswirkung der Oxidationsstufe von FeO_x und der von Nebenoxiden auf die Phasengrenzen dieser ternären Systeme unklar.

Ziel dieser Arbeit ist es, anhand umfassender Auswertungen der Oxidsysteme, die für Raffinationsprozesse mit niedrigem und hohem Phosphorgehalt relevant sind, ein tiefes Verständnis des Zustands industrieller Schlacken in den für den gesamten Prozessverlauf relevanten Bereichen von Zusammensetzung, Temperatur und Oxidationsstufe von FeO_x zu vermitteln. Weiterhin wird eine Bewertung des Entphosphorungspotentials von Industrieschlacken unter diesen Bedingungen vorgenommen.

Für die in der vorliegenden Arbeit durchgeführten thermodynamischen Auswertungen wird ein rechnergestützter Thermodynamikansatz verwendet, bei dem eine neu entwickelte thermodynamische Datenbank mit dem Softwarepaket FactSage™ gekoppelt wird. Das nicht-ideale assoziierte Lösungsmodell wird zur Beschreibung der Gibbs-Energie der flüssigen Phase und der Compound Energy Formalism (CEF) zur Beschreibung der Gibbs-Energie der festen Phase verwendet. Dieser Ansatz wurde aufgrund der Tatsache ausgewählt, dass Modellierungsansätze, die nach der CALPHAD-Methode (CALculation of PHAse Diagrams) entwickelt wurden, eine gute Fähigkeit zur Extrapolation von bewerteten binären Teilsystemen auf Systeme ternärer und höherer Ordnung aufweisen. Somit ist es möglich, mit experimentellen Daten aus Systemen niedrigerer Ordnung völlig neue Phasendiagramme zu erstellen.

Die thermodynamische Bewertung des Oxidsystems CaO-FeO_x-SiO_2-P_2O_5 und seiner ternären Teilsysteme erfolgt über die für die gesamte Prozessdauer relevanten Bereiche von Gesamtzusammensetzung, Temperatur und Oxidationsstufe von FeO_x. Die thermodynamischen Auswertungen werden zur Beurteilung des Zustands von Industrieschlacken mittels Analyse von Messungen aus Anlagenversuchen und industriellen Beobachtungen herangezogen. Die Ergebnisse zeigen, dass industrielle Schlacken während eines Großteils des Prozesses heterogen und in den meisten Fällen mit fester $2CaO.SiO_2$-$3CaO.P_2O_5$ –Phase gesättigt sind. Die meisten in der Literatur beschriebenen Ansätze zur Ermittlung des P-Verschlackungsverhältnis (Lp-Ansätze) wurden jedoch für flüssige Schlacken entwickelt. In der vorliegenden Arbeit wird daher ein neuer Lp-Ansatz entwickelt, der die Auswirkung von Menge, Art und Zusammensetzung der verschiedenen Schlackenphasen berücksichtigt. Die Art und Menge der gebildeten Phasen reagiert sehr empfindlich auf Änderungen von Zusammensetzung, Temperatur und Oxidationsstufe von FeO_x.

Diese Arbeit zeigt, wie neue Methoden und Strategien zur effizienteren Entphosphorung auf der Grundlage einer Kombination aus thermodynamischen, experimentellen und industriellen Bewertungen entwickelt werden können. Diese Methoden beinhalten ein Konzept für die Implementierung der thermodynamischen Datenbank in dynamische Modelle, die Spezifikation einer neuen Zielschlackenzone zur Erzielung optimaler Entphosphorungsergebnisse sowie die Entwicklung einer neuen BOF-Methode zur Gewährleistung einer flexiblen und dennoch genauen Steuerung der Schlackenzusammensetzung in Richtung der Zielregion.

Acknowledgments

The research leading to the results presented in this thesis was carried out during my assignment to the R&D department of the SMS group GmbH in Düsseldorf as a development engineer. In addition, a major part of the research work was carried out within the scope of the BOF DePHos Project, funded by the European Union's Research Fund for Coal and Steel (RFCS) under grant agreement n° [RFSR-CT-2014-0000]. Thus, I would like to express my gratitude to my employer, the SMS group, as well as to the European Union for making this work possible.

My gratitude goes to my supervisor *Univ.-Prof. Dr.-Ing. Rüdiger Deike* for supervising this work as well as for his support and encouragement, which was not limited to this thesis period but from which I profited throughout my student days. It is also through his lectures that I discovered my interest in extractive metallurgy and chose it later as my field of expertise. In this context, I would also like to take the opportunity to express my gratitude to *Univ-Prof. Dr. rer. nat. Johannes Gottschling,* whose trust and recommendation pushed my scientific career forward and opened a world of opportunities for me, including the opportunity to write this thesis.

Furthermore, I would like to thank *Univ-Prof. Dr.-Ing. Karl-Heinz Spitzer* from the University of Clausthal-Zellerfeld for agreeing to co-supervise my thesis.

I would like to express my gratitude to *Prof. Dr. rer. nat. Klaus Hack* as well as to my colleague *Prof. Dr. Ing Hans-Jürgen Odenthal*, who are affiliated with the RWTH Aachen University, for their valuable contribution to the content and quality of this thesis. I am thankful for their critical evaluation, constructive criticism, and the valuable suggestions that they provided in the scope of our common publications. I am especially indebted to *Prof. Klaus Hack* for voluntarily reviewing several parts of this thesis. It was truly a privilege for me to have the opportunity to work with them and to learn from them.

I would like to thank my friend and former colleague, *Dr. Peter Monheim*, for introducing me to the field of computational thermodynamics, which is the fundamental approach adopted in this thesis. I am also thankful for my dear friend, *Anne Monheim*, for the linguistic revision of several parts of this thesis.

I would like to express my gratitude to many colleagues within the R&D department for their constant encouragement and motivation to complete this work (alphabetically): An-

dreas Kemminger, Barbara Sack, Christian Plocienek, Elena Jipnang, Esra Erdem-Hornauer, Fabian Krause, Galina Federau, Kirsten Fieger-Schlangen, Norbert Uebber, Norbert Vogl and Tamara Gusarova. Indeed, the presence of such colleagues gave me the motivating work atmosphere that I needed to thrive and complete this work.

I would like to take this opportunity to give special thanks to many dedicated school teachers who have had a great impact on me personally and academically. I am genuinely grateful to my Mathematics teacher *Mr. Anouar Ben Arbia,* and my Englisch teacher *Mrs. Najoua Dahmeni*. Thank you, Mr. Anouar and Mrs. Najoua, for making my school days truly memorable and for acquainting me with the skills and the motivation that I needed to pursue my academic goals.

I would like to thank my dear husband and best friend, *Hamza Baazaoui*, for his love, support and sacrifice, which made the completion of this thesis possible. I am grateful to my daughters, Sarra and Mariam for being such an inspiration, which lights up every area of my life including my scientific world. I also thank them for their patience and understanding during the time I was absent working on this thesis.

My special thanks go to my entire family for their unconditional love, support, and encouragement that kept me going throughout the entire thesis duration. I am grateful, especially to my sister Asma and to my loving parents, *Rawdha* and *Chedly Khadhraoui*, to whom I dedicate this work. I was truly blessed to have such open-minded parents who were ahead of their time in many aspects and supported me in every way possible to pursue my goals, no matter how unusual and distant they seemed. Finally, my deepest gratitude goes to Allah for granting me the privilege to explore the rules governing His creation and blessing me with such wonderful people during my quest.

Sabrine Khadhraoui

Düsseldorf, November 2019

Patents filed in the scope of this thesis

1. **S. Khadhraoui,** F. Krause, A. Kemminger: inventors; SMS group GmbH, assignee. "*Verfahren zur Bestimmung und Steuerung oder Regelung des Phosphor-Gehaltes"*. German patent office, 13 Dec **2019**. Registration number: 102019219623.3, Germany.

2. **S. Khadhraoui**, U. De fries, A. Hofmann, inventors; SMS group GmbH, assignee. "Verfahren zum Entphosphern einer Stahlschmelze während des Frischprozesses"*.* German patent office, 11 Oct **2019**. Registration number: 102019215678.9, Germany.

3. **S. Khadhraoui**, F. Krause, inventors; SMS group GmbH, assignee. *"Konverter und Verfahren zum Frischen geschmolzenen Metalls"*. German patent office, 24. June **2019**. Registration number: 102019209109.1, Germany.

4. **S. Khadhraoui**, F. Krause F, H-J. Odenthal: inventors, SMS group GmbH: assignee. *"Sauerstoffinjektor für einen Konverter insbesondere zur Stahlherstellung",* German patent office, 29 May **2018**. Registration number: P 10 2018 208 433.5, Germany.
   URL:https://patentscope.wipo.int/search/en/detail.jsf?docId=DE278266447&tab=NATIONALBIBLIO&_cid=P22-K5C8MC-51146-2

5. **S. Khadhraoui**, S. Das, H-J. Odenthal, F. Krause F, A. Kemminger: inventors; SMS group GmbH: assignee. "*Method for Refining Molten Metal Using a Converter".* International patent, 16 Feb **2018**, international publication number: WO 2019/158479.A1.
   URL:https://patentscope.wipo.int/search/en/detail.jsf?docId=WO2019158479&tab=PCTBIBLIO&_cid=P22-K5C94M-56152-3

Publications made in the scope of this thesis

Journal Papers

1. **S. Khadhraoui,** K. Hack, T. Jantzen, and H. Odenthal: Study of the State of Industrial P_2O_5-Containing Slags Relevant to Steelmaking Processes Based on a New Thermodynamic Database Developed for CaO–FeO_x–P_2O_5–SiO_2–MnO–MgO–Al_2O_3 Slags. *Steel research int*. **2019**, *90*, 1900085. DOI:10.1002/srin.201900085. Article selected for the front cover of steel research int. 8/2019, DOI:10.1002/srin.201970081.
2. **S. Khadhraoui**, H.-J. Odenthal, S. Das, M. Schlautmann, K. Hack, B. Glaser and R. Woolf: A new approach for modelling and control of dephosphorization in BOF converter, *La Metallurgia Italiana* **2018**, *n. 11-12*, 5-16

Project reports

M. Schlautmann, B. Kleimt, **S. Khadhraoui**, H.-J. Odenthal, K. Hack, P. Monheim, B. Glaser, R. Antonic, M. Adderley, F. Schrama: *Dynamic online control and end point determination of dephosphorization in BOF converter (BOF DePhos)*, Publication Office of the European Union, Luxembourg, September **2019**.

Conference Papers

1. **S. Khadhraoui***, K. Hack , N. Uebber , W. Klos : *How does solid phase precipitation affect the evolution of phosphorus removal during the BOF Process? Thermochemical and industrial aspects*. The 11th Molten Slags, Fluxes, and Salts (MOLTEN 2020), May 25-29, **2020**, Seoul, Korea (accepted).
2. **S. Khadhraoui*,** H-J. Odenthal, F. Krause, N. Uebber, W. Klos, P. Monheim, K. Hack , M. To Baben: *Modeling and Control of the BOF process: Challenges, solutions and latest developments in SMS group.* METEC and 4th European Steel Technology and Application Days (ESTAD), June 24-28, **2019**, Düsseldorf.
3. **S. Khadhraoui***, H.-J. Odenthal, S. Das, M. Schlautmann, K. Hack, B. Glaser, R. Woolf: *A new Approach for Modelling and Control of Dephosphorisation in BOF Converter*, The 8 th European Oxygen Steelmaking Conference (EOSC), October 2018, Taranto, Italy (selected for publication at the journal: La Metallurgia Italiana **2018**, n. 11-12, 5-16).
4. F. Kaya*, **S. Khadhraoui**, B. Derin: *A Modelling Investigation on the Viscosity of Fayalite Slags by FactSage*, the 19th International Metallurgy and Materials Congress (IMMC), October **2018**, Istanbul, Turkey.
5. M. Schlautmann*, B. Kleimt, **S. Khadhraoui**, K. Hack, P. Monheim, B. Glaser, R. Antonic, M. Adderley, F. Schrama: *Dynamic on-line monitoring and end point control of dephosphorisation in the BOF converter*, 3rd European Steel Technology and Application Days (ESTAD), pp. 1038-1049. June **2017,** Vienna, Austria.

6. S. Petersen*, K. Hack, P. Monheim, P. Scheller, M. Müller, M. Dohrn, **S. Khadhraoui**, *Application Examples of Thermochemical Process Simulation Using SimuSage – Introducing Current Projects from Metallurgy and Combustion Technology*, Materials Science & Technology, pp. 1239-1240, October **2017**, Pittsburgh, USA.

Presentations at Technical Meetings and Events

1. K. Hack*****, P. Monheim, M. to Baben, **S. Khadhraoui**: *Conclusions from the thermochemical Modelling in the BOFdePhos project*, RCCM-GTT User Meeting, November **2019**, Osaka, Japan.
2. **S. Khadhraoui***, P. Monheim, K. Hack, M. to Baben: Application of thermochemistry in BOF process modeling: *What did it teach us about the dynamics of decarburisation reaction?,* GTT Annual User Meeting, June **2019**, in: GTT Technologies, Aachen, Germany.
3. K. Hack*, P. Monheim, T. Jantzen, M. to Baben, **S. Khadhraoui**: *Thermochemical Modelling in the BOFdePhos Project - What did we learn?*, GTT Annual User Meeting, June **2019,** in: GTT Technologies, Aachen, Germany.
4. **S. Khadhraoui *,** K. Hack , T. Jantzen: *Study of the State of Industrial Steelmaking Slags and their Dephosphorisation Potential Based on a computational thermodynamics approach*, Thermoweek, April **2019**, in: Ex Mente, Pretoria, South Africa.
5. **S. Khadhraoui ***, K. Hack, P. Monheim, T. Jantzen: *The importance of computational thermodynamics in process modelling and control*, GTT Annual User Meeting, June **2018**, in: GTT Technologies, Aachen, Germany.
6. **S. Khadhraoui ***: *Findings in the Scope of the BOF DePhos Project*, Meeting of the Technical Committee Development in Steel Plant, Steel Institute VDEh, October **2017**, Düsseldorf, Germany.
7. **S. Khadhraoui***: *BOF DePhos part II: Slag evolution during the blowing process: thermochemical and experimental findings,* GTT Annual User Meeting, June **2017,** Aachen, Germany.
8. K. Hack*, P. Monheim, T. Jantzen, **S. Khadhraoui**: *Advances of Thermochemical Modelling in the BOFdePhos Project*, RCCM-GTT User Meeting, November **2016**, Tokyo, Japan.

**: denotes the presenting author*

Table of Contents

Dedicated to my parents, Rawdha and Chedly Khadhraoui

1 Introduction

Iron is considered as the most widely used, multi-functional and adaptable natural material found on earth. Steel has historically been central to modern economies, synonymous with growth and progress. The reconciliation of Europe after World War II was built on unified coal and steel industries. More recently, the fundamental link between steel and development has been manifested in the enormous increase in production capacity and output in China and, on a smaller scale, in other emerging markets, matching ambitious economic development goals.[1]

The total production of crude steel worldwide has increased by about 35% within the last decade, reaching an amount of 1.808 million tonnes in 2018 [2]. The production of steel is dominated by two production routes: The electrical steelmaking route and the oxygen steelmaking route. Even though the share of the electrical steelmaking route has been increasing steadily for the last 30 years, the oxygen steelmaking route remains the dominant production route, accounting for 70% of total worldwide steel production in 2018.[2]

1.1 Oxygen steelmaking route

"Oxygen steelmaking" is a generic name given to those processes in which gaseous oxygen is used as the primary agent for autothermic heat generation resulting from oxidation reactions.[3] The "electrical" steelmaking processes use electricity and, thus an external energy source as the main source of heat.

Figure 1 shows the sequence of processes making up the oxygen steelmaking route, starting with the blast furnace where the iron ore is reduced to a carbon-rich liquid hot metal. In the majority of steel plants, sulfur is removed afterward in a "desulphurization" station, but it is also possible that the hot metal is sent directly to the "converter" station without prior desulphurization. In the "converter" station, the carbon-rich liquid hot metal is "converted" to a low-carbon liquid steel by means of oxygen blow, which explains why this process is known as the "converter" process. Further major purposes of this process are the reduction of the content of major elements such as silicon and manganese as well as that of impurities such as phosphorus, and to raise the final temperature of the liquid metal to a target value.

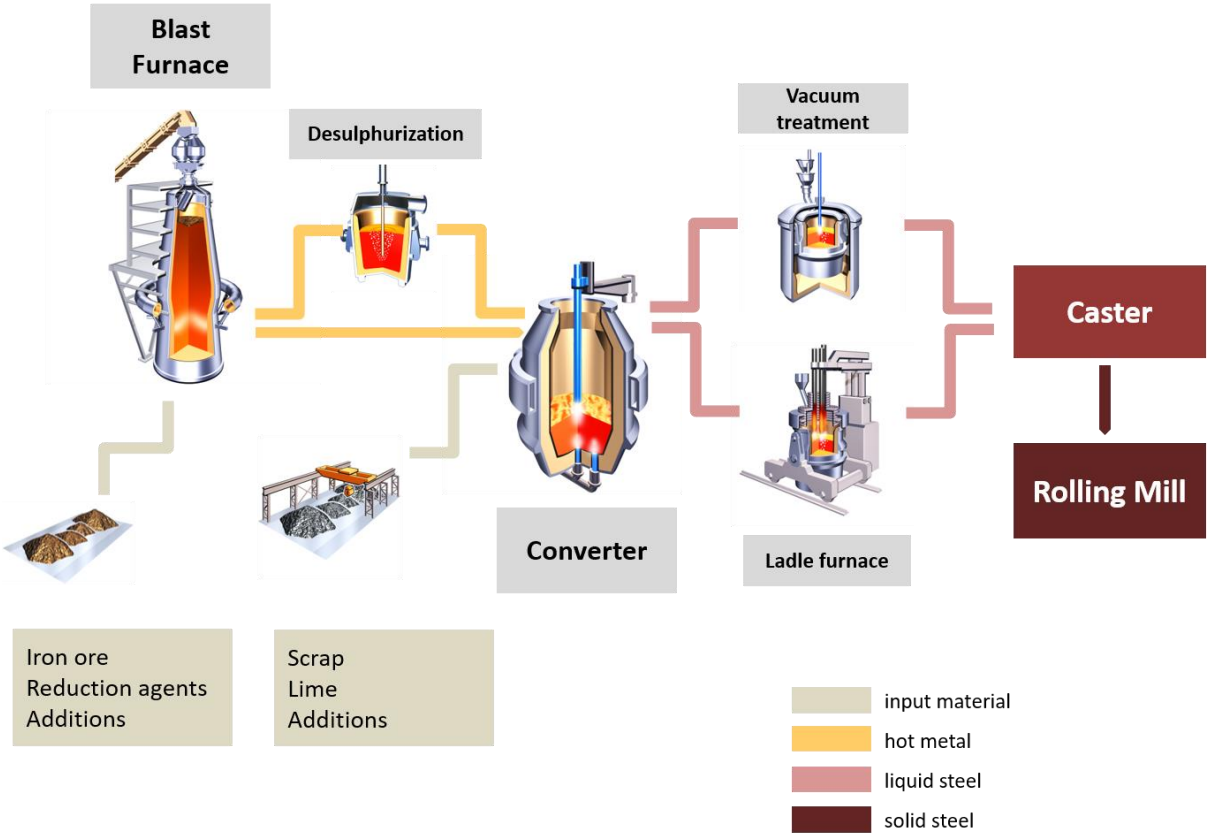

Figure 1: Overview of the sequence of processes during the Oxygen Steelmaking route.

The first commercial operation of steelmaking with a “converter” occurred in the early 1950s at Linz and Donawitz (Austria),[4] where oxygen was blown at supersonic speed onto the melt surface. This manner of steelmaking became known as the Linz-Donawitz or LD process. However, different names for this process are used in different regions:

- In many European steel plants, the process is still called LD
- in the UK, the process is called the BOS process (Basic Oxygen Steelmaking)
- In the United States of America, Canada, and the Far East, the process is called BOF (Basic Oxygen Furnace).

In practice, these annotations refer to the same process, which is the top blown variety of the converter process. A bottom blown variety of the process, noted as the OBM process (Oxygen Bottom Maxhütte), was successfully commercialized in the late 1960s by Maxhütte (Germany). The present work focuses on the top blown converter,

which is the most widespread variety and will be further designated as the BOF process.

Today, the BOF process is typically provided with additional bottom stirring facilities, through which inert gas is blown in order to enhance the mixing conditions. In such a case, the process is called the “combined blowing” BOF process. A typical converter produces a 200-300 tonnes heat, the time of one blow is about 15-20 minutes and the tap-to-tap time (between 2 heats) is in the range of 30-40 minutes.[5]

1.2 Importance, challenges, and potential of phosphorus removal

1.2.1 The phosphorus problem in steel

Phosphorus has a detrimental effect on the quality of steel as it reduces its ductility and toughness. This is because as steel solidifies from the outside in, phosphorus impurities are transported to the center and to grain boundaries, forming brittle cores of high phosphorus concentration in the product.[6]

The requirements for steel regarding the phosphorus content are very strict. This is especially the case for products that require uniform deformability, such as thin sheets, automobile exteriors, and deep drawn components, pipelines for transportation of natural gas, and petroleum products.[6, 7]

In the oxygen steelmaking route, phosphorus is introduced to the blast furnace through the charged coke, iron ore, and flux in the form of P_2O_5, $3CaO.P_2O_5$, and $3FeO.P_2O_5$.[8] In the blast furnace, P_2O_5 is released from the slag phase as gas. The P_2O_5 gas is then reduced by carbon when it passes through the coke layers. The reduction of P_2O_5 is almost complete by the end of the blast furnace process, and the reduced phosphorus is almost entirely dissolved in the liquid iron. In summary, it can be said that more than 90% of the phosphorus that enters the blast furnace is found later in the hot metal, which is then charged into the BOF process (Figure 1). The rest (10%) is either lost to the slag or to the flue gas or is absorbed in the refractory linings.[9]

In general, a final phosphorus content in the range of 0.015-0.06 wt% is required.[10] in liquid steel. For some steel markets, such as those in Europe, Japan, and Korea, more than 50% of the steel sold requires a phosphorus content of less than 0.03 wt%.[11] **Figure 2** shows the phosphorus concentration ranges in iron ores mined in

different regions. In Europe, the majority of processed iron ores are imported from Brazil, Canada, and Australia, which results in a phosphorus content between 0.06 and 0.09 wt% in the hot metal.[12]

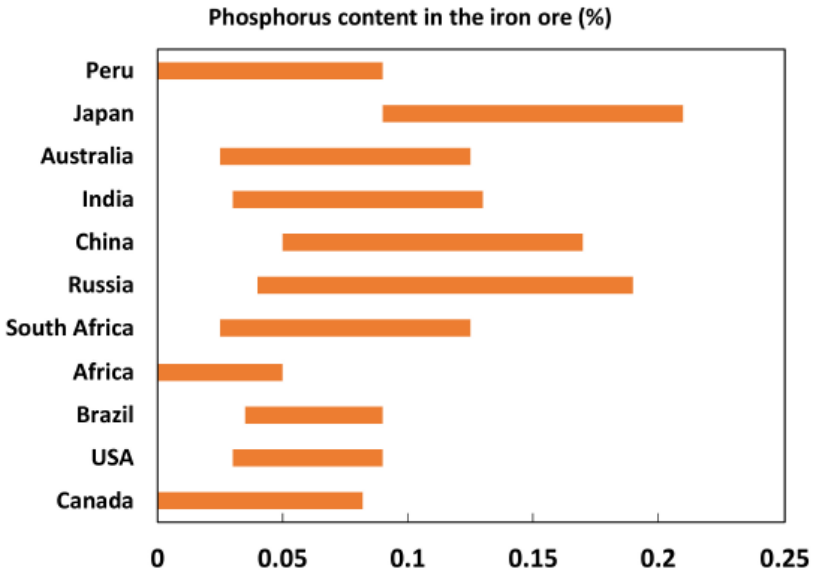

Figure 2: Phosphorus concentration in iron ore in different geographical regions, reprinted with permission from Ref. [13]

It can be seen that while iron ores originating from Russia and China may occasionally contain phosphorus with a content higher than 0.1 wt%, this is the standard case for Japanese iron ores. When the initial phosphorus content of the liquid hot metal is higher than 0.1 wt%, achieving the given phosphorus targets becomes very challenging during a standard BOF operation. This is why Japanese BOF practice is different from that in Europe: Since the 1980s, almost all Japanese steel plants have implemented a double slag process[14, 15]. In Japanese steel plants (and also in some Chinese and Korean plants) phosphorus removal is carried out in a separate step prior to the BOF process, (denoted as “hot metal dephosphorization”) as part of the “hot metal pre-treatment” process.[14, 16-19]This procedure is carried out either in a torpedo car or in a separate BOF vessel, and the phosphorus content of the tapped hot metal is within the typical range of that in the hot metal produced in European steelworks. Afterward, the low-phosphorus hot metal is charged into a typical BOF furnace and the refining procedure is carried out in a similar manner to the typical BOF operation. The second refining step is denoted as the “decarburization step”. More recently, methods to

dephosphorize and decarburize the hot metal continuously in the same BOF furnace were successfully implemented in many Japanese steelworks, but an intermediate de-slagging following the dephosphorization step remains necessary.[18-20]

1.2.2 On the expected increase in phosphorus content and its consequences

Based on the introduction of the phosphorus problem described in section 1.2.1, it can be concluded that the challenges with respect to using high phosphorus iron ores are limited to specific regions, especially Japan, which have accordingly adopted special refining technologies. Thus, it may seem that European steel plants are in a comfortable situation with respect to the initial phosphorus input in the converter. However, recently, a gradual shortage of high-grade raw materials has been reported, which has resulted in an increase in its price.[6] To cover the shortage of high-grade iron ores, low-grade iron ores, which are typically high in phosphorus, will have to be mined and used in the future.[17, 21] The reserves of high-phosphorus iron ores are plentiful all over the world. Some examples are listed below:

- China has up to 7.45 billion tons of high phosphorus iron ore reserves, accounting for above 10% of the national iron ore resource reserves.[21]
- More than 80% of Western Australian iron ore contains an average of 0.15 wt% P.[17]

Steelworkers have responded to the shortage by exploring the possibilities of refining lower-priced high phosphorus iron ores. As a result, the levels of phosphorus in the BOF process are increasing gradually in many regions.[6, 11, 12, 22-25] This is well-illustrated in **Figure 3**, which shows the increasing trend for a higher phosphorus content in hot metal reported by HYUNDAISTEEL.[25] It can be seen that the average phosphorus content has increased by 24% over the last 8 years.

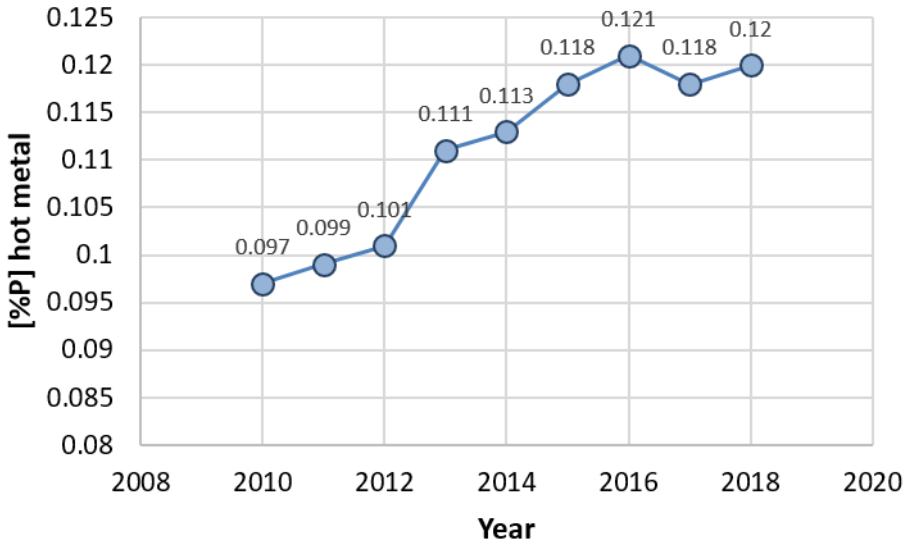

Figure 3: Evolution of initial phosphorus content in hot metal in HYUNDAISTEEL plants within the last decade, reproduced based on the data of Lee et al. [25]

Table 1 shows the mining trend for low and high phosphorus iron ore in a Brazilian mine, as reported by Kitamura et al. [17] It can be seen that the mining of the low-grade iron ore began in the year 2000. The high phosphorus iron ore has now replaced the low phosphorus iron ore as the major mining product. Therefore, the concentration of phosphorus in iron ore is expected to rise steadily, and European steel plants will have to deal with rising phosphorus content in the near future since they mainly import Brazilian, Australian and Canadian iron ores.

Table 1: Mining trends of high and low phosphorus iron ore deposit in the Brockman mine in Brasil.[17, 26]

		Low P deposit	**High P deposit**
Composition (wt%)	Fe	63-64	56-62
	P	< 0.07	> 0.100
	Bonding Water	2.0-3.0	5.0-7.0
Production Year	1965-2000	**Major**	Minor
	2000-2010	Minor	**Major**

Recently a large number of studies were carried out to assess the consequences of this new trend on the BOF operation. Kitamura et al.[17] suggested that it may become

necessary in some regions to replace the standard BOF operation by a double slag practice, which is typically applied in Japanese steelworks as a result of the increasing phosphorus levels.

A further motivation to explore the possibility of using high phosphorus iron ores is the fact that the resulting slag, high in phosphorus, may be used as a source of phosphorus. Phosphorus is a problematic element for steelworks, but it is an essential and irreplaceable element for life [27]. Phosphorus plays a significant role, for example, as an important element in fertilizers.[28] So far, the growing production of phosphorus is mainly based on the processing of non-renewable phosphate ores, often extracted in regions of political instability.[27, 29] Thus, alternative phosphorus sources are being studied and explored.

In addition, phosphate mining and refining have severe negative environmental side effects, which makes the recycling of phosphorus from every suitable phosphorus-containing waste inevitable and desirable in the near future.[29] In this context, the separation of phosphorus from BOF slags is considered a potentially sustainable source of phosphate and has recently been subject to a large number of studies.[21, 30-35] Furthermore, when a hot metal with a phosphorus content of about 0.15 wt% is refined, the resulting slag will contain a P_2O_5 content higher than 10 wt% and can thus be used directly as a fertilizer.[36-38]

In conclusion, it can be stated that the successful refining of hot metal containing high phosphorus levels would be advantageous from both economic and ecological perspectives. At the same time, the restrictions on the final phosphorus content in steel should be maintained in order to ensure the high quality of the finished steel. Thus, it is necessary to derive efficient phosphorus control strategies for refining high phosphorus hot metal in the BOF process. For this purpose, the dephosphorization reaction in the high phosphorus range should be studied in detail at conditions relevant to the BOF process.

2 State of knowledge on the thermodynamics of dephosphorization reaction

2.1 The BOF process: Overview of the main reaction zones and phases

During the BOF process, oxygen gas is blown at supersonic speed onto the liquid metal surface. The resulting reactions between the supplied oxygen gas and the elements take place in several zones and involve a large number of phases. Those phases can be classified into 4 different categories:

- A liquid metal phase: The high-carbon liquid metal charged into the furnace reacts with the blown oxygen gas, resulting in a modification of its composition and temperature throughout the blow: The content of carbon and impurities (Si, Mn, P,…) decrease while the temperature increases gradually due to the exothermic nature of the oxidation reactions.
- A liquid oxide phase containing FeO, CaO, SiO_2, MgO, MnO, and many other minor oxides: This phase is denoted as “liquid slag” in the present work. The formation of a liquid slag results mainly from the Fe-oxidation to FeO as well as from the oxidation of further elements dissolved in the metal, such as Si, Mn, and P. The addition of slag formers during the BOF operation, such as lime (CaO) and occasionally MgO as dolomite, is a general practice for steelworks and is essential for the formation of a reactive liquid slag.
- A large number of solid oxides: The solid oxides precipitate out of the liquid slag when their saturation limit is exceeded. Examples are a variety of calcium silicates such as $2CaO.SiO_2$, $3CaO.SiO_2$. In addition, the charged CaO and MgO (slag formers) require a long dissolution time throughout the blow. Thus, parts of undissolved lime and magnesia are present during a major part of the blowing process and are considered as solid oxide phases in the present work.
- A gas phase containing mainly CO and to a lesser extent CO_2, which represents the products of the main refining reaction in the converter: The carbon oxidation reaction.

In the present work, both types of oxide phases, that is the liquid and the solid oxide phases, are considered to form the so-called “slag phase”. The liquid oxide phase

constitutes the liquid slag part, and the solid oxides constitute the solid part of the slag phase.

A schematic representation of the main reaction zones in the BOF process is provided in **Figure 4**. Once the oxygen blow starts, the slag phase is formed rapidly as the oxidation of the elements dissolved in the liquid metal proceeds at a high rate. This is especially the case for the formation of the FeO oxide. Once lime is charged into the furnace, which usually occurs within the first minutes after the blowing starts, the slag amount increases considerably. Due to its lower density, it floats above the metallic bath.

The strong impact of the supersonic oxygen jet induces a depression on the surface of the liquid metallic bath, which takes the shape of a cavity. This zone is denoted as the “hot spot” as it is characterized by a very high temperature, which has been reported to lie in the range of 2000-2500°C [39, 40]. The “hot spot” zone is considered as part of the primary reaction zone (I), because the oxygen reacts directly in the form of O_2 gas with the elements dissolved in the liquid metal to form a FeO-rich slag phase, a liquid metal phase, and a gas phase. The “metal bath”, which is situated directly underneath the “hot spot”, is also considered as a further primary reaction zone (I) in the present work. In the metal bath zone, the oxygen reacts directly in elementary form, albeit as dissolved [O], with further elements dissolved in the liquid metal phase, which results in the formation of metal and oxide phases as reaction products and, when reacting with dissolved carbon, also in the formation of a gas phase.

A further consequence of the high impact of the supersonic jet on the liquid metal surface is that a substantial number of metal droplets are torn from the cavity and are ejected to the above situated “slag zone” as a result of the shearing action of the gas flow from the impact region when the gases are deflected upwards. This phenomenon is known as “splashing”, and has been studied intensively in the literature from both a computational and an experimental perspective.[41-48] Splashing is largely believed to be responsible for the high amount of metallic droplets residing in the slag as well as for the ejection of materials from the vessel. The ejected metallic droplets, which end up in the slag react with the surrounding slag parts in a way that an oxygen exchange takes place, in the form of the oxidation or reduction of elements, depending on the dominant thermodynamic conditions. When decarburization of the metallic droplets

takes place, CO gas bubbles are generated. The mixture of the slag phase, the metallic droplets residing in it and the entrained gas bubbles is designated as “the emulsion” zone.

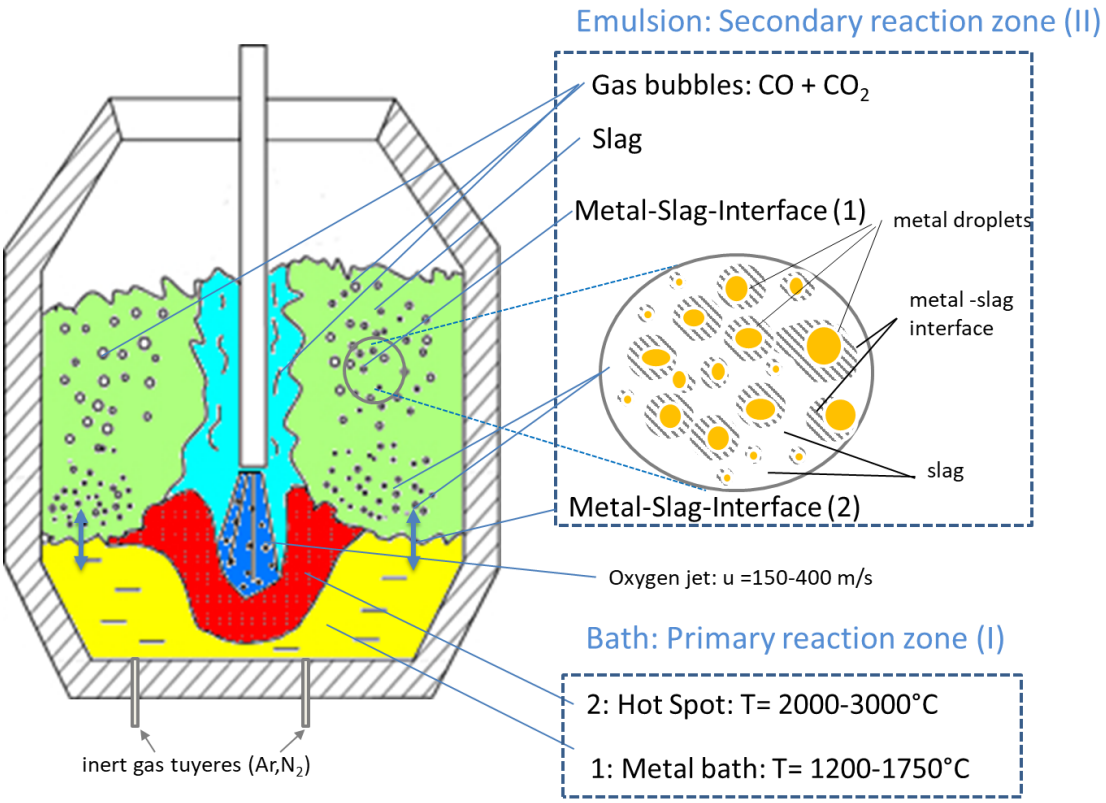

Figure 4: Schematic representation of the main reaction zones and the involved phases in a combined-blown BOF process

The ejected metallic droplets fall back to the “Bath” zone after residing in the slag for a specific duration due to their higher density compared to the density of the entraining slag. The droplets are refined during their trajectory through the “Emulsion” zone, and the composition of the metallic bath changes accordingly upon their return. The residence time of the metallic droplets in the “Emulsion” was reported as high, especially when the slag is foamy, and is largely considered as sufficient for the achievement of chemical equilibrium prior to their return to the “Bath” [49-54]. The refining reactions between the metallic droplets and the slag occur at the interface, and the sum of all interfacial reaction areas is called the “metal-slag-interface (1)” which constitutes a major part of the secondary reaction zone (II). A schematic representation of this reaction zone is shown in Figure 4. The contribution of the “metal-slag-interface (1)” to

the progress and extent of refining reactions in the BOF process has been subject to many studies in the literature [13, 50, 53, 55-59].All of those works agree that this reaction zone plays a major role in the refining reactions, especially with regard to phosphorus, carbon, and manganese removal. Some works considered this zone as the most important reaction zone during the BOF process.[50, 55]

Finally, it can be seen from Figure 4 that parts of the surface of the metallic bath, especially those close to the refractory wall, are constantly in direct contact with the slag phase floating above it. Those sites constitute further reaction sites between the metal and the slag phase. This zone is denoted as the “metal-slag-interface (2)” in the present work. It is generally believed that the metal-slag interfacial area in this zone is much smaller than that between the metallic droplets and the slag, i.e., that of the “metal-slag-interface (2)”. Thus, it is generally considered that the contribution of the “metal-slag-interface (2)” to the refining reactions is very small or even insignificant.[52, 53, 56, 60] In the present work, both zones, “metal-slag-interface (1) and “metal-slag-interface (2), are considered to constitute the “metal-slag-interface” zone.

2.2 Fundamentals of the phosphorus oxidation reaction

Phosphorus is removed from liquid metal by oxidation. The state of equilibrium of the phosphorus reaction between slag and liquid iron has been described and formulated in a variety of ways since the 1940s. Early formulations assumed a molecular nature of phosphorus content in the slag:[4]

$$2[P] + 5[O] \rightarrow (P_2O_5) \quad (1)$$

The following description of the reaction constant of (1) was proposed by Turkdogan:[61]

$$log(Kp_1) = \frac{43480}{T} - 33.0 \quad (2)$$

Examples of further molecular expressions which were used to describe the phosphorus reaction are given by equation (3), (4) and (5):[62]

$$2\,[P] + 5\,(FeO) \rightarrow (P_2O_5) + 5[Fe] \tag{3}$$

$$2\,[P] + 3\,(CaO) + 5\,(FeO) \rightarrow 3CaO.P_2O_5 + 5[Fe] \tag{4}$$

$$2\,[P] + 4\,(CaO) + 5\,(FeO) \rightarrow 4CaO.P_2O_5 + 5[Fe] \tag{5}$$

The following description of the equilibrium constant of equation (3) was proposed by Winkler et al. [63]:

$$log(Kp_3) = \frac{71667}{T} - 28.73 \tag{6}$$

The correct formulation of the phosphorus reaction was first introduced in the late 1960s, as it was realized that phosphorus exists in the slag as a phosphorus pentoxide ion. Phosphorus oxidation requires thus an ionic exchange between the metal and slag phases following the reaction:[60]

$$[P] + \frac{5}{2}[O] + \frac{3}{2}(O^{2-}) \rightarrow ({PO_4}^{3-}) \tag{7}$$

It can be seen from the formulation in (7) that oxygen is required from both the metal and the slag phase in order to remove phosphorus from the metal phase, which implies the necessity of a metal-slag-interface for this reaction to occur. Thus, it is not possible for dephosphorization to take place in the “Bath” (primary reaction zone (I) in Figure 4), contrary to the carbon, silicon, and manganese removal due to the absence of a metal-slag-interface in this zone. Dephosphorization takes place, however, in the “Emulsion” (secondary reaction zone (II) in Figure 4) at the interface between ejected metallic droplets and the slag (metal-slag-interface (1) in Figure 4) as well as at the interface between the bath surface and the slag phase floating above it (metal-slag-interface (2) in Figure 4).

The reaction constant corresponding to (7) can be thus formulated as:

$$Kp_7 = \frac{a(PO_4{}^{3-})}{[\,a(O^{2-})]^{\frac{3}{2}} \cdot a[O]^{\frac{5}{2}} \cdot a[P]} \tag{8}$$

Based on the description of the phosphorus equilibrium reaction, given by (7) and the description of the reaction constant, given by (8), it can be concluded that dephosphorization is promoted by:

1. A high oxygen activity a[O] in the metal phase, which is a strong function of the FeO-activity of the slag.[64] Alternatively, the term a[O] can be substituted by the partial pressure of oxygen in the gas phase $p(O_2)$, which is in equilibrium with the metal, termed largely as the “oxygen potential”. This explains the necessity of oxidizing conditions and, more specifically, the presence of FeO in the slag for dephosphorization to occur.
2. A high activity of free oxygen ions, $a(O^{2-})$, in the slag which is known to be a strong function of the slag basicity. For this purpose, CaO addition is a common practice in the BOF process in order to increase the basicity of the slag and promote phosphorus removal. The effect of basicity on the dephosphorization reaction is further included in the term $a(PO_4^{3-})$, which denotes the activity coefficient of the phosphate ion in the slag: $a(PO_4^{3-})$ decreases with an increase in basicity.[5] This explains the strong ability of highly basic slags to bind phosphorus.

In addition, phosphorus oxidation is known to be highly sensitive to temperature as it is favored by a decrease in temperature. This can be explained by the high value of the coefficient for the 1/T term in equation (2) and equation (6).

2.3 Characterization of the dephosphorization potential of BOF slags

For the evaluation of the dephosphorization potential of BOF slags, the term phosphate capacity $C_{PO_4^{3-}}$, given by equation (10), has been developed based on the formulation of the phosphorus oxidation reaction according to (9):

$$\frac{1}{2}P_2 + \frac{5}{4}O_2 + \frac{3}{2}(O^{2-}) \rightarrow (PO_4{}^{3-}) \tag{9}$$

$$C_{PO_4^{3-}} = \frac{a(PO_4{}^{3-})}{p_{P_2}^{1/2} \cdot p_{O_2}^{5/4}} = Kp_9 \cdot a(O^{2-})^{3/2} \quad (10)$$

In equation (10), the terms p_{O2} and p_{P2} denote the partial pressure of oxygen and phosphorus respectively, while Kp_9 denotes the reaction constant of the dephosphorization reaction according to the formulation presented by equation (9).

The phosphate capacity is considered as a measure of the dephosphorization ability of a slag under a given oxygen potential and is related to the activity of the oxygen ion in the slag.[62] The phosphate capacity has been subject to extensive experimental investigations and accordingly, a large number of formulations were developed for numerous slags and at different temperatures.[65-68] However, due to its complex description, there is a preference for using simpler descriptions of the phosphate capacity in the literature, but they can all be shown to be related to equation (10).[62] The most widely used expressions for phosphate capacity in the literature are shown in equation (11) and equation (12).

$$K_{PO} = \frac{(\%P)}{[\%P]}[\%O]^{-5/2} \quad (11)$$

$$K_{PO} = \frac{(\%P)}{[\%P]}(\%FeO)^{-5/2} \quad (12)$$

It can be seen from (11) and (12) that the phosphorus capacity K_{PO} is expressed as the product of the phosphorus distribution ratio between the slag and the metal, (%P)/[%P], further denoted as Lp, and a term that describes the oxygen potential at the metal-slag interface, which is given either by the oxygen potential of the metal (the term [O]) or the oxygen potential of the slag (the term (%FeO)).

Since the 1930s, extensive experimental studies of metal-slag-equilibria relevant to dephosphorization reaction were made. The purpose was to quantify the phosphorus holding capacity of slags in the form of simplified empirical relations based on regression fitting of measured equilibrium data, which can be used directly for the assessment, prediction, and control of the extent of dephosphorization in the industrial process. As a result, a large number of formulations of the phosphorus capacity K_{PO}

and/or Lp-relations were derived.[18, 63, 69-85] Some examples of the commonly used Lp-equations in the literature are presented in **Table 2**. An overview of a large number of laboratory-based Lp-relations and their validity ranges can be found in the work of Chen et al.[86]

Table 2: Examples of commonly used Lp-relations, which were developed based on fitting experimentally established equilibrium data

Authors	Relations developed based on fitting experimental data
Healy [74]	$log(L_p) = \frac{22350}{T} + 2.5\,log(\%Fe_t) + 0.08(\%CaO) - 16$
Suito et al. [77]	$log(L_p) = \frac{11570}{T} + 2.5\,log(\%Fe_t) + 0.072[(\%CaO) + 0.3(\%MgO) + 0.6(\%P_2O_5) + 0.6(\%MnO)] - 10.52$
Turkdogan [61]	$log(L_p) = \frac{21740}{T} - 9.87 + 0.071 * ((\%CaO) + 0.3\,(\%MgO)) + 2.5\,log(\%Fe_t)$
Ogawa [18]	$log(L_p) = 2.5\,log(\%Fe_t) + 0.0715((\%CaO) + 0.25\,(\%MgO)) + \frac{7710.2}{T} + \left(\frac{105.1}{T} + 0.0723\right)[\%C] - 8.55$
Schürmann et al. [81]	$log(L_p) = \frac{23306}{T} + 2.5\,log(\%Fe_t) + \left(0.06404 - \frac{267.8}{T}\right)(\%Fe_t) - \left(0.0005347 - \frac{1.959}{T}\right)(\%Fe_t)^2 + \left(16.09 - \frac{32941}{T}\right)[\%Mn] - 11.8$

It can be seen from Table 2 that there is general agreement that the dephosphorization potential of slags decreases with temperature but increases with the basicity in terms of (%CaO) and sometimes also of (%MgO), as well as with the FeO-content of the slag. Schürmann et al.[81] did not include the effect of CaO in their equation due to the fact that the experiments were conducted for lime saturated slags. Also, their results indicated that [%Mn] has a strong effect on Lp. This can be explained by the fact that

manganese distribution, defined as the ratio (%MnO)/[Mn], is a strong function of the FeO content of the slag as well as of the temperature.[56, 87-89] As a result, [Mn] can be considered to be strongly correlated with the dephosphorization potential of slags.

The description of the equilibrium state of the dephosphorization reaction in the form of empirical K_{PO} or Lp-relations has found a wide application in dephosphorization modeling and control of the BOF process. Even though the general trends have been in agreement with the experimental behavior, the direct application of laboratory-based Lp-relations to model the dephosphorization behavior in the industrial process generated poor results [24, 90-92]. It was found necessary to modify the laboratory relations by the introduction of regression fitting parameters. This is generally attributed to the fact that laboratory Lp-relations (see examples in Table 2) were developed using equilibrium data while in the industrial process, the equilibrium state for the dephosphorization reaction is usually not achieved due to kinetic restrictions. Examples of industrial Lp-relations reported in the literature are presented in **Table 3.**

Table 3: Examples of industrial Lp-relations developed based on fitting plant trials data

Steel plant	Developed relation based on fitting industrial data
Chukwulebe [93]	$log(L_p) = -0.00218 \cdot T + 0.00382 \cdot (\%FeO) + 0.0228\frac{(\%CaO)}{(\%SiO_2)} - 0.0029 * (\%MgO) - 1.010[\%C] + 5.41$
Tata Steel, 2007 [12]	$log(L_p) = \frac{20254}{T} + 0.3638 \cdot log(\%FeO) - 0.0499(\%MgO) - 6.299$
A large number of data from different steelworks [24]	$log(L_p) = \frac{13536.1}{T} - 0.009 \cdot \log(\%Fe_t) + 0.242 \cdot log[\frac{(\%CaO)}{(\%SiO_2)}] - 1.010[\%C] - 5.235$
Tata Steel, 2013 [91]	$log(L_p) = \frac{7688}{T} + 0.042\ (\%CaO) + 1.405 \cdot log(\%Fe_t) + 0.0156(\%MgO) + 0.0092\frac{(\%MnO)}{[\%Mn]} - 6.2$

It can be seen from Table 3 that, in agreement with the experimentally established Lp-behavior, the temperature, the oxygen potential (expressed in terms of (%FeO), [%O] or [%C]) and the CaO-content of the slag are the main factors controlling dephospho-

rization. In many cases, it proved more suitable to describe Lp-behavior in the industrial process using the term (%CaO)/(%SiO_2), referred to as slag basicity, than using the (%CaO) content of the slag.[93] A major point of disagreement between laboratory- and industrial based Lp-observations is the effect of MgO: Apart from the work of Basu et al. [94], most laboratory-based Lp-investigations in the literature emphasize the positive effect of MgO on dephosphorization [4, 18, 75, 76, 85], but this is in strong contrast with industrial observations. On the contrary, the majority of industrial plant trial results indicate that MgO has either a moderate or even a strongly negative effect on dephosphorization. [10, 12, 24, 95, 96]

Some explanations for the controversial negative effect of MgO in the industrial process are given in the literature, most of which attributed the negative effect of MgO on the kinetics of dephosphorization reaction, due to its effect on viscosity.[97]

2.4 Effect of solid phases on dephosphorization potential of BOF slags

A large number of studies, which investigated the effect of solid phase precipitation on the phosphorus equilibrium reaction and, more specifically, on the phosphorus capacity of slags, are available in the literature.[10, 14, 17, 21, 28, 30-32, 34, 66, 98-120] It is, however, a notable fact that a large majority of those works were carried out at conditions relevant for hot metal dephosphorization processes: The investigated slags had a low basicity which varied in the range of 1-2, the experimental temperature was typically in the range of 1623 K-1673 K and the P_2O_5 content of the slag was higher than 5 wt%. Nevertheless, Lp-measurements in a solid phase containing slag at high temperatures in the range of 1833 K-1873 K, which are relevant for the conventional BOF process, were provided by Inoue and Suito,[113, 114]. In their work,[113, 114] the phosphorus content of the liquid iron phase in equilibrium with slag containing solid phases was measured and it was thus necessary to set the experimental temperature above the liquidus temperature of iron.

In contrast, very few works could be found which studied the effect of solid phases on the dephosphorization potential of BOF slags.[10, 118]

All of those works [10, 14, 17, 21, 28, 30-32, 34, 66, 98-120] indicated that the solid phase di-calcium silicate, 2CaO.SiO_2, further noted as C2S, plays an important role in phosphorus removal from the metal phase due to its large solubility for phosphorus in its solid form.

Inoue and Suito [114] developed an Lp-relation for slags saturated on di-calcium silicate while Kitamura and co-workers [14, 17, 99] developed a kinetic dephosphorization model under consideration of the phosphorus removal potential of the solid C2S phase.

2.4.1 Phosphorus distribution between a multi-phase-slag and liquid iron

In a series of experiments, Inoue and Suito [113, 114] investigated the phosphorus distribution in the temperature range of 1300-1600°C between the di-calcium silicate solid phase and liquid slag phase, termed Lp_{slag}, which is defined as follows:

$$Lp_{slag} = \frac{(\%P)_{C2S}}{(\%P)_{liq}} \tag{13}$$

Their findings [114, 115] indicated that the maximum Lp_{slag}, and thus the maximum enrichment of the solid phase with phosphorus, was obtained at the nose of the C2S primary phase in the CaO–SiO_2–FeO phase diagram (**Figure 5**-a). The relationship between Lp_{slag} and the $(\%FeO)_x$ content of the slag was linear and independent of the oxidation state of FeO_x. Their results were in agreement with earlier findings of Ito and Sano,[121] who carried out their experiments in the temperature range of 1623K-1723 K (**Figure 5**-b). The effect of temperature and basicity on Lp_{slag} was found to be very small and could be considered as negligible in the temperature range of 1673K-1873K.[114, 115] Later, Gao et al.[104, 105], as well as Kitamura et al. [100, 110] confirmed the positive correlation between Lp_{slag} and (%FeO) content of the liquid slag. In addition, Gao et al. [104, 105] reported that (%CaO) had a strong negative effect. However, they reported that a temperature increase from 1350°C to 1400°C had a positive effect. Pahlevani et al.[110] carried out extensive experimental investigations on the activity coefficient of P_2O_5 in the solid phase over the temperature range of 1573 K-1673 K and concluded that (%CaO) is the ruling factor affecting the enrichment. Their results indicated that the activity coefficient of P_2O_5 in the solid phase increased significantly with an increase in (P_2O_5), an increase in (%FeO) and a decrease in (%CaO) content of the liquid phase. The effect of the oxidation state of FeO_x could not be evaluated with certainty and depended on the slag composition. The addition of MgO, Al_2O_3 and MnO had a decreasing effect on the activity coefficient,[110] but their effect was very small compared to that of CaO and P_2O_5.

In a recent work, Xie et al. [119] reported that the phosphorus enrichment of the solid phase in the temperature range of 1573 K-1723 K was not affected by temperature. However, since lime dissolution is enhanced when the temperature increases, the overall effect of temperature on dephosphorization is positive. They further reported that the enrichment was enhanced by increasing the mass ratio of FeO/Fe_2O_3 in the liquid slag while basicity had the opposite effect.

In summary, it can be said that there is general agreement among the experimental investigations that the phosphorus enrichment of the solid phase is a strong function of the composition of the liquid slag phase.

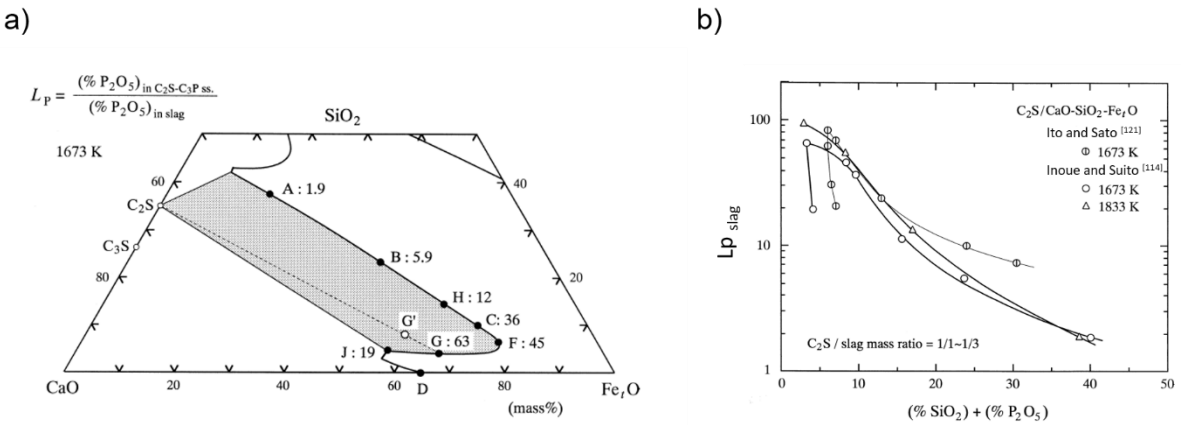

Figure 5: Measured phosphorus distribution values between solid and liquid slag reported by Inoue and Suito [114] in C2S-saturated slags: a) represented in the ternary $CaO\text{-}FeO_x\text{-}SiO_2$ system at 1673 K (1400°C) for slag compositions A-G, b) represented as a function of $(\%SiO_2) + (\%P_2O_5)$ content of the liquid slag together with the data of Ito and Sano [121]. Reprinted with permission from Ref. [114]

Inoue and Suito [114, 115] measured the phosphorus distribution values between the total multi-phase slag (containing both solid and liquid phase) and the metal phase at a temperature of 1560°C and developed the following equation to describe Lp in a C2S-saturated slag:[113]

$$Lp_{tot} = Lp_{liq}\,(1 + Lp_{slag} \cdot \frac{w_{C2S}}{w_{slag_{liq}}}) \Big/ (1 + \frac{w_{C2S}}{w_{slag_{liq}}}) \qquad (14)$$

with Lp_{liq} denoting the phosphorus distribution between the liquid slag phase and the metal phase, which was introduced in section 2.3, and Lp_{slag} denoting the phosphorus distribution between the C2S phase and the liquid slag phase, given by equation (13). The terms W_{C2S} and $W_{slag\ liq}$ denote the weight of C2S and the weight of liquid slag, in kg/ton of metal, respectively.

2.4.2 The enrichment mechanism of the solid C2S_C3P phase with phosphorus

The enrichment mechanism of the solid di-calcium silicate phase C2S with phosphorus has been studied intensively in the literature, and a large number of SEM observations with respect to the enrichment procedure are available. All of those works agree that C2S is capable of dissolving phosphorus by forming the silico-phosphate solid solution phase $2CaO.SiO_2$_$3CaO.P_2O_5$, C2S_C3P. This phase was found to be stable over the total composition and temperature range relevant to the hot metal dephosphorization process.[98, 105]. Kitamura et al. [98, 111] suggested that the enrichment of phosphorus in the solid phase is possible via 2 routes:

1. The precipitation route: The solid solution of C2S_ C3P precipitates directly from the liquid slag. This route occurs when the solid phase precipitates after phosphorus is transferred from the liquid metal to the liquid slag phase.
2. The diffusion route: In this route, phosphorus in the liquid slag phase is transferred to an already precipitated C2S solid phase, which results in the formation of the C2S_C3P phase.

Kitamura et al.[98, 111] and Inoue et al. [114] carried out a series of experiments in which they investigated the mechanism of phosphorus enrichment via both routes. The precipitation route was investigated by cooling $CaO\text{-}FeO_x\text{-}SiO_2\text{-}P_2O_5$ based slags from 1873 K to 1673 K in the experiments of Kitamura et al. [98] and from 1843 K to 1673 K in the experiments of Inoue et al.[114] In both works, the phosphorus enrichment occurred very quickly. The enrichment grade in phosphorus was very high and did not depend on the holding time nor on the cooling rate. The P_2O_5 content in the solid C2S_C3P phase reached 30 wt% in the experiments of Kitamura et al.[98] and 18 wt% in the experiments of Inoue et al. [114]. It should be noted that the initial P_2O_5 content of the slag prior to cooling was in the range of 5 wt% in both works.[98, 114]

The enrichment via the diffusion route was investigated in a large number of experimental works. Kitamura et al. [98, 111] and Yang et al. [102, 106, 107] immersed a C2S rod in a liquid CaO-FeO_x-SiO_2-P_2O_5 slag while Inoue et al.[114] immersed C2S particles with an original size of 20 to 50 µm in a liquid CaO-FeO_x-SiO_2-P_2O_5 slag as well as in liquid CaO-FeO_x-P_2O_5 slag. In all of these experiments, the formation of the C2S_C3P phase occurred on the reaction layer between the C2S phase and the liquid slag. A further point of agreement between these works is that the enrichment occurred more slowly during the diffusion route and that the amount of phosphorus dissolved in C2S_C3P was significantly lower than that dissolved during the precipitation route. Yang et al. [102, 106, 107] indicated that the enrichment of the solid phase is enhanced by an increase in temperature while an increase in the total slag basicity (CaO/SiO_2 ratio) has the opposite effect. The negative effect of a basicity increase was associated with the formation of a $3CaO.2SiO_2$ layer at the interface between the solid C2S_C3P phase and the reacting slag, which restrained the phosphorus condensation in the solid C2S_C3P phase.

Kitamura et al. [98, 111] measured P_2O_5 contents in the range of 3-13 wt% in the C2S_C3P solid phase formed at the reaction layer between the C2S rod and the CaO-FeO_x-SiO_2-P_2O_5 slag depending on the initial slag composition. Inoue et al.[114] could measure P_2O_5 values as high as 5-18 wt% depending on the original particle size. Inoue et al.[114] observed that the thickness of the C2S_C3P layer formed in the reaction layer also depended on the particle size and their distribution: Isolated particles changed completely to uniform C2S_C3P particles within 5 seconds, however, when the particles formed a cluster, only an outside rim of 5 µm changed to C2S_C3P. In both cases, the enrichment occurred within 5 seconds. A further interesting observation made by Inoue et al.[114] is the peeling-off of the phosphorus-enriched C2S_C3P layer: The C2S_C3P grains, which had a size of 5 to 25 µm were peeled off from the surface of the C2S particle shortly after their formation. The peeling-off step was considered crucial for the continuation of the enrichment of the solid phase and was only observed when the C2S particles were in contact with a CaO–FeO_x–P_2O_5 slag. However, this peeling-off was not observed when the C2S particles were in contact with a CaO–SiO_2–FeO_x–P_2O_5 slag. Finally, the authors proposed the following reaction steps

to describe the enrichment mechanism of the solid C2S_C3P phase on phosphorus via diffusion, as illustrated in **Figure 6**:

- Step I: The dissolution of CaO and SiO_2 from the surface of a $2CaO.SiO_2$ particle occurs, thus resulting in the slag composition change from slag D to slag D'.
- Step II: CaO and P_2O_5 in slag D' dissolve into $2CaO{\cdot}SiO_2$, leading to the formation of the C2S_C3P solid solution. The slag composition changes from slag D' to slag D'' with a lower P_2O_5 and CaO and a higher FeO content.
- Step III: The C2S_C3P solid solution layer starts to peel off and the peeled grains separate from the surface.

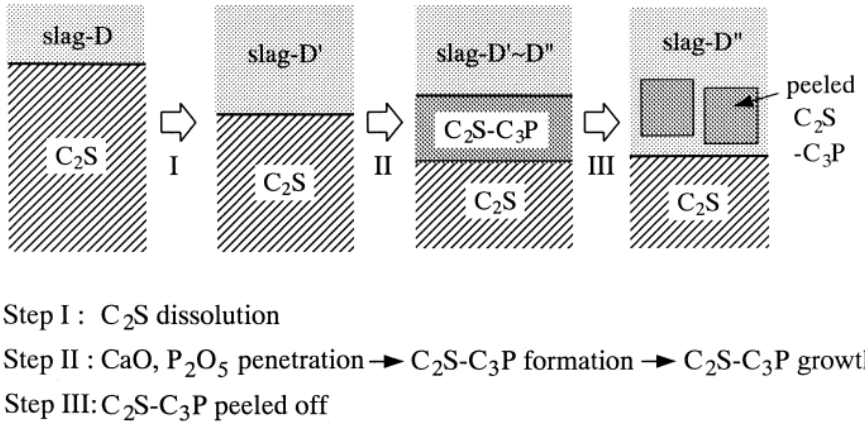

Figure 6: Schematic representation of the reaction sequence of a C2S particle after addition to a $CaO\text{-}FeO_x\text{-}SiO_2$ based slag containing 5 wt% P_2O_5 (slag-D) as illustrated by Inoue and Suito [114]. Reprinted with permission from Ref. [114]

Interestingly, Suito et al. [113] and Hamano et al. [120] observed that the phosphorus-enriched solid phase C2S_C3P is also formed via the diffusion route during the dissolution of CaO-particles in a $CaO\text{-}FeO_x\text{-}SiO_2\text{-}P_2O_5$ slag. A similar phenomenon was observed earlier by Ono et al. [122], as they reported that a solid phosphorus-containing phase, which they designated as ($CaO\text{-}SiO_2\text{-}P_2O_5$), is formed at the reaction layer between solid CaO and the surrounding slag. Yang et al.[102] emphasized that the phosphorus content in the solid C2S_C3P phase, which is formed at the interface between CaO particles and reacting slag is much higher than the phosphorus content in the solid C2S_C3P phase when formed through the addition of C2S particles to the slag.

Suito and Inoue [113] further observed that the phosphorus partition between solid and liquid slag phase, i.e., Lp_{slag}, increased drastically when stirring was applied. They concluded that stirring contributes to the removal of the C2S_C3P layer, which corresponds to step III in Figure 6 and thus to the enhancement of phosphorus enrichment in the solid phase. Despite the importance of this phenomenon, no further measurements under stirring were carried out in their work. This may be due to the fact that their investigations are relevant for the hot metal dephosphorization process, which is a process characterized by a low degree of stirring compared to the conventional BOF process.

3 Introducing the thermodynamic modeling approach

3.1 Why adopting a CALPHAD-based approach for slag modeling?

Even though there is general agreement concerning the importance of slags in controlling the progress of reactions during the oxygen refining of molten iron, their behavior under various process conditions is still not completely understood. This is due to their complex nature, in addition to the fact that they undergo large variations during the process in terms of composition, temperature, and morphology, mainly as a result of the simultaneous oxidation and reduction processes during the blow.

A deep understanding of the behavior of multi-component-steelmaking slags in terms of type, amount, structure, and composition of the phases formed, covering the relevant composition and temperature ranges for the industrial process, provides the key for enhanced process control. For example, undesirable phenomena, such as refractory wear, slopping, spitting, and skulls formation on the BOF (Basic Oxygen Furnace) top lance in the process can become avoidable. Also, better control of the final steel composition, especially in terms of C and P end values, can be achieved.

Considerable experimental efforts were made in order to establish the relevant phase diagrams with respect to basic binary and ternary oxide systems and, to some extent, also under the addition of some minor oxides and their combinations. However, due to the high costs associated with experimental investigations and at the same time, the limitations of the experimental techniques in covering the total temperature and composition range relevant to the industrial process, several thermodynamic modeling approaches were proposed to calculate the activities of the component oxides in the slag, and the distribution of elements between the metal and slag phases, such as manganese, phosphorus, and sulfur. The first slag models were structureless.[123-126] Later, structure related models were developed based on the polymer theory as applied to silicate melts.[127] Although they were successful for simple silicates, a great deal of further work was necessary for multi-component-slags.[128]

The regular solution model,[129] based on the ionic theory of slags, has found a wide application in modeling the thermodynamic behavior of steelmaking slags in terms of the calculation of oxides activities as well as important metal-slag reactions such as P-distribution and Mn-distribution.[83, 130, 131] Recently, a new modeling approach, the

ionic and molecular coexisting theory (IMCT), which considers both ionic and molecular slag nature, was introduced. [107, 117, 132-134]

The introduction of the CALPHAD (CALculation of PHAse Diagrams) methodology in the 1970s provided a consistent approach for thermodynamic modeling of complex multi-component-systems while considerably reducing the experimental effort.[135] This is due to the fact that modeling approaches developed according to the CALPHAD method have a good capability for extrapolating from assessed binary sub-systems to ternary and higher-order systems, which is necessary for application in industrial processes.[136] The availability of commercial thermodynamic computing systems, [137-140] which combine Gibbs energy minimization routines with large databases of optimized thermodynamic data of solutions and compounds, further contributed to the widespread use of the CALPHAD approach. This approach has been successfully used for the description of the state of complex multi-component-slags in general and, more particularly, for slags relevant to steelmaking applications.[141, 142] However, very few works could be found where a CALPHAD based approach was incorporated for equilibrium and non-equilibrium modeling of important metal-slag-reactions in the BOF (Basic Oxygen Furnace) process, such as dephosphorization.[49, 86, 87, 143]

The thermodynamic investigations presented in this work were carried out using a newly developed thermodynamic database. The database was developed in the scope of the European project BOF DePhos,[91] in order to investigate thermodynamic aspects of phosphorus-containing steelmaking slags in the composition, temperature, and oxygen partial pressure ranges relevant for the industrial process. The development of the thermodynamic database, further noted as the BOFdePhos thermodynamic database, was carried out by GTT technologies and Forschungszentrum Jülich [144] according to the CALPHAD-method using the thermodynamic software package FactSage ™.[137] An overview of the procedure adopted for the generation of new datasets is presented in **Figure 7**.[145]

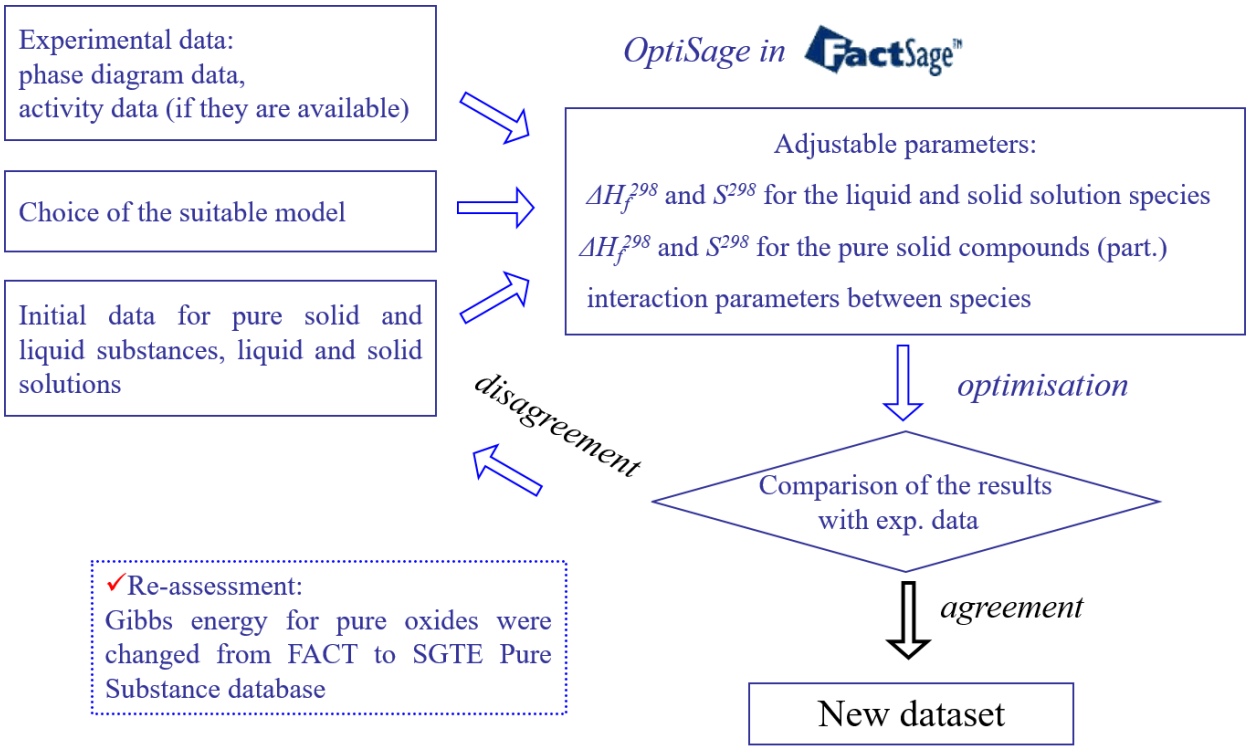

Figure 7: Generation of new thermodynamic datasets according to the CALPHAD method using FactSage. Reprinted with permission from Ref.[145]

In section 3.2, the elements, compounds, and solution phases considered in the BOF-dePhos thermodynamic database are presented. In section 3.3, the Gibbs energy modeling approach considered for the main solution phases is explained. The discussions of the particular data assessments are given elsewhere. [146, 147] The database is suitable for integration in flowsheet modeling and can thus be used for non-equilibrium modeling of industrial processes.[49, 148, 149]

3.2 Elements, compounds and solution phases

A thermodynamic database suitable for the study of multi-component-steelmaking slags has to cover at least the elementary components Fe-Mn-Ca-Ar-S-P-Si-Al-Mg-O-C. Those elements need, in turn, to be incorporated in a set of relevant phases: A gas phase, a liquid steel phase, a liquid slag phase, and a multitude of possible solids, both as solid solutions and as stoichiometric compounds. The vast majority of phases are solid solution oxides. However, since phosphorus is the most important elementary component in this work, it was important to incorporate the phosphorus-containing

solid phases. Those are the silicates, based on lime and silica, as well as the phosphates, based on lime and also containing silica. A concise summary of the major phases considered in the present thermodynamic database is given in **Table 4**.

Table 4: Overview of the major phases considered in the thermodynamic database and their phase constituents.

Phases type	Phase constituents
Gas	P, P_2O_5, N_2, O_2, CO, CO_2, SO_3.
Liquid oxide	P_2O_5 and 18 P_2O_5-containing associate species.
P-containing solid solutions	7 phosphates: M3P ($Mg_3P_2O_8$), C3P-alfa ($Ca_3P_2O_8$), C3P-beta, C2P-MT ($Ca_2P_2O_7$), M2P ($Mg_2P_2O_7$), C3M3P2 ($3CaO{\cdot}3MgO{\cdot}2P_2O_5$), CMP ($CaO{\cdot}MgO{\cdot}P_2O_5$).
	1 silico-phosphate: C2S-C3P (Ca_2SiO_4-$Ca_3P_2O_8$) described as $(Ca^{2+},Mg^{2+},Mn^{2+})_3(Ca^{2+},Va)(P^{5+},Si^{4+})_2(O^{2-})_8$
	1 silicate with limited P_2O_5 solubility: C2S-prime (Ca_2SiO_4).
Examples of non-phosphorus-containing solid solutions with end-members	Monoxide (CaO, MgO, FeO,…), Corundum (Al_2O_3, $Fe_2O_{3,...}$), Spinel (Fe_3O_4, $FeO{\cdot}Al_2O_3$, $MgO{\cdot}Al_2O_3$,…), Wollastonite ($CaSiO_3$).
Stoichiometric compounds	P, P_2O_5 and 56 phosphides, phosphates or silico-phosphates.
Liquid	Fe, P, Al, Si, Ca, Mg, Mn, S, O and C.

3.3 The Gibbs energy modeling approach

3.3.1 Liquid state

In order to answer the need for proper thermodynamic modeling of multi-component-slags, it is essential that the thermodynamic model can, on the one hand, easily be extended to describe ternary and higher-order systems and on the other is suited to describe the phase internal structure of silicate melts.

For melts containing silica, which is the case for steelmaking slags, experimental information shows that the silicate network is the basic structural feature to be considered. When adding further components into the system, this network is either strengthened (network formers) or modified (network modifiers). In addition, silicate-containing melts often exhibit miscibility gaps, which can only be described if the chosen model permits the treatment of concave parts of the Gibbs energy function. For such a situation, the Non-ideal Associate Solution Model,[150] using the Redlich-Kister polynomial for the contribution of the excess Gibbs energy is well suited.[151] For this, the Gibbs energy is calculated as:

$$G_m = \sum x_i G_i^0 + RT \sum x_i \, ln \, x_i + \sum \sum_{i<j} x_i x_j \sum_{v=0} L_{ij}^{(v)} \, (x_i - x_j)^v \qquad (15)$$

with x_i being the mole fractions of the associate species i. These result from a phase internal equilibrium based on the overall compositions of the basic oxide components such as Al_2O_3, CaO, FeO, Fe_2O_3, MgO, and SiO_2. The list of phase constituents in the present database comprises 73 species in total, such as the binary oxide species $CaSiO_3$ and $Al_6Si_2O_{13}$ or the ternary $Ca_2Si_4Al_4O_{16}$. The descriptions of all P_2O_5-containing associate species considered in the liquid oxide phase are given in **Table 5**. These complex associates permit to include the phase internal structure, i.e., the short-range ordering, in the liquid. On the other hand, the repulsive interactions which lead in composition ranges near SiO_2 to miscibility gaps can easily be incorporated in the total Gibbs energy by way of (positive) interaction terms, $L_{ij}^{(\nu)}(T)$, in the Redlich-Kister polynomial.[151] The terms $L_{ij}^{(\nu)}(T)$ relate to the interaction between associate species i and j and the integer power ν in the polynomial term $(x_i\text{-}x_j)^\nu$. Further models which can be found in the literature for modeling ternary and higher-order systems of slags are for

example the quasi-chemical model [152] as modified by Pelton and Blander [153] and the statistical thermodynamics approach from Kapoor and Frohberg [154] as modified by Gaye and Welfringer,[155] noted as the cell model.

The description of the liquid metal phase was taken from the SGTE database,[156] where the liquid metal is treated as a substitutional solution, with the exception of the Fe-P system, which has been assessed in the present work.

Table 5: A list of all-P_2O_5 containing liquid species in the thermodynamic database

System	Associate species with P_2O_5	Description MeO_x:P_2O_5
SiO_2-P_2O_5	SiP_2O_7*2/3	1:1
Me_2O_3-P_2O_5 with Me=Al, Fe, Mn	$AlPO_4$, $FePO_4$, $MnPO_4$	1:1
MeO-P_2O_5 with Me=Ca, Fe, Mg, Mn	$Me_3P_2O_8$*2/5, $Me_2P_2O_7$*1/2, MeP_2O_6*2/3	3:1, 2:1, 1:1
Al_2O_3-MgO-P_2O_5	$P_2Al_2Mg_3O_{11}$*1/7	1:3:1

3.3.2 Solid state

For modeling the solid phases contained in the database, two cases are distinguished: The phase is stoichiometric, or the phase has a homogeneity range, i.e., is a solid solution. The former case (phase is stoichiometric) leads to Gibbs energies, which are solely temperature-dependent and can usually be treated with the following equation:

$$G°(T) = A + B\,T + C\,T\,ln(T) + DT^2 + E\,T^3 + F\,T^{-1} \qquad (16)$$

The parameters C to F in (16) relate directly to the heat capacity of the compound. The parameter A contains a contribution from the enthalpy of formation and from the heat capacity while the parameter B contains in a similar form a contribution from the absolute entropy and from the heat capacity.

The latter case (phase has a homogeneity range) needs to take into account the spatial distribution of the constituents of the phase. That can be achieved by using the multi-sublattice approach, which is also known by the name of Compound Energy Formalism (CEF).[157] The name implies that the major contribution to the Gibbs energy comes from the end-members of the composition range, i.e., particular compounds, which result from the set of all combinations of constituents which are situated on the sublattices chosen for the model. This is demonstrated for a very important example in the present work, namely the phase $2CaO.SiO_2$-$3CaO.P_2O_5$ further noted as C2S-C3P. This phase has been modeled as $(Ca^{2+},Mg^{2+},Mn^{2+})_3(Ca^{2+},Va)(P^{5+},Si^{4+})_2(O^{2-})_8$. [146] This model results in 3*2*2*1=12 end-members, two of which are:

- the dicalcium-silicate $(Ca^{2+})_3(Ca^{2+})(Si^{4+})_2(O^{2-})_8$
- the tricalcium-phosphate $(Ca^{2+})_3(Va)(P^{5+})_2(O^{2-})_8$

The others permit the inclusion of the known small amounts of Mg and Mn in the phase composition. The molar Gibbs energy of this phase was expressed using the compound energy formalism generalized by Sundman et al. [157, 158] as follows:

$$G_m = \sum_{i=1}^{n}\sum_{j=1}^{n}\sum_{k=1}^{n} y_i^I y_j^{II} y_k^{III}\ {}^0G_{i:j:k} + RT\sum_{i=1}^{n} y_i^I \ln y_i^I + RT\sum_{j=1}^{n} y_j^{II} \ln y_j^{II} + RT\sum_{k=1}^{n} y_k^{III} \ln y_k^{III} \qquad (17)$$

The ${}^oG_{i:j:k}$ – terms are the Gibbs energies of the real or hypothetical compounds where the first, second, and third sublattices are occupied by appropriate components *i*, *j,* and *k* as shown above. The oxygen anions are placed on the fourth sublattice ($y_{O^{2-}}^{IV} = 1$). In (17), the variables y_i^N are the so-called site fractions of the sublattice N constituents i.

3.4 Assessment of unary and binary phosphorus-containing systems

Since phosphorus is the elementary component of major importance in the present work, it was necessary to establish the data for phosphorus itself and for P_2O_5, the major oxide containing phosphorus. The data for phosphorus are given in the SGTE

Pure Substance database.[156] However, until recently, the data for P_2O_5 have essentially been taken from standard literature such as JANAF thermochemical tables without further questioning.[159] In 2012, Jung and Hudon [160] have undertaken the work to compile all experimental information available [161-164] and to assess them into a self-consistent set of data for all phases of P_2O_5. Their results indicate that three different solid phases (o and o', both orthorhombic and h, hexagonal) need to be treated, two of which are meta-stable (o and h). In addition, they also found that the liquid state can form a meta-stable and a stable state. For the present database, only the values of the stable orthorhombic (o') and the stable liquid phase ($L_{o'}$) were used.

During the development of the database, a major emphasis was given to the various sub-systems, which contained phosphorus. The major role in this context plays the sub-system Fe-Ca-P-O. Thus, the corresponding unary, binary, and quasi-binary sub-systems were critically assessed, and the relevant Gibbs energy parameters (Figure 7) were optimized. Here, data are given in the literature concerning the Fe-P binary system (**Figure 8**), the $CaO-P_2O_5$ quasi-binary system (**Figure 9**), and the $FeO-P_2O_5$ quasi-binary system (**Figure 10**). It can be seen that the most relevant binary sub-systems of the Fe-Ca-P-O system calculated from the present database are in a very good agreement with available experimental data.

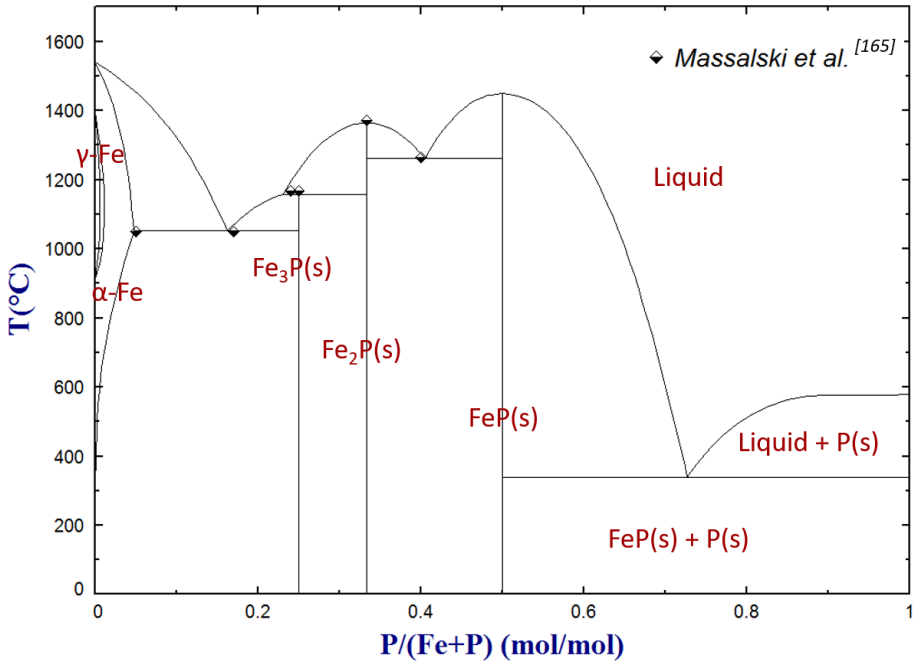

Figure 8: The binary system Fe-P calculated from the present database and compared to experimental data selected from the work of Massalski et al. [165]

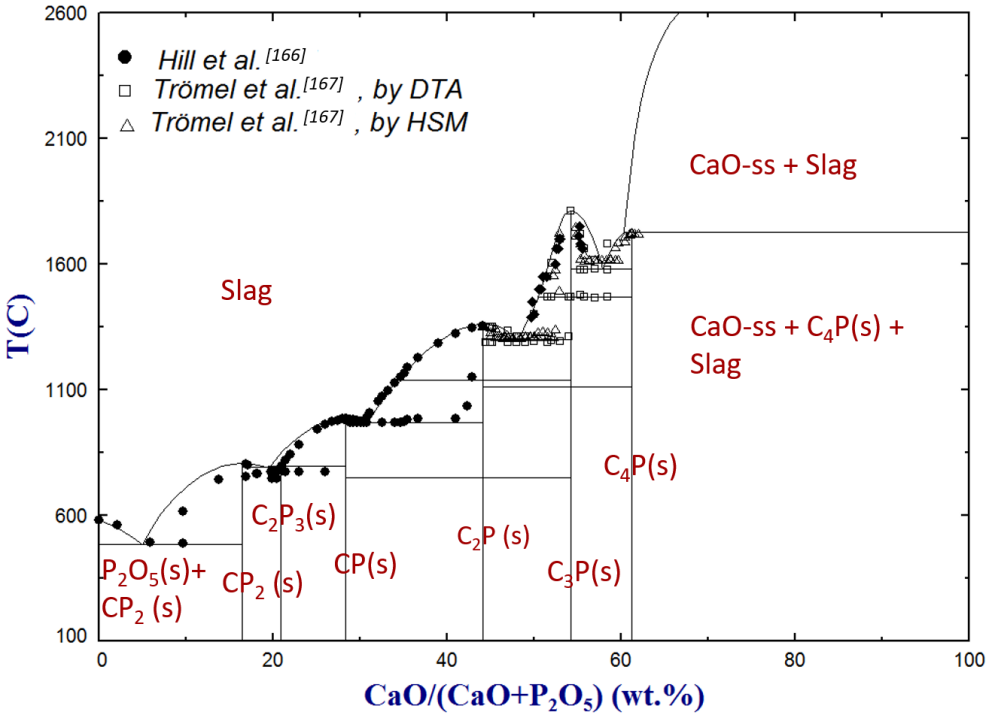

Figure 9: The assessment of the CaO-P_2O_5 binary subsystem based on experimental data of Hill et al.[166] and Trömel et al.[167] C denotes CaO, and P denotes P_2O_5.

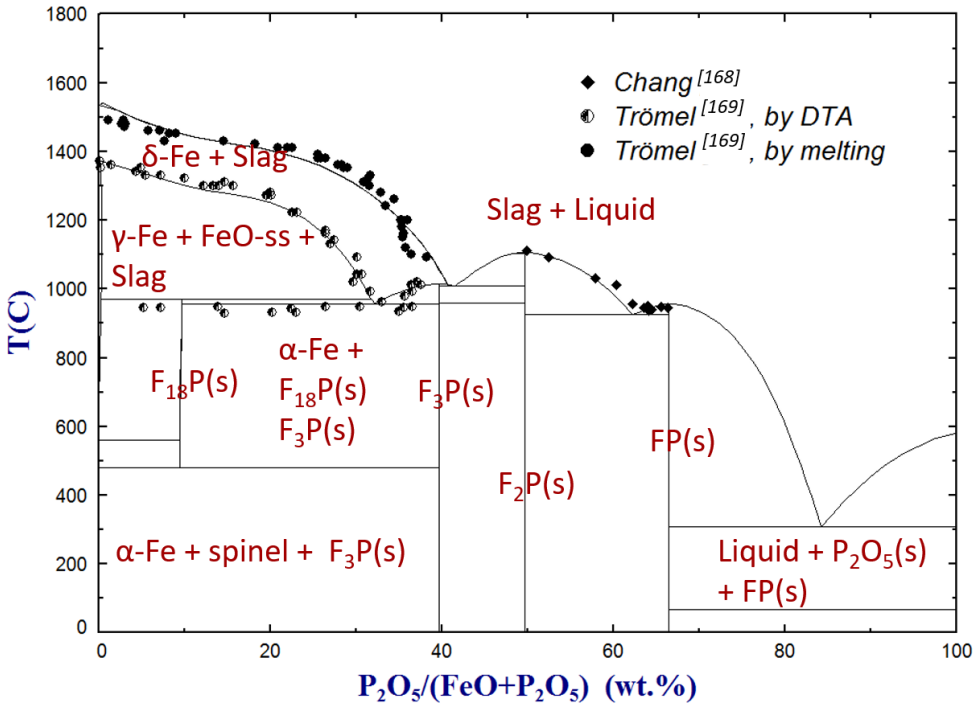

Figure 10: The assessment of the FeO-P_2O_5 pseudo-binary subsystem in equilibrium with metallic Fe based on data of Chang [168] and Trömel et al.[169] F denotes FeO, and P denotes P_2O_5.

3.5 Specification of the oxygen potential state of the slag in the present work

As a result of the oxygen blowing process, considerable amounts of FeO_x are generated by oxidation of Fe from the bath. Thus, the ternary oxide systems CaO-FeO_x-P_2O_5 and CaO-FeO_x-SiO_2 are the basic oxide systems both for high and low P refining processes. In order to study the equilibrium state of FeO_x-containing systems, it is necessary to specify the oxidation state of FeO_x, for example, by setting the ferric to ferrous ratio (Fe^{3+}/Fe^{2+}) or the oxygen partial pressure of the gas phase, further denoted as $p(O_2)$.

During the BOF process, high purity oxygen gas is blown at supersonic speed at the liquid iron surface. A slag is formed above the liquid bath, and its bottom is then in contact with the liquid iron phase. According to Schürmann et al.,[170] the $p(O_2)$ set on the slag-gas-boundary can be considered as 1 atm while $p(O_2)$ on the slag-liquid Fe boundary can be approximated as 10^{-8} atm. As a result, the gradient of $p(O_2)$ throughout the slag layer is expected to be very high. However, at the beginning of the blow, the liquid iron phase, denoted as hot metal, has a high carbon content up to the saturation limit. The carbon is later removed by oxidation throughout the blow and a gas phase with a high CO/CO_2 ratio, typically 90/10 vol% is formed. For a temperature of 1873 K (1600°C), a $p(O_2)$ value of $10^{-8.7}$ atm was calculated for a CO/CO_2 gas containing 90 vol% CO (**Figure 11**) by the „equilibrium module“ of the software FactSage™ 7.1,[137] using the BOFdePhos thermodynamic database. Thus, in case the gas phase in the BOF process has a CO-content of 90 vol%, the $p(O_2)$ value on top of slag (estimated as $10^{-8.7}$ atm according to the calculations) would be in the same range as that at the bottom of the slag (equals 10^{-8} atm when the slag is in contact with liquid Fe according to Schürmann et al.[170]). In such a case, the $p(O_2)$ gradient throughout the slag will not be high.

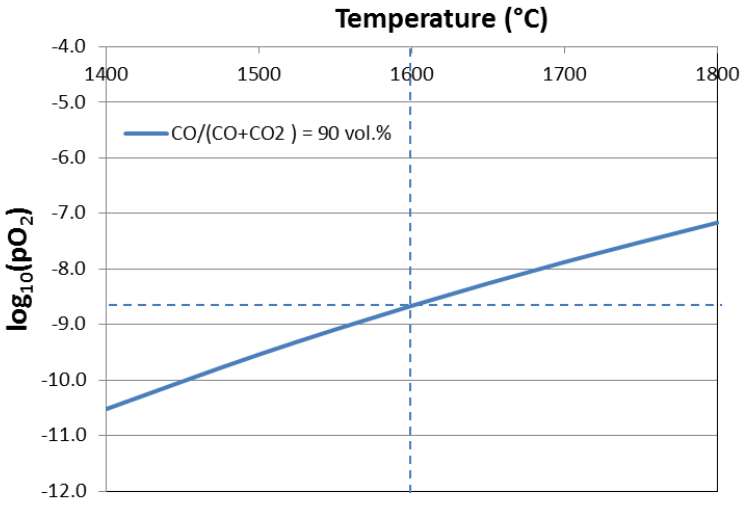

Figure 11: Calculated $p(O_2)$-temperature curve in a CO-CO_2 gas mixture with a CO-content of 90 vol%.

Considering the above analysis of the state of $p(O_2)$ in BOF slags, it can be concluded that a $p(O_2)$ range as wide as [10^{-8}- 1 atm] is relevant for the study of the state of BOF slags. Given the large $p(O_2)$ range, it becomes necessary to clarify the influence of $p(O_2)$ on the internal equilibrium of FeO_x-containing systems.

The $p(O_2)$ set in the experimental works which investigated the equilibrium state of oxide systems relevant to the BOF process ranged from equilibrium with metallic Fe to atmospheric pressure. A large majority of experimental works were carried out at a low $p(O_2)$, by equilibrating the system with metallic Fe. It can be seen from **Figure 12** that $p(O_2)$ values are lowest when the slag is in equilibrium with liquid or solid Fe, depending on temperature. From the diagram, it can be concluded that $p(O_2)$ ranges between 10^{-10} atm and 10^{-7} atm when the temperature is in the range of 1683 K (1400°C) to 1973 K (1700°C). The corresponding Fe_2O_3 content in such a case, which can be read based on the oxygen isobars in the FeO-Fe_2O_3-temperature system (**Figure 13**) is lower than 10 wt%. The case where the system is equilibrated with metallic Fe will be denoted further as the “reduced $p(O_2)$” case.

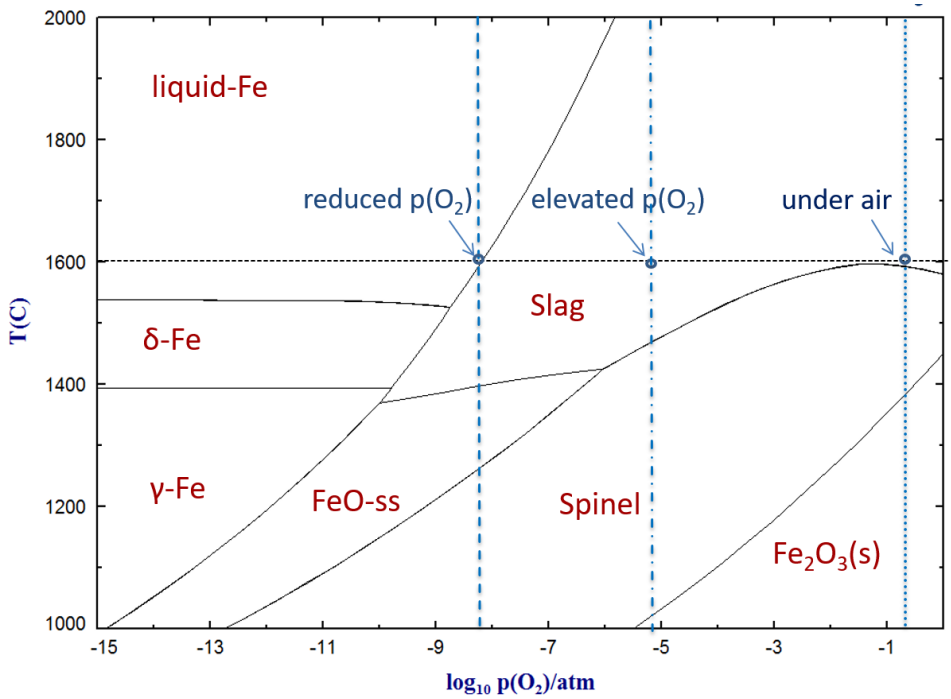

Figure 12: Fe-O_2-temperature diagram calculated using the BOFdePhos thermodynamic database.

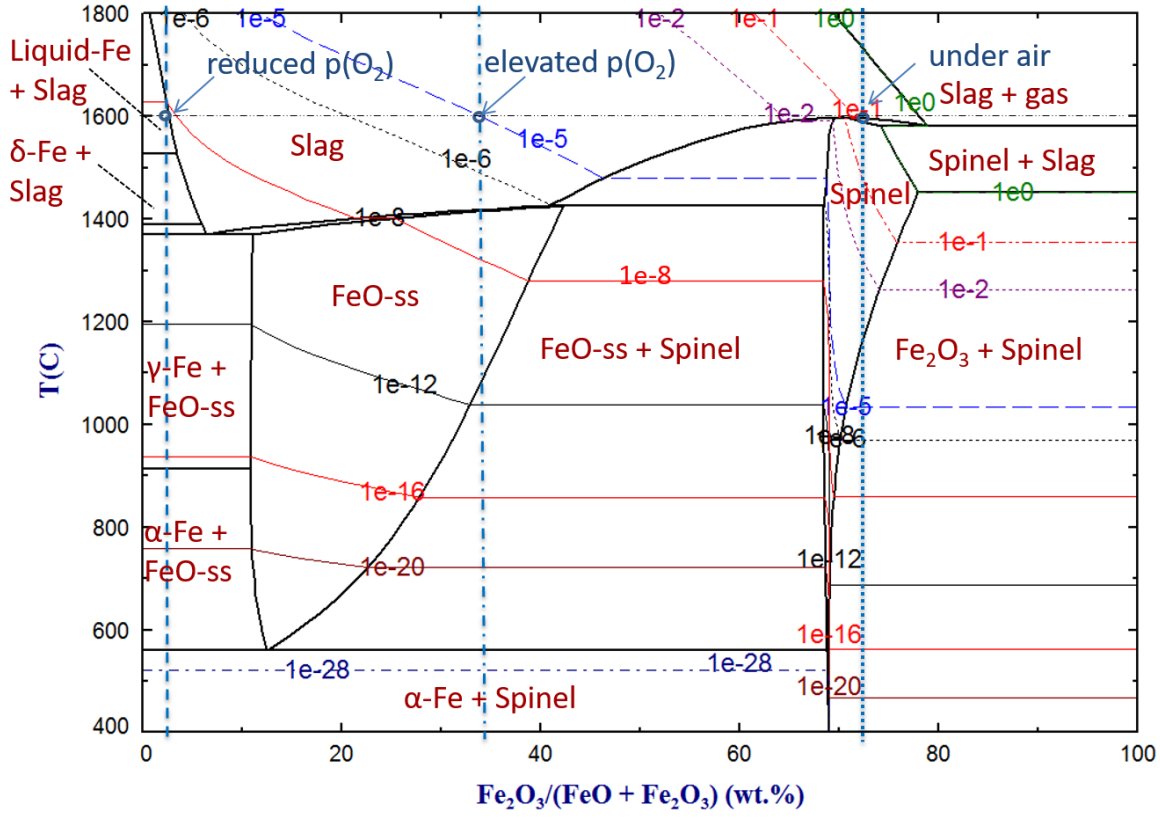

Figure 13: FeO-Fe_2O_3-temperature diagram with oxygen isobars (log(pO_2), atm) calculated using the BOFdePhos thermodynamic database.

Further experimental works are available where an equilibration with a gas phase under a given $p(O_2)$ was made. A large majority of those works were provided by the former IRSID institute, now Arcelor Mittal Maizières, where a $p(O_2)$ value of 10^{-5} atm was set in several experiments. In such a case, the oxidation state of FeO_x will be higher than that in the case of equilibrium with metallic iron (Figure 12). The Fe_2O_3/FeO weight ratio corresponding to a $p(O_2)$ value of 10^{-5} atm and a temperature of 1873 K (1600°C) can be read as 34/66 (in wt%). The cases, where $p(O_2)$ was set as 10^{-5} atm, will be further on designated as the "elevated $p(O_2)$ case". Riboud and coworkers (within IRSID) justified this choice of $p(O_2)$ by the fact that the ferric to ferrous ratio measured in some industrial samples was in the same range of that measured in corresponding laboratory slags when they were in equilibrium with a gas phase at a $p(O_2)$ value of 10^{-5} atm and a temperature of 1873 K (1600°C).[171-173] Unfortunately, despite referring to those samples on several occasions, no details about the plant trials in terms of procedure and sample analysis were published, according to the author's best knowledge.

Further works are available where the oxide systems were investigated under air, that is, at a $p(O_2)$ value of 0.21 atm. This is generally the highest $p(O_2)$ that could be found in related laboratory experiments and will be further denoted as the "under air" case. It can be seen from Figure 12 and Figure 13 that under such conditions, the spinel phase (Fe_3O_4=FeO.Fe_2O_3) is stable below 1873 K (1600°C) for pure FeO_x slags. It can be thus concluded that experimental works for FeO_x containing slags which are carried out below or exactly at a temperature of 1873 K (1600°C) are associated with a high risk of spinel phase precipitation. The Fe_2O_3/FeO weight ratio corresponding to a $p(O_2)$ value of 0.21 atm and a temperature of 1873 K (1600°C) can be read as 73/27.

An overview of the designation of the different $p(O_2)$ cases considered within the present work is presented in **Table 6**.

Table 6: The designation considered for setting the oxidation state of FeO_x-containing oxide systems in the present work.

Designation	$p(O_2)$	Description	Fe_2O_3/FeO (wt%) at 1873 K
Reduced $p(O_2)$	$<10^{-8}$ atm	Equilibration with liquid or solid iron.	3/97
Elevated $p(O_2)$	$\approx10^{-5}$ atm	Equilibrium with a gas phase such as CO-CO_2, H_2-H_2O or H_2-CO_2 mixtures occasionally containing Ar.	34/66
Under air	≈0.21 atm	High oxidation state. If T < 1873 K, the spinel phase is formed.	73/27

Finally, it should be noted that the Fe_2O_3/FeO values given in Table 6 are only true for pure FeO_x slags. Nevertheless, it can be safely considered that for a constant temperature and system composition, the oxidation state of FeO_x in a multi-component oxide will have a similar dependence on $p(O_2)$ as that for the pure Fe-O system. With an increase in $p(O_2)$, the Fe_2O_3/FeO ratio increases and the lowest oxidation state of FeO_x in the system is set when the system is in equilibrium with metallic iron.

4 Study of the oxide systems relevant for high phosphorus slags

The ternary oxide system CaO-FeO_x-P_2O_5, as well as the quaternary CaO-FeO_x-P_2O_5-SiO_2, are the key-systems for modeling the behavior of phosphorus during the refining of P-containing hot metal. Also, this is the basic system of the so-called “Thomas-slags”, resulting from oxygen refining of high phosphorus hot metal (also labeled as Thomas-Hot-Metal) in the 1960s and 1970s, for which the so-called LD-AC or OLP processes were used.[53, 172-175] Since the initial phosphorus content of the hot metal in such processes was higher than 1 wt%, the final P_2O_5 contents in slags typically ranged between 10-20 wt%.

Recently, increased attention has been drawn again to the high phosphorus system due to the expected increase in the phosphorus content of iron ores and, subsequently, in the P_2O_5 contents of the final slags.[17, 21] It was reported that when the phosphorus content of the hot metal is equal to 0.3 wt % or higher (which would be the case when high phosphorus iron ores are used [17]), the P_2O_5 content of the slag will be higher than 10 wt%.[21] For a proper evaluation of the state of high phosphorus industrial slags, it is thus important to study the state of the CaO-FeO_x-P_2O_5 oxide system as well as the state of the quaternary CaO-FeO_x-P_2O_5-SiO_2 oxide system in the composition, temperature, and $p(O_2)$ range relevant for the industrial process.

4.1 Discussion of the quasi-ternary system CaO-FeO_x-P_2O_5

Comprehensive sets of experimental data for this system at reduced $p(O_2)$, that is, in contact with metallic iron (Table 6) and at a temperature of 1873 K (1600°C) were given by Trömel et al. and Knüppel et al.[176-178]. **Figure 14** shows the calculated phase boundaries at 1873 K (1600°C) together with the experimental data. Since the experiments were carried out in equilibrium with liquid Fe, all phase regions in Figure 14 contained liquid Fe. It should be noted that in the calculations, the liquid-Fe phase is treated as a solution, i.e., it contains the equilibrium amounts of Ca, P, and O dissolved in it.

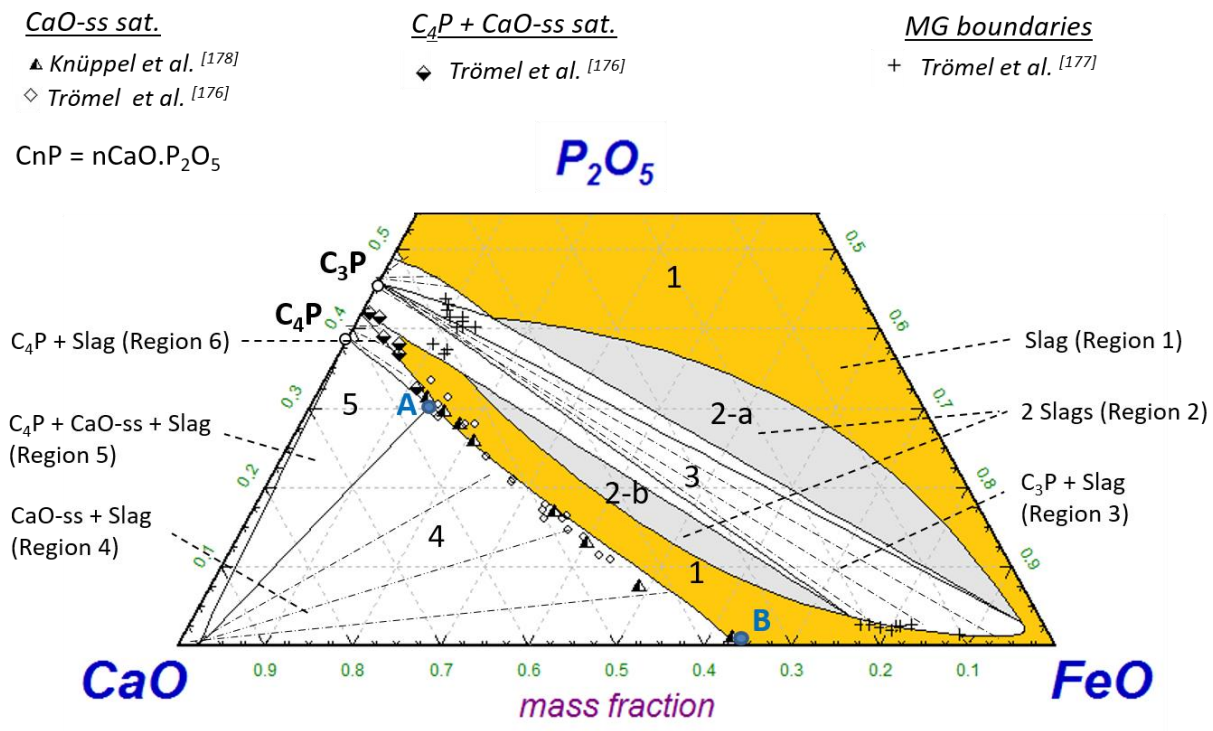

Figure 14: Calculated phase boundaries for the system $CaO\text{-}FeO_x\text{-}P_2O_5$ at T = 1873 K (1600° C) and reduced $p(O_2)$ and comparison with available experimental works from the literature.[176-178]

It can be seen from Figure 14 that the system exhibits a notable feature, which is the presence of a wide lens-shaped miscibility gap (region 2-a and region 2-b), which is cut-off by the precipitation region of the $3CaO.P_2O_5$ solid compound, further noted as C3P (region 3). As a result, 2 parts of the miscibility gap region exist, a lower part, which is rich in CaO (region 2-b), and an upper part, which is low in CaO (region 2-a). In the industrial process, lime saturation of the slag is strived for, and thus, the final slags are high in CaO while their P_2O_5 contents are usually lower than 25 wt%. Thus, only the CaO-rich part of the system is relevant for industrial applications. Correspondingly, it can be seen that most experimental data available on this system focused on the evaluation of the CaO-rich part of the system, especially with regards to the characterization of the lime saturation line (phase boundary between region 1 and region 4). This phase boundary is of utmost importance for the industrial process, and is generally considered as the target slag composition in order to achieve optimal dephosphorization results. Also, the lime saturation line defines the thermodynamic limit as well as the driving force for lime dissolution. It should be noted that the

designation “CaO-ss” indicates the small solubility of FeO in the CaO-based solid solution.

Further important phase boundaries for which experimental data were available are:

- Region 2-a: The boundary liquid slag-upper part of the miscibility gap.
- Region 2-b: The boundary liquid slag- lower part of the miscibility gap.
- Region 5: The (triangular) three-phase region between liquid slag-CaO-ss-C4P. The liquid slag composition in this region, at a constant temperature, remains invariant with respect to changes in the system composition, marked by “point A”.
- Region 6: The boundary liquid slag-$4CaO.P_2O_5$ solid compound, further noted as C4P.

In all cases, the agreement between the calculated phase boundaries and the experimental points can be considered as good.

4.1.1 Effect of $p(O_2)$

Experimental data on the behavior of the system at elevated $p(O_2)$ were provided by Drewes and Olette,[179] while Schwerdtfeger and Turkdogan [180] provided data on the behavior of the system “under air”. **Figure 15** shows the calculated phase boundaries at elevated $p(O_2)$ together with the aforementioned experimental data. [179, 180] For the sake of comparison, the calculated system boundaries at reduced $p(O_2)$ are included in the phase diagram where they are distinguished by a dashed line.

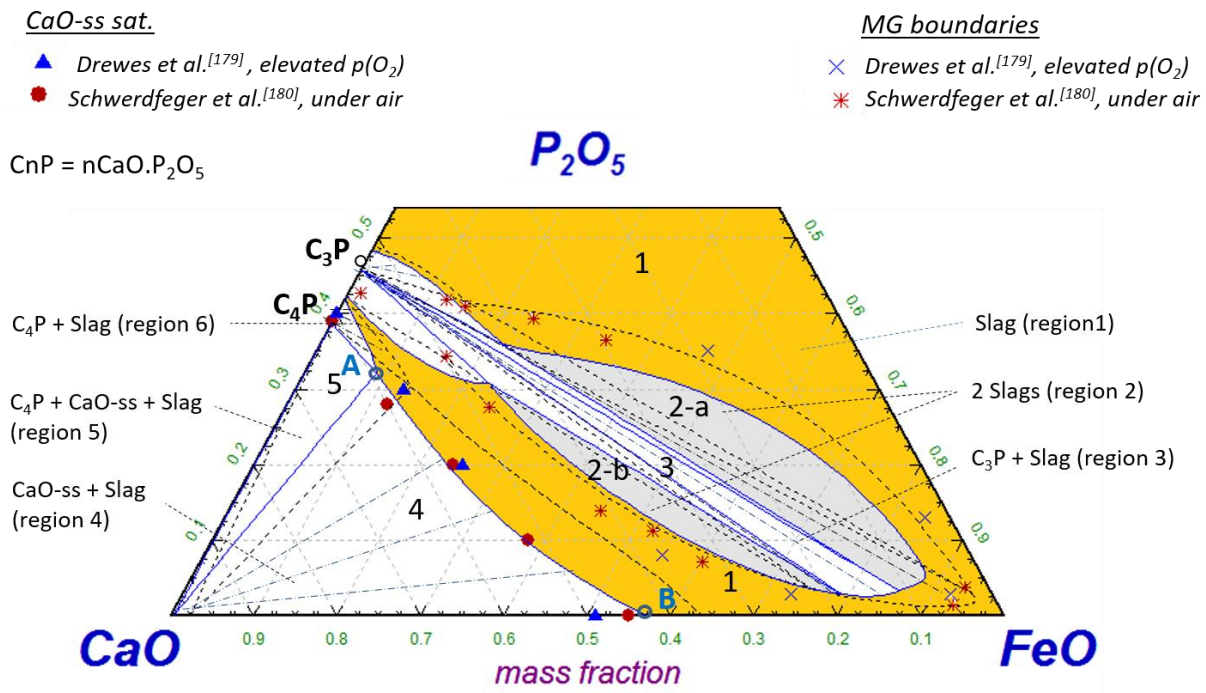

Figure 15: Effect of $p(O_2)$ on the phase boundaries of the CaO-FeO_x-P_2O_5 system at a temperature of 1873 K (1600°C): Full lines represent the elevated $p(O_2)$ case whereas the dashed lines represent the reduced $p(O_2)$ case and comparison with experimental data.[179, 180] The original publication of Schwerdfeger and Turkdogan [180] presented the lime saturation line with no specification of the experimental data points: The data points presented in the phase diagram were selected in the present work from the original lime saturation line.

It can be seen from Figure 15 that an increase in $p(O_2)$ and thus in the ferric to ferrous ratio in the slag, results in a significant increase in lime solubility, noted by a shift of the lime saturation line (A-B) to higher CaO-contents compared to the reduced $p(O_2)$ case. The solubility of CaO in the slag increases by about 3-8 wt%, depending on its FeO_x content. On the other hand, the effect of $p(O_2)$ on the lower part of the miscibility gap (region 2-b) is very small and can be considered as negligible. As a result, an overall expansion of the liquid slag region in the CaO-rich part of the system occurs.

The increase in $p(O_2)$ results furthermore in a significant shrinkage of the upper part of the miscibility gap (region 2-a) in favor of more liquid slag (region 1). Also, the “nose” of the miscibility gap region marking the limiting point with the highest FeO content, shifted slightly away from the FeO-corner. Overall, the miscibility gap region becomes smaller in favor of more liquid slag. However, the experimental data on the upper

boundary of the miscibility gap at elevated $p(O_2)$ as well as under air are consistent with the system boundaries at reduced $p(O_2)$.[179, 180] This means that the experimental findings of Drewes and Olette,[179] and well as of Schwerdtfeger and Turkdogan [180] suggest that the miscibility gap is not sensitive to $p(O_2)$, which is in disagreement with the behavior calculated using the present thermodynamic database BOFdePhos. Since only the CaO-rich part of the system is relevant for the industrial process, no further work was undertaken to clarify the discrepancy between the calculations and the experimental data with respect to the upper boundary of the miscibility gap. However, for studies focusing on this part of the system, both the experimental data and the calculated behavior should be used with precaution. In such a situation, it is highly recommended to carry out further experimental evaluations under variations of $p(O_2)$ on this part of the system.

4.1.2 Effect of temperature

During oxygen refining of high phosphorus hot metal, the temperature of the melt has a large variation range, typically between 1573K (1300°C) and 1973 K (1700°C).[174, 175, 181] It is thus necessary to study the effect of temperature on the system to evaluate the state of industrial slags during a large part of the blowing process. **Figure 16**-a) and -b) show the calculated lime saturation line at 3 different temperatures: 1773 K (1500°C), 1873 K (1600°C) and 1973 K (1700°C) at reduced and elevated $p(O_2)$ respectively.

It can be seen from Figure 16 that the effect of temperature on the CaO-saturation line is very small and can be considered as negligible, especially at elevated $p(O_2)$ (Figure 16-b). The effect of temperature on the 3-phase region, containing liquid slag, CaO-ss and C4P (region 5 in Figure 14), is however considerable: With an increase in temperature from 1773 K (1500°C) to 1973 K (1700°C), the point denoting the double saturation with CaO-ss and C4P for the reduced $p(O_2)$ case shifts from point A, with an FeO_x-content of 25 wt% to point A”, with a FeO_x-content of 2.5 wt%. As a result, the single-phase CaO-ss saturation region (region 4) expands considerably over the double saturation region with CaO-ss and C4P (region 5) when the temperature increases. This expansion is more pronounced in case of reduced $p(O_2)$ than in the case of elevated $p(O_2)$.

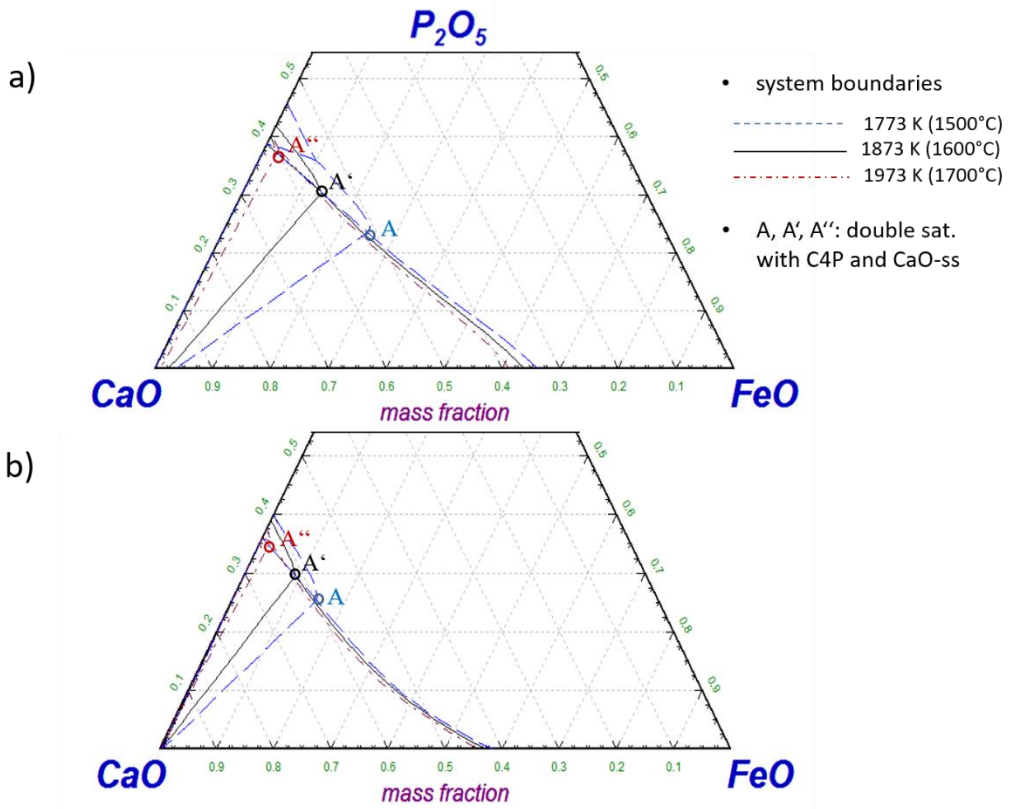

Figure 16: Effect of temperature variation on the lime saturation line of the CaO-FeO_x-P_2O_5 oxide system at a) reduced p(O_2) b) elevated p(O_2)

Finally, equation (18) and equation (19) were derived for the determination of the CaO-saturation values of the slag in case of a single-phase CaO-ss saturation or a double saturation with CaO-ss and C4P for the reduced and elevated p(O_2) cases respectively:

$$(\%CaO)sat._{reduced\ p(O_2),1873K} = -0.3746\ (\%FeO_x) + 61.018 \quad (18)$$

$$(\%CaO)sat._{elevated\ p(O_2),1873K} = -0.0046\ (\%FeO_x)^2 - 0.0401(\%FeO_x) + 59.674 \quad (19)$$

Equation (18) and equation (19) correspond to the (%CaO)-content of slags situated along “line A-B” in Figure 14 and Figure 15, respectively. Since a temperature variation in the range of 1773K (1500°C) to 1973K (1700°C) has no considerable effect on the lime saturation line, equations (13) and (19) are applicable in this temperature range. However, the position of the 3 phase point (A, A’ and A’’ in Figure 16) is temperature-

dependent and shifts to lower FeO_x contents when the temperature increases. The $(\%FeO)_x$ content of the system, corresponding to the 3 phase point (A, A' and A'' in Figure 9) above which the slag is saturated with single-phase CaO-ss, will be further noted as $(\%FeO)_{limit}$. The dependence of $(\%FeO)_{limit}$ on the temperature in case of reduced and elevated $p(O_2)$ can be described by equation (20) and equation (21) respectively:

$$(\%FeO)_{limit,reduced\ p(o_2)} = -0.113\,T + 225.27 \quad (20)$$

$$(\%FeO)_{limit,elevated\ p(o_2)} = -0.0629\,T + 125.97 \quad (21)$$

4.1.3 Consequences for the industrial process

The study of the effect of $p(O_2)$ on the CaO-FeO_x-P_2O_5 system indicated that an increase in $p(O_2)$ results in a significant increase in lime solubility and an overall expansion of the liquid slag region in the CaO-rich part of the system. For the industrial process, this implies the following:

- In case a purely liquid slag is the objective, an increase in $p(O_2)$ and thus in the ferric to ferrous ratio in the slag would provide more flexibility in terms of variation of slag composition while remaining within the liquid slag region.
- If lime saturation is the objective, more lime addition would be required than in the case of reduced $p(O_2)$. At the same time, the driving force for lime dissolution increases, which will accelerate the dissolution process.

As already mentioned, with increasing $p(O_2)$ and thus the ferric to ferrous ratio, the solubility of slag for CaO increases by about 3-8 wt%, while the temperature has a negligible effect. On the industrial scale, this means that for the same slag composition, increasing the ferric to ferrous ratio in the slag is more effective than increasing the slag temperature for enhancing lime dissolution. Another consequence of the increase in lime saturation limit is the avoidance of CaO-ss precipitations. Excessive CaO-ss precipitations increase the slag viscosity and reduce the interfacial area between the liquid and the solid phases of the slag.

4.2 Quaternary system CaO-FeO_x-P_2O_5-SiO_2*

As already mentioned, the ternary system is the basic system for high phosphorus slags. However, the high phosphorus hot metal contains silicon with an initial content in the range of 0.1 - 0.7 wt%,[174] which oxidizes and forms SiO_2 during the BOF process. The SiO_2 content of final slags is low and lies in the range of 4-10 wt%.[172, 178, 182, 183] However, the SiO_2 content of the slag during the process attains higher values and may reach a content of 15 wt%.[175, 183] Such a situation occurs during the main decarburization phase, where the rate of decarburization reaction is very high. The FeO_x contained in the slag at this stage is reduced by carbon to its lowest levels, leading to an increase in the CaO- and SiO_2-content of the slag. Thus, in order to assess the state of industrial high phosphorus slags during the entire process, it is necessary to study the effect of SiO_2 addition on the system in the range of 5-15 wt%.

In this section, the quaternary system CaO-FeO_x-P_2O_5-SiO_2* is investigated using the BOFdePhos thermodynamic database in the composition, temperature, and p(O_2) range relevant for the industrial process.

4.2.1 Effect of SiO_2

The calculated phase boundaries of the system CaO-FeO_x-P_2O_5-SiO_2* at 5 wt% SiO_2 are presented in **Figure 17**-b) while Figure 17-a) shows the phase boundaries of the SiO_2-free system, which has been discussed in section 4.1. Both diagrams were calculated at a temperature of 1873 K (1600°C) and for a reduced p(O_2) state.

It can be seen from Figure 17 that the addition of SiO_2, with a content as low as 5 wt%, has a tremendous effect on the system in terms of a considerable modification in the phase boundaries as well as in the type of solid phase precipitates:

- The regions which were saturated with phosphates (the $3CaO.P_2O_5$ solid compound, further noted as C3P, and the $4CaO.P_2O_5$ solid compound, further noted as C4P) in the SiO_2-free system ((region 3) and (region 5) in Figure 17-a) become saturated with the silico-phosphate solid phase, $2CaO.SiO_2$-$3CaO.P_2O_5$, further noted as C2S_C3P. Only one region (region 5') still contains a phosphate phase, the C4P phase.

- The single-phase CaO-ss saturation region (region (4) in the SiO_2 free system), further noted as lime-only saturation region, is no longer present in the system. This region is now replaced by the double phase saturation with CaO-ss and C2S_C3P (region 4'). This means that when SiO_2 is present with a content equals or higher than 5 wt%, a lime only saturation of the slag is no longer possible and is always coupled by additional precipitation of the C2S_C3P phase.

- The lower part of the miscibility gap (region 2-b) in the SiO_2-free system no longer exists. This is also the case for the liquid slag region, which was situated between the lower part of the miscibility gap (region 2-b) and the lime saturation region (region 4). This region is generally considered as the target slag zone for the industrial process.[174] It can be seen that the C2S_C3P saturation regions ((region 3') and (region 4)) replace both regions when SiO_2 is added to the system.
- Another marking effect of SiO_2 addition on the system is the fact that a purely liquid slag region is now stable only in the low CaO-part of the system, which is not relevant for the industrial process. Slags with CaO-content equal or higher than 40 wt% are thus expected to be in a heterogeneous state and with the C2S_C3P phase as the dominant solid phase. This is in accordance with observations of Koch and Fix, [184], who noted that a purely liquid slag could no longer be found in the CaO-rich part of the system when the SiO_2 content reached a critical value, which ranged between 2 and 3.2 wt%. The liquid slag part of a heterogenous slag contained in (region 3') or (region 4') has a FeO content higher than 50 wt%, a CaO-content, and a P_2O_5 content lower than 5 wt%. It should be noted that a high FeO activity, a high CaO-activity, and a low P_2O_5 activity in the slag are optimal thermodynamic conditions for hot metal and steel dephosphorization.

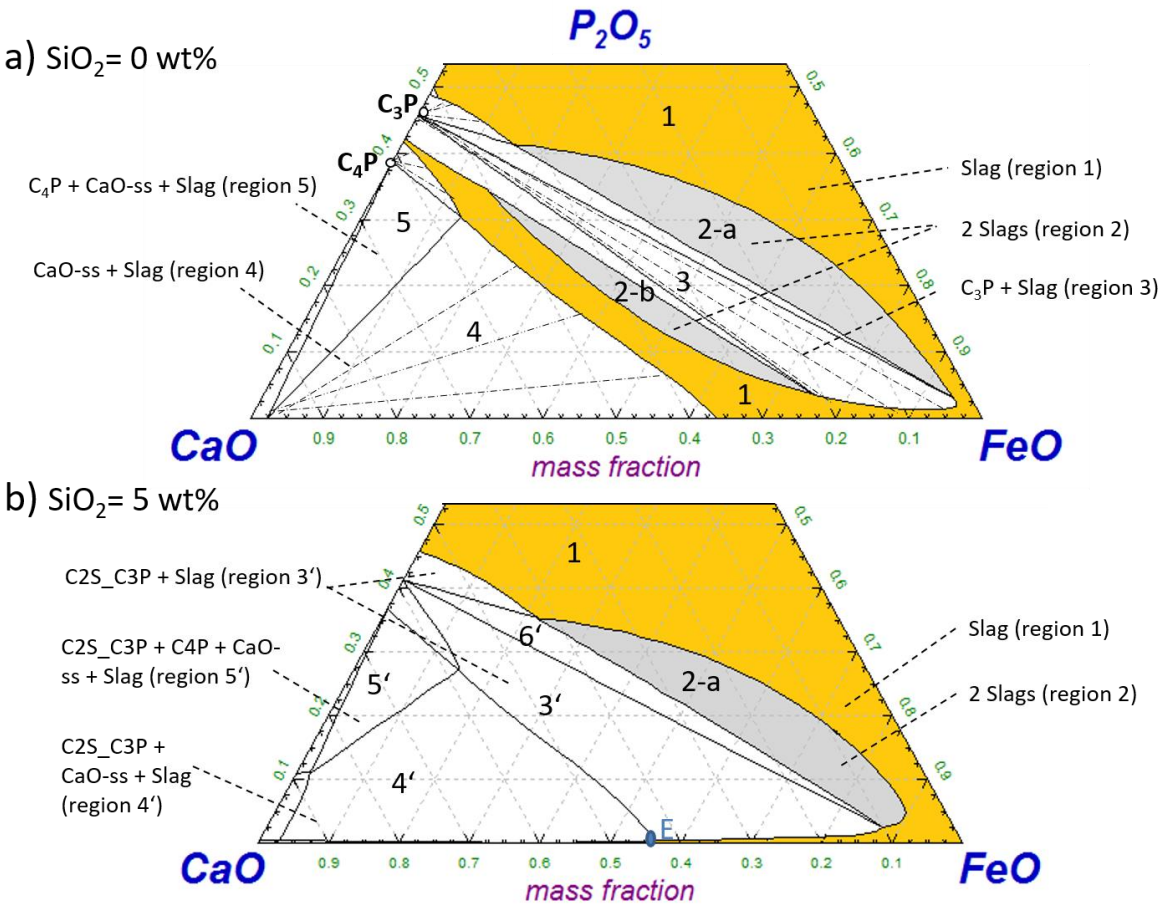

Figure 17: Effect of SiO_2 addition on the quaternary oxide system CaO-FeO_x-P_2O_5-SiO_2* at 1873 K (1600°C) and for a reduced p(O_2): a) SiO_2 = 0 wt% b) SiO_2 = 5 wt%

The reduction of the miscibility gap region under the addition of SiO_2 to the CaO-FeO_x-P_2O_5 system was reported in early investigations by Oelsen and Maetz.[185] Later, Drewes and Olette [179] as well as Fix et al.[176, 184] carried out detailed investigations on the effect of SiO_2 on the CaO-FeO_x-P_2O_5 system at an elevated and a reduced p(O_2), respectively. Those works confirmed the strong reducing effect of SiO_2 addition on the miscibility gap.[176, 179, 184, 185] This effect was explained by Turkdogan [186] by the fact that the miscibility gap in the CaO-FeO_x-P_2O_5 system is presumably caused by preferential coordination of the Ca^{2+} cations with the non-bridging oxygen ions of the phosphate chains. With the addition of silica, the silicate anions enter the phosphate chains causing the so-called “branching”, which presumably reduce the concentration of free oxygen ions. With such a structural change, both the Ca^{2+} and Fe^{2+} cations would be coordinated with the non-bridging oxygen ions of the silico-phosphate anions, resulting in complete liquid miscibility.

The effect of SiO_2 on the quaternary CaO-FeO_x-P_2O_5-SiO_2* system for higher SiO_2-contents is further investigated at a temperature of 1873 K (1600°C) and for a reduced $p(O_2)$. **Figure 18**-a), -b) and -c) show the calculated phase boundaries of the system at a SiO_2 content of 10 wt%, 13 wt%, and 15 wt%, respectively. It can be seen that with an increase in SiO_2, a shrinkage in the C4P saturation region (region 5') occurs: At 10 wt% SiO_2, this region can be reached only when the FeO_x content of the system is below 5 wt%, and is no longer stable in the system when the SiO_2-content reaches 13 wt%. Trömel and Fix reported that C4P saturation could no longer be found in the CaO-FeO_x-P_2O_5-SiO_2* system at a SiO_2 content as low as 2 wt%.[176]

Similar behavior was noted for regions containing a miscibility gap, that is (region 2) and (region 6'). At 13 wt% SiO_2, the triangle (region 6') containing 2 slags and C2S_C3P solid phase disappears completely. This is in agreement with the results of Koch and Fix,[184] who reported that the 3 phase region could no longer be found at 12.5 wt% SiO_2. Furthermore, the miscibility gap (region 2) disappeared completely when SiO_2 reached 15 wt%, which is also in accordance with observations from several experimental works, which were carried out at the same temperature and for both a reduced and an elevated $p(O_2)$ state.[176, 179, 184, 187]

In conclusion, it can be said that when SiO_2 is present with a content equals or higher than 5 wt%, the C2S_C3P phase region expands over the miscibility gap containing regions ((region 2) and (region 6')) as well as the phosphates saturation regions ((region 3), (region 5) and (region 5')). At 15 wt% SiO_2, the miscibility gap regions ((region 2) and (region 6')) are no longer present while the C2S_C3P phase becomes present in all solid phase containing regions ((region 3'), (region 4') and (region 5')). Since the SiO_2 content of industrial slags relevant to high phosphorus refining processes lies generally higher than 5 wt%, it can be concluded that a saturation of industrial slags with C2S_C3P is highly probable. It is thus important to model the thermochemical behavior of this phase for a proper assessment of the state of industrial slags. Thus, in section 4.3, the stability range of this phase has been investigated in detail.

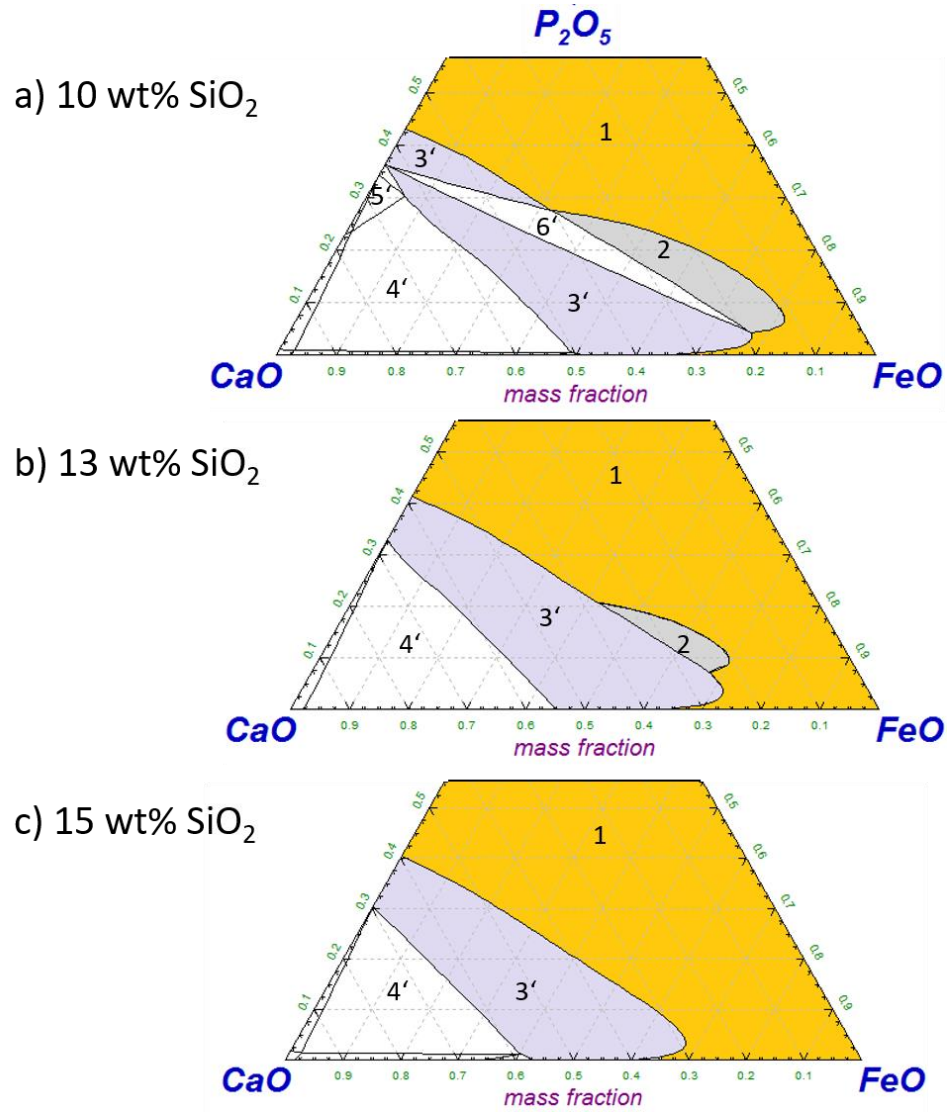

Figure 18: Effect of an increase in SiO_2 on the quaternary $CaO\text{-}FeO_x\text{-}P_2O_5\text{-}SiO_2$* system at a temperature of 1873 K (1600°C) and for a reduced $p(O_2)$ at an SiO_2 content of a) 10 wt% b) 13 wt% c) 15 wt%

4.2.2 Effect of $p(O_2)$

The effect of the oxidation state of FeO_x on the behavior of the quaternary system $CaO\text{-}FeO_x\text{-}P_2O_5\text{-}SiO_2$* at various SiO_2 contents was investigated by means of superimposing the 1863 K (1600°C) isothermals at an elevated and reduced $p(O_2)$. **Figure 19**-a, -b) and –c) show the calculated phase boundaries of the system at a SiO_2-content of 5 wt%, 10 wt%, and 15 wt%, respectively.

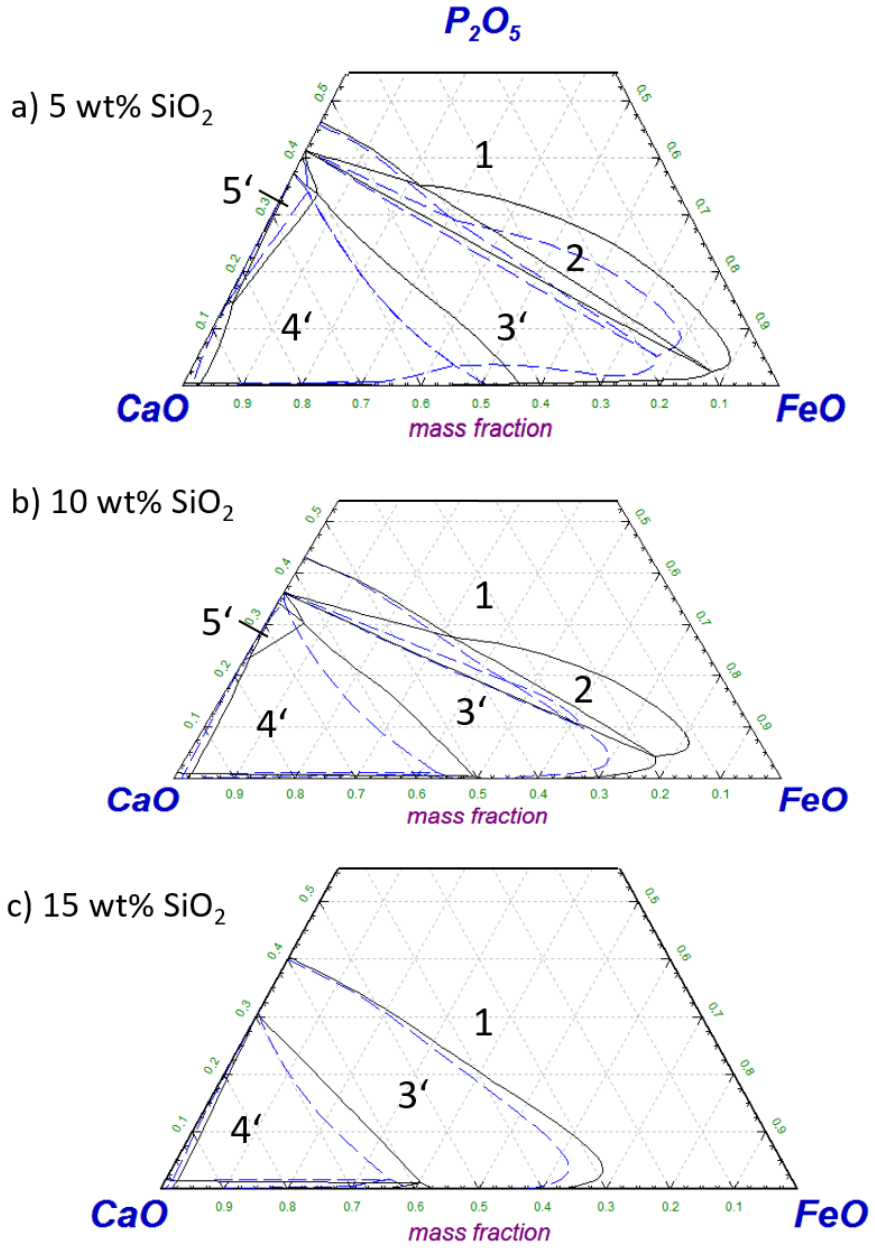

Figure 19: Effect of $p(O_2)$ on the system $CaO\text{-}FeO_x\text{-}SiO_2\text{*-}P_2O_5$ at a temperature of 1873 K (1600°C) and a SiO_2 content of a) 5 wt% b) 10 wt% and c) 15 wt%. The solid lines represent the reduced $p(O_2)$ case, whereas the dashed lines represent the elevated $p(O_2)$ case.

It can be seen from Figure 19 that an increase in $p(O_2)$ and thus in the ferric to ferrous ratio in the slag has a considerable effect on the phase boundaries of the system:

- A strong reduction in the miscibility gap region (2') (which was present at SiO_2 contents of 5 wt% and 10 wt%) is observed. For the elevated $p(O_2)$ case, the miscibility gap becomes very narrow when the SiO_2 content of the system

reaches 10 wt% and disappears completely at 15 wt% SiO_2. This means that under strong oxidizing conditions, the probability of the occurrence of a miscibility gap in the industrial process is very low when the SiO_2 content of the slag reaches 10 wt%. For the reduced $p(O_2)$ case, the miscibility gap region was still pronounced at 10 wt% SiO_2. A similar effect of $p(O_2)$ on the miscibility gap was observed earlier for the ternary $CaO\text{-}FeO_x\text{-}P_2O_5$ oxide system (Figure 15).

- The reduction of the miscibility gap when $p(O_2)$ increases (region 2) results in an expansion of the liquid slag region. Also, it results further in a slight expansion of the C2S_C3P saturation region (region 3') with the upper boundary shifting slightly in the direction of higher P_2O_5 contents.
- The "nose" of the C2S_C3P saturation region (region 3'), marking the boundary between this region and the liquid slag (region S), shifts in the direction of lower FeO contents. Overall, an expansion of the liquid slag region is noted when $p(O_2)$ increases.
- The lower boundary of the C2S_C3P saturation region (region 3') shifts in the direction of higher CaO-contents, marking an increase in the lime solubility of the slag. The phase boundary between regions 3' and region 4', further noted as the lime saturation line, changes its shape from a linear to a curved line. This means that with an increase in $p(O_2)$, the CaO-ss content of slags situated in the 3 phase region (region 4') will decrease in favor of more C2S_C3P precipitation and/or more liquid slag formation.
- The saturation region in C4P (region 5') becomes smaller with an increase in $p(O_2)$ in favor of an expansion of the 3 phase region (region 4') containing liquid slag, C2S_C3P, and CaO-ss and it disappears completely at 10 wt% SiO_2 for an elevated $p(O_2)$. It can be thus concluded that an increase in $p(O_2)$ stabilizes the formation of C2S_C3P solid solution over both the C4P and CaO-ss solid phases.

4.2.3 Effect of temperature

The effect of temperature variations on the phase boundaries of the $CaO\text{-}FeO_x\text{-}P_2O_5$ SiO_2*- oxide system at a fixed SiO_2 content was investigated in the temperature range of 1773 K (1500°C) – 1973 K (1700°C). **Figure 20**-a) and –b) show the calculated

isothermals (1773 K, 1873 K, and 1973 K) at 10 wt% SiO_2 for the reduced and elevated $p(O_2)$ case, respectively.

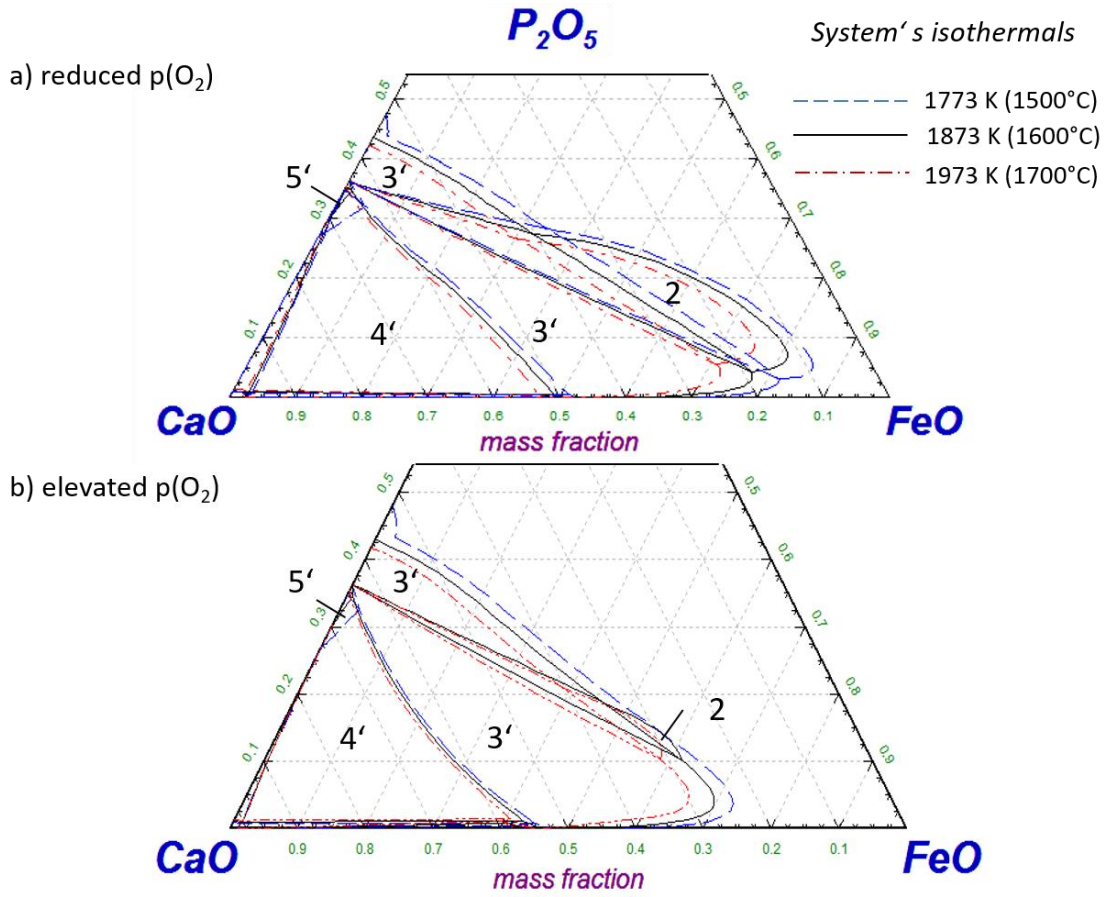

Figure 20: Effect of temperature variation in the range of 1773 K (1500°C) to 1973 K (1700°C) on the CaO-FeO_x-SiO_2*-P_2O_5 at 10 wt% SiO_2 at
a) reduced $p(O_2)$ b) elevated $p(O_2)$

It can be seen from Figure 20 that the temperature does not have a considerable effect on the phase boundaries of the system for both the reduced and the elevated $p(O_2)$ case, especially in comparison to the effect of $p(O_2)$ and SiO_2 content (Figure 19). An increase in temperature by 200 K (from 1773 K to 1973 K) increases lime saturation by 1-2 wt% for the reduced $p(O_2)$ case and by less than 1 wt% for the elevated $p(O_2)$ case. A temperature increase causes further a small shrinkage in both the miscibility gap region (region 2') and the C2S_C3P saturation region (region 3'), which is similar to the effect of increasing $p(O_2)$ (Figure 19), albeit less significant.

4.2.4 Quantification of lime saturation line

The study of the effect of $p(O_2)$ and temperature on the phase boundaries of the CaO-FeO_x- P_2O_5-SiO_2* system, given in section 4.2.2 and section 4.2.3, indicates that the position of lime saturation line is very sensitive to a change in $p(O_2)$ and thus in the oxidation state of FeO_x.

Equation (22) and equation (23) were derived for the determination of the CaO saturation values of the slag at 10 wt% SiO_2, in the temperature range of 1773 K (1500°C) to 1973 K (1700°C), for a reduced (Figure 20-a) and an elevated (Figure 20-b) $p(O_2)$ state, respectively:

$$(\%CaO)_{sat-reduced\,(O_2)} = -0.465\,(\%FeO_x) + 0.012\,T + 43.361 \quad (22)$$

$$(\%CaO)_{sat-elevated\,(O_2)} = -0.0046\,(\%FeO_x)^2 - 0.0401(\%FeO_x) + 59.674 \quad (23)$$

Since the effect of temperature variation in the range of 1773 K (1500°C) to 1973 K (1700°C) on the position of lime saturation line was found very small for the elevated $p(O_2)$ case, equation (23) does not contain a temperature attribute.

The effect of SiO_2 content on the position of lime saturation line was further investigated. **Figure 21**-a) and -b) show the superimposed phase boundaries of the solid CaO-ss phase at 4 different SiO_2-contents (0 wt%, 5 wt%, 10 wt%, and 15 wt%), at a temperature of 1873 K (1600°C) and for a reduced and elevated $p(O_2)$ respectively.

It can be seen from Figure 21 that an increase in the SiO_2 content of the system results in a considerable increase of the lime solubility of the slag, marked by a shift in the lime saturation line to higher CaO-contents. This increase in lime was accompanied by an expansion of the single-phase C2S_C3P saturation region (zone 3' in Figure 18, Figure 19, and Figure 20). The considerable increase in lime solubility occurs for both the reduced and the elevated $p(O_2)$ case. This is in agreement with the experiments of Fix and Koch,[176] where a considerable increase in lime solubility was observed when SiO_2 was added to a CaO-FeO_x-P_2O_5 slag with a content as low as 2.5 wt%.

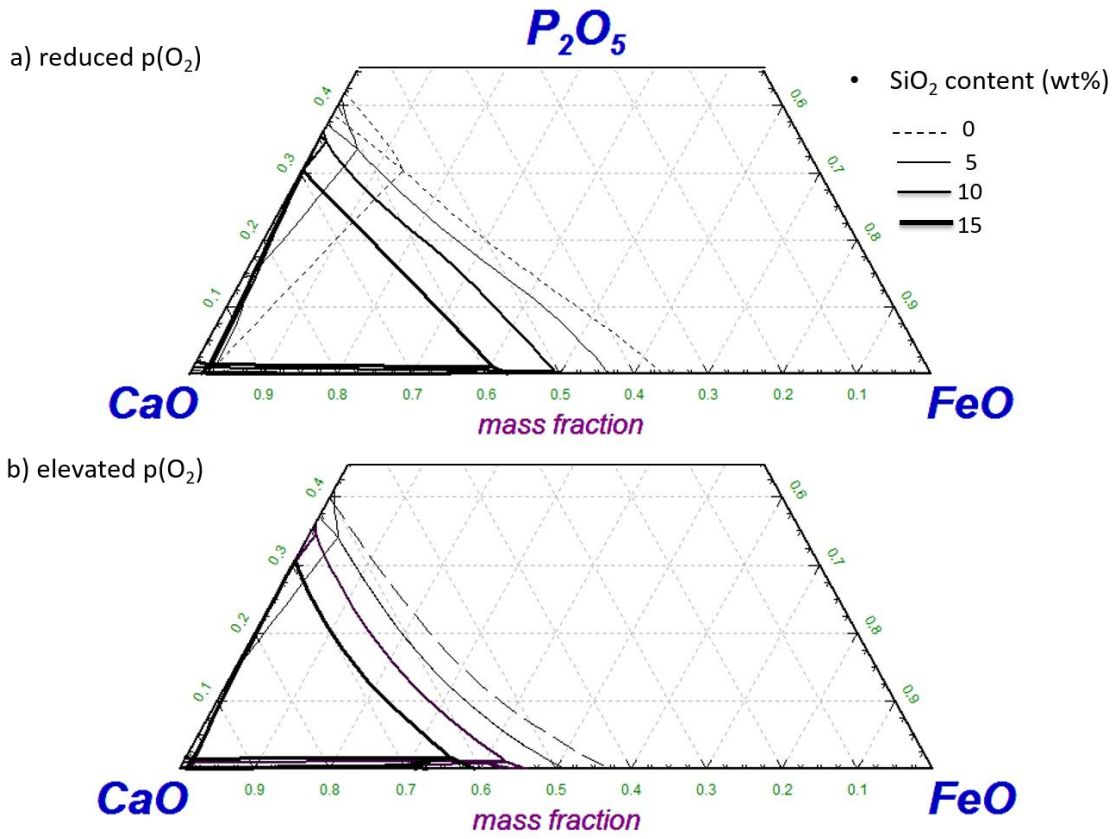

Figure 21: Position of lime saturation line in the quaternary CaO-FeO_x-P_2O_5-SiO_2* system at SiO_2 contents of 0 wt%, 5 wt%, 10 wt% and 15 wt% for
a) reduced p(O_2) b) elevated p(O_2)

4.3 Stability range of the C2S_C3P solid solution

Based on the analysis of the CaO-FeO_x-P_2O_5-SiO_2*-system, provided in section 4.2, it can be concluded that the C2S_C3P phase is expected as the dominant solid phase present in high phosphorus industrial slags. Also, it has been reported earlier (section 2.4) that this solid phase plays a crucial role in phosphorus removal during hot metal dephosphorization processes [10, 14, 17, 21, 28, 30-32, 34, 66, 98-120] due to its solubility for phosphorus. Thus, special attention was given to modeling this phase during the development of the BOFdePhos thermodynamic database. For proper modeling of the thermochemical behavior of this phase, a critical assessment of the ternary system CaO-SiO_2-P_2O_5 is required. A detailed description of the particular data assessment for the CaO-SiO_2-P_2O_5 oxide system is given in a separate publication.[146]

The model used for describing the C2S_C3P solid phase reads: $(Ca^{2+},Mg^{2+},Mn^{2+})_3(Ca^{2+},Va)(P^{5+},Si^{4+})_2(O^{2-})_8$. In this section, the stability range of the

C2S_C3P phase in the $CaO-P_2O_5-SiO_2$ oxide system is investigated for the purpose of clarifying its behavior in the quaternary $CaO-FeO_x-P_2O_5-SiO_2$ oxide system.

Figure 22 shows the isothermal section of the system, calculated at a temperature of 1873 K (1600°C) and under atmospheric pressure. It can be seen that the calculated liquidus line of the C2S_C3P phase is in excellent agreement with the corresponding experimental data of Fix and Koch.[184]

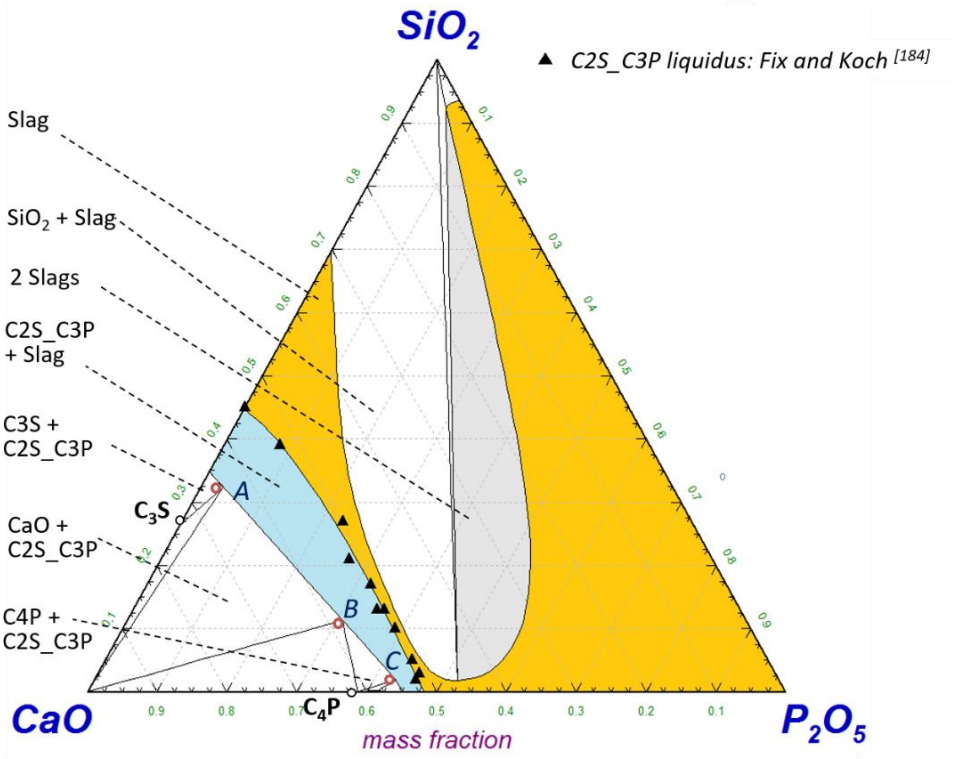

Figure 22: Calculated phase boundaries of the $CaO-P_2O_5-SiO_2$ oxide system at a temperature of 1873 K (1600°C), under atmospheric pressure, and comparison with experimental data of Koch and Fix.[184]

It becomes obvious from Figure 22 that the stability range of both the phosphate phase C4P and the silicate phase $3CaO.SiO_2$, further noted as C3S, is very small in favor of a large stability range of the silico-phosphate phase, the C2S_C3P solid solution. The C2S_C3P replaces C4P gradually with the addition of SiO_2 to the binary $CaO-P_2O_5$ system and is the only solid phase present at an SiO_2 value in the range of 3 to 11 wt% (Position indicated by point B and C respectively) depending on its CaO or P_2O_5 content. For SiO_2 contents higher than 3 wt%, a single saturation of the slag on C4P is no longer possible without additional C2S_C3P saturation, which explains the

shrinkage of the C4P-saturation region in favor of an expansion of C2S_C3P saturation region in the quaternary CaO-FeO_x-P_2O_5-SiO_2* system, observed earlier in section 4.2.1 (Figure 18). Also, the C2S_C3P replaces C3S gradually with the addition of P_2O_5 to the binary CaO-SiO_2 system and becomes the only stable solid phase present in the system when the P_2O_5 content exceeds 3 wt% (point A).

The effect of temperature on the phase boundaries of the CaO-P_2O_5-SiO_2 system was further investigated. **Figure 23** shows the liquidus projection of the CaO-rich part of the system calculated for the temperature range of 1673 K (1400°C) to 3273 K (3000°C). It becomes obvious that the C2S-C3P phase has a very prominent thermal stability in the system. The azeotropic point of C2S_C3P phase dominates the entire composition range up to 60 wt% CaO as well as the entire temperature range of 1673 K (1400°C) to 2473 K (2200°C). Riboud and Margot [172] carried out experimental investigations of the liquidus of the CaO-rich part of the CaO-P_2O_5-SiO_2 system and found out that the lowest liquidus point at which C2S_C3P dissolves corresponds to the composition of point L where a liquidus temperature of 1913 K (1640°C) was measured in their experiments.

Figure 24 shows the temperature-composition diagram of the C2S_C3P phase, calculated using the BOFdePhos thermodynamic database.

It becomes clear from the diagram that there is a complete solubility of P_2O_5 in the C2S phase under the formation of C2S_C3P. The C2S_C3P is the dominant solid phase over the total composition range and in the temperature range of 1773 K (1500°C) to 2573 K (2200°C). There is a complete exchange between the silicate anion $[SiO_4]^{4-}$ and the phosphate anion $[PO_4]^{3-}$ with the amount of CaO changing, in order to keep the electro-neutrality of the phase. This is in accordance with recent findings of Duée et al. [188], who observed that $[PO_4]^{3-}$ units were incorporated into the dicalcium silicate structure by substituting $[SiO_4]^{4-}$ groups, with the charge balance being maintained by creation of calcium vacancies.

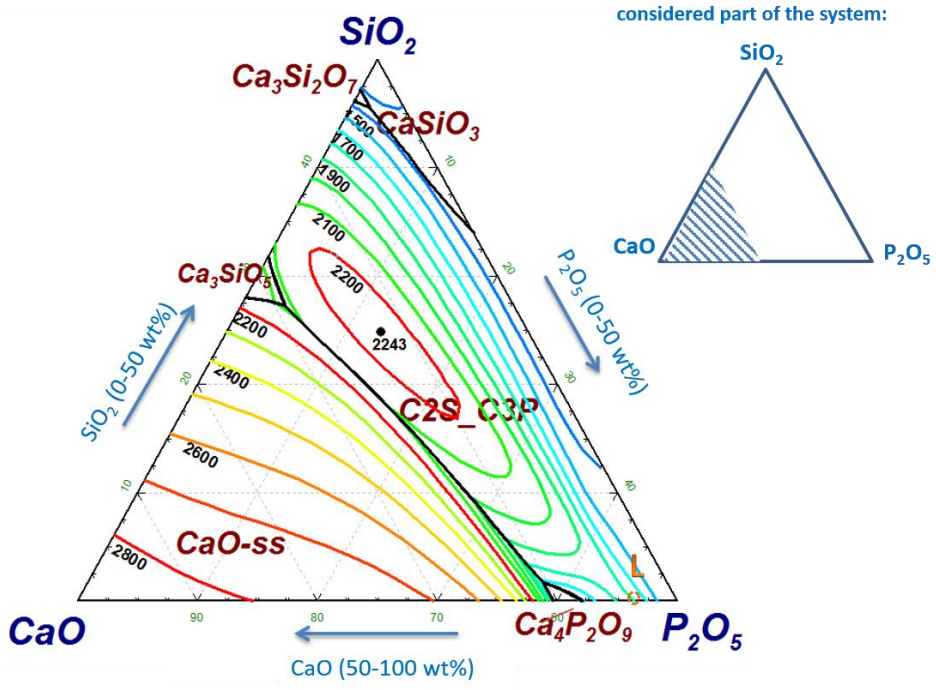

Figure 23: Liquidus projection of the CaO-rich part of the CaO-P_2O_5-SiO_2 system in the temperature range of 1673 K (1400°C) to 3273 K (3000°C). The CaO-content varies between 50-100 wt% while P_2O_5- and SiO_2-content varies between 0-50 wt%.

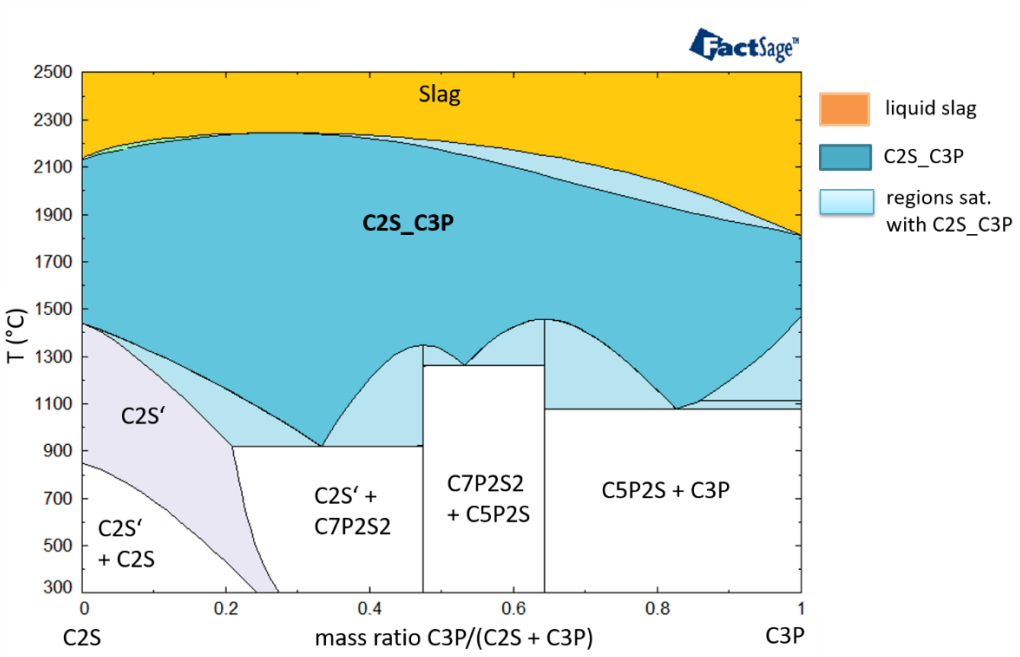

Figure 24: Temperature-composition diagram for the C2S-C3P phase. A major emphasis was given to the reproduction of the solid-liquid equilibria. The sub-solidus range is still preliminary. C denotes CaO, P denotes P_2O_5, and S denotes SiO_2.

4.4 Consequences for the industrial process

The study of the high phosphorus system CaO-FeO_x-P_2O_5-SiO_2* showed that the C2S_C3P saturation regions dominate the CaO-rich part of the system and expand over C4P saturation, CaO-ss saturation, and miscibility gap regions when the SiO_2 content of the system equals or higher than 5 wt%. Due to the high phosphorus dissolving potential of this phase, it can be considered at this stage that the presence of SiO_2 in the system is beneficial for P removal from the liquid metal phase from a thermochemical perspective.

It can be seen from Figure 17-Figure 20 that the liquid part of slags saturated with single-phase C2S_C3P (region 3') is high in FeO and low in P_2O_5, which are optimal thermodynamic conditions for P removal from the liquid metal phase. This indicated that region 3' is expected to have a high dephosphorization potential due to the high phosphorus dissolving potential of the solid C2S_C3P phase and also, due to a high dephosphorization potential of the liquid slag phase. The CaO-content of a liquid slag situated in the single-phase C2S_C3P saturation region is below lime saturation, which should promote lime dissolution.

During the industrial process, it is a common practice to saturate the slag with lime, in order to achieve optimal dephosphorization results.[189] This is due to the well-established increase of P-distribution between the slag and the metal phase with an increase in the CaO-content of the slag (Table 2). Lime saturation of the slag is also advantageous in protecting the refractory lining from wearing.[189] Based on the study of the thermodynamic behavior of the quaternary CaO-FeO_x-P_2O_5-SiO_2* system, provided in the present work, it is found that single-phase CaO-ss saturation cannot be reached when the SiO_2 content of the system equals or higher than 5 wt%.

It should be noted that the equations developed for the description of Lp in the SiO_2-free system were mostly developed for CaO-saturated slags.[82, 83] It is found that the composition of lime saturated slags in the SiO_2-free system (region 1 in Figure 17-a) differs strongly from the composition of lime saturated slags in the SiO_2-containing system (point E in Figure 17-b). In fact, a study of the effect of liquid slag composition over a wide composition range on the dephosphorization potential of CaO-saturated slags in the CaO-FeO_x-P_2O_5-SiO_2* system is not possible since the liquid slag composition varies very little (point E in Figure 17-b). This means that Lp-relations developed

for the SiO_2-free system,[82, 83] can only be applied with precaution for describing Lp-behavior in the quaternary CaO-FeO_x-P_2O_5-SiO_2* system when the SiO_2 content equals or higher than 5 wt%. In addition, it has been reported that the presence of C2S_C3P phase has a strong effect on the dephosphorization potential of the heterogeneous slag (see section 2.4).

A further important observation for the industrial process is the absence of a purely liquid slag region in the CaO-rich part of the quaternary CaO-FeO_x-P_2O_5-SiO_2* system contrary to the SiO_2-free ternary system CaO-FeO_x-P_2O_5, where a purely liquid slag region is stable over the total FeO-variation range. The liquid slag region in the ternary system is generally considered as the target slag region for the industrial process. When SiO_2 is present in the system, the purely liquid region changes to a single-phase C2S_C3P saturation region.

The study of the effect of $p(O_2)$ and temperature variations on the CaO-FeO_x-P_2O_5-SiO_2* system has shown that an increase in $p(O_2)$ increases lime saturation in the slag and reduces the miscibility gap region while variations in temperature are found to have a negligible effect on all phase boundaries of the CaO-rich part of the system.

It can be thus concluded that increasing the oxidation state of FeO_x and thus, the ferric to ferrous ratio in the slag represents an effective measure for increasing lime saturation of the slag, which accelerates the dissolution procedure of lime. A further consequence of increasing lime saturation is the avoidance of CaO-ss precipitations. Excessive CaO-ss precipitations increase the slag viscosity and reduce the interfacial area between liquid slag and undissolved lime, which results in setting unfavorable kinetic conditions for lime dissolution. [190] An increase in temperature is not expected to favor lime dissolution from a thermodynamic perspective.

5 Study of the oxide systems relevant for low phosphorus slags

5.1 Discussion of the quasi-ternary system CaO-FeO_x-SiO_2

The oxide System CaO-FeO_x-SiO_2 is the basic ternary oxide system for slags formed during contemporary oxygen steelmaking (BOF process), and more specifically when a low phosphorus hot metal (P < 0.015 wt%) is used. Experimental data on the behavior of this system in equilibrium with liquid Fe, i.e., at reduced p(O_2) (Table 6) were provided by Görl et al. [191, 192] Drewes and Olette [179] provided experimental data on the system behavior at elevated p(O_2). Muan et al. [193, 194], as well as Margot et al. [195] studied the behavior of the system under air.

5.1.1 System behavior at reduced p(O_2)

Figure 25 shows the calculated isothermal section for the system CaO-FeO_x-SiO_2 for 1873 K (1600°C) and reduced p(O_2). It can be seen that the CaO-rich part of the system, which is the region relevant for the industrial process, is dominated by the presence of silicates: A saturation region for the 2CaO.SiO_2 solid phase (region 2), further denoted as C2S, a double saturation region for the solid phases 2CaO.SiO_2 and 3CaO.SiO_2, further denoted as C3S (region 3) as well as a double saturation region with C3S and with a CaO-based monoxide solution, further denoted as CaO-ss (region 4). The deflection point of the C2S-liquidus (the boundary between regions 1 and 2), marking the composition of a C2S-saturated slag with the highest FeO-content, will be further noted as the “C2S-nose”. It can be seen that the stability range of single-phase C3S saturation is very narrow. It will thus not be considered in the further discussion of this system.

It becomes obvious from Figure 25 that the single-phase CaO-ss saturation (region 5), further denoted as lime-only saturation region, has a small stability range in the system, especially in comparison with the double saturation region with both CaO-ss and C3S (region 4). The lime-only saturation region is generally considered as the target zone for the industrial process.

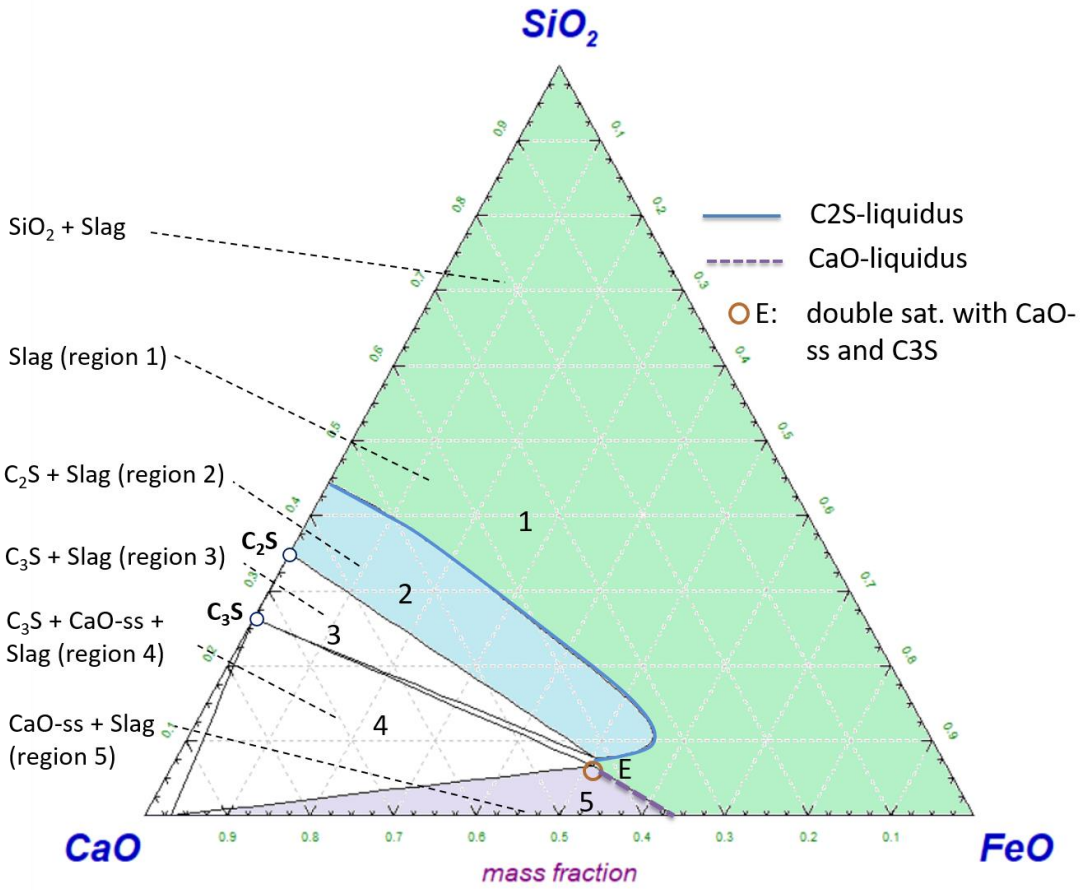

Figure 25: Calculated isothermal section for the system CaO-FeO_x-SiO_2 at 1873 K (1600°C) and reduced p(O_2).

The aforementioned experimental data on the system focused mainly on the determination of the position of the liquidus lines of the CaO-rich part of the oxide system.[179, 191-195] The slag liquidus will be further divided into 2 parts: The “C2S_liquidus” denoting the boundary between (region 1) and (region 2) and the “CaO-liquidus” denoting the boundary between (region 1) and (region 5).

Figure 26 and **Figure 27** show a comparison between the calculated liquidus lines in the present work at 1873 K (1600°C) and the corresponding data in the literature for an elevated and a reduced p(O_2), respectively. It can be seen that in case of a reduced p(O_2) (Figure 26), the calculated phase boundaries were in a very good agreement with the experimental data of Görl et al.,[191, 192] especially regarding the CaO-liquidus, whereas the “C2S-nose” in their experiments was slightly shifted to the FeO_x corner by about 3 wt% compared to the calculated C2S-liquidus.

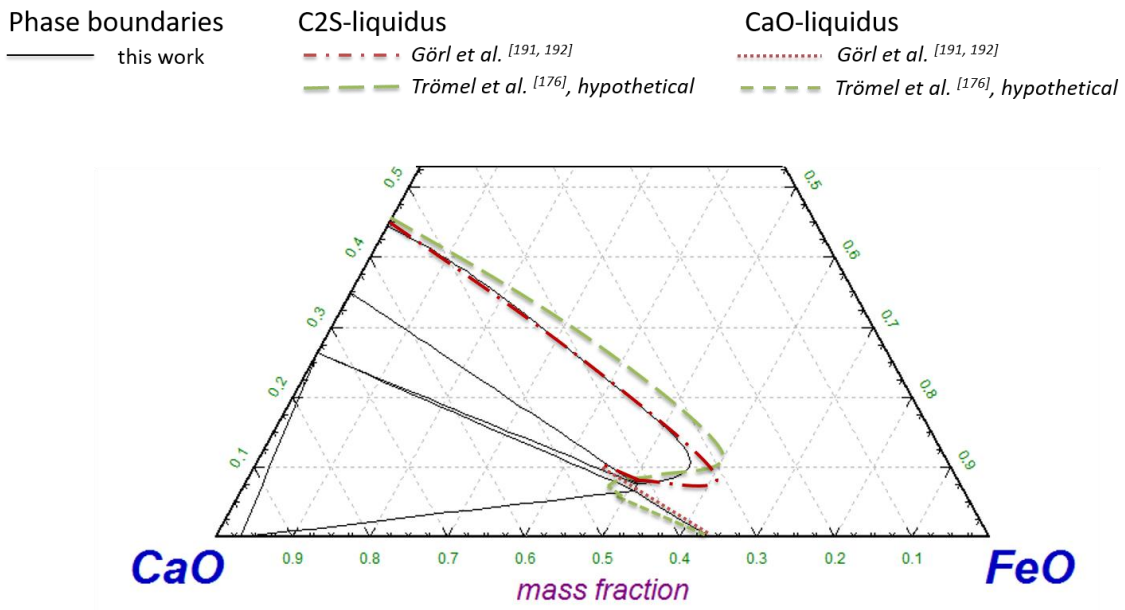

Figure 26: Comparison of the calculated phase boundaries of the system CaO-FeO_x-SiO_2 at 1873 K (1600°C) and reduced p(O_2) with the experimental findings of Görl et al. [191, 192] and estimated liquidus curves from the work of Trömel et al.[176]

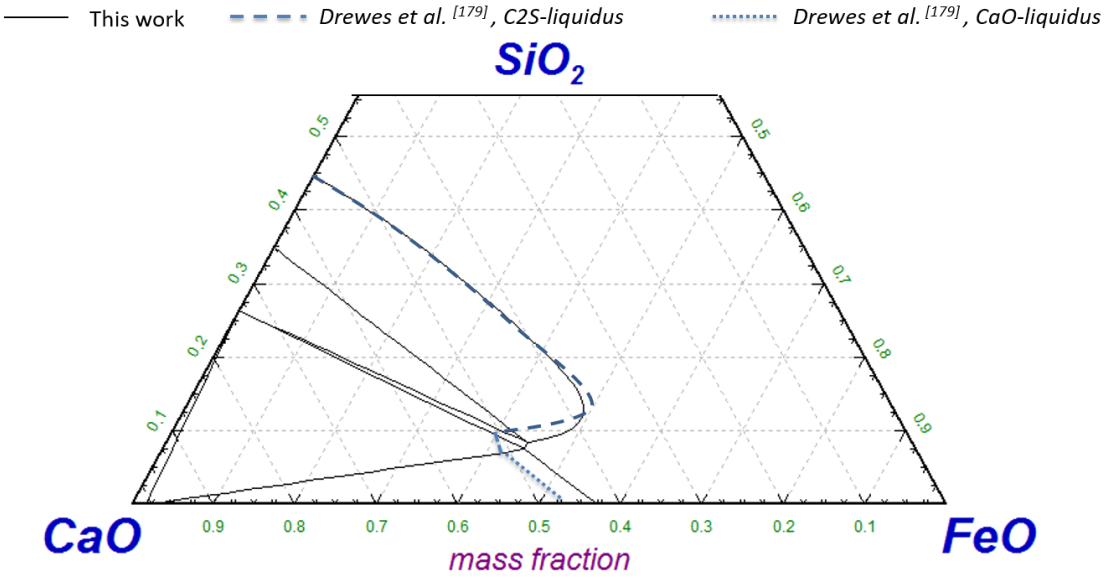

Figure 27: Comparison between the calculated phase boundaries of the system CaO-FeO_x-SiO_2 at 1873 K (1600°C) and elevated p(O_2) with the experimental findings of Drewes and Olette.[179]

For the elevated p(O_2) case (Figure 26-Figure 27), the agreement between the calculated liquidus and the experimental data of Drewes and Olette [179] can also be considered as very good, although a small shift in the CaO-liquidus by about 2 wt% to the

CaO-corner was noted for the experimental data in comparison with the calculated CaO-liquidus.

Experimental data on the behavior of the system at the low temperature of 1673 K (1400°C) could be found in the work of Knüppel et al.[196] At this temperature, metallic iron is in a solid state. An equilibration of slag with solid iron is experimentally very difficult, and thus, the authors investigated the equilibrium state of the system under an inert gas atmosphere (N_2-gas).[196] Their results are presented in **Figure 28** together with the calculated phase boundaries of the system at 1673 K (1400°C) and reduced $p(O_2)$. Even though the calculations suggest a shift in the C2S-nose to lower FeO values by about 7 wt% compared to the experimental data, the general agreement can be considered as acceptable, especially in view of the missing information on the oxidation state of FeO_x in the experimental work. [196]

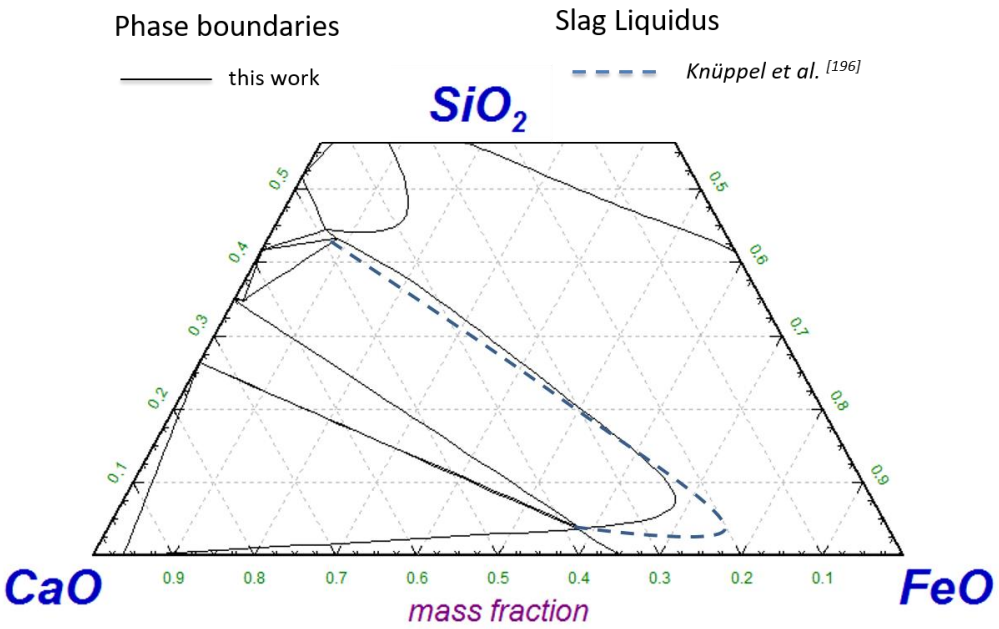

Figure 28: Calculated phase boundaries of the system CaO-FeO_x-SiO_2 at 1673K (1400°C) in equilibrium with solid Fe and comparison with experimental results of Knüppel et al.[196] under inert gas atmosphere ($p(O_2)$ = 0 atm).

5.1.2 System behavior for a high FeO_x oxidation state

Further investigations of the system under air ($p(O_2)$ = 0.21 atm) and thus under strong oxidizing conditions are also available. At such conditions, the ferric (Fe^{3+}) to ferrous (Fe^{2+}) ratio in the system is very high (Table 6). Margot and Riboud provided experimental data at a temperature of 1873 K (1600°C) while Phillips and Muan provided a hypothetical estimation of the slag liquidus, also at a temperature of 1873 K (1600°C).[193, 195] When including their results, the effect of $p(O_2)$ on the system is expected to follow the scheme presented in **Figure 29**. In order to evaluate the effect of the oxidation state of FeO_x on the phase boundaries of the system over a wide $p(O_2)$ range, the phase boundaries of the system at $p(O_2)$ values of 10^{-5} atm and 10^{-9} atm were calculated and included in Figure 29.

It can be seen from Figure 29 that the oxidation state of FeO_x has a considerable effect on the liquidus of the system, with its effect on the C2S-liquidus being much stronger than that on the CaO-liquidus. This means that in case the slag is saturated with C2S, which was occasionally reported as the final state of BOF slags in the industrial process,[10, 118] an increase in $p(O_2)$ would lead to a decrease in C2S precipitations in favor of an increase in the amount of liquid slag. As already mentioned in section 3.1, the oxidation state of FeO_x in industrial slags has not been clarified. In addition, the oxygen partial pressure in BOF slags may not be homogeneous, especially in view of it being a top blowing process: Slag regions surrounding the hot spot (where oxygen gas is in direct contact with the metal bath) may have a higher $p(O_2)$ than those in contact with a CO-containing gas phase (product of the decarburization reaction). Some works considered that the $p(O_2)$ in slag regions surrounding the hot spot may reach values as high as 1 atm.[56]

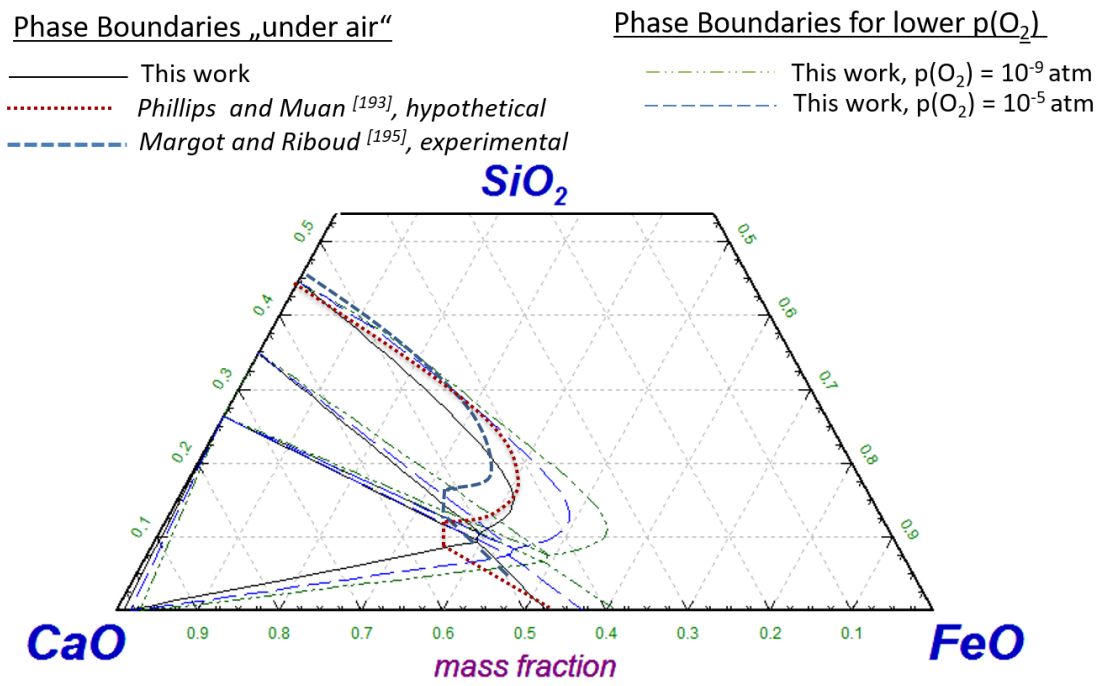

Figure 29: Estimated effect of $p(O_2)$ variation on the phase boundaries of the ternary CaO-FeO_x-SiO_2 system at a temperature of 1873 K (1600°C) based on present calculations and results reported in the literature. [193, 195]

In agreement with the calculated behavior, the hypothetical behavior of the system under air suggested by Phillips and Muan [193] predicted a larger C2S-saturation region than that in the experiments of Margot and Riboud.[195] Considering the analysis of the iron-oxygen-temperature system introduced previously in section 3.5 (Figure 12 and Figure 13), it becomes clear that for a temperature of 1873 K (1600°C), the system under air is very close to the spinel formation region. It is thus possible that in the experiments of Margot and Riboud, [195] some solid phase precipitation may have occurred. This means that under strongly oxidizing conditions, for example, when $p(O_2)$ equals or higher than 0.21 atm, a considerable shrinkage of the C2S-saturation region is expected, and the liquidus of the system may behave similarly to that in the experiments of Margot and Riboud. [195] On an industrial scale, the strong sensitivity of the C2S liquidus to $p(O_2)$ indicates that special attention should be given to preserving the oxidation state of industrial samples during sampling and quenching procedures in order to properly assess the morphology and phase amounts of C2S-saturated BOF slags.

5.1.3 Study of the effect of temperature

During oxygen converting of low phosphorus hot metal, the hot metal temperature increases gradually from an initial temperature in the range of 1250°C-1400°C to a final temperature in the range of 1600°C-1700°C.[174, 197-200] It is thus important to study the effect of temperature on the behavior of the relevant oxide system. The effect of temperature variations on the CaO-FeO_x-SiO_2 system at reduced $p(O_2)$ is illustrated in **Figure 30** by means of superimposing the isothermal sections for 1673 K (1400°C), 1773 K (1500°C), 1873 K (1600°C) and 1973 K (1700°C).

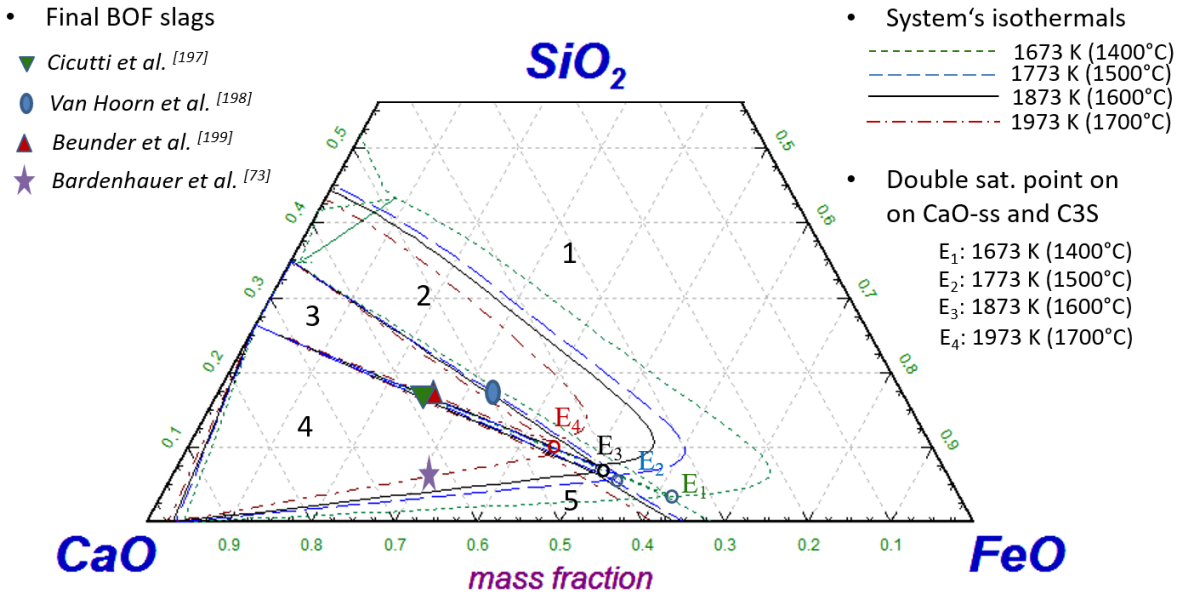

Figure 30: Presentation of the estimated effect of temperature on the phase boundaries of the system CaO-FeO_x-SiO_2 at reduced $p(O_2)$ by means of superimposing the calculated isothermal sections for 1673 K (1400°C), 1773 K (1500°C), 1873 K (1600°C) and 1973 K (1700°C). The positions of final industrial BOF slags in the ternary system, as reported in several works, are also presented.[73, 197-199]

It can be seen from Figure 30 that the silicates saturation regions dominate the CaO-rich part of the system in the entire temperature range of 1673 K (1400°C) to 1973 K (1700°C).

The effect of temperature on the stability range of the C2S saturation region (region 2) can be considered as moderate in the temperature range of 1773 K (1500°C) - 1873 K (1600°C), especially in comparison with the effect of $p(O_2)$ (Figure 29). When the temperature increases from 1773 K (1500°C) to 1873 K (1600°C), the C2S "nose"

shifts away from the FeO corner by 3 wt%. This shift is more pronounced for the lower and the higher temperature regions: When the temperature increased from 1673 K (1400°C) to 1773 K (1500°C) or from 1873 K (1600°C) to 1973 K (1700°C), the C2S "nose" shifts away from the FeO corner by about 10-12 wt%.

On the other hand, the effect of a change in temperature on lime saturation line is very small and can be neglected: An increase in slag temperature from 1773 K (1500°C) to 1873 K (1600°C) increases lime saturation of the slag by less than 1 wt%. The effect is more significant with respect to the expansion of the single-phase CaO-ss saturation (region 5) and the shrinkage of the double saturation with CaO-ss and C3S (region 4). The points which denote the double saturation with CaO-ss and C3S (E_1-E_4) shift along the lime saturation line to lower FeO contents. At a temperature of 1673 K (1400°C) the single-phase CaO-ss saturation (region 5) can be reached only at FeO-contents higher than 62 wt% (point E_1) whereas, at a temperature of 1973 K (1700°C), it is reached at a FeO-value of 44 wt% (point E4). This means that region 5 becomes more "accessible" at lower FeO contents when the temperature increases. This is an important indication for the industrial process since lime saturation is strived for, and at the same time, high FeO contents of the slag are avoided in order to minimize iron losses to the slag as well as refractory wear. Similar observations were made earlier with respect to the effect of temperature on lime saturation with the ternary CaO-FeO_x-P_2O_5 system (section 4.2.2) when considering the C4P phase as the equivalent of the silicate phase C3S in the CaO-FeO_x-SiO_2 system.

Finally, equation (24) was derived for the description of the lime saturation line in the CaO-FeO_x-SiO_2 oxide system at reduced p(O_2) and in the temperature range 1823 K (1550°C) to 2023 K (1750°C):

$$(\%CaO)sat._{reduced\ p(O_2)} = -0.465\ (\%FeO_x) + 0.012\ T + 43.361 \qquad (24)$$

It should be noted that equation (24) is only applicable when the FeO-content of the slag is higher than that of the 3 phase point (point E_1-E_4 in Figure 30), further noted as "$FeO_{x\ limit}$". The position of the 3 phase point (E_1-E_4) depends on temperature and can

be approximated by equation (25) when the temperature is within the range of 1673 K (1400°C) to 2023 K (1750°C) and for a reduced $p(O_2)$:

$$(\%FeO_x)_{limit,reduced\ p(O_2)} = -0.0623\,T + 166.72 \quad (25)$$

By using equation (24), it becomes possible to estimate the maximum solubility of CaO in a CaO-FeO_x-SiO_2 slag at a given temperature by inserting the corresponding $(\%FeO_x)_{limit}$ value (calculated by equation (25)) as the value of the $(\%FeO_x)$ term in equation (24).

5.1.4 Conclusions and industrial consequences

The study of the state of CaO-FeO_x-SiO_2 slags given in the previous sections (3.3.1, 3.3.2 and 3.3.3) for different oxidation states of FeO_x as well as for different temperatures showed that the silicate phases C2S and C3S dominate the CaO-rich part of the system, which is the relevant section for the industrial process. The saturation state of BOF slags on solid phases is thus expected as follows:

- When the system is below lime saturation, the slag is situated within silicate saturation regions: A single-phase saturation with C2S (region 2) or a double phase saturation with both silicates C2S and C3S (region 3) is reached. It can be seen from Figure 30, that the industrial slags reported by Van Hoorn et al.[198] are not saturated with CaO-ss but rather in silicates: Depending on the temperature, the reported slags are either within the single-phase C2S saturation (region 2) or lie exactly at the double saturation line with both C2S and C3S (the boundary between region 2 and region 3).
- When lime saturation is achieved, a double phase saturation with both C3S and CaO-ss. (region 4) is expected. This is because the single-phase CaO-ss saturation (region 5) has a small stability range in the system and high FeO contents are required to reach it: For a temperature of 1973 K (1700°C) and reduced $p(O_2)$, the required FeO_x-content must be higher than 44 wt%, and this value is higher for lower temperatures. The slag analysis, reported in the plant trials of Cicutti et al.[197] as well as in that of Beunder et al. [199] (Figure 30) lie exactly along the lime saturation line and are saturated additionally with C3S

independent of temperature. The saturation state of the slag analysis reported by the plant trials of Bardenheuer et al.[73] depends however on the temperature: At temperatures equals or below 1873 K (1600°C), the slag is double saturated with C3S and CaO-ss, whereas at a higher temperature of 1973 K (1700°C), the slag lies exactly at the double saturation line in C3S and CaO-ss (boundary between region 4 and region 5) and no C3S precipitations would occur in such a case.

Similar to the CaO-FeO_x-P_2O_5 system, the temperature did not have a significant effect on the lime saturation line for the CaO-FeO_x-SiO_2, system. However, it was observed that an increase in temperature resulted in an expansion of the single-phase CaO-ss saturation region over the double phase saturation region with CaO-ss and C3S. This was also observed for the CaO-FeO_x-P_2O_5 system, with the solid phase being C4P instead of C3S. Thus, the same conclusions which were drawn for lime saturation in the CaO-FeO_x-P_2O_5 system further hold for the CaO-FeO_x-SiO_2 system: Even though an increase in temperature does not increase lime solubility in the slag, it will indirectly result in promoting lime dissolution. This is due to the fact that less silicates precipitations will occur in favor of an increase in liquid slag amount. As a result, the contact area between liquid slag and lime particles increases, which was reported as crucial for the continuation of lime dissolution, especially under foaming conditions.[201]

The strong effect of $p(O_2)$ on the phase boundaries of the system, shown in Figure 29, indicates the importance of this aspect in modeling and assessment of the state of industrial slags. With an increase in $p(O_2)$ and thus, in the ferric to ferrous ratio, a shrinkage in the silicate saturation regions occurs, and the “C2S nose” shifts to lower FeO-contents. Also, a moderate increase in lime solubility in the slag is observed, which is, however, less significant than the increase noted for the CaO-FeO_x-P_2O_5 system (Figure 15). In section 4.3, it is found that the C2S solid phase has a large phosphorus solubility under the formation of the C2S_C3P phase. Thus, the C2S saturation region is highly interesting for phosphorus removal in the BOF process. The estimation of the oxidation state of FeO_x in the slag can be thus considered as important in the assessment of the dephosphorization potential of BOF slags due to its strong effect on the stability range of the C2S phase in the CaO-FeO_x-SiO_2 oxide system.

It should be further clarified whether the effect of $p(O_2)$ on the system is temperature-dependent. **Figure 31**-a) and –b) show the calculated phase boundaries, for both a reduced and an elevated $p(O_2)$, at a temperature of 1723 K (1450°C) and 1973 K (1700°C) respectively. It can be seen that the effect of $p(O_2)$ on the C2S-liquidus is very pronounced at a temperature of 1723 K (Figure 31-a) and diminishes completely at a temperature of 1973 K (Figure 31-b).

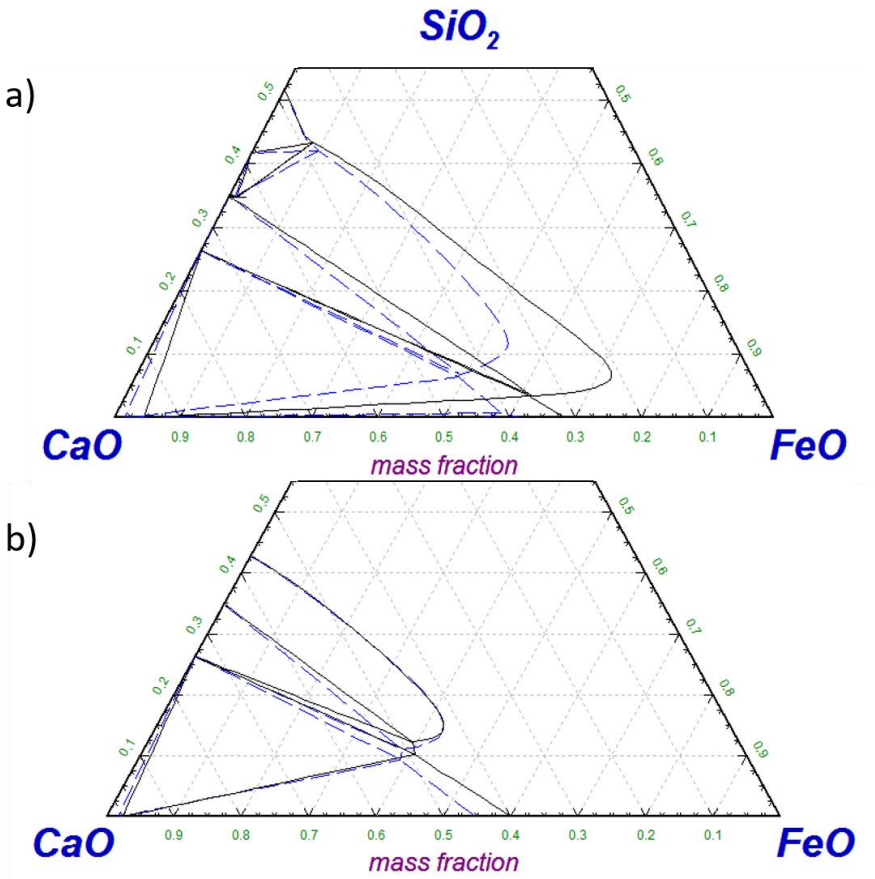

Figure 31: Effect of $p(O_2)$ on the a) 1723 K (1450°C) b) 1973 K (1700°C) isothermal sections of the CaO-FeO_x-SiO_2 system: The solid lines represent the reduced $p(O_2)$ case whereas the dashed lines represent the elevated $p(O_2)$ case.

A study of the morphology of industrial slags, carried out by Fix and Koch,[182] indicated that early slags, formed during the first 1/3 of the blowing time, were saturated with silico-phosphates. The morphology of the corresponding samples was investigated and showed an irregular structure with zones dominated by solid phases precipitations and others dominated by liquid slag. The authors attributed this to an irregular temperature distribution in the slag.[182] Even though the observed solid phase was the silico-phosphate phase, the C2S_C3P phase, it can be assumed that the thermochemical

behavior of this phase is similar to that of the phosphate-free C2S phase. Based on the discussion of the CaO-FeO_x-SiO_2 and CaO-FeO_x-P_2O_5 systems given in the present work regarding the effect of temperature and $p(O_2)$ on silicates and phosphates stability regions, it can be concluded that the irregular structure may have resulted from a non-homogeneous oxidation state of FeO_x in the slag, and thus from $p(O_2)$ irregularities: Regions with high $p(O_2)$ were liquid or had small precipitation amounts of solid phases while regions with lower $p(O_2)$ experienced excessive solid phase precipitations. This is supported by the fact that the C2S saturation region was found to be highly sensitive to a change in $p(O_2)$ (Figure 29), especially at low temperatures (Figure 31-a). The temperature of the bath during the first 1/3 of blowing time and thus, that of early slags in the BOF process was reported as lower than 1773 K (1500°C) in several works. [58, 175, 199]

Inhomogeneities in $p(O_2)$ within the slag may exist on a microscopic level due to the dispersion of C-containing metallic droplets from the bath into the slag and their subsequent decarburization by FeO_x. This results in CO and, to a lesser extent, CO_2-gas formation. As a result, $p(O_2)$ in slag regions in contact with CO/CO_2 gas bubbles will be lower than in “bubble-free” regions.

Even though it was found that the temperature also affects the C2S saturation region, temperature-caused irregularities in C2S precipitations will require high-temperature gradients, higher than 50 K, compared to the required $p(O_2)$ gradients, especially in the temperature range of 1500-1600°C (Figure 30). The difference between the temperature measured in the metal bath (thus at the lower side of the slag) and the temperature measured in the slag was reported to lie in the range of 30-100 K.[91] The observed irregularities occurred within very small specimen areas (with a dimension less than 0.2 * 0.2 $mm^{2)}$. Thus, it seems unlikely that the temperature gradient within such a small dimension was high enough to cause the observed irregularities in the slag structure.

The authors further reported that the slags remained heterogeneous until the end of the blow; however, the irregularities in its structure diminished.[182] This can be explained by the high temperature reached for the final slags compared to the temperature of early slags: The C2S saturation region becomes less sensitive to changes in

the oxidation state of FeO_x and thus, to $p(O_2)$ irregularities in the slag, at high temperatures (Figure 31-b).

Recently, there has been increased interest in measuring the oxygen partial pressure, $p(O_2)$ in industrial slags at multiple sampling positions in the BOF converter in order to get online information about the extent of dephosphorization.[91] Such measurements, if successfully correlated with the ferric to ferrous ratio, would deliver the missing information about the state of oxidation of FeO_x in BOF slags. The dependence of $p(O_2)$ on the sampling position would clarify the extent of $p(O_2)$ gradients in the slag.

5.2 Quaternary CaO-FeO-SiO_2-P_2O_5* system in the low P_2O_5 range

5.2.1 Effect of P_2O_5

The low P_2O_5 part of the quaternary CaO-FeO-SiO_2-P_2O_5* system is the relevant oxide system for the slags resulting from conventional BOF operation. During the BOF process, the initial P content of the hot metal is in the range of 0.07-0.15 wt%, and thus, low P_2O_5 contents in the final slags are obtained, which fall generally within the range of 1-5 wt%.[10, 35, 174] In European BOF plants, the initial phosphorus content is usually less than 0.09 wt%, while Japanese steel plants use hot metal with higher initial phosphorus contents.[12] Even though the slag composition in terms of its CaO, FeO and SiO_2 contents undergoes a large variation during the refining process, the P_2O_5 content of the slag varies within a small range throughout the blow and usually remains below 5 wt%. This is due to the fact that during the main decarburization phase, the FeO content decreases considerably and may reach values as low as 5 wt%.[199] The P_2O_5 content at those conditions does not increase in terms of concentration as in the case of CaO and SiO_2 but decreases instead as a result of the phosphorus reversion from the slag to the metal phase, which occurs at such low FeO-contents in the slag.

Despite the importance of phosphorus control in the BOF process, the thermochemical behavior of the quaternary system CaO-FeO-SiO_2-P_2O_5* at P_2O_5 contents in the range of 1- 5 wt% remains unclear. The composition of BOF slags is usually reduced to the ternary CaO-FeO_x-SiO_2 system during the evaluation of the thermodynamic state of the slag, especially when the P_2O_5 content of the system is less than 2 wt%. Apart from the work of Gao et al.,[104, 105] where the phase diagram of the system was

investigated at 5 wt% P_2O_5 and at a temperature of 1673 K (1400°C), no further experimental works focusing on studying the phase boundaries of the CaO-FeO-SiO_2-P_2O_5* system in the low P_2O_5 range are available, to author's best knowledge.

Figure 32-a) and –b) show the calculated phase boundaries of the CaO-FeO-SiO_2-P_2O_5* oxide system by the BOFdePhos thermodynamic database at a P_2O_5 content of 1 wt% and 3 wt%, respectively, at a temperature of 1873 K (1600°C) and for a reduced $p(O_2)$.

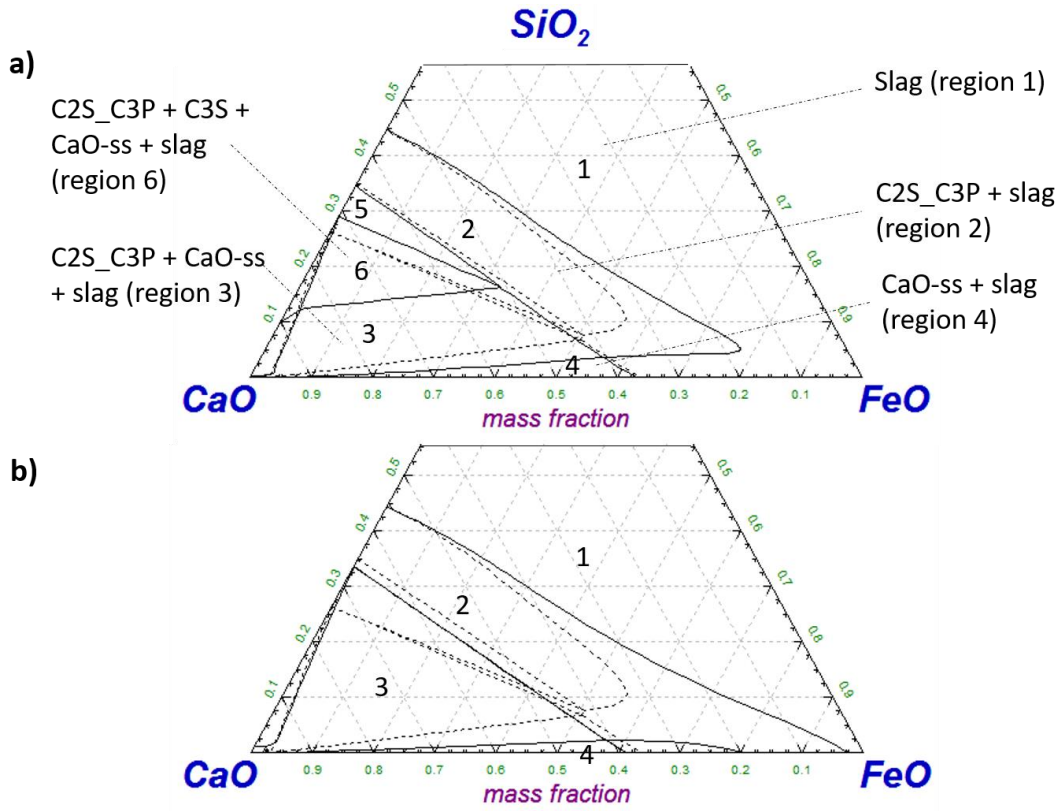

Figure 32: Calculated phase boundaries of the quaternary CaO-FeO_x-SiO_2-P_2O_5* system at a temperature of 1873 K (1600°C) and for a reduced $p(O_2)$ at a) 1 wt% P_2O_5 b) 3 wt% P_2O_5. The dashed lines represent the corresponding phase boundaries of the P_2O_5-free system.

It can be seen from Figure 32 that a P_2O_5 addition at values as low as 1 wt% has a tremendous effect on the system. It was reported in section 4.2.1 that the addition of SiO_2 to the ternary CaO-FeO_x-P_2O_5 oxide system results in the stabilization of the silico-phosphate phase C2S_C3P over the phosphates C3P and C4P phases. Similarly, the addition of P_2O_5 to the CaO-FeO_x-SiO_2 oxide system results in the stabilization of the silico-phosphate C2S_C3P over the silicates C3S and C2S. The

effect of P_2O_5 on the silicate saturation region (of the P_2O_5-free system) can be described as follows:

- The C2S-phase, which dominated the P_2O_5 free system, is now replaced completely by the C2S_C3P phase (region 2). The C3S saturation regions shrink massively in favor of C2S_C3P saturation (region 3 and region 6) at 1 wt% P_2O_5 and disappear completely at 3 wt% P_2O_5. The replacement of C3S phase by the C2S_C3P phase under P_2O_5 addition can be explained by the observed instability of C3S in the ternary CaO-SiO_2-P_2O_5 system when P_2O_5 is added in the range of 2-3 wt% (Figure 22 and Figure 23). The study of the behavior of the quaternary system shows that the C2S_C3P saturation region expands over C3S saturation when the P_2O_5 content of the system is as low as 1 wt%.

- The “nose” of C2S_C3P phase expands in the direction of the FeO corner of the system in comparison to the position of the “C2S nose” in the P_2O_5 free system. At 3 wt%, P_2O_5, the liquid slag region situated between “C2S_C3P nose” and the FeO corner of the system diminishes almost completely in favor of an expansion of the single-phase C2S-C3P saturation region (region 2).

- The single-phase CaO-saturation region (region 4) shrinks massively in favor of the double saturation with CaO-ss and C2S_C3P (region 3). At 1 wt% and 3 wt% P_2O_5, this region can be reached only at SiO_2 contents below 4 wt% and 2 wt%, respectively.

Experimental data on the behavior of the quaternary system were provided by Gao et al.[105] at a P_2O_5 content of 5 wt%, a $p(O_2)$ of $9.24 * 10^{-11}$ atm and a temperature of 1673 K. Such conditions are relevant for dephosphorization in Japanese steelworks, where the hot metal is usually dephosphorized in a separate step prior to decarburization.[18]

Figure 33 shows the position of the C2S_C3P regions reported in these experiments within the corresponding system’s isothermal, which was calculated using the BOF-DePhos database. It can be seen that in accordance with the calculated phase boundaries, the experiments of Gao et al.[105] reported the presence of C2S_C3P phase in

both the low and the high FeO part of the system, up to a FeO content of 90 wt%. Furthermore, the authors reported that no traces of C3S phase could be found in the experimental samples [105], which is in agreement with the calculated phase diagram. It should be noted that similar observations with respect to the expansion of C2S_C3P saturation regions and the instability of C3S phase are observed for the higher temperature (1873 K) and the lower P_2O_5 (1-3 wt%) case (see Figure 32) which fall within the conditions relevant for BOF operation in European steelworks.

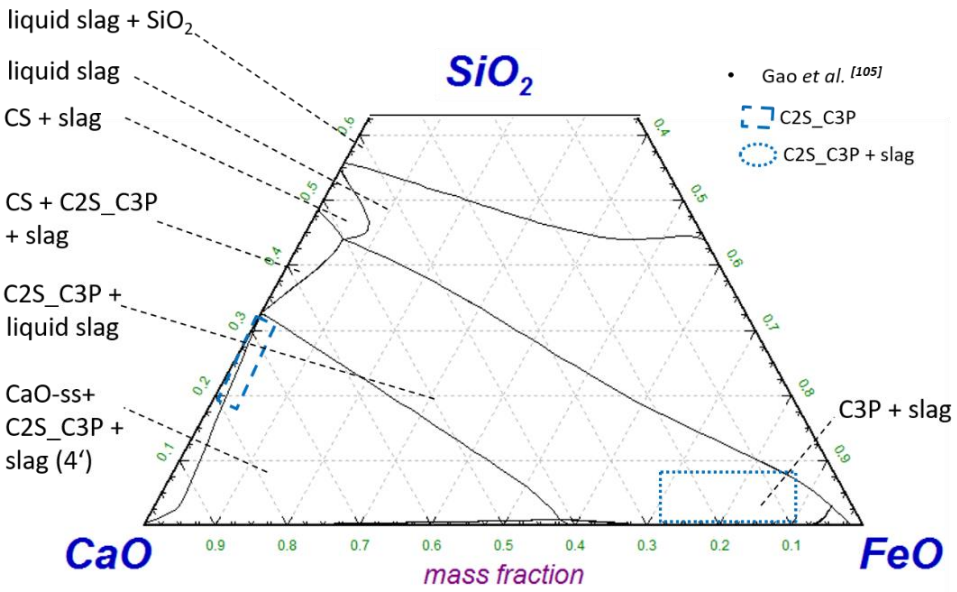

Figure 33: Position of C2S_C3P saturated slags from the experiments of Gao et al. [105] in the calculated phase boundaries of the CaO-FeO_x-SiO_2-P_2O_5* system at 5 wt % P_2O_5, a temperature of 1873 K (1600°C), and a p(O_2) of 9.6 10^{-11} atm: CS denotes the $CaO.SiO_2$ phase (Wollastonite).

5.2.2 Effect of p(O_2)

It should be further clarified whether a change in the oxidation state of iron has a significant effect on the phase boundaries of the CaO-FeO_x-SiO_2-P_2O_5* system. **Figure 34**-a) and -b) show the calculated phase boundaries at a P_2O_5 content of 1 wt% and 3 wt% respectively, a temperature of 1873 K (1600°C) and for both a reduced (solid lines) and an elevated (dashed lines) p(O_2) state. It can be seen that when p(O_2) increases, a significant shrinkage in the C2S_C3P containing regions in favor of an expansion of the liquid slag region occurs. A similar effect was observed previously for the ternary CaO-FeO_x-SiO_2 system with respect to the C2S saturation region. The

shrinkage of the C2S_C3P saturation region with an increase in $p(O_2)$ was observed for the quaternary CaO-FeO_x-SiO_2^*-P_2O_5 system in the high P_2O_5 range (section 4.2.2). A further effect observed in association with an increase in $p(O_2)$ is the expansion in the single-phase CaO-ss saturation region (region 4) in the direction of higher SiO_2 contents as well as a shift in the lime saturation line in the direction of higher CaO-contents, indicating an increase in the lime solubility of the slag. The increase in lime solubility following an increase in $p(O_2)$ was also observed for the CaO-FeO_x-SiO_2^*-P_2O_5 system in the high P_2O_5 range (section 4.2.2) as well as in the ternary system CaO-FeO_x-P_2O_5 (Figure 15) and to a lesser extent, also in the ternary system CaO-FeO-SiO_2 (Figure 29).

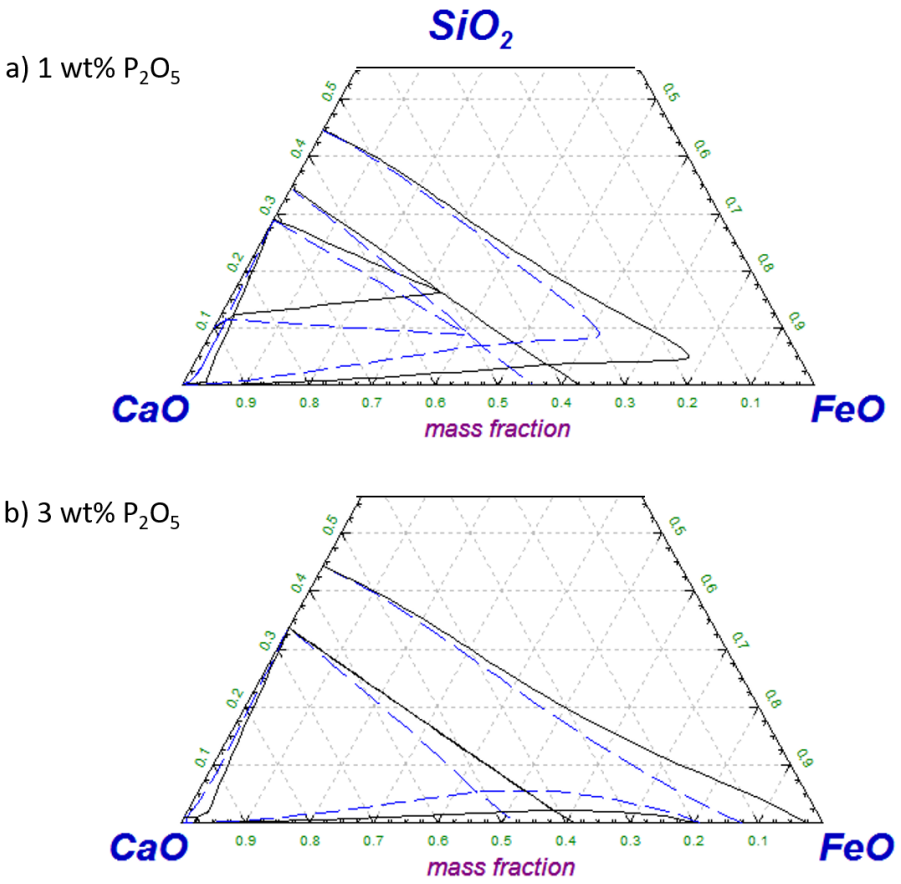

Figure 34: Effect of $p(O_2)$ on the phase boundaries of the system CaO-FeO_x-SiO_2-$P_2O_5^*$ at a temperature of 1873 K (1600°C) at a P_2O_5 content of a) 1 wt% b) 3 wt%. The solid lines represent the reduced $p(O_2)$ case, whereas the dashed lines represent the elevated $p(O_2)$ case.

5.2.3 Effect of temperature

The thermochemical behavior of the CaO-FeO_x-SiO_2-P_2O_5* system in the temperature range 1773 K-1973 K was investigated by means of superimposing the 1773 K (1500°C), 1873 K (1600°C) and 1973 K (1700°C) isothermals, which were calculated using the BOF DePhos database. **Figure 35**-a) and –b) show the calculated phase boundaries of the CaO-rich part of the system at a P_2O_5 content of 3 wt%, for a reduced and an elevated $p(O_2)$, respectively.

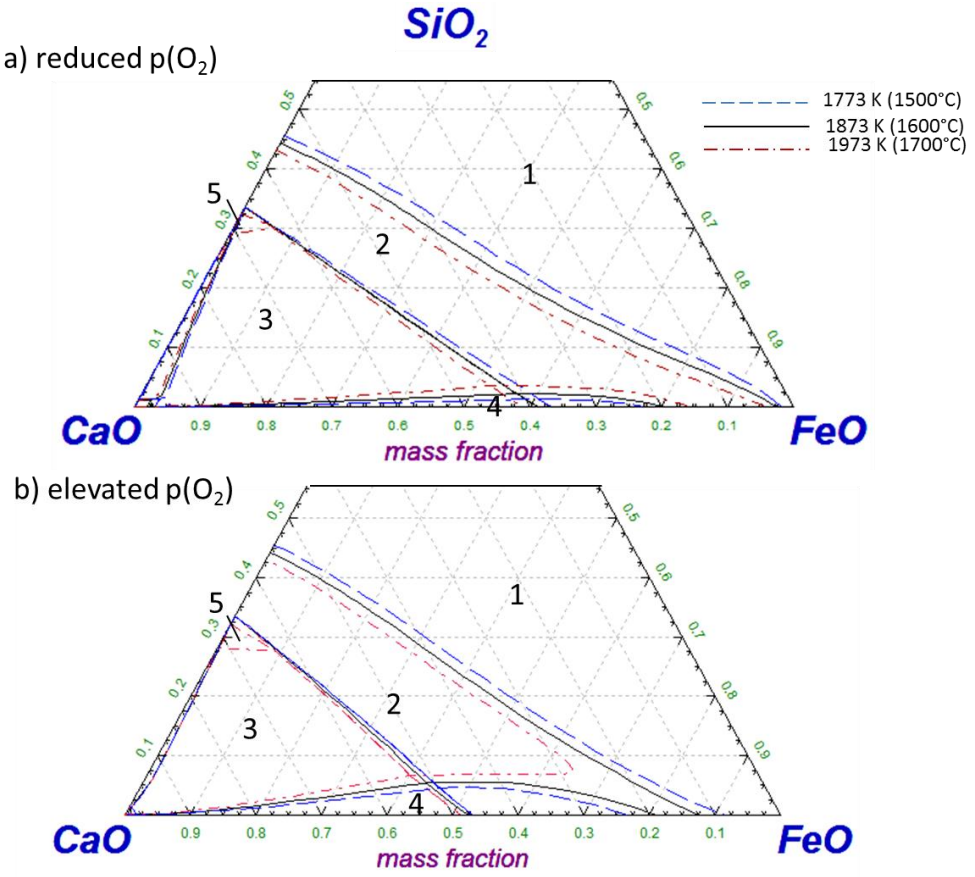

Figure 35: Effect of a temperature variation in the range of 1773 K (1500°C) to 1973 K (1700°C) on the quaternary CaO-FeO_x-SiO_2-P_2O_5* system at 3 wt% P_2O_5, for a) reduced $p(O_2)$ b) elevated $p(O_2)$

It can be seen from Figure 35 that the effect of the temperature on the phase boundaries of the system is very small. The effect of increasing the temperature is similar to that of increasing $p(O_2)$, albeit less significant: A shrinkage of C2S_C3P saturation region in favor of more liquid slag and an increase in lime solubility of the slag is observed, which is more pronounced for the elevated $p(O_2)$ case (Figure 35-b). It can be

seen that at a high temperature of 1700°C and for an elevated p(O_2), the single-phase C2S_C3P saturation region (region 2) no longer covers the total FeO-range, but takes rather a “nose” shape, similar to that of the single-phase C2S saturation region in the P_2O_5-free ternary system (Figure 32).

5.2.4 Conclusion and industrial consequences

Based on the study of the behavior of the quaternary CaO-FeO_x-SiO_2-P_2O_5* system in the low P_2O_5 range of 1-5 wt%, for a temperature range of 1773 K-1973 K, and at different p(O_2) conditions (Figure 32-Figure 35), it can be concluded that low phosphorus industrial BOF slags, which usually lie in the CaO-rich part of the system, are expected to be either saturated with silico-phosphates or double saturated with silico-phosphates and CaO-ss. This means that lime-saturation, which is usually considered as the target slag region in the industrial process, cannot be reached without causing additional silicates precipitations. A single lime saturation can only be achieved at very low SiO_2-contents, lower than 8 wt% (Figure 35), which are not within the typical SiO_2 range for the industrial BOF slags. For example, the maximum SiO_2 content allowed in the slag in case single lime saturation region is the target, at a temperature of 1973 K (1700°C) and for an elevated p(O_2) (Figure 35-b), corresponds to a value of 7 wt% at a P_2O_5 content of 1 wt% and to 4 wt% at a P_2O_5 content of 3 wt%. The limiting SiO_2 value is even lower at lower temperatures and lower p(O_2) values. With an increase in both the temperature and the oxidation state of FeO_x in the slag, the possibility of achieving a purely liquid or single lime saturation region becomes more realistic from a thermodynamic point of view. During the BOF process operation, such conditions may be achieved during the last blowing stage (after 70-80% of the total oxygen is blown), when the main decarburization phase is completed, and the slag temperature and oxidation state increase considerably.

It is also an interesting observation that the C2S_C3P saturation region dominates the CaO-rich part of the system and expands over both the C2S and C3S saturation region at P_2O_5 contents as low as 1 wt%. Due to the high phosphorus dissolving potential of this phase, [87, 91] its stability in the system is highly advantageous for dephosphorization. However, at such low P_2O_5 contents, the formation of the C2S_C3P phase may be rather dominated by the diffusion route rather than by the precipitation route (section 2.4.2). The precipitation of a large amount of solid phase, which is more probable

when the slag is situated in the double saturation region with C2S_C3P and CaO-ss, may inhibit the diffusive mass transfer of phosphorus between the liquid slag and the solid C2S_C3P phase resulting in a poor enrichment of phosphorus in C2S_C3P. Thus, it is recommended to avoid the double saturation region with C2S_C3P and CaO-ss, due to the associated risk of excessive solid phase precipitations. Based on the present findings. An optimal slag zone for dephosphorization is thus considered to lie within the single saturation region with C2S_C3P. At the same time, the amount of precipitated solid phase shall be controlled carefully in order to avoid excessive solid phase precipitations, and the associated kinetic withdraws for dephosphorization. The specification and the control of the target slag region for the achievement of optimal dephosphorization are discussed in detail in section 7.2.

5.3 Effect of addition of minor oxides MgO, Al_2O_3, and MnO

5.3.1 Effect of MgO and Al_2O_3

The effect of MgO- and Al_2O_3-addition on the phase boundaries of the CaO-FeO_x-SiO_2 system at 1873 K (1600°C) and reduced p(O_2) is illustrated in **Figure 36**. The formation of C3S-phase was suppressed during the simulations for the sake of enhanced readability of the diagrams. Thus, the C2S phase is considered representative of the silicate phases of the system. It can be seen that the addition of Al_2O_3 or MgO up to a value of 7 wt% resulted in the shrinkage of the single-phase C2S saturation region (marked blue) in favor of an expansion of both liquid slag (marked green) and single lime saturation regions (marked purple) with the effect of Al_2O_3 being stronger than that of MgO. For MgO-content equal or higher than 4 wt%, a miscibility gap occurs in the monoxide phase, and two monoxide solutions, CaO-ss and MgO-ss, are formed. As a result, the single CaO-ss saturation (marked purple) shrinks at the lower SiO_2 part in favor of the formation of a new double saturation region with both CaO-ss and MgO-ss. Also, a new four-phase-region is formed, which contains a liquid slag and three solid phases, a silicate phase (C2S or C3S), CaO-ss and MgO-ss (marked grey). The formation of the four-phase-region results in the shrinkage of the single-phase C2S saturation region (marked blue). The area of the four-phase-region (marked grey) increases with an increase in MgO and covers a considerable part of the single-phase C2S saturation region (marked blue) in the low FeO part of this region at a MgO-content of 7 wt%.

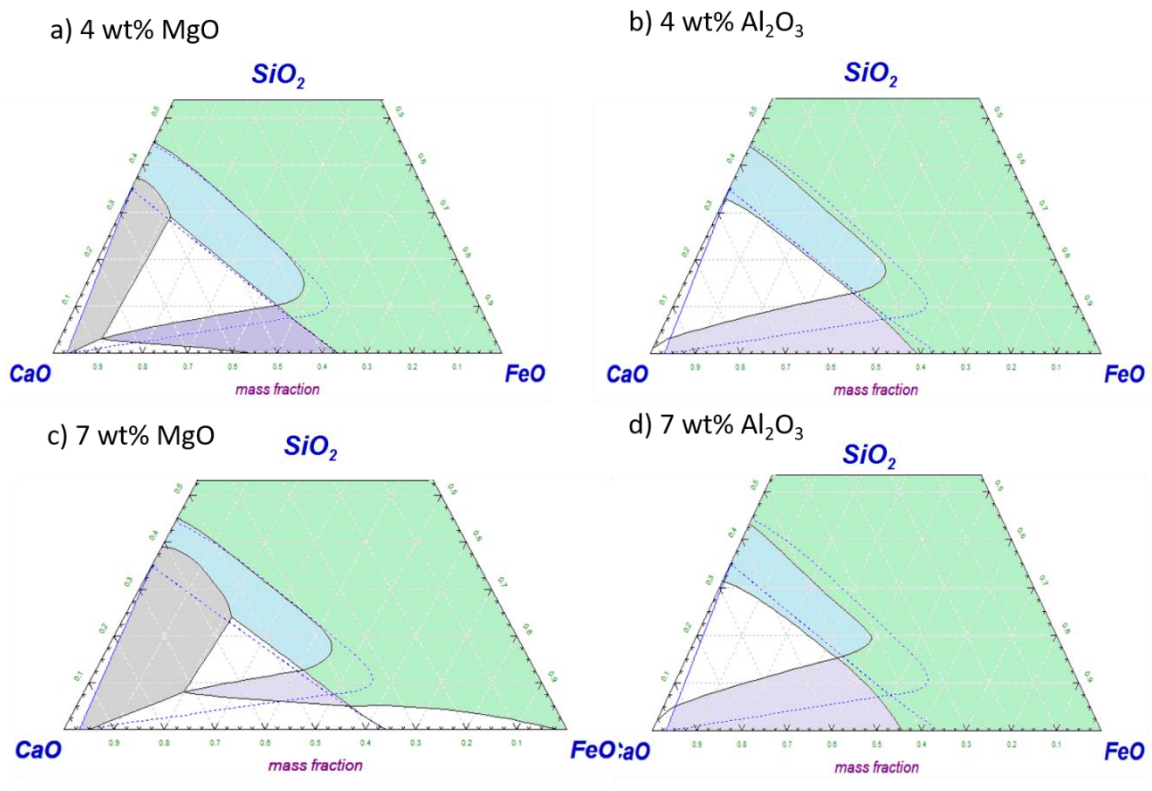

Figure 36: Effect of the addition of 4 wt% a) MgO b) Al_2O_3, and of 7 wt% c) MgO d) Al_2O_3 on the phase boundaries of the CaO-FeO_x-SiO_2 system at 1873 K (1600°C) and reduced p(O_2). The dashed lines represent the phase boundaries of the ternary CaO-FeO_x-SiO_2 system. The formation of C3S-phase was suppressed during the simulations for the sake of simplification.

5.3.2 Effect of MnO addition

Figure 37-a) shows the effect of adding 7 wt% MnO to the CaO-FeO_x-SiO_2 system at 1873 K (1600°C) and reduced p(O_2) while Figure 37-b) shows the effect of the combined addition of 7 wt% MnO and 7 wt% MgO.

It can be seen from Figure 37-a) that the effect of MnO on the phase boundaries of the CaO-FeO_x-SiO_2 system at a content of up to 7 wt% is negligible. However, Figure 37-b) shows that the effect of the addition of 7 wt% MnO to the CaO-FeO_x-SiO_2-7% MgO system (Figure 36-c)) is considerable: The single C2S saturation region (marked blue) shrinks massively in the low FeO part in favor of the formation of a three-phase-region containing liquid slag, C2S and a monoxide phase, which contained mainly FeO, MgO, and MnO.

It can be thus concluded that for a proper evaluation of the state of CaO-FeO_x-SiO_2 based slags, which is the case for BOF slags, it is crucial to include the effect of minor oxides addition. The effect of a minor oxide might be negligible at a single addition but may become considerable when added in a certain combination, as observed in the case of MnO addition. In this context, the usage of a consistent thermodynamic database, developed according to the CALPHAD-approach, such as the present BOFdePhos thermodynamic database, is a powerful method to gain valuable insights on the behavior of a specific system under consideration of a large number of components and possible phases.

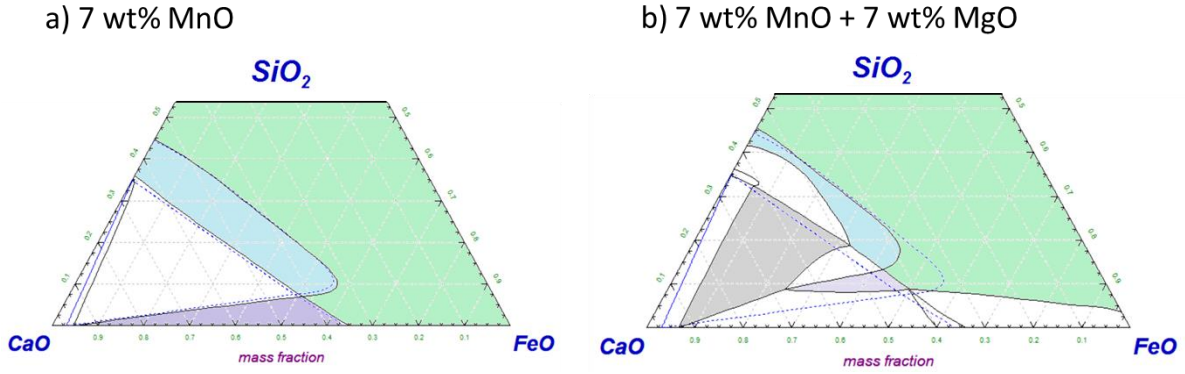

Figure 37: Effect of MnO-addition at 7 wt% on a) CaO-FeO_x-SiO_2 system, and b) CaO-FeO_x-SiO_2-7% MgO system, at 1873 K (1600°C) and reduced p(O_2). The dashed lines represent the phase boundaries of the original CaO-FeO_x-SiO_2 system. The formation of C3S-phase was suppressed during the simulations for the sake of simplification.

5.4 Modeling of the phosphorus distribution in heterogeneous slags

Based on the analysis of the oxides systems relevant for BOF slags in the previous sections (5.1-5.3), it can be concluded that BOF slags are heterogeneous and saturated with different silicates and monoxides. However, most Lp-approaches available in the literature are developed for purely liquid CaO-FeO_x-SiO_2 based slags (Table 2). In this section, an attempt is made to develop an Lp-relation, which is applicable for heterogeneous slags in the total composition and temperature range relevant for the BOF process. Thus, a large number of Lp-calculations were carried out in the present work using the developed BOFdePhos thermodynamic database. In total, 550 calculation data were generated in the temperature range of 1673 K-2023 K.

It should be noted that for temperatures below 1811 K (1538°C), the formation of solid iron solution phases (α-Fe, γ-Fe, and δ-Fe) was suppressed in the simulations. Thus, an extrapolation to the case where a liquid-Fe solution is stable at such conditions is made. In the industrial process, the presence of carbon in the hot metal lowers the melting point of the liquid metal phase, and thus, the metal phase remains liquid throughout the entire process even though the initial temperature is lower than 1673 K (1400°C). In the simulations, the addition of the element carbon to the liquid iron phase would lead to a reduction of FeO_x and, thus, to a modification of the initial slag composition. This is also the reason behind the non-availability of experimentally established Lp-relations below 1823 K (1550°C): A reduction of FeO_x contained in the slag by the carbon contained in the metal phase and in some cases, also with the carbon contained in the gas phase occurred [97].

5.4.1 Phosphorus distribution in a liquid slag

The following Lp-correlation was developed for purely liquid $CaO\text{-}FeO_x\text{-}SiO_2$ based slags by means of regression fitting of the calculation data with an R2 value of 0.83:

$$Log(Lp_{liq}) = 0.09 * (\%CaO)_{liq} + 0.07 * (\%FeO)_{liq} - 6.05 * 10^{-4} * (\%FeO)_{liq}{}^2 + 16456.469 * 1/T - 12.336 \quad (26)$$

It should be noted that the decimal logarithm is used in equation (26). The terms $(\%CaO)_{liq}$ and $(\%FeO)_{liq}$ denote the CaO- and the FeO-content of the liquid slag, respectively.

Equation (26) is also applicable for describing the phosphorus distribution in the liquid slag part of a heterogeneous slag. This will be described in detail in section 5.4.2.

5.4.2 Phosphorus distribution in a C2S_saturated slag

As discussed in the previous sections (5.1-5.3), BOF converter slags are saturated with silicates and monoxides for a large part of the blowing process. Thus, the investigation of the effect of the presence of these solid phases on the phosphorus distribution of heterogeneous slags is important for a proper assessment of the equilibrium state of the dephosphorization reaction during the industrial process. The results of the thermodynamic evaluations of the quaternary $CaO\text{-}FeO_x\text{-}SiO_2\text{-}P_2O_5$

system revealed that the presence of P_2O_5 oxide in the slag stabilized the C2S_C3P phase over the C2S and C3S phases. It is found that phosphorus dissolves in the solid C2S_C3P solution phase, by substituting some of the silicates with phosphates. As a result, P_2O_5 can be dissolved in the C2S_C3P phase up to its stoichiometric solubility limit of about 22 wt%.

The calculations results for Lp between C2S-C3P saturated slags and liquid metal using the BOFdePhos thermodynamic database are presented in **Figure 38** as a function of the mass ratio between C2S_C3P and liquid slag, further denoted as W. It can be seen that Lp-values in the range of 10^3 and higher were calculated when W was equal or higher than 0.3. Also, Lp increased with the basicity of the liquid slag part, termed basicity $_{liq}$, which is defined as the CaO/SiO_2 weight ratio in the liquid slag part.

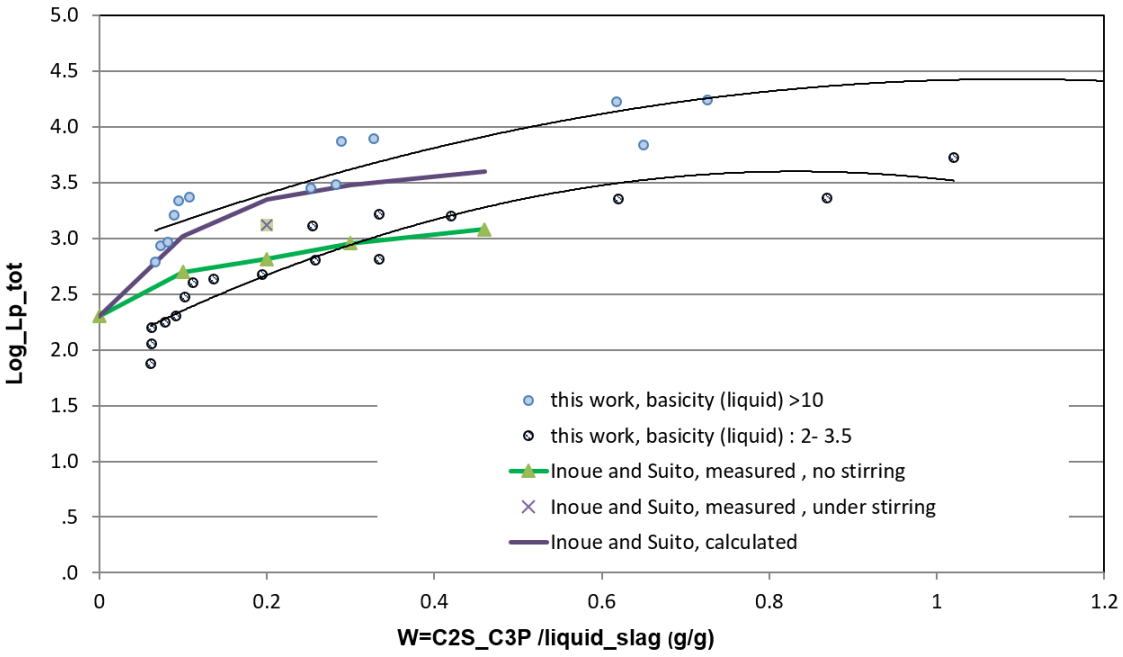

Figure 38: Presentation of the results of the thermodynamic simulations for C2S_C3P saturated slags in the system $CaO\text{-}FeO_x\text{-}SiO_2$-2 wt% P_2O_5, for a temperature range of 1823 K-1873 K, and comparison with the results of Suito and Inoue [113] at 1833 K, [%P]= 0.5 wt% and a slag/metal ratio of 1/10.

In a series of experiments, Inoue and Suito [113-115] investigated the phosphorus enrichment in solid C2S_C3P phase via both the precipitation (by heating up and subsequently cooling a C2S-saturated slag) and the diffusion route (by adding C2S particles

to a liquid slag). In addition, they performed a variety of phosphorus distribution measurements in C2S_C3P containing slags. The authors reported that by adding C2S particles to liquid slags, Lp increased drastically compared to the case of purely liquid slag, as a result of the formation of the C2S_C3P phase. Some of their results with respect to Lp-measurements and Lp-calculations, which were made using their own Lp-approach, [113] are presented in Figure 38. The results show that the calculated Lp-values by Suito and Inoue [113] were in the same range as those resulting from the present thermodynamic simulations for the high basicity case, exceeding 10^3 when W was higher than 0.1. The experimental behavior was in agreement with the results of the thermodynamic simulations and showed an increasing trend when W increased. Even though the experimental results of Suito and Inoue [113] were generally below the calculation results, and attained a maximum of 10^3 at a W value of 0.45, they are still considerably higher than in the case of purely liquid slags (case W = 0). Thus, their results [113] confirm that the C2S_C3P phase has a strong potential in dissolving phosphorus. However, their results also suggest that the enrichment of solid C2S_C3P phase with phosphorus is associated with kinetic limitations and that a limiting W value exists, above which no further Lp increase occurs in the laboratory experiments. Interestingly, the authors observed that Lp increased by about 80% when stirring was applied for a slag at a W of 0.2 (Figure 38). This may be an indication of a possible blocking layer removal phenomenon, probably similar to that observed during lime dissolution [202]. In recent work, Gu et al. [203] observed that the overall mass transfer coefficient for dephosphorization in a liquid slag increased by a 2 order of magnitude when carbon is present in the metal phase due to the stirring effect provided by the formation of CO. It is possible that the stirring effect of CO gas may additionally contribute to Lp-enhancement in a heterogeneous slag in a similar manner to the observed Lp-increase in the experiments of Suito and Inoue. At the same time, the presence of CO gas may decrease the interface between C2S_C3P and liquid slag, and thus, it may inhibit the mass transfer of phosphorus between liquid slag and solid C2S_C3P. Thus, additional experimental studies are required to clarify the behavior of Lp in C2S-saturated slags under foaming conditions.

Finally, the following Lp-equation was developed by means of multi-linear-regression fitting of the simulation results for C2S_C3P containing slags in the temperature range of 1673 K-2023 K with a regression coefficient of 0.922:

$$Log(Lp_{C2S-sat.}) = 2.361W + 0.1071\ basicity_{liq} + \frac{14537.691}{T} - 5.938 \qquad (27)$$

The industrial analysis of the morphology of BOF slags provided by Preßlinger et al. [118] from the Voestalpine plant and DeO et al. [10] from several European and Indian steel plants confirmed that the final slags were C2S-saturated and that a large part of P_2O_5 was present in this solid phase under formation of C2S_C3P phase. Thus, the contribution of C2S_C3P to phosphorus removal is not restricted to hot metal dephosphorization processes, which are part of the refining route in Japanese steelworks, but is also confirmed for industrial slags taken during the standard BOF operation. However, the maximum P_2O_5-contents, which were measured in the C2S_C3P phase in those slags was in the range of 5 wt%, [10, 118] which is much lower than its solubility limit. In general, the Lp-values measured in the industrial process are much lower than those predicted by the present thermodynamic simulations (Figure 38) as well as those measured in a number of experimental investigations [113-115]. This can be explained by the fact that BOF slags have a low P_2O_5 content, usually lower than 3 wt%, which implies that the diffusion route is the dominant route for phosphorus enrichment of the solid C2S_C3P phase. The enrichment grade of the solid phase with phosphorus through the diffusion route is reported to be much lower than that achieved through the precipitation route [98, 111, 113, 114] (see section 2.4.2).

5.4.3 Description of phosphorus distribution in BOF slags

Based on the findings introduced in the present work, it can be concluded that an adequate description of the P-distribution between a CaO-FeO_x-SiO_2 based heterogeneous slag and a liquid metal phase should consider the amount, type and composition of the different slag phases. However, most Lp-approaches reported in the literature were developed for purely liquid slags. At the same time, the direct application of the Lp-relation given by (27) would lead to an overestimation of Lp since no kinetic

limitations on the phosphorus enrichment of the solid phase can be considered in the thermodynamic simulations.

Even though some industrial observations [10, 118] confirmed that the C2S_C3P phase made a considerable contribution to the removal of phosphorus, little attention was given to the incorporation of the role of this solid phase in phosphorus removal or prediction strategies during the conventional BOF operation. Apart from some few works, such as the work of Deo and al. [10], little effort has been made to incorporate the formation and dissolution of the C2S phase in the development of industrial-based Lp-relations. As a result, systematic industrial evaluations of the phosphorus distribution between the solid C2S phase and the liquid slag (Lp $_{slag}$) are not available to the author's best knowledge. On a laboratory scale, several investigations are available in the literature (see section 2.4). The maximum phosphorus distribution ratio measured between the C2S phase and CaO–SiO_2–Fe_tO slags reported in those works [114, 121] was obtained at the nose of the single-phase C2S saturation region (Figure 5-a).

The results of experiments carried out by Ito and Sato [121] and later by Inoue and Suito [114] showed, that phosphorus distribution between the C2S_C3P phase and the liquid slag phase, termed Lp $_{slag}$ (see equation (13)), depended mainly on the liquid slag composition and had maximum values at the nose of C2S_saturation region (see Figure 5-a). The following relation was developed within the present work to fit the experimental data of Suito and Inoue [114]:

$$Log\left(Lp_{slag}\right) = -0.0602 * (\%SiO_2)_{liq} + 2.1652 \quad (28)$$

In equation (28), $(\%SiO_2)_{liq}$ denotes the SiO_2-content of the liquid slag part.

The temperature dependence of the phosphorus distribution ratio between the C2S and the liquid slag phase is found to be very small, and no direct dependence on the slag basicity could be established in those works. [114, 121]

Finally, equation (29) has been developed in the present work to describe the phosphorus distribution between a heterogeneous slag (containing C2S, and/or C3S and/or monoxide phases) and liquid metal phase based on the formulation provided by Inoue and Suito [114], given by equation (14):

$$Lp_{tot} = \frac{Lp_{liq}\left(1 + Lp_{slag} * W_{<lim}\right)}{1 + W}\left(1 - f_{non-P-dissolving\ phases}\right) \quad (29)$$

The term W is defined as the ratio of the C2S_C3P and liquid slag phase fractions in the heterogeneous slag (W = C2S/slag $_{liq}$), $W_{<lim}$ is this ratio with a maximum value of W_{lim} and f $_{non\text{-}P\text{-}dissolving\ phases}$ denotes the total fraction of the phases which do not dissolve phosphorus, such as C3S, CaO-ss, and MgO-ss in the heterogeneous slag. The term Lp $_{liq}$ corresponds to the phosphorus distribution between the liquid slag and the liquid metal, given by equation (26). In addition, a large number of formulations are available for Lp $_{liq}$ in the literature (Table 2). The results of the thermodynamic simulations, carried out in the present work indicate that Lp $_{liq}$ is a strong function of temperature, CaO- and FeO-content [2]. The limiting value $W_{<lim}$ has been introduced into equation (29) to limit the diffusive mass transfer from liquid slag to the solid phase when the C2S/slag $_{liq}$ ratio exceeds a certain value, which is estimated to lie in the range of 0.3-0.45 based on the experiments of Suito and Inoue [113-115].

It can be seen from equation (29) that the determination of the type, amount and composition of the different slag phases (liquid and solid) of a heterogeneous BOF slag is essential for the evaluation of its dephosphorization potential. Here, the application of a CALPHAD-based approach presents a powerful method for the accurate determination of the type, amount and composition of a large number of oxide systems combination over the entire temperature, composition, and oxygen partial pressure range relevant for the BOF process.

5.5 Effect of minor oxides on the dephosphorization potential of BOF slags

Even though the Lp-approach developed in the present work (equation (29)) does not explicitly include the effect of minor oxides addition to CaO-FeO_x-SiO_2 based slags, their effect is indirectly incorporated through the consideration of the type and amount of the different phases in the slag. It is found that minor oxides such as MgO, Al_2O_3, and MnO have a considerable effect on the phase boundaries of CaO-FeO_x-SiO_2 based slags (see section 5.3). The formulation of Lp $_{tot}$, given by equation (29), takes into account the effect of temperature, oxygen partial pressure, and minor oxides on the phase boundaries of the CaO-FeO_x-SiO_2 based slags based on the following:

- The type and the ratio of the different solid phases (C2S, C3S, CaO-ss, MgO-ss,…) are included in the terms W = C2S/slag $_{liq}$ and f $_{non\text{-}P\text{-}dissolving\ phases}$.
- Changes in the phase boundaries of the system will result in a modification of the composition of the liquid slag phase. The terms Lp $_{liq}$ and Lp $_{slag}$ in equation (29) are a strong function of the liquid slag composition, as shown in equation (26) and (28), respectively.

It was mentioned in section 2.3 that there is a large discrepancy between laboratory and industrial observations with respect to the effect of MgO on dephosphorization. Apart from the work of Basu et al. [94], Lp-relations developed based on fitting experimentally established equilibrium data (see examples in Table 2) reported a positive effect of MgO on Lp, similar to that of CaO, while the majority of industrial plant trials reported either a moderate or a strong negative effect. [10, 12, 24, 92, 95, 96, 204] Chen et al. [92] reported that Lp measured in samples taken from an 80 tons BOF converter was reduced significantly from a value of 120.7 to 75.7 when the average MgO content in the final slag increased from 7 to 9.8%, respectively.

Based on the study of the CaO-FeO_x-SiO_2 system provided in section 5.1, it was concluded that industrial slags are heterogeneous and contain different types of solid phases (C2S, C3S, CaO-ss,…). Since laboratory-based studies were carried out in purely liquid slags, it is possible that the positive effect of MgO on Lp is only valid for purely liquid slags or in the liquid slag part of heterogeneous slags. It has been found that the presence of MgO has a decreasing effect on the stability range of the phosphorus dissolving C2S phase (Figure 36) and an increasing effect on the stability range of non-phosphorus dissolving monoxide type of phases (CaO-ss, MgO-ss,…), the resulting overall effect on Lp $_{tot}$ (given by equation (29)) is negative. A further possibility is that the presence of MgO inhibits the enrichment of solid phase C2S_C3P with phosphorus through the diffusion route, due to its increasing effect on the amount of solid phase precipitates. The diffusion route is considered as the significant enrichment route for C2S_C3P phase with phosphorus during the BOF process.

The effect of Al_2O_3 addition on CaO-FeO_x-SiO_2 based slags has been subject to several investigations in the literature.[10, 24, 205, 206] Recently, Drain et al. [24] assessed more than 90 Lp-equations based on industrial data and concluded that Al_2O_3 had a weak

negative effect, except at low oxygen potential ranges, where a positive effect was observed. It was reported at TATA Steel's Plant in IJmuiden (the Netherlands) [205, 206] that Al_2O_3-contents above 3.5 wt% had a negative effect on dephosphorization. DeO et al. [10] observed that the presence of Al_2O_3 decreased the amount of solid C2S phase in the slag as well as its phosphorus content and overall, a negative effect on dephosphorization was observed. Thus, it can be concluded that, so far, there is no agreement on the effect of Al_2O_3 on the dephosphorization potential of industrial slags, and that the majority of works reported a negative effect.

Based on the analysis of the effect of Al_2O_3 addition on the phase boundaries of the CaO-FeO_x-SiO_2 system, provided in section 5.3, it was concluded that Al_2O_3 has a strong decreasing effect on the stability range of the phosphorus dissolving C2S phase in favor of more liquid slag formation (Figure 36). It is thus possible that the negative effect of Al_2O_3 addition on dephosphorization, observed during the industrial investigations, is related to its decreasing effect of C2S phase amount, which results in decrease Lp_{tot}. The positive effect of Al_2O_3 in the low oxygen potential range that is, in the low FeO_x range, reported by Drain et al. [24], can be explained as follow: At low FeO_x contents in the slag, excessive C2S precipitations are expected which may result in exceeding the optimal $W = C2S/slag_{liq}$ ratio, denoted as W_{lim} in equation (29). At such conditions, the presence of Al_2O_3 in the slag may result in the setting of an adequate C2S/liquid ratio by increasing the liquid slag amount without increasing monoxide precipitations, as in the case of MgO addition. This results in a positive effect of Al_2O_3 on Lp_{tot}, which explains the observations of Drain et al. [24] for BOF slags in the low oxygen potential range.

6 Analysis and discussion of industrial plant trial results

6.1 Morphology of high P slags

6.1.1 Samples from an LD-AC process

Fix and Koch [182] studied the morphology of a large number of industrial slags, resulting from the refining of high phosphorus hot metal in an LD-AC converter, which were taken from 4 different steel plants in Germany: Salzgitter, Dillingen, Peine and Maximilianhütte. A representation of the measured composition of the slags in the quaternary system CaO-FeO_x-P_2O_5-SiO_2 was provided by the authors,[182] which is shown in **Figure 39** for 2 steel plants. In both plants, the oxygen blow was carried out over 2 blowing periods, with an intermediate slag tapping. The slag tapped after the first blowing period is designated as “1 st slag” and the final slag tapped at the end of the second blowing period is designated as “2 nd slag”. It can be seen from Figure 39 that both slags have a high P_2O_5 content, which varied between 20 and 30 wt% for „1st slag“ type, and between 5 and 15 wt% for “2 nd slag” type. In addition to a lower P_2O_5 content, slags of type “2 nd slag” had a lower SiO_2 content ranging between 3-6 wt% compared to slags of type “1 st slag” which had a SiO_2 content ranging between 6-12 wt%.

The authors reported that the microscopic examination of the samples indicated the presence of solid C2S_C3P phase with a high content in the large majority of the samples. This is an interesting observation considering the fact that slags of type „2 nd slag“ had a low SiO_2-content with an average value of 4 wt%. Those observations are in agreement with the thermodynamic evaluations of the quaternary CaO-FeO_x-P_2O_5-SiO_2 oxide system (Figure 17) and confirm the stability of this solid phase in the industrial process.

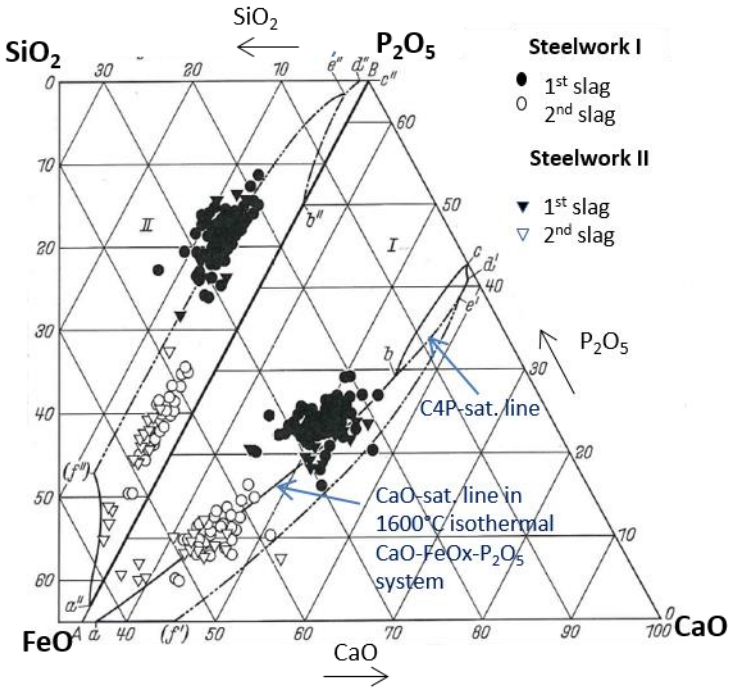

Figure 39: Composition of industrial slag samples taken from 2 steel plants in Germany equipped with an LD-AC converter with a double slag operation, presented in the quaternary system FeO-CaO-P_2O_5-SiO_2. The terms „1 st slag“ and „2 nd slag“ designate the slags tapped after the first blowing period and after the second blowing period, respectively. Adapted with permission from Ref.[182]

In order to evaluate the lime saturation state of the industrial samples, the authors drew the lime saturation line, which they determined for the ternary CaO-FeO_x-P_2O_5 system at 1873 K (1600°C), in the quaternary system presentation in Figure 39. It can be seen that the large majority of the slag samples of type „1 st slag“ lie outside or very close to the considered lime saturation region. Accordingly, the authors found no evidence of lime saturation in the samples. However, even though slag samples of type „2 nd slag“ lie exactly along or below the lime saturation line, no trace of lime saturation was found in the corresponding samples. The authors [182] concluded that the phase diagram presentation of the ternary CaO-FeO_x-P_2O_5 system is not sufficient to evaluate the lime saturation state of quaternary FeO-CaO-P_2O_5-SiO_2* slags, and that the phase boundaries of the quaternary CaO-FeO_x-P_2O_5-SiO_2 system as well as of higher-order systems should be determined for a proper evaluation of the state of industrial samples.

In order to verify this statement, the lime saturation line of the quaternary system is calculated using the BOFdePhos thermodynamic database for 4 different SiO_2 contents (0, 5, 10 and 15 wt%), for a temperature of 1873 K (1600°C), and for an elevated $p(O_2)$ state (**Figure 40**). When including the average composition of „1st slag“ and „2 nd slag“ samples in Figure 40, which is determined using the data provided in Figure 39, it becomes obvious that samples of type „ 2 nd slag“ are situated close or exactly underneath the lime saturation line for the SiO_2-free system (dashed line in Figure 40). However, when considering an SiO_2 content equal to or higher than 5 wt%, the samples of type „ 2 nd slag“ become situated outside of the lime saturation region. Since the average SiO_2 content of the industrial slags of type “2 nd slag” was reported as higher than 4 wt%, it can be concluded that they will not be lime saturated (region 4’ Figure 17-b) but rather saturated with C2S_C3P (region 3’ Figure 17-b). This is in accordance with the results of the microscopic examination of the samples, which indicated that the samples were C2S_C3P saturated and no evidence of lime saturation could be found.[182] It should be mentioned here that the evaluation of the effect of temperature on lime saturation showed that the temperature has a negligible effect in both the ternary and the quaternary system (Figure 20, Figure 30, Figure 35). Thus, a higher process temperature does not explain the absence of lime saturation in the industrial samples. It can be concluded that the observations of Fix and Koch [182] can be explained by the thermochemical behavior of the quaternary system CaO-FeO_x-P_2O_5-SiO_2 and point to the limitations associated with using the ternary system CaO-FeO_x-P_2O_5 for the evaluation of industrial plant trials results.

Furthermore, the authors reported that increasing lime consumption during the first blowing period of the process did not result in reaching lime saturation. The higher the amount of lime charged during the process, the higher the amount of undissolved lime, which was found later in the samples despite the absence of lime saturation. Based on the thermodynamic evaluations provided in section 4.2.1, those observations can be explained by the difficulty in accessing the lime saturation region in the quaternary FeO-CaO-P_2O_5-SiO_2* system. This is due to the fact that a single-phase CaO-ss saturation is not possible to achieve in this system without additional saturation with the C2S_C3P solid phase. An increase in the CaO amount of the slag will result in increasing the amount of C2S_C3P precipitation. As a result, a significant decrease in

the slag liquid amount, an increase in the slag viscosity, as well as a decrease in the interface between liquid slag and undissolved lime, occurs. Those factors contribute to the inhibition of lime dissolution procedure in the slag. The fact that this behavior was reported as more typical of „1st slag“ than of „ 2 nd slag“ type can be attributed to the lower FeO-content of „1st slag“ and thus to the higher C2S_C3P precipitations. In summary, the presence of high amounts of solid C2S_C3P precipitations provides unfavorable kinetic conditions for lime dissolution. As a result, the slag remains within the C2S_C3P saturation (region 3') and does not enter lime saturation (region 4') despite the addition of high amounts of lime during the process.

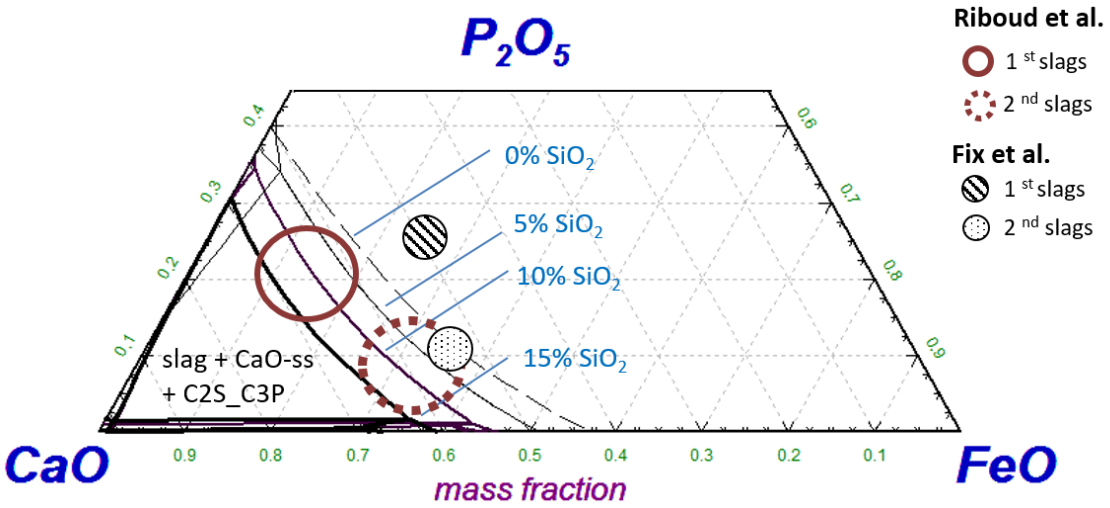

Figure 40: Presentation of the average composition of „1 st slag“ and „2 nd slag“ sample types taken from the LD-AC process, which were reported by Fix and Koch [182] as well as those reported by Riboud and Margot [172], in the quaternary FeO-CaO-P_2O_5-SiO_2* system. The lime saturation lines were calculated using the BOFdePhos thermodynamic database, at a temperature of 1873 K (1600°C), for an elevated $p(O_2)$ state and for 4 different SiO_2 contents: 0, 5, 10 and 15 wt%

6.1.2 Samples from an OLP process

A further investigation of the state of industrial high phosphorus slags was provided by Riboud and Margot,[172] where 43 slag samples of type „1 st slags“ and „2 nd slags“ were taken from a 30 tons OLP-converter, which is very similar to the LD-AC process.

The estimated average compositions of the „1 st slags „ and „2 nd slags“ investigated by Riboud and Margot [172] are presented in the quaternary system FeO-CaO-P_2O_5-SiO_2 along with that of Koch and Fix [182] (Figure 40). The SiO_2 content of „1 st slags „

and „2 nd slags“ was in the range of 4-8 wt% and 2-3 wt%, respectively. The samples further contained small amounts of MnO, MgO, and Al_2O_3 with an average value of about 2, 1.5 and 0.4 wt%, respectively.[172]

It can be seen from Figure 40 that the composition of „1 st slags” samples investigated by Riboud and Margot,[172] which had an SiO_2 content in the range of 4-8 wt%, lies within the double saturation region with C2S_C3P and CaO-ss. However, contrary to the results of Fix and Koch,[182] the authors reported that the microscopic examination of the samples did not show any evidence of C2S_C3P saturation of the samples, apart from some few exceptions.[172] Interestingly, the authors reported that the microscopic examination of synthetic laboratory slags, which had a similar composition to the industrial samples and which were investigated at an experimental temperature of 1773 K (1500°C) showed that they were saturated with the C2S_C3P solid phase. The authors [172] attributed the discrepancy between the experimental and industrial observations to the fact that the process temperature is probably higher than 1773 K (1500°C), and that the C2S_C3P phase is not stable for this temperature range which explains the absence of C2S_C3P saturation of the industrial samples. However, the thermodynamic evaluations of the corresponding quaternary system, indicate that the temperature has a negligible effect on the phase boundaries of the system (Figure 20) and that the C2S_C3P phase dominates the CaO-rich part of the system for the entire temperature range of 1773 K (1500°C) to 1973 K (1700°C).

Considering the discrepancy between the results of the microscopic examination of industrial high phosphorus slags between both works [172, 182] as well as the discrepancy between laboratory and industrial investigations of Riboud and Margot [172] concerning the presence of the C2S_C3P solid phase, it can be concluded that the structure of industrial slag samples investigated by Riboud and Margot [172] was possibly modified during the sampling and/or quenching procedure. Such a modification in the slag structure may have resulted from a change in the oxygen partial pressure, $p(O_2)$, of the system during the sampling and/or quenching procedure. This presumption is based on the evaluation of the effect of $p(O_2)$ on the phase boundaries of the relevant ternary and quaternary system, presented in section 4.1.1 and 4.2.2, respectively. It was shown that $p(O_2)$ has a strong effect on the boundaries of the C2S_C3P saturation regions (Figure 19). The description of the sampling and quenching procedure in both

works [172, 182] indicates that the samples were taken by a “slag spoon” from the surface of the slag. Strong oxidation of the sample may occur if the transport and quenching of the sample are not quick enough, which may have been the case for the plant trials of Riboud and Margot [172].

The results of the microscopic analysis of „2 nd slags“ samples reported by Riboud and Margot [172] showed that they were all saturated on CaO-ss. The SiO_2 content of those slags was in the range of 2-3 wt% with an average value of 2.4 wt%. Thus, the system components can be reduced to the ternary CaO-FeO_x-P_2O_5 system. It can be seen from Figure 40 that those samples fall within the single-phase CaO-ss saturation region (underneath the dashed line), which is in accordance with the findings of the authors.[172] In the ternary CaO-FeO_x-P_2O_5 system, lime saturation can be reached easily. However, when SiO_2 is present with a content equals or higher than 5 wt%, the system is dominated by C2S_C3P saturation regions, and lime saturation cannot be reached without additional saturation on C2S_C3P. This further supports the assumption that excessive C2S_C3P precipitations have a negative effect on the kinetics of lime dissolution.

6.1.3 Conclusion

In this section, different sets of industrial samples from high phosphorus slags were investigated. The following conclusions were derived based on a comparison between the microscopic analysis of the samples reported in the literature, [172, 182] and the thermodynamic evaluations of the quaternary CaO-FeO_x-P_2O_5-SiO_2* system provided in the present work:

- The presence of C2S_C3P in samples where SiO_2 content equals or higher than 5 wt% is confirmed for a large number of industrial slags. This indicates the risk involved with reducing the system to its basic components as this phase in not present in the ternary CaO-FeO_x-P_2O_5 system.
- Riboud and Margot [172] did not find evidence of C2S_C3P presence in the industrial samples and referred to the fact that synthetic laboratory slags with a similar composition were C2S_C3P saturated at 1773 K. The authors [172] attributed the discrepancy to a higher process temperature. However, based on the thermodynamic evaluations of the corresponding system presented in this

work, this explanation was considered as unrealistic. The present work suggests that a modification of the slag structure may have occurred during the sampling procedure as a result of a change in $p(O_2)$ state, which was possibly caused by a long exposure time of the sample to air and/or by an inefficient quenching. This indicates the importance of preservation of $p(O_2)$ state of industrial samples during sampling and quenching for a proper evaluation of their structure. This is especially the case for C2S and C2S_C3P saturated slags due to the sensitivity of those solid phases to the oxidation state of the slag.

- It is reported that lime saturation could not be reached in industrial slags with a SiO_2 content equals or higher than 4 wt%, independently of the amount of lime added during the industrial process. This can be explained by the difficulty in accessing the lime saturation region in the quaternary $CaO\text{-}FeO_x\text{-}P_2O_5\text{-}SiO_2$* system: An increase in the CaO amount of the slag will result in increasing the amount of C2S_C3P precipitations. As a result, a significant decrease in the liquid slag amount, an increase in slag viscosity, as well as a decrease in the interface between liquid slag and undissolved lime, occurs. All of those factors contribute to the inhibition of lime dissolution. This explains the non-achievement of lime saturation despite adding high amounts of lime during the process.

6.2 Morphology of low P slags

The thermodynamic evaluations of the quaternary $CaO\text{-}FeO_x\text{-}SiO_2\text{-}P_2O_5^*$ system provided in chapter 5 indicated that the C2S_C3P phase dominates the CaO-rich part of the system in the composition, temperature, and $p(O_2)$ range relevant for the BOF process. However, apart from some few works,[10, 35, 118] the presence of the silicophosphate phase C2S_C3P in industrial samples taken from conventional BOF converter has rarely been reported in the literature. This may be due to the fact that, in most cases, elementary analysis and not mineralogical analysis of the slags are provided. Also, most investigations of the morphology of BOF slag samples focused in general on the clarification of the extent of lime dissolution in the samples and little attention was given to the identification of silicates. In many cases, the presence of the C2S phase, which is capable of dissolving phosphorus under the formation of the C2S_C3P phase, is reported in association with its negative effect on lime dissolution,

as it forms a blocking layer around the lime particles.[207, 208] For hot metal dephosphorization processes, where dephosphorization and decarburization are carried out as 2 separate steps with an intermediate deslagging,[16, 18] the presence of the C2S_C3P phase has been evidenced in industrial samples taken during both decarburization and dephosphorization steps. [98] Dehosphorization slags are characterized by a low basicity, defined as the CaO to SiO_2 ratio, as well as by a low temperature, usually lower than 1723 K (1450°C). Decarburization slags have a higher basicity, usually higher than 2, and a higher temperature, usually is in the range of 1900 K, which is the case for conventional BOF slags.

Table 7 presents an overview of the results of several plant trials [10, 35, 118] carried out in a variety of BOF converters where the morphology of slag samples was investigated, and which reported that phosphorus was found dissolved in solid phases.

Table 7: Overview of the results of several industrial plant trials carried out in a BOF converter, where the presence of phosphorus-containing solid phases was reported.

Authors	Samples/ process characteristics	Relevant observations
Deo et al.[118]	Samples taken from European and Indian steelworks with an initial [%P] content of hot metal in the range of 0.067-0.25 wt%.	No indication of C3S phase presence. C2S found in all samples and P was found dissolved in C2S.
Preßlinger et al.[118]	15 slag samples taken from the Voestalpine steel plant.	P contained in both C2S and C3S solid phases by 4.9% and 2.3 wt%, respectively.
Wu et al.[35]	3 different BOF samples taken from Chinese steelworks with a P_2O_5 content of 2.8-4.6 wt%	P was found dissolved in C2S and C3S by 7.1 wt% and 3.1 wt%, respectively.

It can be seen from Table 7 that all of those works agree that the industrial slags are heterogeneous and saturated with silicates: the C2S phase, and/or the C3S phase.[10, 35, 118] Also, they indicate that P_2O_5 is found mainly dissolved in the C2S phase with a

content in the range of 5-7 wt%. Thus, the phosphorus-containing “C2S” phase, which is referred to in those works represents the silico-phosphate phase C2S_C3P. Those works further reported that the content of P_2O_5 measured in the solid phase was much higher than that measured in the liquid slag phase. [10, 35, 118]

It is interesting that Wu et al.[35] and Preßlinger et al.[118] reported the presence of C3S phase in their samples while Deo et al.[10] did not find any evidence of C3S saturation, even though their slag samples [10] were taken during the refining of a hot metal with a large phosphorus variation range (Table 7). The analysis of the quaternary CaO-FeO_x-SiO_2-P_2O_5* system, given in section 5.2, showed that the C3S phase is no longer stable in the system when P_2O_5 is present with content equal or higher to 3 wt %. The C3S saturation regions shrink massively in favor of C2S_C3P saturation at 1 wt% P_2O_5 and disappear completely at 3 wt% P_2O_5 (Figure 32). Furthermore, the experimental study of the quaternary system at 5 wt% P_2O_5 and a temperature of 1673 K, carried out by Gao et al.[105] indicated that the C3S phase is no longer present in the system in favor of an expansion of the C3S_C3P stability range. Margot and Riboud [173] studied the quaternary system CaO-FeO-SiO_2-P_2O_5 with either a fixed FeO or SiO_2 content, over a temperature range of 1300-2000 K, and for the elevated pO_2 case. They reported that when the P_2O_5 content of the system is below 10 wt%, the C3S phase is no longer found in the samples for all composition ranges as well over the total temperature range of 1300-2000 K.

Thus, it can be considered that the state of the slag samples of Deo et al. [10] was closer to the equilibrium state than that of Wu et al. and Preßlinger et al. [35, 118], which found C3S in their samples. The reported presence of C3S in those industrial samples [35, 118] can be considered as an indication that at low P_2O_5 values, probably lower than 3-5 wt%, the C3S phase may not be entirely replaced by the C2S_C3P phase in the industrial process, contrary to the equilibrium state of the system. It can be further concluded that the C3S phase observed in the samples [35, 118] is thermodynamically unstable. Thus, in order to achieve optimal dephosphorization results, it is recommended to avoid C3S saturation regions during the BOF process operation, as this phase may not be entirely replaced by C2S_C3P when phosphorus oxidizes, contrary to the thermodynamic equilibrium state. The thermodynamic evaluation of the low phosphorus system, provided in chapter 5, showed that reaching lime saturation in the

ternary CaO-FeO_x-SiO_2 oxide system is associated with additional precipitation of the C3S phase. Also, it is shown that the formation of the C3S phase has a negative effect on the dephosphorization potential in the slag (section 5.4). It is thus recommended to avoid C3S saturation of the slag during the BOF process operation. Alternatively, setting the single-phase C2S saturation region as the target zone may provide optimal dephosphorization results due to the high dephosphorization potential of C2S_C3P saturated slags.

It is also an interesting fact that Wu et al.[35] and Preßlinger et al.[118] reported that P_2O_5 was found dissolved in both C2S and C3S solid phases. The measured P_2O_5 content of the C2S and C3S phase was reported to lie in the range of 5-7 wt% and 2-3 wt%, respectively. While the phosphorus dissolving potential of the C2S phase is widely reported in the literature, [10, 14, 17, 21, 28, 30-32, 34, 66, 98-120], no evidence on the solubility of phosphorus in C3S phase could be found, to author's best knowledge. The C3S phase dissociates to free lime and C2S phases at room temperature, and thus, it is very difficult to investigate this phase during laboratory experiments. Wu et al. [35] noted that the C3S phase could be identified in the samples by the XRD analysis, but it could not be found by the SEM analysis, which is an indication of the challenges associated with the identification of this phase at room temperature. It is thus possible that the phosphorus was falsely attributed to C3S instead of C2S in those works [35, 118], as a result of the challenges associated with the identification of this phase. In addition, the analysis of the quaternary CaO-FeO_x-SiO_2-P_2O_5 * system, given in section 5.2, showed that the C3S phase is no longer stable when P_2O_5 is present with a content equal or higher than 3 wt%, in favor of C2S_C3P formation. It is thus possible that some parts of the C3S-saturated slag samples have reached thermodynamic equilibrium state in terms of the formation of the phosphorus-containing solid phase C2S_C3P, which was then falsely identified as a phosphorus-containing C3S phase. A further possibility is that the C3S phase is indeed capable of dissolving phosphorus, but relevant experimental assessments are lacking due to the aforementioned laboratory challenges associated with investigating the C3S phase at room temperature. In conclusion, it is highly recommended to carry out experimental works to clarify the controversial phosphorus solubility in the solid C3S phase reported by Wu et al.[35] and Preßlinger et al.[118]

6.3 Evaluation of the equilibrium state of phosphorus in the metal during the industrial process

During the BOF process, dephosphorization reaction takes place mainly on the interface between the slag and metallic droplets residing in the slag. Those reaction sites are designated as the “metal-slag-interface” (Figure 4). It is largely assumed in the literature that several refining reactions, including dephosphorization, attain chemical equilibrium at the metal-slag-interface.[13, 50, 53, 55-59] Thus, in order to assess the equilibrium state of the dephosphorization reaction during the industrial process, the measured phosphorus content of the metallic droplets residing in the slag should be considered.

In this section, several industrial measurements of the P-content of metallic droplets residing in the slag, which were provided in the literature, are evaluated. The aim is to clarify which measurements are representative of the equilibrium state of phosphorus in the metal phase and can thus be used for the evaluation of the extent of achievement of equilibrium with respect to dephosphorization reaction during the industrial process. In this section, an attempt is made to clarify whether the phosphorus equilibrium content is reached in all metallic droplets residing in the slag or only for a specific type of droplets.

6.3.1 Analysis of the plant trials of Schoop and co-workers

In a series of plant trials, carried out in an LD-AC converter, Schoop et al.[52, 53, 175] measured the evolution of the P-content in the metal bath as well as in a large number of metallic droplets during the total blowing process for 2 types of heats. The authors measured the amount, size, and P-content of a large number of metallic droplets, which were found embedded in a variety of slag samples, and divided them into several size groups. The average P-content for each size group, as well as for all metallic droplets was determined. The details with respect to the sampling procedure adopted in their work, the process operation as well as the measured slag evolution is given in section 6.4. **Figure 41** shows the measured evolution of phosphorus content of the metal bath as well as the evolution of average P-content in all metallic droplets for heat type 1. It can be seen from Figure 41 that the average P-content measured in the metallic droplets was at least one order of magnitude smaller than the corresponding

values measured in the bath for the entire blowing period. This supports the assumption that phosphorus equilibrium is achieved only in the metallic droplets residing in the slag, while the extent of dephosphorization in the bath depends on major kinetic aspects such as the droplets generation rate from the bath to the slag [41-48] and their residence time [49-54] in the slag prior to returning to the metal bath.

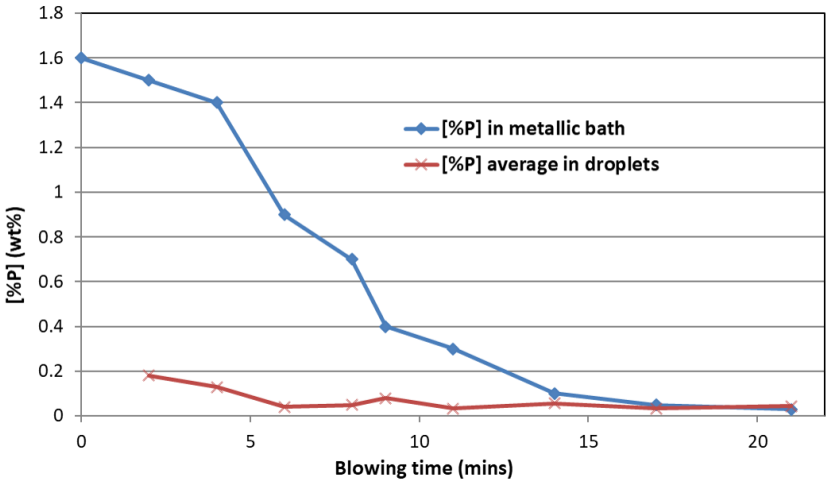

Figure 41: Evolution of the [%P] content of the metallic bath as well as of the average [%P] content of the metallic droplets embedded in the corresponding slag samples, reproduced based on the data of Schoop et al. [52, 53, 175]

Schoop et al. [52, 53, 175] reported that the size of the metallic droplets investigated in their work showed a large variation range, as their diameter varied between 0.1 and 2 mm while their phosphorus content was a strong function of their size. **Figure 42**-a) and –b) show the measured P evolution for 6 different size groups, and for type 1 and type 2 heats, respectively.

It can be seen from Figure 42 that the P-content of size group 1, 2 and 3 which had a diameter higher than 0.8 mm, was above that of the smaller-sized groups, for most of the blowing time, albeit some few exceptions are noted. It is also notable that despite different P-contents, the evolution of phosphorus was similar for all metallic droplets of different sizes: During a large part of the blowing period, phosphorus reversion behavior, as well as a recovery in phosphorus removal, occurred simultaneously in all droplets size groups.

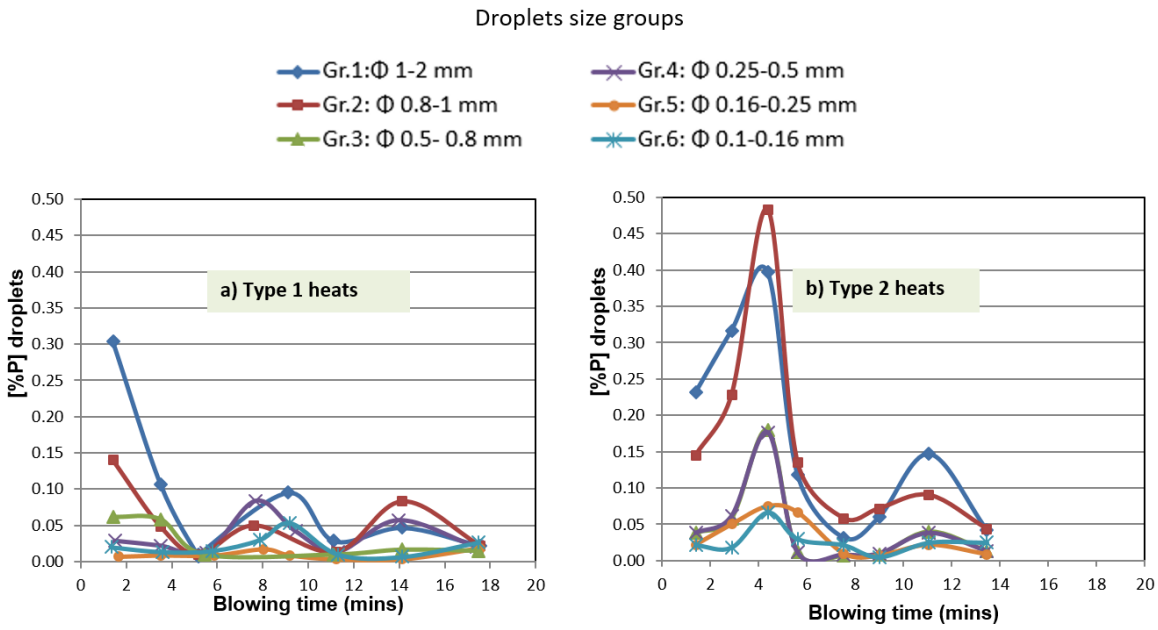

Figure 42: P evolution in the metallic droplets of different size groups, which were found embedded in slag samples, reproduced based on the measurements of Schoop et al. [52, 53, 175] for a) Type 1 heats b) Type 2 heats

Based on the measurement of the P-content in different metallic droplets, carried out by Schoop et al. [52, 53, 175], it can be concluded that the equilibrium with respect to dephosphorization reaction is not achieved for all metallic droplets, and that it is a strong function of their size: The smaller the droplet size is, the closer the P-content will be to the equilibrium value. It can be assumed, based on those measurements, that small-sized metallic droplets, for example, those with a diameter smaller than 0.8 mm, are closer to the equilibrium state than droplets with a larger size. A further conclusion which can be drawn from Figure 42 is that, even though the P content depended strongly on the size of the droplets, the behavior of phosphorus in all size group is similar (increasing or decreasing behavior) and may thus indicate the behavior of phosphorus at the equilibrium state. This means that an increase in the P content in one size group indicates an increase in the P equilibrium content in the metal phase and vice versa.

6.3.2 Analysis of further plant trial results

Further plant trial results, where the P-content in metallic droplets was measured, are available in the literature. Kozakevitch [50] examined samples taken by Hergat et al.[209]

from a 30 tons OLP converter, a process similar to the LD-AC converter, during the refining of a high phosphorus hot metal. More recently, plant trials carried out in the scope of the IMPHOS project [210] provided data on the dephosphorization behavior of a low phosphorus hot metal refined in a 7 tons pilot converter.

In accordance with the results of Mahn et al.,[52, 53, 175] Kozakevitch [50] observed a strong correlation between the P-content of the metallic droplets and their size. **Table 8** presents some examples, selected from the work of Kozakevitch [50], where the measured P-content of metallic droplets for 4 different size ranges and the corresponding P-content of the bath are given. It can be seen from Table 8 that the P-content of the metallic droplets with a larger size, specifically those with a diameter higher than 2.5 mm, was at least twice as high as the P-content in smaller sized droplets. Also, the P content of the droplets decreased with the diameter of the droplet. Interestingly, the P-content in droplets with a diameter smaller than 0.6 mm was less than 0.01 wt%, which is in accordance with the results of Schoop et al. [52, 53, 175] for droplets with a similar diameter range (see P-content for size groups 4, 5 and 6 in Figure 42) during the last 2 minutes of the blow: During this blowing period, the corresponding P-content in the bath measured by Schoop et al. [52, 53, 175] was below 0.1 wt% (Figure 41), which is similar to the P-content in the bath reported by Kozakevitch [50], at the time the samples were taken (Heat 1 in Table 8).

Table 8: Measured P-content in the bath and in the metallic droplets taken from a 30 tons OLP converter by Hergat et al. [209], reproduced from the work of Kozakevitch [50].

Heat N°	[%P] Bath	[%P] Droplets (Emulsion)			
		Droplet diameter [mm]			
		>2.5	2.5 to 1.2	1.2 to 0.6	<0.6
1	0.1	-	0.006	0.005	0.004
2	0.136	0.028	0.011	0.008	0.007

In addition, the results of plant trials measurements carried out in a 7-tons-BOF converter in the scope of the IMPHOS project [210] further confirmed the strong correlation between the P-content of metallic droplets and their size. This indicates that this correlation is not a characteristic of the LD-AC or the OLP process and that it is also valid for the conventional oxygen top blowing process, regardless of the adopted blowing strategy and the initial P content of the hot metal. The sampling method used in those plant trials is different from the method used in the plant trials investigated earlier, [52, 53, 175, 209] where samples were taken either during or after slag tapping [209]. Instead, a special sampling system was used where several samples can be taken simultaneously from bath and emulsion zones and at different locations. **Figure 43**-a) shows the measured P content of the droplets as a function of their approximated diameter, whereas Figure 43-b) shows the measurement results for manganese, for the purpose of comparison. It can be seen from Figure 43-a) that a large amount of droplets with a diameter equals or smaller than 0.6 mm had P contents less than 0.015 wt%, while droplets with a higher diameter had significantly higher P contents.

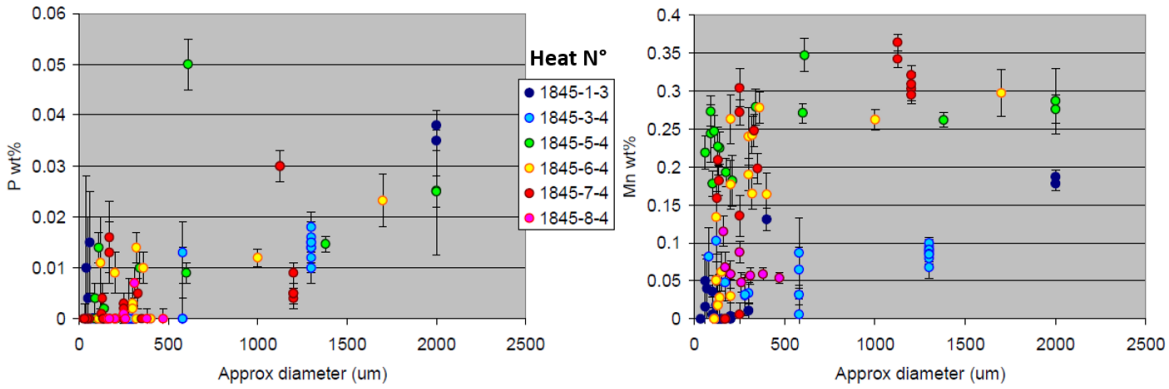

Figure 43: Measured a) phosphorus b) manganese content of metallic droplets as a function of their approximated diameter, which were embedded in slag samples taken from a 7 tons pilot BOF converter in the scope of the IMPHOS project [210]. Reprinted with permission from Ref. [210]

The authors [210] emphasized on the reliability of the phosphorus measurements in the metallic droplets, especially in comparison to the quality of the measurements for other elements such as Mn, Si, and V. The measurements for phosphorus were reproducible with three accelerating voltages, indicating no adverse effect of secondary fluores-

cence from surrounding slag. [210] Interestingly, a correlation between the element content and the droplet size was a characteristic of phosphorus and could not be reliably established for Mn, Si, and V. It can be seen from Figure 43-b), that such a correlation could not be established for manganese, especially for metallic droplets with a diameter smaller than 0.6 mm.

6.3.3 Conclusion

Based on the examination of the phosphorus measurements in the metallic droplets, it can be concluded that the extent of achievement of equilibrium with respect to dephosphorization in metallic droplets depends mainly on their size. It is thus reasonable to assume that only the smaller sized droplets and more specifically, the droplets with a diameter equal or less than 0.5 mm, are more likely to achieve equilibrium, or to behave closer to the equilibrium state than the droplets of a larger size. The correlation between the P-content in a droplet and its size could be established for different types of converters: A 200 tons LD-AC converter, a 30 tons OLP converter as well as 7 tons conventional top-blown BOF converter. Thus, this correlation can be considered as generally valid for top blown refining processes independently of the:

- converter size,
- lime type (lump, powdered), feeding rate, and addition strategy (single batch or several batches, continuous feeding, …),
- blowing conditions: A hard blow or a soft blow.

Figure 44-a) and b) present further measurement results reported by Shoop et al.[52, 53, 175], which show the size distribution of metallic droplets, which were embedded in 2 slag samples (sample x and sample y, taken at 2 different blowing intervals), for type 1 and type 2 heats, respectively. It can be seen from Figure 44 that the percentage of metallic droplets with a diameter equals or smaller than 0.5 mm was in the range of 20- 35 % for type 1 heats and 14-38 % for type 2 heats. It can be thus concluded that the average P-content of the metallic droplets, which is usually approximated using the P-measurement data for all metallic droplets independently of their diameter, is not representative of the equilibrium behavior of phosphorus in the metal phase. This is especially the case for samples where the presence of large size droplets was dominant. Such a situation is depicted by the cumulative frequency curves of sample y in

type 1 and type 2 heats, where the percentage of droplets that had a diameter equals or smaller than 0.5 mm was less than 20% of the total amount of metallic droplets found in the slag sample.

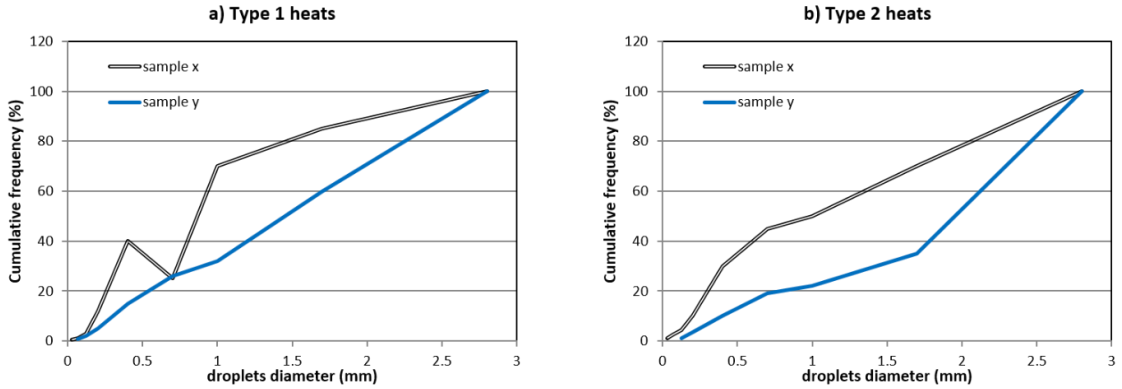

Figure 44: Cumulative frequency of metallic droplets (in %), embedded in 2 different slag samples (x and y) as a function of their diameter (in mm), selected from the data of Shoop et al.[52, 53, 175] for a) type 1 heats b) type 2 heats

In order to investigate the behavior of phosphorus equilibrium state in the metal phase during the industrial process, which is carried out in section 5.4, only the phosphorus evolution in metallic droplets with a diameter equals or less than 0.5 mm should be considered. Also, in order to study the factors affecting the evolution of phosphorus at equilibrium, only the phosphorus evolution for one single size group should be observed instead of considering the evolution of the average phosphorus content for all droplets independently of their size. It can be deduced from Figure 44, that the average P-content of the metallic droplets for sample x and sample y will be different even when the P-content of each size group is the same in both samples. The difference in the behavior of the droplets size distribution between sample x and sample y may be caused by a modification in the blowing conditions (lance height, oxygen flow rate,…) or the decarburization rate (the onset of decarburization in the droplets may lead to a bloating and a subsequent explosion of large droplets to smaller-sized droplets, which will increase the number of smaller-sized droplets). If the evolution of the average P-content in all droplets is considered as representative of the P equilibrium state, a modification in the average P-content of the droplets will be falsely attributed to a modification in the P-equilibrium state rather than to a modification in the blowing conditions. Thus, in the following, the P-evolution in one size group and precisely, in size

group 6 with a diameter range of 0.1- 0.16 mm (Figure 42), will be considered as representative of the behavior of phosphorus at equilibrium in the metal phase.

Finally, it should be noted that in order to evaluate the state of dephosphorization in the metallic droplets residing in the emulsion zone, the deviation of the P-content of the metallic droplets from the equilibrium state, which is found to be a strong function of their size, should be considered. Since only the evaluation of the phosphorus equilibrium state is of interest in the present work, the deviation from the equilibrium state will not be further assessed in the present work.

6.4 Simulation of the evolution of slag phases and their composition

In this section, the evolution of the slag phases and their composition will be simulated using the BOFdePhos thermodynamic database, based on the measurement results of Schoop et al.[52, 53, 175], which were introduced in section 6.3.

6.4.1 Setting input data for the thermodynamic simulations

Schoop et al.[52, 53, 175] provided measurement data with respect to the evolution of several oxide contents in the slag for 2 types of heats. **Figure 45**-a) and -b) show the evolution of the CaO-, P_2O_5- and total FeO-content (originating from both FeO and Fe_2O_3) of the slag for type 1 and type 2 heats, respectively.

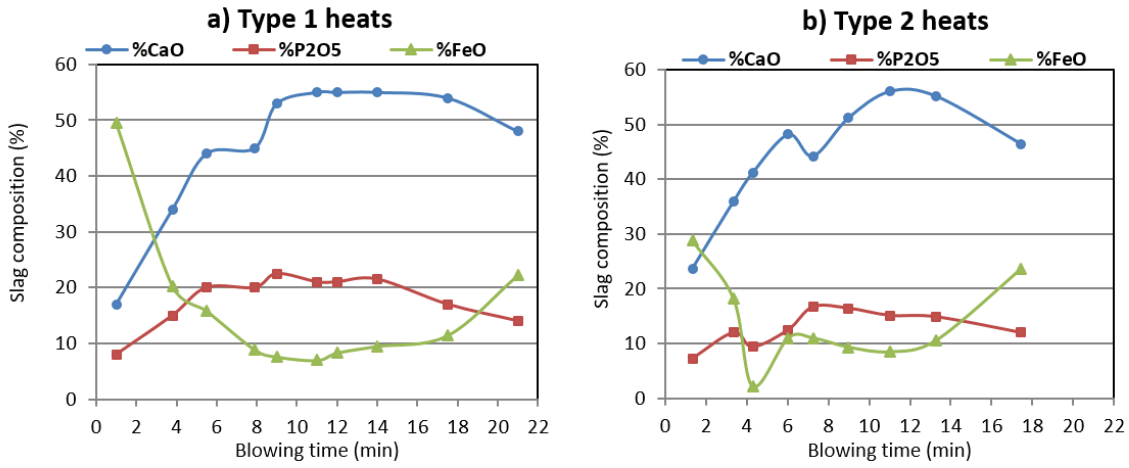

Figure 45: Evolution of the FeO, CaO and P_2O_5 contents of the slag during the blow measured by Schoop et al. [52, 53, 175] for a) type 1 heats b) type 2 heats

The initial hot metal composition reported by Schoop et al. [52, 53, 175] contained 0.6 wt% Si and 0.6 wt% Mn. Thus, significant contents on SiO_2 and MnO_x are expected in the

slag. Also, it can be seen from Figure 45 that the sum of FeO_x, P_2O_5, and CaO analysis is less than 100 wt% for all measurement points. However, only the analysis with respect to CaO, FeO_x, and P_2O_5 in the slag was provided by the authors [52, 53, 175]. In the work of Resch [175], graphs containing a large number of measurement data for each of the oxides FeO_x, CaO, P_2O_5, SiO_2 values as well as for the temperature of the metallic bath could be found, however without indicating whether the data belong to samples taken from type 1 heats or type 2 heats. **Figure 46** –a) and -b) shows the measurement data of the SiO_2 –content and the temperature of the metallic bath, respectively, reproduced from the work of Resch [175].

Due to the strong effect of SiO_2 on the phase boundaries of the high phosphorus system (Figure 17-Figure 19), it is necessary to estimate the evolution of the SiO_2-content of the slag for a proper thermodynamic evaluation of the state of those industrial slags. The measurement data corresponding to the evolution of the SiO_2-content of the slag and the temperature of the metallic bath were fitted with the curves presented in Figure 46-a) and -b), respectively. Those fitting curves were then considered representative of the evolution of the SiO_2-content and the temperature of the metallic bath as a function of the blowing fraction for type 1 and type 2 heats.

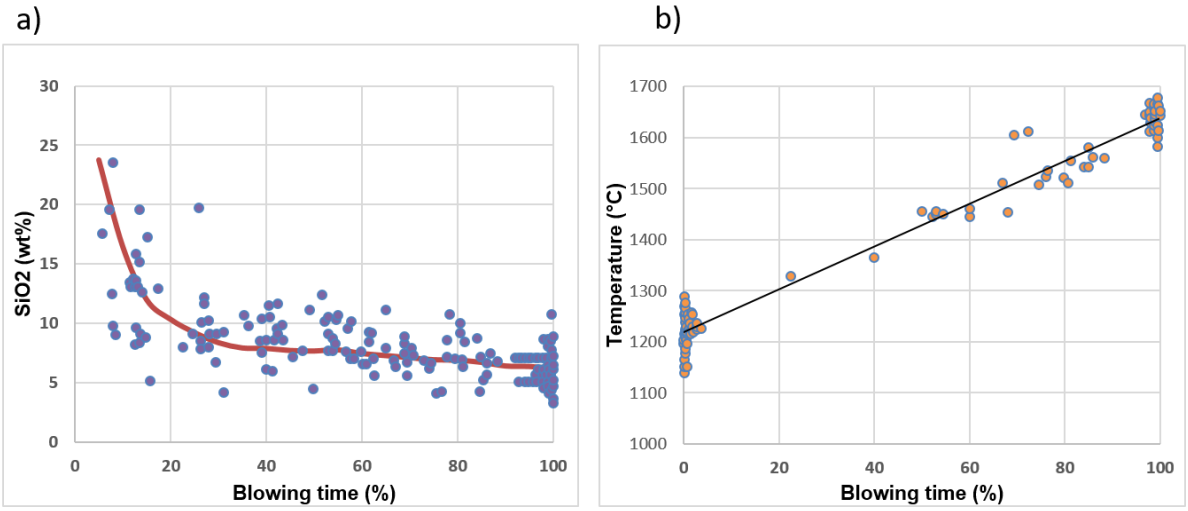

Figure 46: Measurements data for the evolution of a) SiO_2 b) Temperature of the metallic bath, reproduced from the work of Resch [175]. In the present work, fitting curves were developed to describe the behavior of the original data, which were used to describe the evolution of SiO_2 (red fitting curve, left) and bath temperature (black straight line, right) in type1 and type 2 heats.

6.4.2 Description of the simulation method

The thermodynamic simulations were carried out using the “Equilib”-module of the thermodynamic software FactSage 7.1 [137]. The thermodynamic models for all phases considered were taken from the BOFdePhos thermodynamic database, presented in chapter 3. The measurement data for the evolution of CaO, FeO_x, P_2O_5, and SiO_2 contents of the slag as a function of the blowing fraction, presented in Figure 45 and Figure 46, were given as input into the calculations. The oxide system composition was set in equilibrium with the liquid-Fe solution phase. Thus, the oxidation state of FeO_x in the slag set for the thermodynamic simulations corresponds to the reduced $p(O_2)$ state (Table 6). **Figure 47** presents an overview of the input window of the “Equilib”-module of the software.

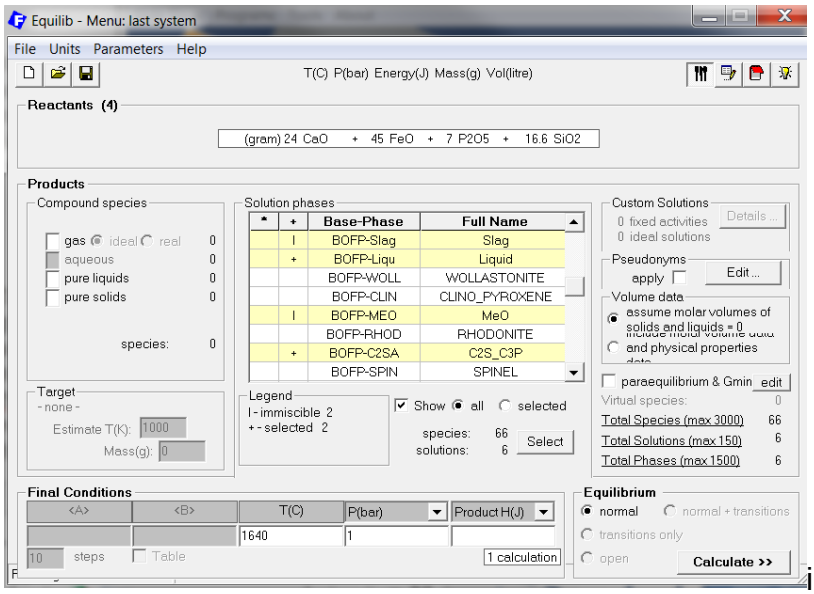

Figure 47: Overview of the input window of the “Equilib”-module of FactSage 7.1 TM

In addition to specifying the oxide system composition, the slag temperature is also required as input into the thermodynamic simulations. However, only the evolution of the temperature of the metallic bath (Figure 46-b) was measured by Schoop et al. [52, 53, 175]. It is reported in the literature that, in general, the slag temperature can be estimated as approximately 50 °C higher than that of the metallic bath [62, 211]. Ishiguro [212] measured the temperature gradient between the slag and the metallic bath, and reported that the slag temperature was always above that of the bath, with a temperature gradient in the range of 20°C-100°C. The initial P-content of the hot metal in the plant

trials of Schoop et al. [52, 53, 175] was considerably high, with an initial content of 1.6 wt%. Thus, based on the fact that the P oxidation reaction is highly exothermic and that it occurs within the slag (or within the “Emulsion”, presented in Figure 4), the temperature gradient between the metallic bath and the slag is expected to be very high. Thus, the temperature of the slag is set as 100°C above the bath temperature, that is, at the upper limit of the temperature gradient interval reported by Ishiguro [212].

6.4.3 Analysis and discussion of the simulation results

The simulation results with respect to the evolution of the slag phases during the entire blowing period for type 1 and type 2 heats are presented in **Figure 48** and **Figure 49**, respectively. The results with respect to the evolution of (%FeO_x)-, (%CaO)-, (%SiO_2)- and (%P_2O_5)-content of the purely liquid slag part for type 1 and type 2 heats are presented in **Figure 50** and **Figure 51**, respectively. In order to investigate the effect of the evolution of the slag phases on the phosphorus equilibrium state in the metal phase, the evolution of the P-content in the metallic droplets, measured for Gr.6 droplets (Figure 42), is drawn in Figure 48-Figure 51. Those metallic droplets are considered representative of the equilibrium state of phosphorus in the metal phase in the present work, due to their small size, as they have a diameter in the range of 0.1-0.16 mm (detailed explanation is given in section 6.3).

In order to analyze the factors affecting the behavior of P removal in the metallic droplets, the entire blowing period was divided into several blowing intervals based on the behavior of P content in Gr.6 droplets. Those blowing intervals will be further described as the „dephosphorization stages“. The difference between 2 consecutive stages is the alternation in dephosphorization behavior from a phosphorus removal (decrease in [%P]) to a phosphorus reversion (increase in [%P]) and vice versa. Finally, five dephosphorization stages could be distinguished for type 1 heats (Figure 48 and Figure 50) as well as for type 2 heats (Figure 49 and Figure 51).

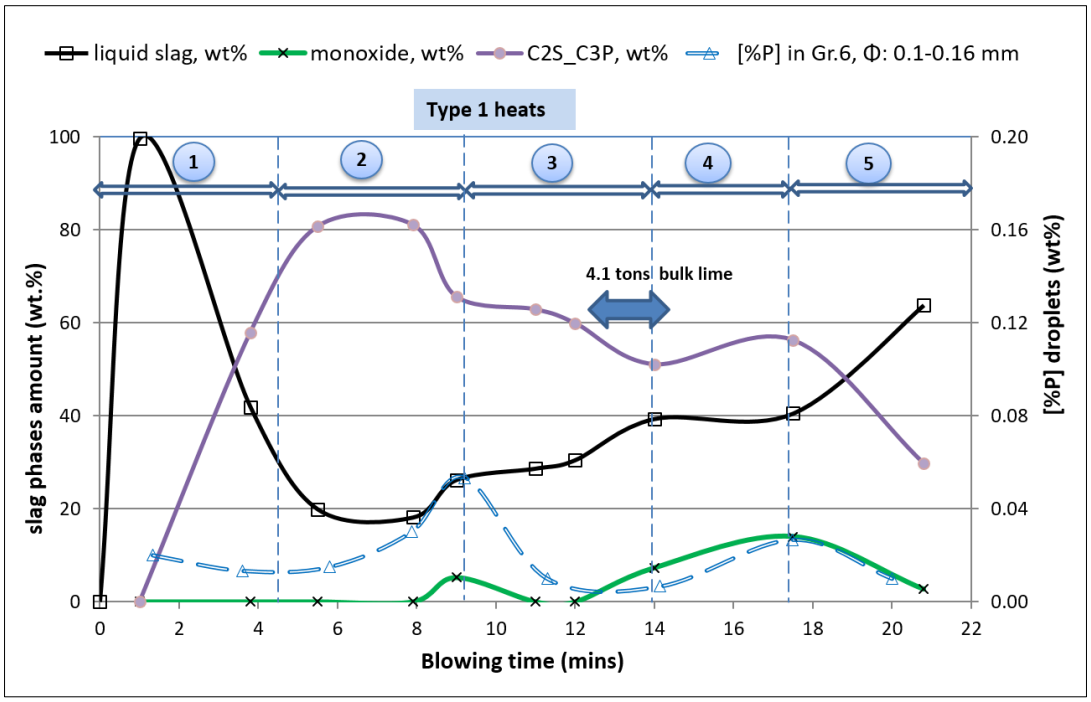

Figure 48: Evolution of the slag phases for type 1 heats, calculated in the present work in comparison with the evolution of phosphorus in Gr.6 droplets, measured by Schoop et al. [52, 53, 175]

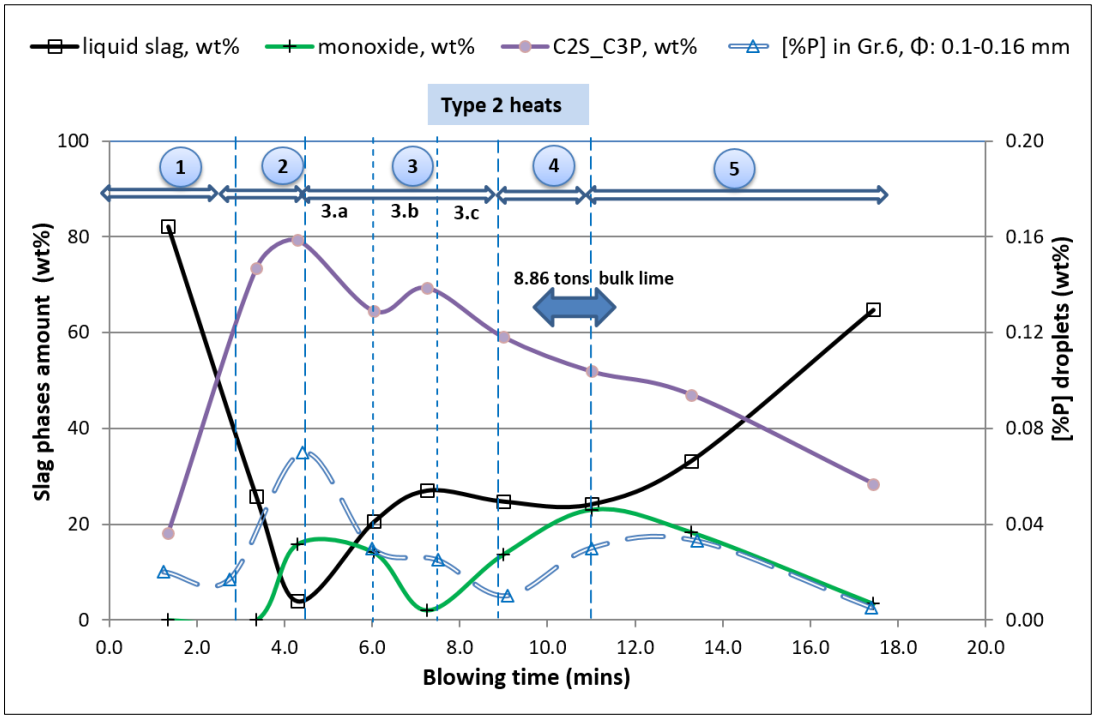

Figure 49: Evolution of the slag phases for type 2 heats, calculated in the present work in comparison with the evolution of phosphorus in Gr.6 droplets, measured by Schoop et al. [52, 53, 175]

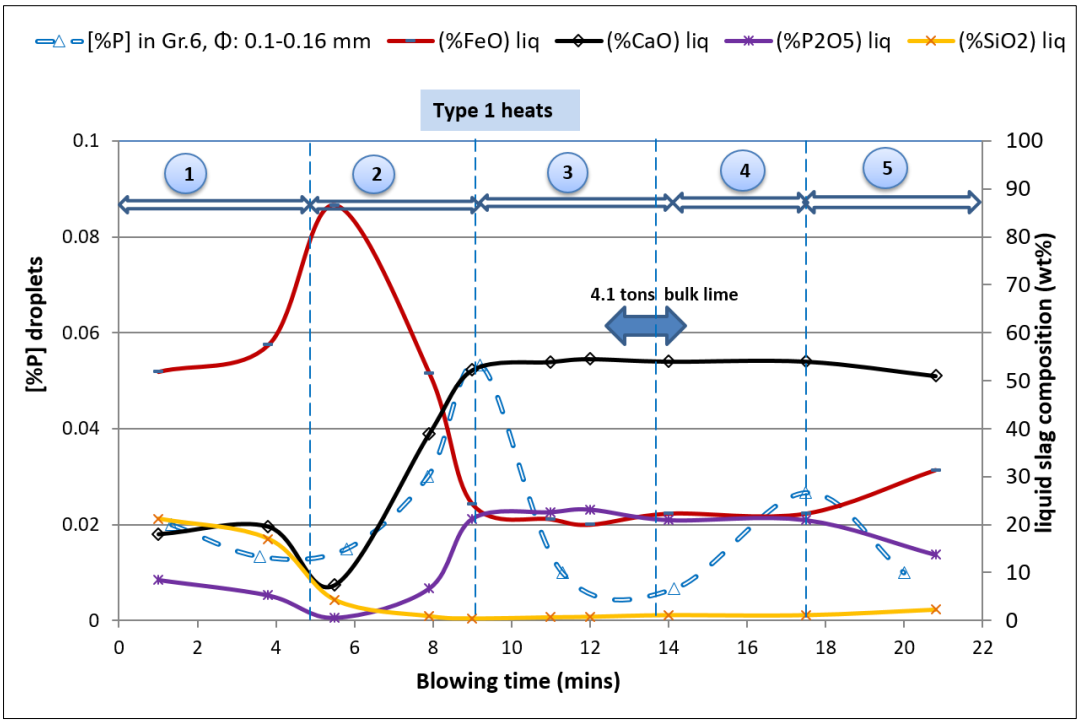

Figure 50: Evolution of the liquid slag composition for type 1 heats, calculated in the present work in comparison with the evolution of phosphorus in Gr.6 droplets, measured by Schoop et al. [52, 53, 175]

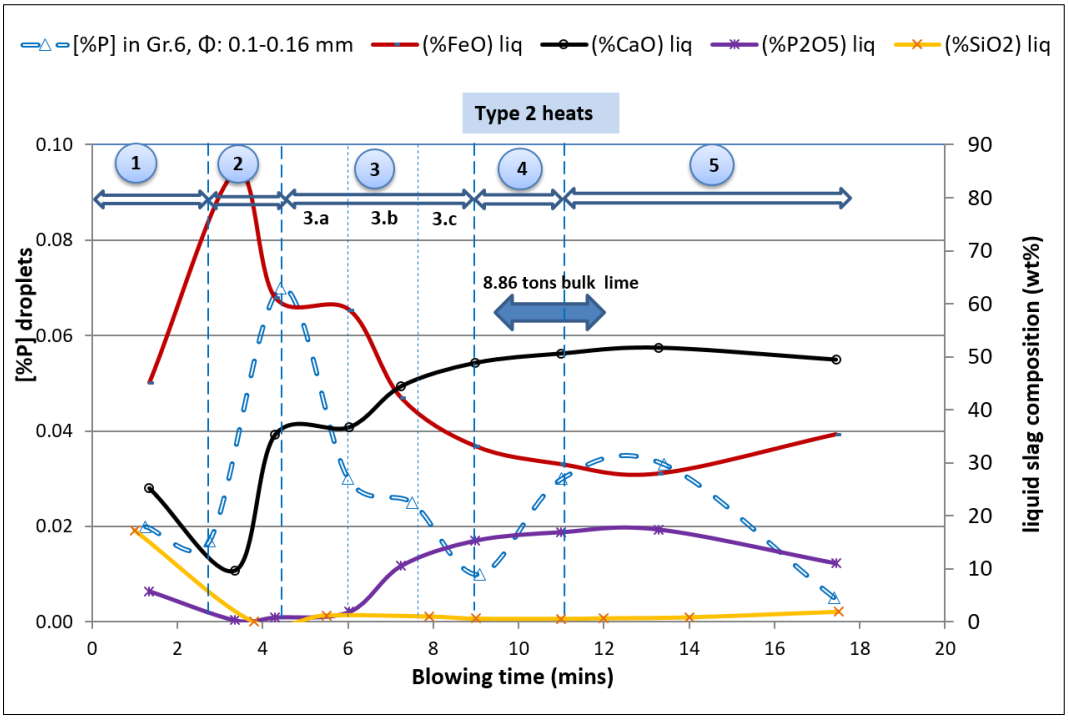

Figure 51: Evolution of the liquid slag composition for type 2 heats, calculated in the present work in comparison with the evolution of phosphorus in Gr.6 droplets, measured by Schoop et al. [52, 53, 175]

The P-content of size group 6 droplets, which had a diameter in the range of 0.1-016 mm, were considered representative of the equilibrium state of phosphorus in the metal phase, due to their small size (see section 6.3 for details). The behavior of phosphorus in the metal phase will be evaluated based on the analysis of the thermochemical state of the corresponding slag, which is determined using the BOFdePhos thermodynamic database. Thus, factors affecting the kinetics of the dephosphorization reaction, such as the mass transfer in the metal or in the slag, are not considered during the analysis of the dephosphorization behavior of the metallic droplets.

The evolution of slag phases for type 1 heats and type 2 heats, presented in Figure 48 and Figure 49, respectively, show that the slag became heterogeneous within 2 minutes after the start of blow and remained in such a state for the entire blowing period. The heterogeneous slag was always C2S_C3P saturated and occasionally, saturated on the monoxide phase, CaO-ss, too.

An overview of the characteristics of the different dephosphorization stages for type 1 and type 2 heats is provided in **Table 9** and **Table 10**, respectively. Some stages were further divided into substages (a,b,c), in case a considerable modification in the removal or reversion rate of phosphorus is observed within the same stage (a slowdown, an increase, or a decrease).

Table 9: Overview of the different dephosphorization stages and the corresponding slag state for type 1 heats.

deP Stages	Duration (mins)	Description of [%P] behavior	Description of the state of slag phases (based on the thermodynamic simulations)
1	0-4.5	Removal	C2S_C3P ↑ till 60 wt%, Liquid ↓,
2	4.5-9	Reversion	C2S_C3P ↑ till 80 wt%, Liquid ↓,
3	9-14	Removal	C2S_C3P ↓ 55%, Liquid ↑, Monoxide < 10 wt%
4	14-17.5	Reversion	C2S_C3P ↑ (slightly), Liquid ≈, Monoxide ↑ > 15 wt%
5	17.5-21	Removal	C2S_C3P ↓ till 30 wt%, Liquid ↑, Monoxide ↓ to 3 wt%

Table 10: Overview of the different dephosphorization stages and the corresponding slag state for type 2 heats: (+) denotes a moderate removal rate, (+ +) denotes a strong removal rate.

deP Stages	Duration (mins)	Description of [%P] behavior	Description of the state of slag phases (based on the thermodynamic simulations)
1	0-3	Removal (+)	C2S_C3P ↑ till 60%, Liquid ↓,
2	3-4.5	Reversion	C2S_C3P ↑ till 80%, Liquid ↓, Monoxide ↑
3.a	4.5-6	Removal (++)	C2S_C3P ↓ till 65 wt% , Liquid ↑, Monoxide ↓
3.b	6-7.5	Removal (+)	C2S_C3P ↑ (slightly) , Liquid ↑, Monoxide ↓
3.c	7.5-9	Removal (++)	C2S_C3P ↓ till 60 wt%, Liquid ↑, Monoxide ↑
4	9-11	Reversion	C2S_C3P ↑, Liquid ≈, Monoxide ↑> 20 wt%
5	11-17.5	Removal (+)	C2S_C3P ↓ 30%, Liquid ↑, Monoxide ↓ < 5%

It can be seen from Table 9 and Table 10 that for both heat types, a phosphorus removal behavior is observed in the metallic droplets during stage 1, stage 3, and stage 5. Thus, stages 1, 3, and 5 can be considered as optimal dephosphorization stages for the industrial process. It is notable that for both heat types, those stages (1, 3, and 5) were characterized by the presence of the C2S_C3P phase with content less than 50-60 wt% and in some cases, additional monoxide phase (CaO-ss) precipitation occurred, indicating reaching lime saturation. During stage 2 and stage 4, a rephosphorization was observed for both heat types, which was more pronounced in the case of stage 2. Stage 2 was characterized by the presence of C2S_C3P phase with amounts higher than 50-60 wt%. During stage 4, the slag was lime saturated, the content of the monoxide phase had an increasing behavior, and reached its highest value for the entire blowing duration.

Based on the analysis of the evolution of the liquid, the C2S_C3P, and the monoxide phase during all dephosphorization stages, it can be concluded that while C2S_C3P precipitations have a positive effect on dephosphorization, a limiting value exists upon

which no further improvement in phosphorus removal is achieved, and a P reversion might occur. The limiting C2S_C3P content, further denoted as C2S_C3P $_{limit}$, is reached at the end of stage 1 and stage 3, where the lowest phosphorus content was measured. It is estimated to lie in the range of 50-60 wt%. The strong P reversion observed during stage 2 can be attributed to excessive C2S_C3P precipitations, which exceeded C2S_C3P $_{limit}$. However, a P reversion also occurred during stage 4, even though the C2S_C3P content remained lower than C2S_C3P $_{limit}$. It should be noted that stage 4 is characterized by the highest amounts of monoxide phase CaO-ss for the entire blowing process: The monoxide content in the slag increased throughout stage 4, reaching 17 wt% for type 1 heats and 23 wt% for type 2 heats. It can be thus concluded that the presence of CaO-ss, which is an indication of reaching lime saturation, has a strong negative effect on dephosphorization in a C2S_C3P saturated slag, even if the C2S_C3P amount is below C2S_C3P $_{limit}$. However, when CaO-ss is present in limited amounts, which seem to lie in the range of 10-15 wt%, no indication of a negative effect on dephosphorization is found and in some cases, a P removal is observed (stage 3) which can be explained by the positive effect of lime saturation on the dephosphorization potential of the liquid slag.

Figure 52 shows a presentation of the slag path of type 1 heats in the quaternary system CaO-FeO_x-P_2O_5-10%SiO_2 at a temperature of 1873 K (1600°C), and for a reduced (solid lines) and elevated (dashed lines) p(O_2) state. It can be seen that under consideration of a reduced p(O_2) state, the slag path for type 1 heats was either within the single-phase C2S_C3P saturation region or slightly below its boundary with the double saturation region in monoxide (CaO-ss phase) and C2S_C3P. In case of an elevated p(O_2), the slag will be completely situated within the single-phase C2S_C3P saturation, albeit the transition point between stage 4 and stage 5 will be situated very close to the lime saturation line in such a case.

In the following, the dephosphorization stages 1-5, will be analyzed and discussed in detail in order to evaluate the effect of the evolution of the different slag phases on the extent of dephosphorization in the metal phase during the industrial process.

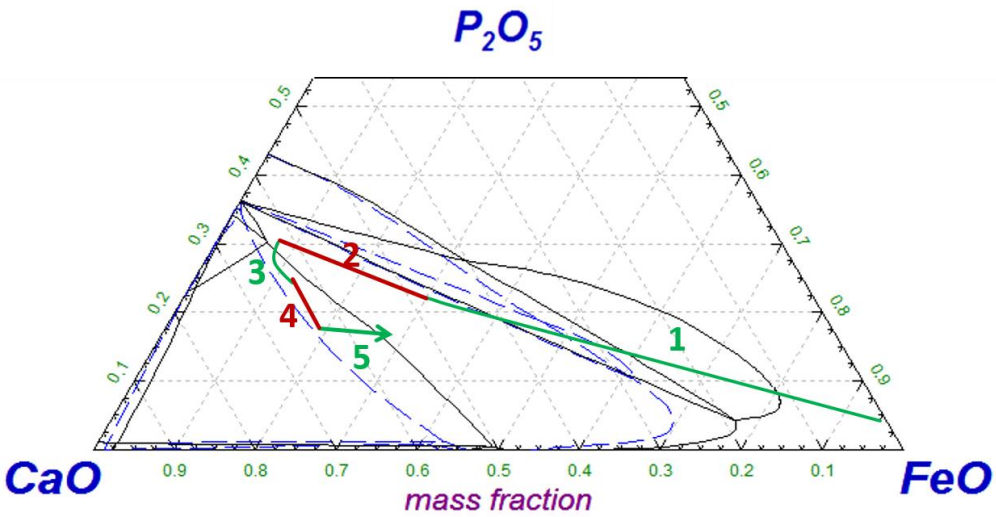

Figure 52: Presentation of the slag path for type 1 heats during the plant trials of Schoop et al.[52, 53, 175] in the quaternary system CaO-FeO_x-P_2O_5-10%SiO_2 at a temperature of 1873 K (1600°C) and for a reduced (solid lines) and elevated p(O_2) (dashed lines) state. The numbers refer to the corresponding dephosphorization stage (Table 9), where either a removal (green colored path) or a reversion (red-colored path) of phosphorus is observed in the metallic droplets.

A. Dephosphorization stage 1

The first dephosphorization stage, which had a duration of 4.5 mins for type 1 heats and 3 minutes for type 2 heats, represents the starting phase of the process. Within this short blowing period, a high P removal rate occurred, and the phosphorus content of Gr.6 droplets reached values below 0.02 wt%. It can be seen from Figure 41 that the corresponding phosphorus content of the metallic bath was very high and lay in the range of 1.3-1.6 wt% for type 1 heats. This stage is characterized by the early precipitation of C2S_C3P phase within 1 minute after the start of the blow.

The high dephosphorization rate observed during this stage is an indication of the strong dephosphorization potential of the C2S_C3P saturated slags and that, under certain conditions, the enrichment of this phase with phosphorus may occur very quickly. This is in agreement with the experimental results of Inoue and Suito [114] which indicated that the enrichment of precipitated C2S_C3P with phosphorus occurs very fast. It can be seen from Figure 52 that the slag composition is situated far from the lime saturation line, while Figure 50 and Figure 51 show that the liquid slag part was low in CaO (less than 20 wt%), high in FeO (more than 60 wt%) and very low in P_2O_5

(less than 5 wt%) for both heat types. It can be thus concluded that such a liquid slag composition is highly favorable for the enrichment of the solid phase C2S_C3P with phosphorus. Interestingly, Inoue and Suito [114] came to a similar conclusion based on their experimental evaluations of the phosphorus distribution Lp_{slag} (see equation(13)) between solid C2S_C3P phase and liquid CaO-FeO-SiO_2 slags. The authors investigated low P_2O_5 slags, [114] and observed that the maximum Lp_{slag} values are obtained at the nose of C2S precipitation region (Figure 5-a) where the liquid slag is high in FeO, low in CaO, and very low in SiO_2, which is very similar to the state of the liquid slag during stage 1. It can be seen from Figure 52 that the liquid slag composition at the end of stage 1 is also situated at the nose of the C2S_C3P saturation zone. It should be noted that CaO-FeO-SiO_2 slags situated at the “nose” of C2S saturation region and CaO-FeO-P_2O_5-SiO_2 slags situated at the „nose“ of C2S_C3P saturation region share the properties of having a very high FeO activity (highest in the corresponding region). It can be thus concluded that a high FeO activity increases the P transfer in a C2S_C3P saturated slag between the liquid and the solid C2S_C3P phase. According to Inoue and Suito, [114] the low SiO_2 content of liquid slags situated at the nose of C2S in the low P_2O_5 system has contributed to the enrichment of the C2S_C3P phase during their experiments. However, it is not clear what is behind the negative effect of SiO_2 on Lp_{slag} in their experiments. Some works reported that dephosphorization of metallic droplets is controlled by the mass transfer in the slag.[99, 213-215] Thus, the negative effect of SiO_2 on dephosphorization may be associated with its increasing effect on viscosity, which subsequently decreases the mass transfer in the slag and thus, the P removal from the metallic droplets as well as the phosphorus enrichment of the solid C2S_C3P phase. Inoue and Suito [114] noted that the peeling-off of C2S_C3P layer, which was an essential condition for the continuation of P enrichment of the C2S particles (which were added to the liquid slag in their experiments), [114] was only observed in CaO-FeO-P_2O_5 slags and was not observed in CaO-FeO-SiO_2 slags. It is thus possible that an increase in liquid slag viscosity when SiO_2 is present inhibits the peeling-off of C2S_C3P phase after its enrichment, which results in inhibiting the continuation of the enrichment process.

Another interesting possibility is that due to the surface-active nature of both SiO_2 and P_2O_5, [216, 217] their presence with considerable contents in the liquid slag may lead to

the formation of a blocking layer on the surface of the liquid slag, which subsequently slows down or completely blocks the transfer of P_2O_5 to the solid phase. In such a case, the application of stirring may remove the blocking layer and lead to the continuation of the enrichment procedure. This explains the strong increase in the phosphorus distribution between C2S_C3P saturated slag and liquid metal (Lp_{tot}) in the experiments of Inoue and Suito [114] when stirring was applied (Figure 38). It is thus highly recommended in the present work to carry out further experimental investigations to clarify whether those possibilities are realistic.

Considering the high phosphorus removal rate observed during stage 1 for both types of heats, the composition range and the evolution of the slag during this stage is of great interest to the industrial process. The CaO-content of the slag lay considerably below the values required for reaching lime saturation, which indicates that optimal dephosphorization results can be achieved without lime saturation of the slag and, thus, at a low lime consumption and with less slag formation.

B. Dephosphorization stage 2

This stage is characterized by the occurrence of a strong phosphorus reversion in the droplets, as the phosphorus content of Gr. 6 droplets increased from 0.015 wt% to 0.055 wt% for type 1 heats and from 0.017 wt% to 0.07 wt% for type 2 heats.

For type 1 heats, the reversion rate started slowly as the C2S_C3P increased beyond 65 wt% and reached a value of 80 wt%. Afterward, the C2S_C3P started dissolving in favor of liquid slag formation, and the corresponding reversion rate increased. The P reversion ended when the C2S_C3P phase amount decreased to 65 wt%.

As for type 2 heats, the C2S_C3P phase content increased from 60 wt% to 80 wt%, and the monoxide phase precipitation occurred, reaching 20 wt% at the end of this stage.

Based on those observations, it can be concluded that even though the formation of C2S_C3P phase enhances dephosphorization, it seems that a critical C2S_C3P phase amount exists, above which no further improvement in phosphorus removal can be attained, and a phosphorus reversion might occur. This is in accordance with the experimental observations of Inoue and Suito [114], which indicated that a C2S_C3P

content higher than 35-45 wt% no longer contributed to an increase in Lp_{total} (Figure 38). Based on the analysis of dephosphorization stages during the plant trials of Schoop et al. [52, 53, 175], the limiting value, $C2S\_C3P_{lim}$, is estimated to lie in the range of 50-60 wt%. The fact that $C2S\_C3P_{lim}$ estimated based on plant trial results is higher than $C2S\_C3P_{lim}$ estimated based on experimental data can be attributed to the fact that the industrial process is characterized by a high stirring. Another possibility is the difference in the composition of the oxide system investigated: The P_2O_5 content of the slags during the plant trials [52, 53, 175] ranged between 5-20 wt% while the P_2O_5 content of the slags during the experiments [114] was less than 5 wt%.

The existence of a limiting C2S_C3P content for the achievement of optimal dephosphorization results confirms that a large interface between the liquid slag and the solid C2S_C3P phase is crucial to ensure the transfer of phosphorus from the liquid to the solid phase. The increase of C2S_C3P amount beyond $C2S\_C3P_{lim}$ increases the viscosity of the heterogeneous slag, which may inhibit the peeling-off of the P-enriched C2S_C3P phase (Figure 6). Also, it can be seen that monoxide phase precipitation increased during this stage and reached 18% for type 2 heats. It can be concluded that the formation of the monoxide phase in C2S_C3P saturated slags when the C2S_C3P phase amount is higher than the limiting value $C2S\_C3P_{lim}$, further contributes to the increase of the phosphorus content of the metal phase. This effect can be explained by the further decrease in the liquid slag amount and the subsequent decrease in the interface between liquid slag and solid C2S_C3P phase as well as by the increase in the slag viscosity.

C. Dephosphorization stage 3

During stage 3, a recovery from rephosphorization is observed for both heat types. The phosphorus content of type 6 droplets dropped from a value of 0.05-0.07 wt% to 0.006-0.007 wt% by the end of this stage, which are the lowest values achieved during the entire process. Thus, the state of the slag at the end of this stage represents an optimal composition for the achievement of low phosphorus contents in the metal phase during the industrial process.

A decrease in both the C2S_C3P and in the monoxide phase amount in favor of an increase in liquid slag amount was observed for both heat types. The representation

of the slag path during stage 3 in the corresponding phase diagram, shown in Figure 52, indicates that, for type 1 heats, the slag is situated slightly below lime saturation for reduced p(O_2) case and slightly above lime saturation for the elevated p(O_2) case. Thus, it can be stated that independently of the oxidation state of FeO_x in the slag, the slag was very close to the lime saturation line.

It is interesting that the variation range of the slag composition during this stage was very small, especially compared to the variations observed during stage 1 and stage 2. However, the effect of those small variations on the extent of the evolution of P in the metallic droplets was very pronounced. Also, this stage is characterized by a long duration than all of the other stages and for both heat types as it has a duration of 5 and 4.5 minutes for type 1 heats and type 2 heats, respectively. The increase in liquid slag amount and the long duration of this stage may have contributed to the enhancement of the diffusive mass transfer of phosphorus between liquid slag and C2S_C3P phase and thus to an increase in Lp_{slag}. The dephosphorization behavior of the metallic droplets during this stage can be thus considered as an evidence of the importance of the diffusion route (see section 2.4.2) in the enrichment of the C2S_C3P phase with phosphorus during the industrial process.

The behavior of the P removal rate for type 2 heats can be divided into 3 parts: A high P removal rate during the first 1.5 minutes (stage 3.a), a slow-down or standstill afterward with a duration of 1.5 minutes (stage 3.b) and finally, a moderate removal rate for the last 1.5 minutes. It is not clear what is behind the slow-down in P removal during stage 3.b, but it may be associated with the slight increase in C2S_C3P by about 7 wt%, and the considerable decrease in the monoxide phase amount. An increase in C2S_C3P content coupled with a decrease in monoxide content is expected to enhance P removal, but a slow-down is observed instead during stage 3.b. This can be explained by the fact that the C2S_C3P content during this substage is higher than 60 wt% and thus, is already above $C2S\_C3P_{lim}$, which is estimated to lie in the range of 50-60 wt% based on the analysis of stage 1 and stage 2. It seems that, under such conditions, only a decrease in C2S_C3P amount will enhance phosphorus removal. Another possibility is that the diffusive mass transfer of phosphorus from liquid slag to solid C2S_C3P phase is inhibited by an abrupt change in the evolution of the slag

phases, which is observed during stage 2.b. As the C2S_C3P phase amount is decreasing and the liquid slag amount is increasing during substages 3.a and 3.c, the P transfer between the liquid and solid slag phase is enhanced but may have been restrained during stage 2.b due to the abrupt formation of new C2S_C3P precipitations. It can be thus concluded that when the C2S_C3P content is above $C2S\_C3P_{lim}$, the diffusive route becomes the dominant enrichment route for P enrichment of the solid C2S_C3P phase. Under such conditions, a long duration together with a continuous and moderate increase in liquid slag amount is required in order for dephosphorization to continue.

It should be further noted that the monoxide phase was present occasionally during this stage with a content less than 10 wt% for type 1 heats and less than 15 wt% for type 2 heats. The positive dephosphorization behavior observed in the metallic droplets during this stage, indicates that when the monoxide phase is present in limited amounts, which is estimated to lie in the range of 10-15 wt%, no indication of a negative effect on dephosphorization is found and in some cases, a P removal can be observed, which can be explained by the positive effect of lime saturation on the dephosphorization potential of the liquid slag.

D. Dephosphorization stage 4

During this stage, a moderate rephosphorization in the metallic droplets of Gr.6 occurred for both heat types. This stage is characterized by an increase in the monoxide content of the heterogeneous slag, reaching its highest values for the entire process. The behavior of C2S_C3P phase during this stage was different for each heat type: For type 1 heats, the dissolution of C2S_C3P, which already started in stage 3, stopped completely and a slight increase by 5 wt% was observed, while for type 2 heats, the dissolution of C2S_C3P has continued.

The description of the lime addition profile provided by Schoop et al. [52, 53, 175] indicates that lump lime was added exceptionally at the start of this stage with an amount of 4 tons for type 1 heat and 8.86 tons for type 2 heats. This explains the high amount of monoxide phase, formed exceptionally during this stage, which reached a content of 16 wt% for type 1 heats and 23 wt% for type 2 heats. The lump lime requires a longer dissolution time than the lime powder, which has been blown continuously into the

melt during this process. [52, 53, 175] This indicates that possibly, 3 types of solid phase were present in the slag during this stage: The C2S_C3P phase, the monoxide phase and undissolved lime parts. The rephosphorization observed in the droplets confirms the negative effect of the monoxide phase on the dephosphorizing potential of C2S_C3P saturated slags.

The negative effect of excessive monoxide precipitations on the dephosphorization potential of C2S_C3P saturated slags can be explained based on the description of phosphorus distribution in a heterogeneous slag given by equation (29). The formation of the monoxide phase, which does not dissolve phosphorus, decreases the amount of liquid slag and solid C2S_C3P, and, eventually, it counteracts the positive effect of lime saturation on the dephosphorization potential of the liquid slag. In addition, its presence decreases the interface between liquid slag and C2S_C3P phase as well as the fluidity of the heterogeneous slag, which are important factors for promoting P transfer from liquid to solid C2S_C3P via the diffusion route. Similarly, the presence of undissolved lime parts has a negative effect on the diffusive mass transfer of phosphorus, which may be more considerable than the effect of monoxide phase formation: The lump lime parts are expected to be larger in size than the monoxide particles (which are formed by precipitation) and are thus more likely to form large clusters and inhibit the diffusion process.

E. Dephosphorization stage 5

This stage corresponds to the last blowing stage during the plant trials [52, 53, 175]. A recovery from rephosphorization is observed in the metallic droplets during this stage.

The representation of the slag path during stage 5 in the corresponding phase diagram, shown in Figure 52, indicates that, for type 1 heats, the slag lay exactly along the lime saturation line when a reduced $p(O_2)$ state is considered. Accordingly, the simulation results show that the monoxide phase dissolved almost completely for both heat types, and its content was below 3 wt% at the end of this stage. The final phosphorus content achieved in the metallic droplets was in the range of 0.02 wt%. This stage was further characterized by an increase in the FeO content of the heterogeneous slag and by a strong increase in the liquid slag amount, while the C2S_C3P phase dissolved gradually, reaching a final content in the range of 30 wt% for both heat types.

It can be thus concluded that high amounts of C2S_C3P phase are not required to achieve low phosphorus contents in the metal phase and that values in the range of 30-40 wt% are sufficient to achieve optimal dephosphorization results.

6.5 Conclusion and consequences for the industrial process

In section 6.4, the phosphorus evolution behavior measured by Schoop et al. [52, 53, 175] in Gr. 6 metallic droplets, which had a diameter of 0.1-0.16 mm, has been divided into five stages. Each stage corresponds to a specific blowing interval where either a phosphorus removal or reversion behavior was observed. Based on the analysis of the P equilibrium state, provided in section 6.3, it is assumed that droplets with a diameter smaller than 0.5 mm are representative of the equilibrium state of P in the metal phase. Each stage was analyzed by means of comparing the evolution of the P content in these metallic droplets with the evolution of slag phases, which is simulated using the thermodynamic BOF DePhos database, presented in chapter 3.

The results indicate that the slag became heterogeneous within 2 minutes after the start of the blow and remained in such a state for the entire blowing process. The heterogeneous slag was always C2S_C3P saturated and occasionally also saturated with the monoxide phase CaO-ss.

Optimal dephosphorization results could be observed when the C2S_C3P content attained a specific value, which is estimated in the range of 50-60 wt% when no other solid phase is present. This value is designated as the $C2S\_C3P_{limit}$ and is defined as the C2S_C3P content at which optimal dephosphorization results are obtained. In many cases, a reversion and a subsequent recovery in phosphorus removal could be observed in conjunction with an increase followed by a decrease in the monoxide phase amount, respectively. The negative effect of the monoxide phase is observed when its content exceeds a certain critical value, which is estimated to lie in the range of 10-15 wt%. Below this range, the monoxide phase precipitation does not negatively affect dephosphorization, and in many cases, a positive effect on dephosphorization is observed.

The negative effect of the monoxide phase on the dephosphorization potential of C2S_C3P saturated slags can be explained based on the description of the phosphorus distribution in equation (29), derived from the thermodynamic evaluations of the

low P_2O_5 system, presented in section 5.4. The formation of the monoxide phase indicates reaching lime saturation and, thus, the achievement of a high phosphorus distribution in the liquid part of the slag (a high Lp_{liq}, given by equation (26)). This explains the positive effect of the monoxide phase on dephosphorization, observed when its content remains below a certain value, which is estimated to lie in the range of 10-15 wt%. However, the presence of the monoxide phase decreases the amount of liquid slag and solid C2S_C3P phase, which eventually counteracts its positive effect upon exceeding this limitation range, thus resulting in an overall decrease in Lp_{tot}. It is further concluded that the presence of the monoxide phase in high amounts decreases the phosphorus enrichment potential of the C2S_C3P phase via the diffusion route, mainly due to the following aspects:

1. The monoxide precipitations may decrease the interface between the liquid slag and solid C2S_C3P where the transfer of P_2O_5 from liquid to solid slag phase takes place.
2. During the analysis of stage 1, it is observed that an increase in the SiO_2 content of the liquid slag phase has a negative effect on dephosphorization, which is potentially linked to its increasing effect on viscosity. Similarly, the negative effect of monoxide precipitations may also be associated with a resulting increase of the apparent viscosity of the heterogeneous slag, which is a strong function of the fraction of solid phase [218]. Shiraishi et al.[219] investigated the viscosity of Fe_xO-SiO_2 slags containing solid particles, and observed a sharp viscosity increase when the solid fraction increased. Ono et al.[220] observed that the fluidity of C2S saturated slags at a temperature of 1823 K (1550°C) decreased with an increase in their C2S content. This can be explained by the fact that an increased viscosity results in a decrease of the mass transfer coefficient in the slag, which will eventually affect the mass transfer of P_2O_5 from the liquid slag to the C2S_C3P solid phase. In their kinetic dephosphorization model, Kitamura and co-workers [99] introduced a factor accounting for the effect of the solid fraction on the mass transfer coefficient in the slag.

Similarly, the negative effect of excessive C2S_C3P precipitations, upon exceeding the value of the C2S_C3P $_{limit}$, can be attributed to its decreasing effect on the slag fluidity as well as on the interface between liquid slag and solid C2S_C3P phase.

It is further observed that the addition of bulk lime at the initial phase of stage 4 causes rephosphorization in the metallic droplets due to excessive monoxide precipitation. A recovery in phosphorus removal after bulk lime addition is possible, provided that a subsequent increase in the amount of liquid slag and a decrease in the amount of monoxide takes place over a sufficient duration.

The initial phosphorus content of the hot metal, reported by Schoop et al.[52, 53, 175] was higher than 1 wt%. As a result, the P_2O_5 content of the corresponding slag was higher than 10 wt% during the entire blowing period. Under such conditions, it is expected that the precipitation route would be dominant over the diffusion route for C2S_C3P enrichment on phosphorus (see section 2.4.2). The phosphorus enrichment grade in the solid phase via the precipitation route was reported as very high [98, 111, 114], which explains the high phosphorus distribution values established during the process. However, the strong correlation between an increase in the liquid or apparent viscosity of the slag and the occurrence of a phosphorus reversion in the metallic droplets is evidence of the significance of the diffusion route for the enrichment of the solid phase during this process.

7 Exploitation and impact of the results for dephosphorization modeling and control

7.1 Application of computational thermodynamics to online process control

Based on the analysis of the dephosphorization stages presented in section 6.4, it can be concluded that the dephosphorization potential of C2S_C3P saturated slags is mainly controlled by the evolution of the different slag phases (liquid, C2S_C3P, and monoxide). This is supported by the fact that the correlation between the measured P evolution in the small-sized droplets of Gr.6, which have been considered representative of the P equilibrium state in the metal phase (see section 6.3), and the simulated evolution of the slag phases did not depend directly on the temperature or on the blowing conditions. It is observed, based on the analysis of 2 different types of heats (type 1 and type 2 heats), that when the evolution of slag phases was similar for a specific dephosphorization stage, the corresponding phosphorus evolution in the metallic droplets was also similar independently of the heat type. It should be noted that type 1 and type 2 heats had very distinguished blowing profiles in terms of oxygen blowing rate and the lance height profile. The results indicate that a successful simulation of the evolution of slag phases and their composition is essential for the accurate prediction of the evolution of phosphorus in the metal phase. In this context, the application of a CALPHAD-based approach presents a powerful method for the accurate determination of the type, amount and composition of a large number of oxide systems over the entire temperature, composition, and oxygen partial pressure range relevant for the industrial process. However, the evolution of the oxide content and the temperature of the slag is required as input data for the thermodynamic simulations. For this purpose, dynamic models based on the principle of conservation of mass and energy can be used.[221] Such models are capable of calculating the amount and total composition of the metal and slag during the blow based on online process data, such as the oxygen blowing rate, the lance height profile, the input time and the input amount of additions.[49, 91, 222]

An implementation concept of the BOFdePhos thermodynamic database into a comprehensive “dynamic BOF process model” is presented in **Figure 53**. The “BOF Process Model” determines the evolution of metal and slag temperature as well as the

evolution of the main slag components, such as CaO, FeO, MnO, SiO_2, MgO, mainly on the basis of mass and energy balance equations.[91] Further information from kinetic functions or models is required for these calculations, such as the amount of lime or scrap dissolved during the process, which are determined based on lime dissolution [223, 224] and scrap melting models [225] respectively. The slag composition and temperature, calculated using the "BOF Process Model", can be given as input data into the thermodynamic database, which in turn calculates the amount and composition of the involved slag phases. The calculation output of the thermodynamic database can be used for the following:

- Determination of the equilibrium phosphorus content in the metal $[\%P]_{eq}^{t}$, by using a phosphorus distribution equation suitable for heterogeneous slags such as equation (29), which has been developed based on the thermodynamic calculations for the low phosphorus system presented in this work.
- The phosphorus equilibrium value $[\%P]_{eq}^{t}$, is then used as input to the "Kinetic dephosphorization model" as it defines the driving force for the dephosphorization reaction.
- Determination of the lime saturation value of the slag, $(\%CaO)_{sat}$, which is a strong function of the slag composition and temperature.[226] For CaO-FeO_x-P_2O_5 and CaO-FeO_x-SiO_2 based slags with a low content of further oxides, equations (18)-(19) and equations (24)-(25) can be used for example to calculate lime saturation values, respectively. The difference between the actual lime content of the slag and its saturation value, $(\%CaO)_{sat}$, defines the thermodynamic driving force for lime dissolution.[227]
- Characterization of the transport properties of the slag: The mass transfer coefficient of the slag is known to be a strong function of the slag composition [228] and the solid phase fraction [99], both of which can be determined accurately by the BOFdePhos thermodynamic database. The mass transfer coefficient of the slag is an important parameter for the determination of the dephosphorization rate [99] as well as for estimating the dissolution rate of CaO and MgO [224, 227].

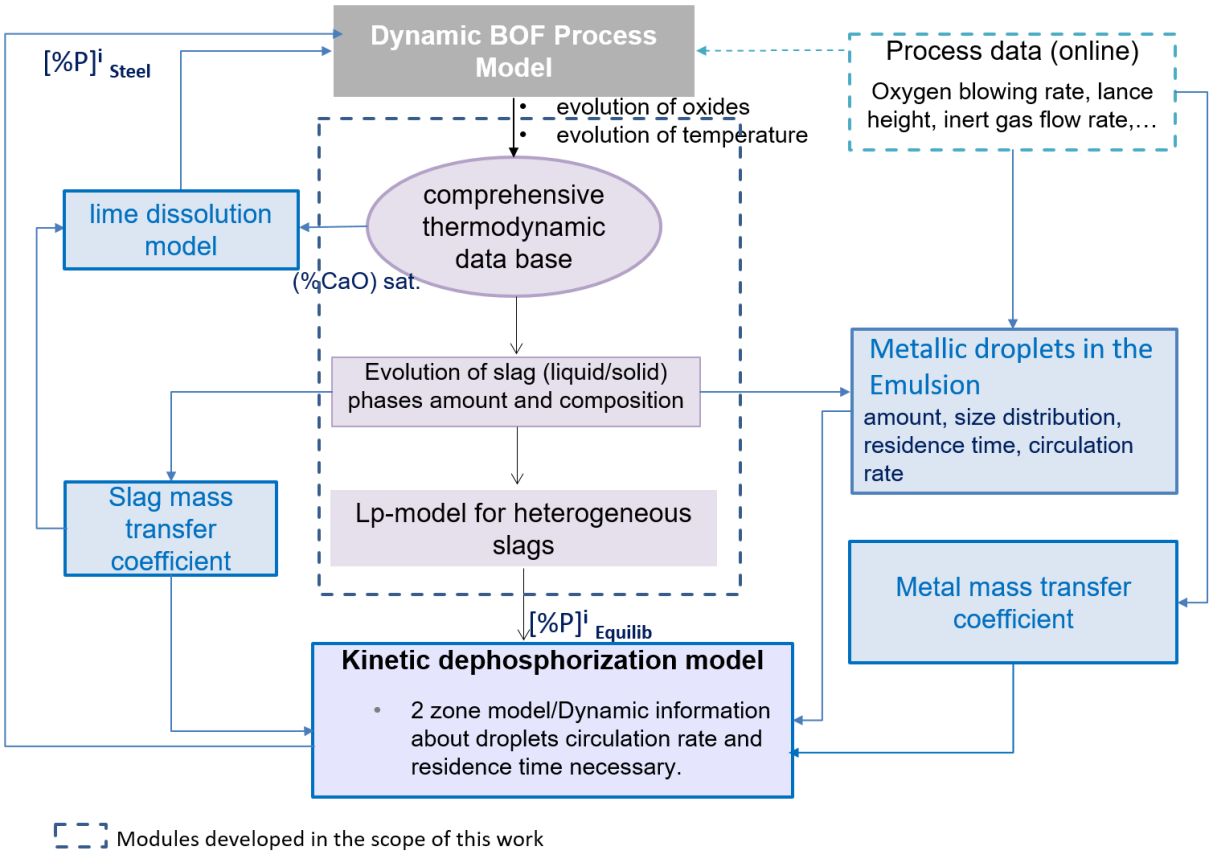

Figure 53: Implementation concept for the thermodynamic database in a comprehensive dynamic model for the purpose of modeling and control of the dephosphorization reaction.

The implementation of the thermodynamic database contributes to the enhancement of the accuracy of dynamic BOF process models. In general, dynamic process models are used for the continuous monitoring of the actual heat state in the BOF converter, as well as for the prediction of its further evolution until the end of the blow. Such information can be assessed by dynamic control functions for adaption of the amount of oxygen to be blown, lime to be charged, and heating or cooling materials to be added in order to adjust the targets for temperature, carbon, and phosphorus content. Thus, the enhancement of the accuracy of such models will subsequently lead to better attainment of the target values and therefore, to significant economic benefits for the industrial process. When the target composition is not met, a reblow is required, which consists of further blowing oxygen and charging additions. A reblow is associated with a considerable loss of production time, a decrease in the iron yield as well

as with an increase in refractory wear and deoxidant amount. Thus, a better adjustment and control of the process leads to cost savings and improves the liquid steel quality in terms of lower phosphorus content.

Furthermore, the thermodynamic database is suitable for integration in flowsheet modeling of industrial processes, which is based on the principle of inter-linked local equilibria [148, 149], also widely designated as the effective equilibrium method [143, 229] in the literature. In the scope of the BOFdePhos project,[91] a flowsheet model, denoted as LD-Sage, has been developed and the BOFdePhos thermodynamic database was used for the determination of the metal-slag-gas equilibrium state in the different equilibrium zones. Details about the model concept and results can be found in separate publications.[49, 91, 230, 231]

7.2 Specification of the target slag composition for optimal dephosphorization results

Based on the thermodynamic evaluation of low P_2O_5-systems presented in section 5.2, it can be concluded that the single-phase CaO-ss saturation region is not accessible under the conditions relevant to the standard BOF process operation (SiO_2 content in the slag higher than 10 wt%, temperatures lower than 1973 K (1700°C), MgO is usually present in the slag, …). When MgO is present in the system with a content equal to or higher than 7 wt%, a monoxide phase, MgO-ss, becomes stable over a large part of the lime saturation region. It is concluded based on the analysis of a large number of industrial data in section 6, that the presence of monoxide phase CaO-ss with a content higher than 10-15 wt% has a strong negative effect on dephosphorization. The low phosphorus system is characterized by the presence of the same monoxide phase, CaO-ss, when lime saturation is reached. In the presence of MgO, a second monoxide phase, the MgO-ss phase is formed additionally. Furthermore, it is found that reaching lime saturation is always associated with an additional saturation with the C3S solid phase. All of those solid phases, which are stable at lime saturation (CaO-ss, MgO-ss, and C3S) do not dissolve phosphorus and their effect on dephosphorization in the low P_2O_5 system is estimated to be similar to the effect of the monoxide phase in the high P_2O_5 system:

- From a thermodynamic perspective: The precipitation of CaO-ss, MgO-ss, and C3S leads to a decrease in the amount of liquid slag and in some cases, also in the C2S phase. This means that non-P-dissolving phases are formed at the cost of P-dissolving phases (the liquid slag and the C2S phase). As a result, the phosphorus distribution between the heterogeneous slag and liquid metal decreases considerably, following the Lp-formulation in a heterogeneous slag given by equation (29).
- From a kinetic perspective: The formation of the monoxide phases CaO-ss and MgO-ss as well as the formation of the C3S phase result in a decrease of the liquid slag amount and subsequently, of the interface between liquid slag and solid C2S-C3P phase, as well as of the interface between liquid slag and undissolved lime. In addition, the viscosity of the slag increases drastically when the solid phase fraction increases.[99, 219] Eventually, the formation of large precipitations of those solid phases inhibits the enrichment of the solid phase C2S_C3P through the diffusion route and slows down lime dissolution, which leads to poor dephosphorization results.

Based on the present findings, it is highly recommended to aim at the C2S-saturation region in order to ensure the establishment of a high phosphorus distribution while avoiding the risk of excessive solid phase precipitation, associated with reaching lime saturation. In low phosphorus slags, which is mostly the case for European BOF slags, it is expected that the enrichment of the C2S_C3P phase on phosphorus would be dominated by the diffusion route (see section 2.4.2) due to the low P_2O_5 content in the slag. It is thus important to provide suitable conditions for the enhancement of the mass transfer of phosphorus between the liquid slag and the solid C2S_C3P phase in order to exploit the phosphorus removal potential of the C2S_C3P phase. Based on the analysis of the industrial plant trials of Schoop et al.[52, 53, 175], it is concluded that the optimal amount of C2S_C3P precipitation, denoted as $C2S\_C3P_{lim}$ is estimated to lie in the range of 50-60 wt%. It is possible that the presence of the C3S phase, which has a large stability range in the low phosphorus system, has also a negative effect on the dephosphorization potential of BOF slags, similar to that of the monoxide phase.

Based on the present findings, a new slag region considered as the optimal region for dephosphorization during the BOF process is determined, which is indicated by “zone A” in **Figure 54**, where the calculated phase boundaries of the CaO-FeO_x-SiO_2 system are presented at a temperature of 1973 K (1700°C) and for a reduced p(O_2) state. This target region A has been selected based on the following four criteria:

1- The dephosphorization potential of the slag is found highest when the slag is saturated with C2S_C3P. This means that the slag composition should be situated within the C2S saturation region (region 2). The enrichment of the C2S_C3P phase in BOF slags is expected to be dominated by the diffusion route due to the low P_2O_5 content of BOF slags (usually lower than 5 wt%). In such a case, the C2S phase is precipitated first without phosphorus, and P_2O_5 is transferred afterward from the liquid slag to the solid C2S phase (see section 2.4.2).

2- It is important that the C2S precipitations remain below a limiting value, which is estimated to lie in the range of 50-60 wt%, based on the analysis of industrial plant trials of Schoop et al. [52, 53, 175] (see section 6.4). In addition, it is crucial that the precipitation of non-phosphorus dissolving phases (monoxide and C3S) is avoided or at least restricted to values lower than 10-15 wt%. This is due to the fact that the mass transfer of phosphorus from the liquid to the solid C2S_C3P phase is inhibited by the presence of an excessive amount of solid phases, especially with regard to the non-phosphorus dissolving phases CaO-ss, MgO-ss, and C3S. The negative effect of excessive solid phase precipitation is attributed to the resulting decrease in the phosphorus distribution in the heterogeneous slag (equation (29)), the reduction of the interface between liquid slag and C2S_C3P phase, the reduction in the interface between liquid slag and undissolved lime as well as to its increasing effect on viscosity which decreases the mass transfer coefficient in the slag.

3- Inoue and Suito [114] reported that the maximum phosphorus distribution values between the C2S_C3P phase and the liquid slag (Lp_{slag}) were measured when the liquid slag was situated at the “nose” of the C2S-saturation region (Figure 5-a). The liquid part of slag situated in zone A is situated very close to the C2S “nose,” and the corresponding Lp_{slag} values are expected to be higher than 10, according to the measurements of Inoue and Suito [114].

4- Small fluctuations in the slag composition, for example, in the direction of lower or higher CaO-contents, may shift the composition from zone A to zone A' or A", respectively. In such a case, the slag will either remain C2S-saturated (zone A') with a liquid part situated close to the C2S "nose" (Thus further satisfying criteria 2- and 3-), or the slag will enter the double saturation region with C3S and CaO-ss (zone A''). In the second case, the slag would no longer be saturated with C2S. However, the liquid part of the slag is lime saturated, and at the same time, the amount of CaO-ss and C3S precipitations is small, due to the fact that zone A'' is situated far from the C3S and CaO corners. Thus, the dephosphorization potential of the slag in both cases (zone A' and zone A'') remains high, albeit lower than that of zone A.

It should be noted that zone "B", shown in Figure 54, also satisfies criteria 1-3 and, at the same time, is highly interesting for the industrial process: A slag situated within zone B has a low FeO content (In the range of 15-23 wt%) which has considerable economic benefits, such as achieving a high iron yield and less refractory wear during the process. Also, the CaO content required for achieving zone B is slightly lower than that required for zone A, which implies less lime consumption and less slag formation. However, zone B is not recommended as an optimal target region for dephosphorization due to the fact that small fluctuations in the slag composition, for example in the direction of lower or higher CaO contents, may shift the composition from zone B to zone B' or zone B'' respectively, which may induce a negative effect on dephosphorization due to the following:

- Even though zone B' is situated within the single saturation zone regarding C2S, the liquid part of the slag is now situated far from the C2S "nose". Thus, criterion 3- is no longer satisfied. According to the measurements of Inoue and Suito [114], the resulting Lp_{slag} values will be low (Figure 5-a), and eventually, a low Lp_{tot} will be established in the slag according to equation (29).

- Zone B'' is situated in the double saturation region with C2S and C3S. The amount of C3S precipitation will be high, especially compared to that in the case of zone A''. The resulting dephosphorization potential of the slag is low, since excessive C3S precipitations are estimated to have a negative effect on Lp_{tot}, similar to the effect of excessive monoxide precipitations.

Thus, zone B is recommended for dephosphorization in processes where the slag composition can be controlled very accurately in a way that such small fluctuations can be avoided. For the standard BOF process, where changes in slag composition are a strong function of the carbon removal rate, zone A is recommended as the optimal target slag zone.

It can be seen from Figure 54 that the CaO-content of the total slag required for reaching zone A is about 5-12 wt% lower than the values required for reaching lime saturation. This means that the lime amounts which should be charged during the process are lower, which brings considerable economic benefits to steelmakers, such as decreased lime consumption, less final slag amounts, and decreased refractory wear.

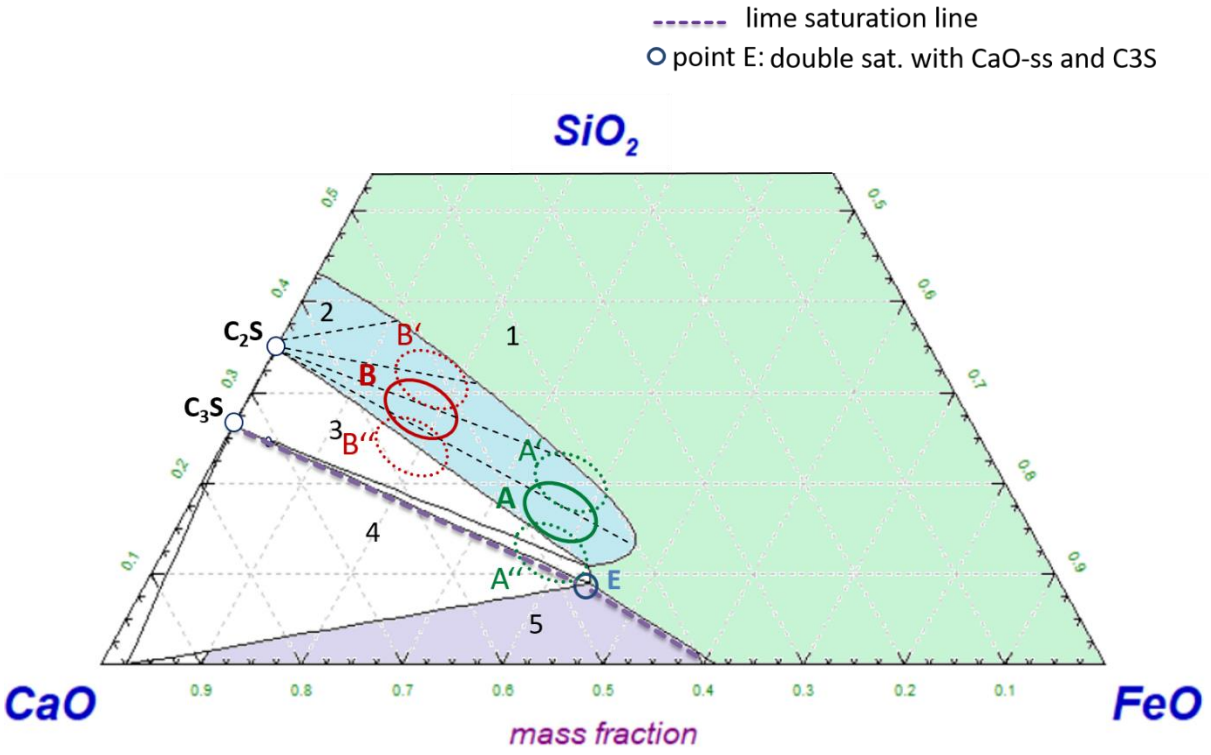

Figure 54: Position of the alternative target slag regions A and B, suggested in the present work for optimal dephosphorization results in the CaO-FeO_x-SiO_2 system, at 1973 K (1700°C), and for a reduced p(O_2) state.

Finally, it should be mentioned that the phase boundaries of the CaO-FeO_x-SiO_2 oxide system are found to be a strong function of the process temperature (Figure 30), the p(O_2) state (Figure 29), as well as of the minor oxide contents (Figure 36-Figure 37) in the present work. This implies that the composition of the target slag region A should

be adjusted to take into account the changes in temperature, $p(O_2)$ state or minor oxide content of the system, in order to continue satisfying criteria 1-4.

Figure 55-a), –b), –c) and -d) present some examples for setting the position of the target region at different temperatures and minor oxide contents for the reduced $p(O_2)$ state, as calculated using the BOFdePhos thermodynamic database. It becomes obvious that the determination of the dynamic evolution of the slag composition and temperature, as well as the accurate simulation of the corresponding phase boundaries under these specific conditions, is crucial for setting the optimal target slag region. This can be achieved, for example, by the implementation of a consistent CALPHAD-based thermodynamic approach suitable for multi-component and multi-phase systems, such as the BOFdePhos thermodynamic database, in a dynamic process model, for example by following the scheme presented in Figure 53.

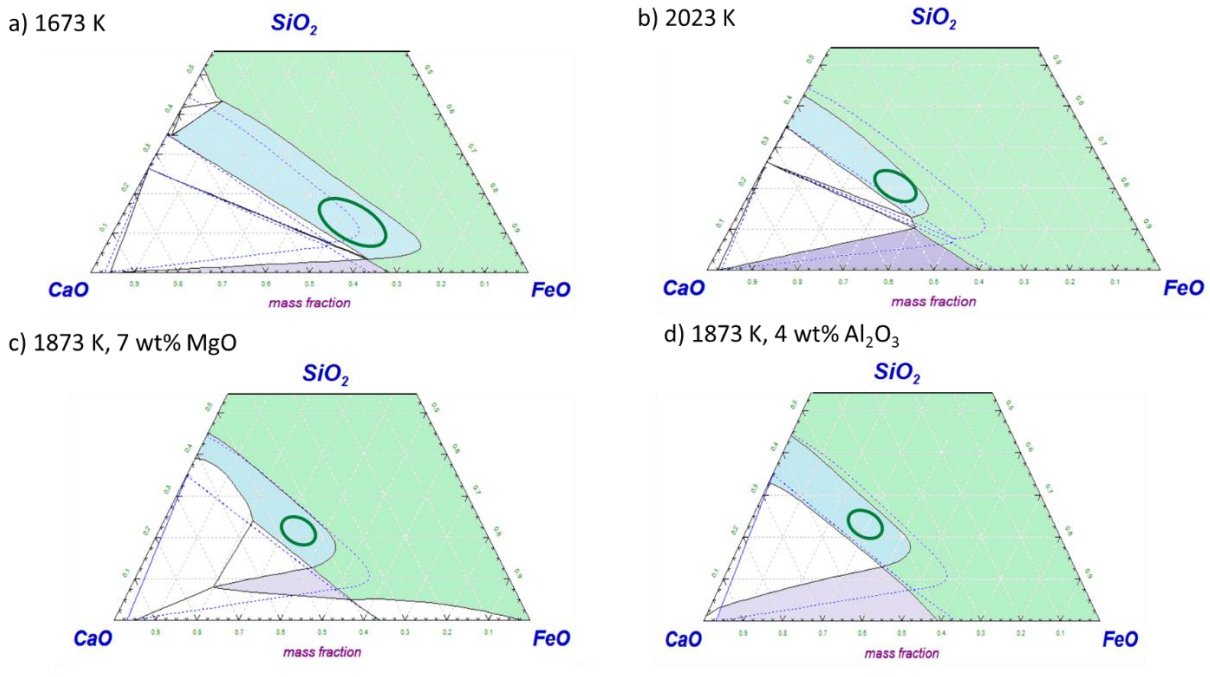

Figure 55: Examples of the adjustment of the position of the optimal target slag region (green circle) in the $CaO\text{-}FeO_x\text{-}SiO_2$ oxide system at reduced $p(O_2)$ state as a function of temperature: a) 1673 K (1400°C), b) 2023 K (1750°C), and depending on the minor oxide content of the system: c) 7 wt% MgO at 1873 K (1600°C), d) 4 wt% Al_2O_3 at 1873 K (1600°C). The dashed lines represent the phase boundaries of the ternary system at 1873 K.

7.3 Development of a new BOF method for controlling dephosphorization

Apart from the necessity of an accurate determination of the optimal slag composition, explained in section 7.2, an accurate slag control during the BOF process in a way that the target composition can be set under specific conditions is also required. For this purpose, a method has been developed to provide the required flexibility in controlling the slag composition during the BOF process. This method is presented in **Figure 56**, and consists of the injection of fluxes, mainly lime powder, directly into the slag through sidewall nozzles.[232] The purpose of the method is ensuring a flexible control of the slag composition in order to achieve a high dephosphorization potential of the corresponding slag based on the following mechanisms:

- By injecting CaO particles into a C2S-saturated slag, a high phosphorus enrichment of the solid phase is expected. Suito et al.[113] and Hamano et al.[120] reported that the enrichment grade of C2S_C3P was high when this phase is formed at the rim of CaO particles during their dissolution into the slag. Yang, Matsuura et al.[102] emphasized that the amount of C2S_C3P phase formed at the interface between the CaO particles and the reacting slag was much higher than in the case when C2S particles were added.
- By continuously injecting small lime particles, the CaO-content of the slag will gradually increase. Thus, the C2S phase is expected to precipitate gradually in small amounts. In such a case, the C2S precipitates are more likely to be distributed as isolated particles and the formation of C2S clusters is avoided, which is necessary for the establishment of a high phosphorus enrichment (see section 2.4.2). In addition, the enrichment of the solid phase by the diffusion route is enhanced when the interface between the liquid slag and the C2S precipitates is large and the slag viscosity is low, which can be maintained by a continuous injection of lime powder. On the contrary, when bulk lime is added in high amounts, the CaO content may increase rapidly. This may result in excessive C2S precipitations, thus increasing the risk of the formation of C2S clusters. Under such conditions, a low enrichment of the solid phase C2S_C3P on phosphorus is expected.

By using the sidewall nozzles for lime injection, the following disadvantages associated with alternative lime blowing methods (For example, through top oxygen lance or bottom tuyeres) are avoided:

- The top oxygen lance is a laval nozzle of convergent-divergent type, which produces supersonic gas velocities approximately at twice the speed of sound. When lime is injected through this type of nozzle, the particles are accelerated up to a high speed by the supersonic gas. The particles will be grinding against the nozzle walls, which will induce a rapid wear on those walls. Since the top lance is water-cooled, an unforeseen water leakage might occur if the wall thickness becomes too thin, with hazardous consequences.
- It is considered that restricting the powder injection to the bottom nozzles is not sufficient to achieve the total lime amounts required for achieving optimal dephosphorization. The mass transfer of phosphorus in the bath is generally considered as a rate-limiting step for the dephosphorization reaction [13], and in the case of bottom lime injection, it is expected to be also the rate-limiting step for lime dissolution. This is especially the case when an oxygen-free gas is used for the bottom injection. Also, due to the relatively small outlet area, the injection of lime powder solely through the bottom nozzles is limited, and the required powder injection rates will not be achieved. The powder injection will further limit the inert gas-flow rates through the bottom nozzles and decrease their life span.

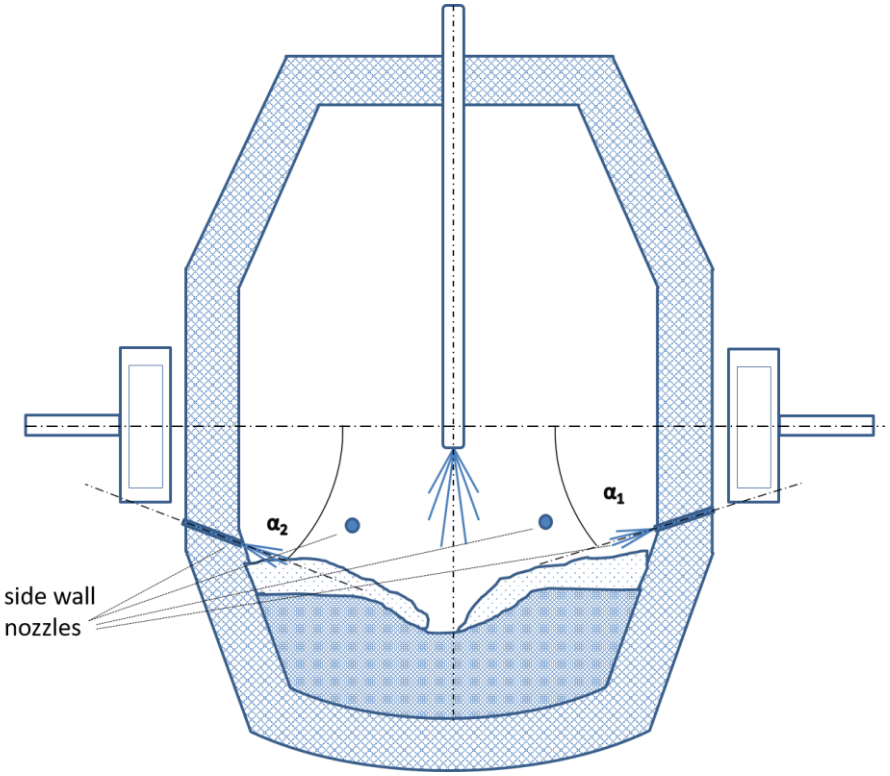

Figure 56: Method for dephosphorization control in the BOF process developed in the present work [232]

Furthermore, the method presented in Figure 56 has been optimized to provide additional flexibility in the control of the decarburization rate. It is found that lime injection in the slag may initiate a kinetically impeded CO-nucleation, which is found to be responsible for slopping occurrence.[230] By optimizing the position, number, blowing angle and carrier gas flowing rate of the sidewall nozzles, the mixing intensity in the slag (or emulsion) zone can be controlled independently of the mixing intensity in the bath (which is usually controlled by modifying the position of the top oxygen lance). In **Figure 57**-a) and –b), two examples of possible arrangements of the sidewall nozzles, which have been developed in the scope of the present work, are shown.

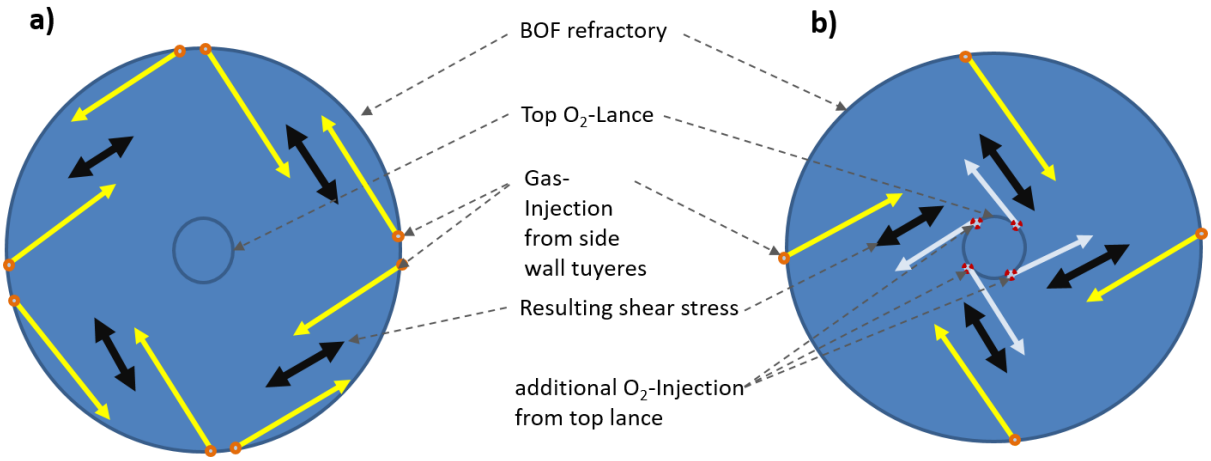

Figure 57: Arrangement of sidewall nozzles for optimal dephosphorization and decarburization control, which is suggested in the present work: a) case of a conventional top oxygen lance, b) case of a special top oxygen lance equipped with tangential outlets.

In Figure 57-a), the mixing (carrier) gas is blown through the pairwise sidewall nozzles in a direction tangential to the furnace circumference. The nozzles are arranged in such a way that opposing jets act on the slag at the points of impact. This ensures that the slag layer does not rotate uniformly but that a stirring effect is obtained through the induced shear stress to ensure that only the slag and not the melt is stirred. Blowing must be as flat as possible so that the mass exchange between the bath and the slag is not affected.

Figure 57-b) presents another possibility of enhancing mixing in the slag without affecting mixing in the bath. According to this method, the top oxygen lance is additionally equipped with nozzles, which are tangentially aligned. The gas is blown through those additional lances parallel but in the opposite direction to that of the gas blown through the sidewall nozzles. Thus, a shear stress results in the slag layer without affecting the mass exchange between the bath and the slag.

The developed methods can be used to avoid slopping and excessive foaming in the first place and thus to serve as a preventive measure. In addition, the method incorporates the possibility of quick intervention by initiating the decarburization reaction at a controlled rate if slopping risk is detected. Further details about the presented method are provided in separate publications.[87, 230]

8 Potential, limitations and future aspects of the present work

The work undertaken in the scope of this thesis revealed major findings with respect to the thermodynamics of the dephosphorization reaction and the important role of the solid phase C2S_C3P during the dephosphorization in the industrial process. It is found that dephosphorization in the BOF process has not reached its full thermodynamic potential and that dephosphorization control strategies have focused solely on enhancing the dephosphorization potential of liquid slags, while the role of the solid phase C2S_C3P in the industrial process has not been given the attention it deserves. The exploitation of the great potential of the solid phase in removing phosphorus is lacking, and thus highly recommended as it provides new possibilities for the successful refining of high phosphorus hot metal in a standard BOF furnace. In this work, the phase diagrams required for the identification of the stability range of this solid phase over the total variation range of temperature, oxygen partial pressure, and P_2O_5 content are provided. In addition, the effect of minor oxides such as MgO, MnO, and Al_2O_3 on several ternary systems is discussed.

In this context, a large emphasis is put on providing a simplified, yet powerful visualization of the phase diagrams relevant for the industrial process without losing information on the behavior of the system in the relevant composition, temperature, and $p(O_2)$ ranges. For this purpose, the phase diagrams were presented in most cases as a superposition of different system's isothermals, calculated at different $p(O_2)$ states and temperature values in order to clarify how the phase boundaries are affected by a modification in the process conditions. Those diagrams were then used for the interpretation of experimental and industrial observations. Similarly, steelmakers can use the diagrams generated in this work to interpret plant trial results, define target compositions, derive new control strategies, or design completely new processes with economic and/or ecological advantages.

Based on the findings presented in the current work, new methods and strategies for enhancing dephosphorization control are developed and presented. This includes an implementation concept of the BOFdePhos thermodynamic database into a dynamic BOF process model, the specification of a new target slag zone for achieving optimal dephosphorization results, and a new BOF method for ensuring accurate control of

the slag composition towards the specified target region. The new methods and strategies were derived based on the thermodynamic evaluations of relevant slag systems, together with the analysis of a large number of laboratory and industrial data.

It is found that, although several experimental works investigating the enrichment behavior of phosphorus in the solid C2S_C3P phase are available in the literature, the majority of those works were related to the hot metal dephosphorization process, which is part of the double slag strategy adopted in Japanese steelworks. Even though the results are very useful, a transfer of the results to the standard BOF practice adopted in European steelworks can only be made with precaution.

The majority of the industrial slag samples investigated in the present work were high in phosphorus. In such a case, the enrichment of the solid C2S_C3P with phosphorus is expected to be dominated by the precipitation route (section 2.4). Still, the diffusion route is found to play a significant role. The analysis of the industrial plant trials of Schoop et al. [52, 53, 175], provided in section 6.4, indicated that the enrichment was inhibited by excessive solid phase formation. It seems that the enrichment via the diffusion route is strongly affected by the viscosity of the slag. In the low phosphorus part of the quaternary CaO-FeO_x-SiO_2-P_2O_5 system, which is the relevant part for the standard BOF practice, the diffusion route is expected to be the dominant route for the phosphorus enrichment of the C2S_C3P phase and should be thus investigated in more detail. In addition, this part of the system is characterized by a large stability range of the C3S phase, which is expected to have a similar effect, if not more critical, as that of the monoxide phases (CaO-ss and MgO-ss) in decreasing the phosphorus enrichment of the solid C2S_C3P phase. It is thus highly recommended to carry out further work to clarify the phosphorus enrichment mechanism of the solid C2S_C3P phase in the low phosphorus part of the system, and how it is affected by process conditions. Thus, rigorous experimental and industrial investigations are needed. In this context, the phase diagrams and the thermodynamic evaluations presented in this work provide a firm basis for setting the experimental conditions or planning the plant trials.

The heterogeneous nature of high and low phosphorus BOF slags throughout the entire blowing process is underlined in this work. In general, BOF slag sampling is carried out with a steel bar, which is immersed in the slag. After taking out, a layer of slag is

sticking on the bar, which mainly originates from the liquid slag part. Thus, it is suspected that the slag sampling techniques currently available in the market provide information about the liquid slag part only and do not necessarily represent the state of the heterogeneous slag. Thus, it is highly recommended to develop alternative sampling techniques, which ensure that the samples are representative of the total slag state and not only the liquid part. The availability of representative slag samples is an important pre-requisite for the success of industrial-based investigations of the enrichment procedure of the C2S_C3P phase with phosphorus. The present work aims at motivating steelworks as well as suppliers of process and sampling technologies into carrying out further research and developments on this matter through pointing out the importance of determining the evolution of the solid phases in modeling and control of dephosphorization in the BOF process. The great potential of the C2S_C3P solid phase in removing phosphorus opens promising opportunities for steelworks in overcoming the challenges associated with phosphorus removal.

Furthermore, the effect of the oxidation state of FeO_x, which is set mainly by the oxygen partial pressure $p(O_2)$, on the phase boundaries of the $CaO\text{-}FeO_x\text{-}SiO_2\text{-}P_2O_5$ oxide system is underlined in this work. It is found that increasing the ferric to ferrous ratio is more effective for enhancing lime dissolution and lowering solid phase precipitation than increasing the slag temperature. The effect of the oxidation state of FeO_x is pronounced for both the high and the low P_2O_5 parts of the system, especially compared to the effect of temperature. However, neither is there a general conclusion about the dominant ferric to ferrous ratio in industrial slags, nor are there correlations with the slag composition available. While measurements of the oxygen potential in the metal phase are a general practice for steelworks, little effort has been made to measure the oxygen potential in the slag. The availability of such $p(O_2)$ measurements in the slag, together with a successful correlation with the ferric to ferrous ratio, would deliver the missing information about the oxidation state of FeO_x in BOF slags.

9 Conclusion

In the present work, the quaternary oxide system CaO-FeO_x-SiO_2-P_2O_5 and its ternary subsystems were intensively investigated in the total composition, oxygen partial pressure and temperature ranges relevant for low and high phosphorus refining processes. A computational thermodynamics approach is used for those evaluations, which involves coupling a newly developed thermodynamic database, which is developed according to the CALPHAD method in the scope of the European project BOF-dePhos, to the thermodynamic software package FactSage ™.

The results indicate that the liquidus of the C2S phase and the liquidus of the C2S_C3P phase are highly sensitive to changes in temperature: An increase in temperature results in a considerable decrease of the C2S-saturation region in the CaO-FeO_x-SiO_2 system and a moderate decrease of the C2S_C3P saturation region in the quaternary CaO-FeO_x-SiO_2-P_2O_5 system. On the other hand, temperature variations have a small effect on the lime saturation line for all oxide systems considered.

The effect of the oxidation state of FeO_x, which is set by the oxygen partial pressure $p(O_2)$, on the phase boundaries of those systems is investigated. It is found that an increase in the oxidation state of FeO_x results in a considerable increase in the lime solubility of the slag in all systems considered, in a significant decrease of the C2S saturation region for the CaO-FeO_x-SiO_2 system, as well as in a moderate decrease of the C2S-C3P saturation region for the quaternary system. It is thus concluded that increasing the ferric to ferrous ratio in the slag is more effective than increasing the temperature in promoting lime dissolution and, subsequently, dephosphorization. It is further found that the effect of $p(O_2)$ on the oxide systems is temperature-dependent and was more pronounced at higher than at lower temperatures. Thus, the inhomogeneities reported in slag samples taken early in the blow are, contrary to the general belief, attributed to irregularities in $p(O_2)$ rather than in temperature. The effect of $p(O_2)$ on the phase boundaries of the relevant systems and its significance for the dephosphorization reaction is presented for the first time in the present work. Mathematical descriptions of the dependency of lime saturation in different systems on the temperature and the oxidation state of FeO_x are provided.

The widely observed agreement between the calculated phase boundaries and the experimental data at different temperature and $p(O_2)$ conditions confirms the capability of the adopted computational thermodynamics approach in predicting the thermodynamic behavior of chemical sub-systems in composition ranges and for thermodynamic conditions where no experimental or industrial data are available. This is an important characteristic given the high costs and the strong limitations associated with experimental measurements and industrial plant trials.

The results of the thermodynamic evaluations presented in this work were further used to analyze the state of industrial slags, for which industrial data are provided in the literature. The industrial slags, investigated in the present work, are found to be heterogeneous and, in most cases, saturated with solid C2S_C3P phase. However, most Lp-approaches reported in the literature were developed for liquid slags. Thus, a new Lp-approach is developed in the present work, which considers the effect of the amount, type, and composition of the different phases on the dephosphorization potential of industrial slags. The type and amount of phases formed are found to be highly sensitive to the system's composition, temperature, and $p(O_2)$ state. In addition, the presence of minor oxides such as MgO, MnO, and Al_2O_3 is found to have a considerable effect on the type and amount of phases formed and, subsequently, on dephosphorization. Several controversies between experimental and industrial observations, such as the effect of MgO on dephosphorization, could be explained based on the new Lp-approach.

Furthermore, the evolution of the slag phases is simulated for two industrial heats during the refining of a high phosphorus hot metal. The simulation results indicate that the slag becomes saturated with C2S_C3P phase within 2 minutes after the start of the blow. When comparing the simulated evolution of the slag phases with the measured evolution of the phosphorus content of the metallic droplets, the negative effect of the monoxide phase on dephosphorization, which is indicated by the new Lp-approach, could be confirmed. However, the positive effect of the C2S_C3P phase is observed only up to a certain limit, which is estimated to lie in the range of 50-60 wt%. The negative effect of monoxide precipitation as well as of excessive C2S_C3P precipitation is explained by the resulting decrease in the slag fluidity as well as by the

reduction of the interface between the liquid slag and the C2S_C3P phase, which inhibits the enrichment of the C2S_C3P phase with phosphorus via the diffusion route.

Finally, it is concluded that the exploitation of the thermodynamic potential of the solid phase C2S_C3P in dissolving phosphorus opens promising opportunities for steelworks in overcoming the challenges associated with phosphorus removal. This work demonstrates how new methods and process control strategies for enhancing dephosphorization in the BOF process can be developed under consideration of the phosphorus removal potential of the C2S_C3P phase. This includes an implementation concept of the BOFdePhos thermodynamic database into a dynamic process model, the specification of a new target slag region, as well as the development of a new BOF method for ensuring the accurate control of the slag composition towards the specified target region. However, further work is needed to understand the phosphorus enrichment behavior of the solid C2S_C3P phase under industrial conditions and its inhibiting factors.

References

[1] Publications Office of the European Union, The wind of change: energy in future steelmaking, steel in the energy market applications, greening European steel, 2018, https://op.europa.eu/en/publication-detail/-/publication/fb63033e-2671-11e8-ac73-01aa75ed71a1

[2] World Steel Association: World steel in figures, https://www.worldsteel.org/

[3] B. Deo, R. Boom, Fundamentals of steelmaking metallurgy, Chapter 4, Prentice-Hall, 1993.

[4] E. Turkdogan, Fundamentals of steelmaking, London, The Institute of Materials, 1996.

[5] H. Jalkanen, L. Holappa, Chapter 1.4 - Converter Steelmaking, in: S. Seetharaman (Ed.), Treatise on Process Metallurgy, Elsevier, Boston, 2014, pp. 223-270.

[6] M.A. Tayeb, S. Spooner, S. Sridhar, Phosphorus: The noose of sustainability and renewability in steelmaking, JOM 66(9), 2014, 1565-1571.

[7] T. Bloom, The Influence of Phosphorus on the Properties of Sheet Steel Products and Methods Used to Control Steel Phosphorus Levels in Steel Product Manufacturing. Iron and Steelmaker 17(9) (1990) 35-41.

[8] Y. Yang, K. Raipala, L. Holappa, Chapter 1.1 - Ironmaking, in: S. Seetharaman (Ed.), Treatise on Process Metallurgy, Elsevier, Boston, 2014, pp. 2-88.

[9] A. Biswas, Principles of Blast Furnace Ironmaking: Theory and Practice, Cootha, URL: https://books. google. com. au/books (1981).

[10] B. Deo, J. Halder, B. Snoeijer, A. Overbosch, R. Boom, Effect of MgO and Al_2O_3 variations in oxygen steelmaking (BOF) slag on slag morphology and phosphorus distribution, Ironmaking & steelmaking 32(1) (2005) 54-60.

[11] Y. Ghobara, I. Cameron, Removal of phosphorus-technology alternatives, Iron Steel Technol. 14(4) (2017) 80-89.

[12] D.-I.W. Urban, I.M. Weinberg, I.J. Cappel, De-Phosphorization Strategies and Modelling in Oxygen Steelmaking, Stahl Eisen 134(8) (2014) 27–39.

[13] B.K. Rout, Modelling of dephosphorization in oxygen steelmaking, Ph.D. thesis, Swinburne University of Technology, Melbourne, Australia, 2018.

[14] S.-y. Kitamura, Hot metal pretreatment, Treatise on process metallurgy, Elsevier, 2014, pp. 177-221.

[15] L. Lynn, How Japan innovates: A comparison with the US in the case of oxygen steelmaking, Routledge, 2019.

[16] Y. Wang, S. Yang, J. li, J. Feng, F. Wang, Dephosphorization by Double-Slag Process in Converter Steelmaking, 2017.

[17] S.-y. Kitamura, Solution of the steelmaking process to prepare the increase in the phosphorus content of iron ore, 8th European Oxygen Steelmaking Conference (EOSC), Taranto, 2018.

[18] O. Yuji, Y. Masataka, K. Shin-ya, H. Hiroshi, Development of the Continuous Dephosphorization and Decarburization Process Using BOF, steel research international 74(2) (2003) 70-76.

[19] M. Iwasaki, M. Matsuo, Change and development of steel-making technology, nippon steel technical report 391 (2011) 88.

[20] O. Yuji, M. Yano, S. Kitamura, H. Hirata, Development of the continuous dephosphorization and decarburization process using BOF, Tetsu-to-Hagané 87(1) (2001) 21-28.

[21] L. Lin, Y.-p. Bao, M. Wang, W. Jiang, H.-m. Zhou, P_2O_5 Solubility Behavior and Resource Utilization of P-Bearing Slag, ISIJ International 54(12) (2014) 2746-2753.

[22] M. Lee, Dephosphorisation in steelmaking: Back to the future?, Steel Times International 32(4) (2008) 40-42.

[23] T. Fuji, Trans. Iron Steel Inst. Japan 25 (1985) 658.

[24] P. Drain, B. Monaghan, G. Zhang, R. Longbottom, M. Chapman, S. J. Chew, A review of phosphorus partition relations for use in basic oxygen steelmaking, Ironmaking & Steelmaking 44 (2017) 721-731.

[25] C.O. Lee, J.O. Jo, B.J. Song, C.H. Chang, Y.D. Jeon, T.I. Yoon, S.H. Kim, J.G. Won, Improvement of De-Phosphorus in BOF process, 8 th European Oxygen Steelmaking Conference (EOSC), Taranto, 2018.

[26] Y. Matui, Reserved state of high phosphorus iron ore, Symposium on the contribution of iron and steel industry to phosphorus resource security, Tokyo, 2013, pp. 29-30.

[27] S. Arnout, E. Nagels, Modelling thermal phosphorus recovery from sewage sludge ash, Calphad 55 (2016) 26-31.

[28] C.-m. Du, X. Gao, S. Ueda, S.-y. Kitamura, Effect of Slag Composition on the Dissolution of Phosphorus from Steelmaking Slag by Selective Leaching, ISIJ International 58(9) (2018) 1659-1668.

[29] Publication Office of the European Union, RECOPHOS (Recovery of Phosphorus from Sewage Sludge and Sewage Sludge Ashes with the thermo-reductive-RecoPhos-Process), Luxembourg, 2015. https://cordis.europa.eu/project/rcn/102600/reporting/en.

[30] L. Lin, Y.-P. Bao, M. Wang, X. Li, Effect of MgO and MnO on Phosphorus Utilization in P-Bearing Steelmaking Slag, High Temperature Materials and Processes 35(4) (2016) 425.

[31] L. Lin, Y. Bao, M. Wang, H. Zhou, L. Zhang, Influence of SiO_2 modification on phosphorus enrichment in P bearing steelmaking slag, Ironmaking & Steelmaking 40(7) (2013) 521-527.

[32] L. Lin, Y.-P. Bao, M. Wang, H.-M. Zhou, Influence of Al_2O_3 modification on phosphorus enrichment in P bearing steelmaking slag, Ironmaking & Steelmaking 41(3) (2014) 193-198.

[33] Q.F. Shu, Y. Liu, Effects of basicity, MgO and MnO on mineralogical phases of $CaO–FeO_x–SiO_2–P_2O_5$ slag, Ironmaking & Steelmaking 45(4) (2018) 363-370.

[34] T. Teratoko, N. Maruoka, H. Shibata, S.-y. Kitamura, Dissolution behavior of dicalcium silicate and tricalcium phosphate solid solution and other phases of steelmaking slag in an aqueous solution, High Temperature Materials and Processes 41(4-5) (2012) 329–338.

[35] X.R. Wu, P. Wang, L.S. Li, Z.J. Wu, R.H. Chen, Distribution and enrichment of phosphorus in solidified BOF steelmaking slag, Ironmaking & Steelmaking 38(3) (2011) 185-188.

[36] H.-J. Li, H. Suito, M. Tokuda, Thermodynamic analysis of slag recycling using a slag regenerator, ISIJ international 35(9) (1995) 1079-1088.

[37] M. Ishikawa, Reduction behaviors of hot metal dephosphorization slag in a slag regenerator, ISIJ international 46(4) (2006) 530-538.

[38] K. Yokoyama, H. Kubo, K. Mori, H. Okada, S. Takeuchi, T. Nagasaka, Tetsu-to-Hagané 92 (2006) 683.

[39] T. DI, Upravlenie plavkoi stali v konvertere [Steel melting control in a converter]. Moscow: Metallurgiya, 1971, 360 p, Russ.

[40] Y.E. Lee, L. Kolbeinsen, An Analysis of Hot Spot Phenomenon in BOF Process, ISIJ International 47(5) (2007) 764-765.

[41] Z. Wang, Q. Liu, L. You, S. Wei, L. Cao, Experimental study on slag splashing of an 80 t combined blown converter, Ironmaking & Steelmaking 45(4) (2018) 379-385.

[42] L. Cao, Y. Wang, Q. Liu, X. Feng, Physical and Mathematical Modeling of Multiphase Flows in a Converter, ISIJ International 58(4) (2018) 573-584.

[43] S. Sabah, G. Brooks, Study of cavity modes in BOF by analysis of sound, Ironmaking & Steelmaking 43(6) (2016) 473-480.

[44] M.J. Luomala, T.M.J. Fabritius, E.O. Virtanen, T.P. Siivola, J.J. Härkki, Splashing and spitting behaviour in the combined blown steelmaking converter, ISIJ international 42(9) (2002) 944-949.

[45] M. Iguchi, Generation of Fine Bubbles, Metal Droplets, and Slag Droplets in Reactors Agitated by Bottom Gas Injection, Tetsu to Hagane -Journal of the Iron and Steel Institute of Japan, 103(3) (2017) 119-133.

[46] S.C. Koria, K.W. Lange, A new approach to investigate the drop size distribution in basic oxygen steelmaking, Metallurgical Transactions B 15(1) (1984) 109-116.

[47] Subagyo, B. GA, C. KS, I. GA, Generation of droplets in slag-metal emulsions through top gas blowing, ISIJ international 43(7) (2003) 983-989.

[48] B.K. Rout, G. Brooks, M.A. Rhamdhani, Z. Li, Modeling of droplet generation in a top blowing steelmaking process, Metallurgical and Materials Transactions B 47(6) (2016) 3350-3361.

[49] M. Schlautmann, B. Kleimt, S. Khadhraoui, K. Hack, P. Monheim, B. Glaser, R. Antonic, M. Adderley, F. Schrama, Dynamic on-line monitoring and end point control of dephosphorisation in the BOF converter, 3rd European Steel Technology and Application Days (ESTAD), Vienna, 2017, pp. 1038-1049.

[50] P. Kozakevitch, T.G. John, Foams and Emulsions in Steelmaking, JOM 21(7) (1969) 57-68.

[51] Subagyo, G.A. Brooks, K.S. Coley, Residence time of metal droplets in slag-metal-gas emulsions through top gas blowing, Canadian Metallurgical Quarterly 44(1) (2005) 119-130.

[52] E. Schürmann, G. Mahn, J. Schoop, W. Resch, Model Conception and Calculations of the Kinetics of Dephosphorization and the Circulation of Droplets in the Basic O Process, Arch. Eisenhuttenwes., Oct. 1977, 48,(10), 515-519 (1977).

[53] J. Schoop, W. Resch, G. Mahn, Reactions occurring during the oxygen top blown process and calculation of metallurgical control parameters, Ironmaking Steelmaking 5(2) (1978) 72-79.

[54] D. Price, LD steelmaking: Significance of the emulsion in carbon removal, Process Engineering of Pyrometallurgy Symposium, 1974.

[55] H. Meyer, W. Porter, G. Smith, J. Szekely, Slag-metal emulsions and their importance in BOF steelmaking, JOM 20(7) (1968) 35-42.

[56] B. Rout, G. Brooks, M.A. Rhamdhani, Z. Li, F. N. H. Schrama, W. van der Knoop, Dynamic Model of Basic Oxygen Steelmaking Process Based on Multizone Reaction Kinetics: Modeling of Manganese Removal, Metallurgical and Materials Transactions B 49(5) (2018) 2191-2208.

[57] S. Spooner, J. Marc Warnett, R. Bhagat, M. Williams, S. Sridhar, Calculating the Macroscopic Dynamics of Gas/Metal/Slag Emulsion during Steelmaking, 2016.

[58] M.S. Millman, A. Overbosch, A. Kapilashrami, D. Malmberg, M. Brämming, Study of refining performance in BOS converter, Ironmaking & Steelmaking 38(7) (2011) 499-509.

[59] K.S. Coley, Progress in the kinetics of slag-metal-gas reactions, past, present and future, Journal of Mining and Metallurgy B: Metallurgy 49(2) (2013) 191-199.

[60] H. Jalkanen, M. Suomi, M. Wallgren, Simulation of oxygen converter process (BOF), Joint Finnish-South African Symposium on Metallurgical Research, Johannesburg, 1998, pp. 1-21.

[61] E. Turkdogan, Assessment of P_2O_5 activity coefficients in molten slags, ISIJ international 40(10) (2000) 964-970.

[62] B. Deo, R. Boom, Fundamentals of steelmaking metallurgy, Chapter 2, Prentice-Hall1993.

[63] T.B. Winkler, J. Chipman, An equilibrium study of the distribution of phosphorus between liquid iron and basic slags, Trans. Aime 167 (1946) 111-133.

[64] H.W. Gudenau, Eisenhüttenmännische Verfahrenstechnik: vom Erz zum Stahl; Materialsammlung zum Praktikum" Eisenhüttenmännische Verfahrenstechnik", Inst. für Eisenhüttenkunde1989.

[65] Y. Kobayashi, N. Yoshida, K. Nagai, Thermodynamics of Phosphorus in the MnO-SiO2-FetO System, ISIJ International 44(1) (2004) 21-26.

[66] F. Tsukihashi, M. Nakamura, T. Orimoto, N. Sano, Thermodynamics of Phosphorus for the CaO-BaO-CaF_2-SiO_2 and CaO-Al_2O_3 Systems, Tetsu-to-Hagane 76(10) (1990) 1664-1671.

[67] J.C. Wrampelmeyer, S. Dimitrov, D. Janke, Dephosphorization equilibria between pure molten iron and CaO-saturated FeOn–CaO–SiO_2 and FeO_n–CaO–Al_2O_3 slags, Steel research 60(12) (1989) 539-549.

[68] J.C. Wrampelmeyer, S. Dimitrov, D. Janke, Dephosphorization equilibria between pure molten iron and CaO-saturated FeOn–CaO–CaF_2 slags, Steel Research 61(1) (1990) 1-7.

[69] K. Balajiva, P. Vajragupta, The effect of temperature on the phosphorus reaction in the basic steelmaking process, Journal of the Iron and Steel Institute 155(4) (1947) 563-567.

[70] P. Vajragupta, Note on further work on the phosphorus reaction in basic steelmaking, Journal of the Iron and Steel Institute 158(4) (1948) 494-496.

[71] H. Flood, K. Grjotheim, Thermodynamic calculation of slag equilibria, Journal of the Iron and Steel Institute 71 (1952) 64-80.

[72] W. Fischer, H.v. Ende, Die Verteilung des Phosphors zwischen Eisenschmelzen und kalkgesättigten Schlacken für Temperaturen von 1530ºC-1700ºC, Stahl Eisen 72 (1952) 1398-1408.

[73] F. Bardenheuer, P.G. Oberhäuser, Bereich unterschiedlicher Entphosphorung im system CaO-FeO-SiO2 und Folgerungen zur Erzielung niedrige Phosphorgehalte beim verblasen vom Phosphorarmen Roheisen, Stahl und Eisen 89 (1969) 988-994.

[74] G. Healy, New look at phosphorus distribution, J Iron Steel Inst 208(7) (1970) 664-668.

[75] H. Suito, R. Inoue, M. Takada, Phosphorus Distribution between Liquid Iron and MgO Saturated Slags of the System CaO-MgO-FeO_x-SiO_2, Tetsu to hagane 67 (1981) 2645-2654.

[76] H. Suito, R. Inoue, Effect of calcium fluoride on phosphorus distribution between MgO-saturated slags of the system CaO-MgO-FeO_x-SiO_2 and liquid iron, Tetsu-to-Hagané 68(10) (1982) 1541-1550.

[77] H. Suito, R. Inoue, Phosphorus Distribution between MgO-saturated CaO-Fe_tO-SiO_2-P_2O_5-MnO Slags and Liquid Iron, Tetsu to hagane 70 (1984) 186-193.

[78] R. Inoue, X.P. Zhang, H. Li, H. Suito, Distribution of Nb, P, Mn between Liquid Iron and MgOsat.-Fe_tO-SiO_2-NbO_x-MnO Slags, Tetsu-to-Hagane 74(9) (1988) 1765-1769.

[79] E.T. Turkdogan, Rationale on composition of slags in oxygen steelmaking processes, Ironmaking & Steelmaking 26(5) (1999) 358-362.

[80] K. Ide, R. Fruehan, Evaluation of phosphorus reaction equilibrium in steelmaking, Iron & steelmaker 27(12) (2000) 65-70.

[81] E. Schürmann, H. Fischer, Einfluß der Metall- und Schlackengehalte sowie der Temperatur auf die Entphosphorung mit kalkgesättigten Frischschlacken bei 1600 und 1700°C, Steel Research 62(7) (1991) 303-313.

[82] Y. Shirota, K. Katohgi, K. Klein, H.-J. Engell, D. Janke, Phosphate capacity of FeO-Fe_2O_3-CaO-P_2O_5 and FeO-Fe_2O_3-CaO-CaF_2-P_2O_5 slags by levitation melting, Transactions of the Iron and Steel Institute of Japan 25(11) (1985) 1132-1140.

[83] R. Nagabayashi, M. Hind, S. Ban-ya, Distribution of Phosphorus between Liquid Iron and FetO-(CaO+ MgO)-(SiO_2+ P_2O_5) Phosphate Slags, Tetsu-to-Hagané 74(9) (1988) 1770-1777.

[84] R. Selin, Studies on MgO Solubility in Complex Steelmaking Slags in Equilibrium With Liquid Iron and Distribution of Phosphorus and Vanadium Between Slag and Metal at MgO Saturation, Scandinavian Journal of Metallurgy(20) (1991) 279-299.

[85] A. Assis, R. Fruehan, S. Sridhar, Phosphorus equilibrium between liquid iron and CaO-SiO_2-MgO-FeO slags, AISTech 2012 Iron and Steel Technology Conference and Exposition, 2012, pp. 861-870.

[86] C. Chen, L. Zhang, J. Lehmann, Thermodynamic Modelling of Phosphorus in Steelmaking Slags, High Temperature Materials and Processes 32(3) (2013) 237.

[87] S. Khadhraoui, H.-J. Odenthal, S. Das, M. Schlautmann, K. Hack, B. Glaser, R. Woolf, A new approach for modelling and control of dephosphorization in BOF converter, La Metallurgia Italiana n. 11-12 (2018) 5-16.

[88] H. Suito, R. Inoue, Manganese equilibrium between molten iron and MgO-saturated CaO-Fe_tO-SiO_2-MnO-slags, Transactions of the Iron and Steel Institute of Japan 24(4) (1984) 257-265.

[89] H. Suito, R. Inoue, Thermodynamic Assessment of Maganese Distribution in Hot Metal and Steel, ISIJ international 35(3) (1995) 266-271.

[90] X-m. You, N-c. Yang. L. Wu, D-g. Li, Behavior of Phosphorous and Its Distribution Ratio in Combined Oxygen Converter, publication of CISDI R&D CO, funded by Chongqing Science and Technology Committee, item number CSTC, 2011AC7048.

[91] Publications Office of the European Union, Dynamic online control and end point determination of dephosphorisation in BOF converter (BOF DePhos), unpublished, Luxembourg, 2019.

[92] G.J. Chen, S.P. He, Effect of MgO content in slag on dephosphorisation in converter steelmaking, Ironmaking & Steelmaking 42(6) (2015) 433-438.

[93] B.O. Chukwulebe, A.N. Klimushkin, G.O. Kuznelsov, The Utilization of High-Phosphorus Hot Metal in BOF Steelmaking, Iron & Steel Technology, Ohio, 2006, pp. 613-622.

[94] S. Basu, A. Lahiri, S. Seetharaman, Phosphorus partition between liquid, steel and CaO-SiO_2-P_2O_5-MgO slag containing low FeO, Metallurgical and Materials Transactions B 38((3)) (2007) 357-366.

[95] X.-M. Yang, J.-P. Duan, C.-B. Shi, M. Zhang, Y.-L. Zhang, J.-C. Wang, A thermodynamic model of phosphorus distribution ratio between CaO-SiO2-MgO-FeO-Fe_2O_3-MnO-Al_2O_3-P_2O_5 slags and molten steel during a top–bottom combined blown converter steelmaking process based on the ion and molecule coexistence theory, Metallurgical and Materials Transactions B 42(4) (2011) 738-770.

[96] X.-M. Yang, C.-B. Shi, M. Zhang, J.-P. Duan, J. Zhang, A Thermodynamic Model of Phosphate Capacity for CaO-SiO_2-MgO-FeO-Fe_2O_3-MnO-Al_2O_3-P_2O_5 Slags Equilibrated with Molten Steel during a Top–Bottom Combined Blown Converter Steelmaking Process Based on the Ion and Molecule Coexistence Theory, Metallurgical and Materials Transactions B 42(5) (2011) 951-977.

[97] M. Ek, J.C. Huber, G. Brosse, D. Sichen, Capacities of some CaO–SiO_2–FeO–MnO–MgO slags and slag–solid mixtures in capturing phosphorous, Ironmaking & Steelmaking 40(4) (2013) 305-311.

[98] S.-y. Kitamura, H. Shibata, K. Shimauchi, S. Saito, The importance of dicalcium-silicate on hot metal dephosphorization reaction, Revue De Métallurgie 105(5), (2008) 263-271.

[99] S.-y. Kitamura, K.-i. Miyamoto, H. Shibata, N. Maruoka, M. Matsuo, Analysis of Dephosphorization Reaction Using a Simulation Model of Hot Metal Dephosphorization by Multiphase Slag, ISIJ International 49(9) (2009) 1333-1339.

[100] K.-i. Shimauchi, S.-y. Kitamura, H. Shibata, Distribution of P_2O_5 between Solid Dicalcium Silicate and Liquid Phases in CaO–SiO_2–Fe_2O_3 System, ISIJ International 49(4) (2009) 505-511.

[101] C.-m. Du, X. Gao, S. Ueda, S.-y. Kitamura, Distribution of P_2O_5 and Na_2O Between Solid Solution and Liquid Phase in the CaO-SiO_2-Fe_2O_3-P_2O_5-Na_2O Slag System with High P_2O_5 Content, Metallurgical and Materials Transactions B 49(1) (2018) 181-189.

[102] X. Yang, H. Matsuura, F. Tsukihashi, Reaction Behavior of Phosphorus in Multi-phase CaO–FeO_X–SiO_2–P_2O_5 Flux System: Proceedings of the First Global Conference on Extractive Metallurgy, 2018.

[103] S. Xie, W. Wang, Y. Liu, H. Matsuura, Effect of Na2O and B2O3 on the distribution of P2O5 between solid solution and liquid phases slag, ISIJ international 54(4) (2014) 766-773.

[104] X. Gao, H. Matsuura, M. Miyata, F. Tsukihashi, Phase Equilibrium for the CaO–SiO_2–FeO–5mass%P_2O_5–5mass%Al_2O_3 System for Dephosphorization of Hot Metal Pretreatment, ISIJ International 53(8) (2013) 1381-1385.

[105] X. Gao, H. Matsuura, I. Sohn, W. Wang, D. Joon Min, F. Tsukihashi, Phase Relationship of CaO-SiO_2-FeO-5 mass pct P_2O_5 System with Low Oxygen Partial Pressure at 1673 K (1400 A degrees C), 2012.

[106] X. Yang, H. Matsuura, F. Tsukihashi, Reaction Behavior of P_2O_5 at the Interface between Solid 2CaO· SiO_2 and Liquid CaO–SiO_2–FeO_x–P2O5 Slags Saturated with Solid 5CaO· SiO_2· P_2O_5 at 1 573 K, ISIJ international 50(5) (2010) 702-711.

[107] X. Yang, H. Matsuura, F. Tsukihashi, Condensation of P_2O_5 at the interface between $2CaO\cdot SiO_2$ and $CaO–SiO_2–FeO_x–P_2O_5$ slag, ISIJ International 49(9) (2009) 1298-1307.

[108] H. Matsuura, M. Kurashige, M. Naka, F. Tsukihashi, Melting and solidifying behaviors of the $CaO–SiO_2–FeO_x$ slags at various oxygen partial pressures, ISIJ International 49(9) (2009) 1283-1289.

[109] C.-m. Du, X. Gao, S. Ueda, S.-y. Kitamura, Recovery of phosphorus from modified steelmaking slag with high P_2O_5 content via leaching and precipitation, ISIJ International 58(5) (2018) 833-841.

[110] F. Pahlevani, S.-y. Kitamura, H. Shibata, N. Maruoka, Distribution of P_2O_5 between solid solution of $2CaO\cdot SiO_2–3CaO\cdot P_2O_5$ and liquid phase, ISIJ international 50(6) (2010) 822-829.

[111] S.-y. Kitamura, S. Saito, K. Utagawa, H. Shibata, D.G. Robertson, Mass transfer of P_2O_5 between liquid slag and solid solution of $2CaO\cdot SiO_2$ and $3CaO\cdot P_2O_5$, ISIJ international 49(12) (2009) 1838-1844.

[112] S.-y. Kitamura, F. Pahlevani, Process simulation of dephosphorization treatment of hot metal with high phosphorus content. Tetsu-To-Hagane/Journal of the iron and steel institute of Japan 100(4) (2014), 500-508.

[113] H. Suito, R. Inoue, Behavior of phosphorous transfer from $CaO–Fe_tO–P_2O_5$ ($–SiO_2$) slag to CaO particles, ISIJ international 46(2) (2006) 180-187.

[114] R. Inoue, H. Suito, Phosphorous partition between $2CaO\cdot SiO_2$ particles and $CaO–SiO_2–Fe_tO$ slags, ISIJ international 46(2) (2006) 174-179.

[115] R. Inoue, H. Suito, Mechanism of dephosphorization with $CaO–SiO_2–Fe_tO$ slags containing mesoscopic scale $2CaO\cdot SiO_2$ particles, ISIJ international 46(2) (2006) 188-194.

[116] S. Xie, W. Wang, Z. Luo, D. Huang, Mass Transfer Behavior of Phosphorus from the Liquid Slag Phase to Solid $2CaO\cdot SiO_2$ in the Multiphase Dephosphorization Slag, Metallurgical and Materials Transactions B 47(3) (2016) 1583-1593.

[117] J.-y. Li, M. Zhang, M. Guo, X.-M. Yang, Enrichment Mechanism of Phosphate in CaO-SiO2-FeO-Fe_2O_3-P_2O_5 Steelmaking Slags, Metallurgical and Materials Transactions B 45(5) (2014) 1666-1682.

[118] H. Preßlinger, J. Fluch, R. Apfolterer, Mikroanalytische Untersuchungen über die Einbindung von Phosphor in LD-Schlacken, BHM Berg-und Hüttenmännische Monatshefte 157(3) (2012) 136-143.

[119] S. Xie, W. Wang, D. Huang, H. Li, Y. Du, Clarification of the Dissolution of Solid CaO and the Phosphorus-Enrichment Capability of Calcium Silicates in the Multiphase Slag Based on the Ion and Molecule Coexistence Theory, steel research international 89(2) (2018) 1700317.

[120] T. Hamano, S. Fukagai, F. Tsukihashi, Reaction mechanism between solid CaO and $FeO_{(X)}$-CaO-SiO_2-P_2O_5 slag at 1573K, Tetsu-to-Hagane 92(11) (2006) 649-654.

[121] K. Ito, N. Sano, Phosphorus Distribution between CaO-containing Slag and Carbon-saturated Iron at Hot Metal Temperatures, Tetsu-to-Hagane 69(15) (1983) 1747-1754.

[122] H. Ono, T. Masui, H. Mori, Dephosphorization Kinetics of Hot Metal by Lime Injection with Oxygen Gas, Tetsu-to-Hagane 69(15) (1983) 1763-1770.

[123] K. Endell, J. Hellbrugge, Naturwissenschaften 30 (1942) 421-422.

[124] J.O'.M. Bockris, J.D. Mackenzie, J.A. Kitchner, Trans. Faraday Soc. 51 (1955) 1734-1748.

[125] J. Flood, T. Förland, Acta chem. scand. 1 (1947) 592-604 and 781-789.

[126] C.J.B. Fincham, F.D. Richardson, Proc. R. Soc. A223 (1954) 40-62.

[127] C.R. Masson, Proc. R. Soc. A 28 (1965) 201.

[128] K.C. Mills, M. Hayashi, L. Wang, T. Watanabe, Chapter 2.2 - The Structure and Properties of Silicate Slags, in: S. Seetharaman (Ed.), Treatise on Process Metallurgy, Elsevier, Boston, 2014, pp. 149-286.

[129] J. Lumsden, Physical chemistry of process metallurgy, Part I, Interscience Publisher, N. Y, 1961.

[130] Y.-q. Hou, G. Xie, D.-p. Tao, X.-h. Yu, R.-x. Li, Activity Calculation in Complex Metallurgical Molten Slag Systems Based on Regular Solution Model, Journal of Iron and Steel Research, International 19(3) (2012) 6-10.

[131] S. Ban-Ya, Mathematical expression of slag-metal reactions in steelmaking process by quadratic formalism based on the regular solution model, ISIJ international 33(1) (1993) 2-11.

[132] C. Shi, X.-M. Yang, J.-s. Jiao, C. Li, H.-j. Guo, A Sulphide Capacity Prediction Model of CaO–SiO_2–MgO–Al_2O_3 Ironmaking Slags Based on the Ion and Molecule Coexistence Theory, ISIJ International 50 (2010) 1362-1372.

[133] X.-M. Yang, M. Zhang, J.l. Zhang, P.c. Li, J.y. Li, J. Zhang, Representation of Oxidation Ability for Metallurgical Slags Based on the Ion and Molecule Coexistence Theory, steel research international 85(3) (2014) 347-375.

[134] S.-c. Duan, C. Li, X.-l. Guo, H.-j. Guo, J. Guo, W.-s. Yang, A thermodynamic model for calculating manganese distribution ratio between CaO–SiO_2–MgO–FeO–MnO–Al_2O_3–TiO_2–CaF_2 ironmaking slags and carbon saturated hot metal based on the IMCT, Ironmaking & Steelmaking 45(7) (2018) 655-664.

[135] H. Lukas, S.G. Fries, B. Sundman, Computational thermodynamics: the Calphad method, Cambridge university press2007.

[136] R. Schmid-Fetzer, J. Gröbner, Focused development of magnesium alloys using the calphad approach, Advanced engineering materials 3(12) (2001) 947-961.

[137] E .B. C. W. Bale, P. Chartrand, S. A. Decterov, G. Eriksson, A.E. Gheribi, K. Hack, I. H. Jung, Y. B. Kang, J. Melançon, A. D. Pelton, S. Petersen, C. Robelin. J. Sangster, P. Spencer and M-A. Van Ende, FactSage Thermochemical Software and Databases - 2010 - 2016, Calphad vol. 54(2016) (2016) 35-53.

[138] R. Davies, A. Dinsdale, J. Gisby, J.A.J. Robinson, S.M. Martin, MTDATA-thermodynamic and phase equilibrium software from the national physical laboratory, Calphad 26(2) (2002) 229-271.

[139] J.-O. Andersson, T. Helander, L. Höglund, P. Shi, B. Sundman, Thermo-Calc & DICTRA, computational tools for materials science, Calphad 26(2) (2002) 273-312.

[140] L. Jahanshahi, Recent developments in physico-chemical characterization and modelling of ferroalloy slag systems, Journal of the Southern African Institute of Mining and Metallurgy 104(9) (2004) 529-540.

[141] T.I. Barry, A.T. Dinsdale, J.A. Gisby, Predictive thermochemistry and phase equilibria of slags, JOM 45(4) (1993) 32-38.

[142] I.-H. Jung, Overview of the applications of thermodynamic databases to steelmaking processes, CALPHAD 34(3) (2010) 332-362.

[143] I.-H. Jung, P. Hudon, M.A. Van Ende, W.Y. Kim, Thermodynamic database for P_2O_5-containing slags and its application to the dephosphorization process, AISTech-Iron and Steel Technology Conference Proceedings, Indianapolis, 2014, pp. 1257-1268.

[144] K. Hack, T. Jantzen, M. Müller, E. Yazhenskikh, G. Wu, A novel thermodynamic database for slag systems and refractory materials, Proceedings of the 5th International Congress on the Science and Technology of Steelmaking, ICS, 2012.

[145] E. Yazhenskikh, K. Hack, M. Müller, Thermodynamic optimisation of the system Al_2O_3-K_2O-Na_2O-SiO_2, GTT User Meeting, Aachen, 2010.

[146] T. Jantzen, E. Yazhenskikh, K. Hack, M. Müller, Thermodynamic assessment of the $CaO–P_2O_5–SiO_2–ZnO$ system with special emphasis on the addition of ZnO to the Ca2SiO4–Ca3P2O8 phase, Calphad 67 (2019) 101668.

[147] E. Yazhenskikh, T. Jantzen, K. Hack, M. Müller, A New Multipurpose Thermodynamic Database for Oxide Systems, Расплавы, 2019 - elibrary.ru.

[148] M. Modigell, A. Traebert, D. Liebig, P. Monheim, A Process Modelling Technique for High Temperature Reactors, Chemie Ingenieur Technik 73(6) (2001) 672-672.

[149] S. Petersen, K. Hack, P. Monheim, P. Scheller, M. Müller, M. Dohrn, S. Khadhraoui, Application Examples of Thermochemical Process Simulation Using SimuSage – Introducing Current Projects from Metallurgy and Combustion Technology, Materials Science & Technology Pittsburgh, 2017, pp. 1239-1240.

[150] T.M. Besmann, K.E. Spear, Thermochemical modeling of oxide glasses, Journal of the American Ceramic Society 85(12) (2002) 2887-2894.

[151] Y.A. Chang, W.A. Oates, Materials thermodynamics, John Wiley & Sons, New jersey, 2010.

[152] E. Guggenheim, Proc. Roy. Soc.(London) A148, 304 (1935), Proc. Roy. Soc.(London) 148 (1935) 304.

[153] A.D. Pelton, M. Blander, Thermodynamic analysis of ordered liquid solutions by a modified quasichemical approach—application to silicate slags, Metallurgical and Materials Transactions B 17(4) (1986) 805-815.

[154] M. Kapoor, M. Frohberg, Chemical metallurgy of iron and steel, Iron and Steel Institute, London, 1971, pp. 17-21.

[155] H. Gaye, J. Welfringer, Modelling of the thermodynamic properties of complex metallurgical slags, The Second International Symposium on Metallurgical Slags and Fluxes, Warrendale, Pittsburgh, 1984, pp. 357-375.

[156] I. Ansara, B. Sundman, The scientific group thermodata Europe, Elsevier, Amsterdam, 1987.

[157] B. Sundman, J. Ågren, A regular solution model for phases with several components and sublattices, suitable for computer applications, Journal of physics and chemistry of solids 42(4) (1981) 297-301.

[158] B. Sundman, Q. Chen, Y. Du, A Review of Calphad Modeling of Ordered Phases, Journal of Phase Equilibria and Diffusion 39(5) (2018) 678-693.

[159] M. Chase, J.L. Curnutt, A. Hu, H. Prophet, A. Syverud, L. Walker, JANAF thermochemical tables, 1974 supplement, Journal of Physical and Chemical Reference Data 3(2) (1974) 311-480.

[160] I.-H. Jung, P. Hudon, Thermodynamic Assessment of P_2O_5, Journal of the American Ceramic Society 95(11) (2012) 3665-3672.

[161] J.C. Southard, R.A. Nelson, The Vapor Pressure of Phosphorus Pentoxide, J. Am. Chem. Soc., 59 (1937) 911–6.

[162] A. Smits, E.P.S. Parve´, P.G. Meermann, H.C.J. deDecker, Die Komplexität des Phosphorpentoxyds. III. Das Auftreten von Zwei Flüssigen Phasen, Z. Physik. Chem. B 46 (1940) 43–61.

[163] A. Smits, A.J. Rutgers, Part I.The Complexity of the Solid State. Part II. The Behaviour of Phosphorus Pentoxide, J. Chem. Soc., 125 (1924) 2573–9.

[164] M.A. Hoeflake, F.E.C. Scheffer, Les Tensions de Vapeur du Pentoxyde de Phosphore, Rec. Trav. Chim., 45 (1926) 191–200.

[165] W.T. Massalski, H. Okamoto, P. Subramanian, L. Kacprzak, Binary Alloy Phase Diagrams–Second edition. ASM International, Advanced Materials 3(12) (1991) 628-629.

[166] W. Hill, G. Faust, D. Reynolds, The binary system P_2O_5-2CaO.P_2O_5; Part II, American Journal of Science 242(10) (1944) 542-562.

[167] G. Trömel, W. Fix, Untersuchungen im System Kalk-Phosphorsäure, Archiv für das Eisenhüttenwesen 32(4) (1961) 209-212.

[168] L. Chang, Phase equilibria in iron phosphate system, Dissertation, Missouri University of Science and Technology (2010).

[169] G. Trömel, K. Schwerdtfeger, Untersuchungen im System Eisen–Phosphor–Sauerstoff, Archiv für das Eisenhüttenwesen 34(1) (1963) 55-59.

[170] E. Schürmann, K.-H. Obst, L. Fiege, H.-P. Kaiser, Effect of bottom stirring and post stirring on the oxygen distribution between metal and slag at the end of the LD process, Steel Research 56(8) (1985) 425-431.

[171] P. Kozakevitch, P. Riboud, Estimation du pouvoir déphosphorant des laitiers suroxydés, Revue de Métallurgie 63(11) (1966) 871-876.

[172] P. Riboud, H. Margot-Marette, Étude des laitiers phosphatés influence des différents constituants du laitier sur la quantité optimale de chaux a enfourner, Revue de Métallurgie 65(7-8) (1968) 477-492.

[173] H. Margot-Marette, P. Riboud, Study of the liquidus of the CaO-P_2O_5-SiO_2-FeO system. Part 3. less than 50 percent FeO section, MEM SCI REV MET LXIX(9) (1972) 593-604.

[174] H. Burghardt, S. Krauß, G. Neuhof, Stahlerzeugung, Deutscher Verlag für Grundstoffindustrie, 1982.

[175] W. Resch, Die Kinetik der Entphosphorung beim Sauerstoffaufblasverfahren für phosphorreiches Roheisen, Dissertation, Technische Universität Clausthal, 1976.

[176] G. Trömel, W. Fix, Die Gleichgewichte zwischen Eisenschmelzen und kalkhaltigen Phosphatschlacken bei Gegenwart von Kieselsäure und Manganoxyd, steel research international 33(11) (1962) 745-755.

[177] G. Trömel, H.W. Fritze, Arch. Eisenhüttenwesen, 30 (1959) 398-401.

[178] H. Knüppel, F. Oeters, H. Gruss, Arch. Eisenhüttenwesen 30 (1959) 253-265.

[179] E.J. Drewes, M. Olette, Untersuchungen über den Einfluß der Kieselsäure und des Oxydationsgrades auf die Phasengrenzen, besonders der Mischungslücke, im System $CaO–P_2O_5–FeO–Fe_2O_3–SiO_2$ bei 1600°C, Archiv für das Eisenhüttenwesen 38(3) (1967) 163-175.

[180] K. Schwerdtfeger, E. Turkdogan, Miscibility Gap in the System Iron Oxide-CaO-P_2O_5 in Air at 1625ºC, Trans. Metall. Soc. AIME 239 (1967) 589-590.

[181] W.A. Fischer, H.J. Fleischer, F. Höfer, Archiv für das Eisenhüttenwesen 35(4) (1964) 279-285.

[182] W. Fix, K. Koch, Untersuchung über den Schlackenzustand beim Sauerstoffaufblas-Verfahren mit phosphorreichem Roheisen, Archiv für das Eisenhüttenwesen, doi:10.1002/srin.196803484 39(1) (1968) 9-22.

[183] H.J. Fleischer, H. Fischer, Arch. Eisenhuettenwes 38(3) (1967) 185-190.

[184] K. Koch, W. Fix, Untersuchungen im Schlackensystem $Fe–CaO–FeO_n–P_2O_5–SiO_2$ bei 1600° C, steel research international 41(2) (1970) 111-118.

[185] W. Oelsen, H. Maetz, Das Verhalten des Flusspates und der Kalziumphosphate gegenüber dem Eisenoxydul im Schmelzfluss und seine metallurgische Bedeutung, Mitt. Kais. Wilh. Inst. f. Eisenforsch. Bd 23 (1941) 195.

[186] E.T. Turkdogan, Physicochemical properties of molten slags and glasses, Chapter 3, The Metals Society, London, 1984.

[187] E. Schürmann, F. Bardenheuer, S. Döhler, Sättigungszustände und Entmischung in kalkreichen, flüssigen Schlacken der Stahlerzeugung bei 1600°C, Archiv für das Eisenhüttenwesen 50(10) (1979) 423-428.

[188] C. Duée, C. Bourgel, E. Véron, M. Allix, F. Fayon, F. Bodénan, J. Poirier, Phosphorus speciation in dicalcium silicate phases: Application to the basic oxygen furnace (BOF) slag, Cement and Concrete Research 73 (2015) 207-214.

[189] F. Oeters, Die physikalische Chemie der Eisen- und Stahlerzeugung, Chapter: Grundlagen der Frischereaktionen, Schlackenarbeit, Verlag Stahleisen, Germany, 1964.

[190] S. Khadhraoui, K. Hack, T. Janßen, H.-J. Odenthal, Study of the state of industrial P_2O_5-containing slags relevant to Steelmaking processes based on a new thermodynamic database developed for CaO- FeO- P_2O_5- SiO_2 -MnO-MgO-Al_2O_3 slags - Part I: Ternary and lower order systems, Steel research international (2019) 1900085.

[191] E. Görl, F. Oeters, R. Scheel, Archiv für das Eisenhüttenwesen 37 (1966), 441-451.

[192] E. Görl, R. Klages, R. Scheel, G. Trömel, Gleichgewichte zwischen flüssigem Eisen und gesättigten Schlacken des Systems CaO–FeO–MnO–SiO_2 bei 1600° C unter Berücksichtigung der Schwefelverteilung, Archiv für das Eisenhüttenwesen 40(12) (1969) 959-967.

[193] B. Phillips, A. Muan, Phase Equilibria in the System CaO-Iron Oxide-SiO_2, in Air, Journal of the American Ceramic Society 42(9) (1959) 413-423.

[194] E.F. Osborn, A. Muan, Phase equilibrium diagrams of oxide systems, Am. Ceram. Soc., Columbus, Ohio, 1960.

[195] H. Margot-Marette, P.V. Riboud, Fusibilité et cristallisation des laitiers basiques peu phosphatés d'aciérie, Revue de Métallurgie 61(9) (1964) 709-713.

[196] R. Knüppel, H. Helfmeier, F. Oeters, Thermodynamic database development modeling and phase diagram calculation in oxide systems, Archiv für das Eisenhüttenwesen 46 (1975) 549-554.

[197] C. Cicutti, M. Valdez, T. Pérez, J. Petroni, A. Gómez, R. Donayo, L. Ferro, Study of slag-metal reactions in an LD-LBE converter, 6th International Conference on Molten Slags, Fluxes and Salts, 2000.

[198] A. Van Hoorn, J. van Konynenburg, P. Kreyger, Evolution of slag composition and weight during the blow, in: L. W-K (Ed.), The Role of Slag in Basic Oxygen Steelmaking Processes, McMaster University Press, Hamilton, Ontario, 1976.

[199] E.M. Beunder, A. Overbosch, F.N.H. Schrama, H.J. Visser, K. Gu, N. Dogan, K.S. Coley, Steel and slag analysis during converter blowing compared to model calculations 8th European Oxygen Steelmaking Conference (EOSC), Taranto, 2018.

[200] H. Jalkanen, L. Holappa, On the role of slag in the oxygen converter process, VII International Conference on Molten Slags Fluxes and Salts, 2004, pp. 71-76.

[201] J. Martinsson, B. Glaser, D. Sichen, Lime Dissolution in Foaming BOF Slag, Metallurgical and Materials Transactions B 49(6) (2018) 3164-3170.

[202] T. Deng, D. Sichen, Study of lime dissolution under forced convection, Metallurgical and Materials Transactions B 43(3) (2012) 578-586.

[203] K. Gu, N. Dogan, K. Coley, Dephosphorization Kinetics between Bloated Metal Droplets and Slag Containing FeO: The Influence of CO Bubbles on the Mass Transfer of Phosphorus in the Metal, Metallurgical and Materials Transactions B 48.6 (2017) 2984-3001.

[204] K. Chattopadhyay, S. Kumar, Thermodynamic Analysis for Enhancing Phosphorus Removal in Steelmaking. AISTech-Iron and Steel Technology Conference (AISTech), Indianapolis, 2014.

[205] G. Thornton, A. D, Ironmaking and Steelmaking 21 (1994) 247.

[206] W. Van der Knoop, G. Van Unen, A. Snoeijer, R. Boom, Steel Times 222 (1994) 141.

[207] F. Oeters, R. Scheel, Untersuchungen zur Kalkauflösung in CaO-FeO-SiO_2-Schlacken, Archiv für das Eisenhüttenwesen 45(9) (1974) 575-580.

[208] B. Deo, R. Boom, Fundamentals of steelmaking metallurgy, Chapter 5, Prentice-Hall, 1993.

[209] V. Hergat, Contribution à l'étude du mécanisme de l'affinage à l'oxygène. Etude du comportement des billes de métal en suspension dans la phase laitier-métal. Reports Pilot Plant IRSID.

[210] Publications Office of the European Union, Improving phosphorus refining (IMPHOS), 2011, https://cordis.europa.eu/project/rcn/80409/factsheet/en.

[211] W. T. Lankford, ed. The making, shaping, and treating of steel. Association of Iron & Steel Engineers, 1985.

[212] M. Ishiguro, Tetsu-to-Hagane 57 (1971) 267-270.

[213] B. Monaghan, R. J. Pomfret, K. Coley, The Kinetics of Dephosphorization of Carbon-Saturated Iron Using an Oxidizing Slag, Metallurgical and Materials Transactions B 29(1) (1998) 111-118.

[214] M. Nasu, K.C. Mills, B.J. Monaghan, A. Jakobsson, S. Seetharaman, Effect of slag/metal interfacial tension on kinetics of dephosphorisation, Ironmaking & Steelmaking 26(5) (1999) 353-357.

[215] T. Sato, K. Nakashima, K. Mori, Dephosphorization rate of high carbon iron melts by CaO-based slags, Tetsu-to-Hagane 87(10) (2001) 643-649.

[216] D. Woolley, U. Pal, Mechanistic analysis of the kinetics of reactions between iron oxides in slag and carbon in liquid iron, 58 th Ironmaking Conference, 1999, pp. 413-429.

[217] W.M. Kim, G. Gränzdörffer, H.A. Fine, The kinetics of reduction of iron oxide from molten slag, Steel Research 60(3-4) (1989) 166-170.

[218] R. Roscoe, The viscosity of suspensions of rigid spheres, British journal of applied physics 3(8) (1952) 267.

[219] Y. Shiraishi, K. Ikeda, A. Tamura, T. Saito, On the viscosity and density of the molten FeO–SiO_2 system, Transactions of the Japan Institute of Metals 19(5) (1978) 264-274.

[220] H. Ono, A. Inagaki, T. Masui, H. Narita, T. Mitsuo, S. Nosaka, S. Gohda, Removal of phosphorus from LD converter slag by floating of dicalcium silicate during solidification, Tetsu-to-Hagané 66(9) (1980) 1317-1326.

[221] S. Khadhraoui, Analysis of Static Models for the Oxygen Steelmaking Process, Master Thesis, University of Duisburg-Essen, 2010.

[222] B.K. Rout, G. Brooks, M.A. Rhamdhani, Z. Li, F.N. Schrama, J. Sun, Dynamic Model of Basic Oxygen Steelmaking Process Based on Multi-zone Reaction Kinetics: Model Derivation and Validation, Metallurgical and Materials Transactions B 49(2) (2018) 537-557.

[223] M. Matsushima, S. Yadoomaru, K. Mori, Y. Kawai, Fundamental Study on the Dissolution Rate of Solid Lime Into Liquid Slag, Trans. Iron Steel Inst. Jpn. 17(8) (1977) 442-449.

[224] N. Dogan, G.A. Brooks, M.A. Rhamdhani, Kinetics of flux dissolution in oxygen steelmaking, ISIJ international 49(10) (2009) 1474-1482.

[225] C. Chigwedu, J. Kempken, W. Pluschkell, A new approach for the dynamic simulation of the BOF process, 2006.

[226] S. Eberhard, S. Peter, K. Ingo, Verlauf der Kalksättigung im System FeO–Fe_2O_3–CaO–SiO_2–P_2O_5–MgO–MnO beim Gleichgewicht mit einer Eisenschmelze, Steel Research 56(7) (1985) 369-378.

[227] Y. Lytvynyuk, J. Schenk, M. Hiebler, A. Sormann, Thermodynamic and kinetic model of the converter steelmaking process. Part 1: The description of the BOF model, Steel research international 85(4) (2014) 537-543.

[228] S. Amini, M. Brungs, O. Ostrovski, S. Jahanshani, Effects of additives and temperature on dissolution rate and diffusivity of lime in Al_2O_3-CaO-SiO_2 based slags, Metallurgical and Materials Transactions B 37(5) (2006) 773-780.

[229] M.-A. Van Ende, Y.-M. Kim, M.-K. Cho, J. Choi, I.-H. Jung, A kinetic model for the Ruhrstahl Heraeus (RH) degassing process, Metallurgical and materials transactions B 42(3) (2011) 477-489.

[230] S. Khadhraoui, H.-J. Odenthal, F. Krause, N. Uebber, W. Klos, K. Hack, P. Monheim, M. to Baben, Modeling and control of the BOF process: Challenges, solutions and latest developments in SMS group, METEC and 4th European Steel Technology and Application Days (ESTAD), Düsseldorf, 2019.

[231] S. Khadhraoui, P. Monheim, K. Hack, M. To Baben, Application of Thermochemistry in BOF process modeling: What did it teach us about the dynamics of decarburisation reaction?, GTT Technologies, GTT Annual User Meeting 2019, 2019.

[232] S. Khadhraoui, S. Das, H.-J. Odenthal, F. Krause A. Kemminger: inventors; SMS group GmbH: assignee. Method for Refining Molten Metal Using a Converter. International patent, 16 Feb **2018**, international publication number: WO2019/158479.A1.
URL:https://patentscope.wipo.int/search/en/detail.jsf?docId=WO2019158479&tab=PCTBIBLIO&_cid=P22-K5C94M-56152-3

List of Symbols

Latin characters

a	Activity	
E	Energy	J/mole
G	Gibbs energy	J/mole
h	Enthalpy	J/mole
K	Reaction constant	-
n	Number of moles	mole
m	Mass	g
p	Partial pressure	atm
R2	Multi-linear-regression-coefficient	-
T	Temperature	K
Vol%	Volume percent	Nm^3/Nm^3
Wt%	Weight percent	g/g
x_i	mole fraction of the species i	mole/mole

Greek characters

α-Fe	solid solution phase of iron with a body-centered cubic crystal structure
γ-Fe	solid solution phase of iron with a face-centered cubic crystal structure
δ-Fe	solid solution phase of iron with body-centered cubic crystal structure

Abbreviations

BOF	Basic Oxygen Furnace
Gr.	Group
LD-AD	Linz- Donawitz-ARBED-CRM
Meas.	Measured
MG	Miscibility Gap
ppm	Particle per million
Ref.	Reference
SEM	Scanning Electron Microscope
SGTE	Scientific Group Thermodata Europe
Va	Vacancy in the sublattice
XRD	X-Ray Diffraction

Indices

liq	liquid
sat.	saturation
s	solid
ss	solid solution
x	oxidation state of iron: equals 1 for pure FeO and 1.5 for pure Fe_2O_3

List of Figures

List of Tables

DOI: 10.17185/duepublico/74066
URN: urn:nbn:de:hbz:464-20210226-153814-8